Using nanoparticle stabilised emulsions to encapsulate low molecular weight species in a metallic shell

Kirsty Scott Stark

School of Chemical and Process Engineering

University of Leeds

A thesis submitted for the degree of

Doctor of Philosophy

January 2018

The candidate confirms that the work submitted is her own. The candidate confirms that appropriate credit has been given within the thesis where reference has been made to the work of others.

Experimental data collected by another user (with the author present) included the collection of Cryo-TEM data operated by Dr Nicole Hondow and Cryo-SEM data operated by Stuart Micklethwaite.
Experimental data for uncoated polymer capsules in Figure 7.4 used as a comparison for the gold coated emulsion capsules was collected by Alison Tasker while at the University of Leeds[101].
NIR irradiation and ultrasound shell fracture experiments were carried out by Dr Hui Gao at Queen Mary University in the laboratories of Prof. Gleb Sukhurokov.

Acknowledgements

I would like to start my thanking my supervisor Dr Olivier Cayre for his support, guidance and feedback throughout my PhD. In particular thank you for putting up with my wobbles and constantly encouraging me to carry on despite my own doubts and providing me with many great opportunities.

Additionally I would like to thank those at Procter & Gamble who were involved with the project, including Dr Elaine Baxter and Alastair MacGregor who provided many helpful insights and guidance. I would also like to express my thanks to the EPSRC and Procter & Gamble for the funding towards this project, without which it would have not been possible.

There are a number of people I would like to thank within the School of Chemical and process engineering, including those in the Colloids and Polymer Engineering group and everyone at LEMAS, for their time and expertise. In particular I would like to express my gratitude to all the people that I have met along the way that I have become privileged enough to call my friends, without their constant support for the past few years I would not have made it to his stage. In particular, frequent tag team pep talks from EJ James have motivated me through particularly long teary days and great advice from Ian Rosbottom and many others has kept me going. It also turns out that an in house psychology team was required to get me through many of the years and I am forever grateful for the support, understanding and escape from work when I needed to vent about life, especially to Tom Matthews for his continued support. Forming such friendships

has made this whole process worthwhile and made Leeds much more enjoyable!

Finally I would like to thank my family for supporting me throughout my PhD and and my undergraduate degree, especially my Mum who has always been on the other end of the phone when I have needed her, despite some challenging times for us all. A special thanks goes to my long standing friends who have been there every step of the way and had to put up with all of the highs and lows. They have provided constant encouragement and often reminded me of the words of J.K Rowling; 'Hard work is important but there's something that matters even more. Believing in yourself.'

Abstract

Encapsulation and controlled release of active ingredients in formulated products can provide benefits to a number of industries such as cosmetics, pharmaceuticals, agrochemicals, home and personal care products and fragrances. The main roles of encapsulation are to isolate an active material from its surroundings so as to act as a form of protection from exterior environments and to provide a mechanism for controlled release. One of the prominent challenges of encapsulating small compounds, such as those found in drugs, vitamins, fragrance and flavour oils, arises from the fact that the permeation of such species through most microcapsule membranes is fast because current capsule shell materials (polymeric/lipid based membranes/ particulate) have large diffusion coefficients. Although this can be compensated for in some ways, the unavoidable active ingredient leaching resulting from common processes occurring during the application/storage (i.e. lifetime) of the product such as dilution or interaction with other formulation ingredients (surfactants, polymers, biological species) is a significant challenge. Such process often leads to wastage of the valuable active and to side effects.

In this work, a method for preventing the loss of encapsulated actives whereby an impermeable metallic film is deposited directly onto an emulsion droplet, hence allowing 100 % of the emulsion core (potentially corresponding to 100 % of the active material depending on conditions) has been developed. A metallic nanoparticle emulsifier, stabilised by a polymer, is used as a catalyst for the electroless deposition of a secondary metal film at the emulsion droplet interface, thereby forming an impermeable shell. In this case a platinum-catalysed gold

film electroless deposition mechanism is used as a model system to demonstrate the feasibility of the process.

Polyvinylpyrrolidone (PVP) stabilised platinum nanoparticles (Pt-PVP NPs) were specifically synthesised to reduce the quantity of excess polymer in the resulting nanoparticle dispersion, in order to reduce competition for adsorption at the oil-water interface for the Pt nanoparticles and hence to maximise the nanoparticle packing at the interface. Successful adsorption of the Pt nanoparticles at the oil-water interface was confirmed by electron microscopy techniques and energy dispersive x-ray (EDX) spectroscopy, whereby a densely packed nanoparticle array was observed at curved interfaces. Interfacial rheology experiments also showed the build up of a nanoparticle film over time at a planar oil-water interface, which as a result exhibited increasing elastic properties. Cryo-transmission electron microscopy (cryo-TEM) illustrated the importance of reducing the amount of excess PVP in the nanoparticle dispersion as the polymer was found to competitively adsorb at the interface. This observation was supported by interfacial tension measurements of the nanoparticles in oil, whereby dispersions on the nanoparticles took significantly longer to reach equilibrium than those with added polymer.

The optimised Pt-PVP NP dispersions were used to stabilise hexadecane emulsions and key parameters in the emulsification process were investigated to demonstrate control over the resulting emulsion. Emulsification with excess PVP in the nanopartcle dispersion further confirmed that the PVP was competitively adsorbing and reduced the density of catalytic nanoparticles at the oil-water interface. For a given nanoparticle concentration stable emulsions could be produced with oil volume fractions between 5% and 13 % The influence of electrolyte concentration was investigated and the significance of screening interactions between the charged oil-water interface and the charged nanoparticle surface for efficient nanoparticle adsorption was highlighted.

Finally, the Pt-PVP NP stabilised emulsions were used as scaffolds for the electroless deposition of a secondary gold film, thereby encapsulating the oil core. Retention of the core was demonstrated over 35 days in an ethanol:water (4:1) environment at 40 °C and was compared to the rapid release of oil from uncoated polymeric shells. The effect of the polymeric stabiliser in the gold plating solution was investigated, with longer chained polymers appearing to provide better stabilisation of the microcapsules during the electroless deposition process. The shell thickness and therefore density of the microcapsules was controlled by altering the concentration of gold salt in the plating solution. Preliminary ultrasound and IR irradiation experiments were also carried out to demonstrate the possibility of remotely triggering the metallic film fracture and associated release of the capsule payload. These initial tests show promise and offer potential for applications such as controlled drug delivery.

List of Symbols

Abbreviations

CNT	Classical nucleation theory
DCM	Dichloromethane
DWR	Double wall ring
EDX	Energy dispersive x-ray
ELP	Electroless plating
FCC	Face-centred cubic
FTIR	Fourier transform infrared
GC	Gas chromatography
GLN	Gelled lipid nanoparticles
HAADF-STEM	High-angle annular dark-field scanning transmission electron microscopy
HLB	Hydrophilic-lipophilic balance
HRTEM	High-resolution transmission electron microscopy
IFT	Interfacial tension
NP	Nanoparticle
PCMs	Phase change materials
PEG	Poly(ethylene glycol)
PFPE	Perfluoropolyether
PMMA	Poly(methyl methacrylate)
Pt-PVP NPs	Polyvinylpyrrolidone stabilised platinum nanoparticles
PTFE	Polytetrafluoroethylene
PVA	Poly(vinyl alcohol)
PVP	Polyvinylpyrrolidone
SAED	Selected area electron diffraction

SEM	Scanning electron microscopy	
SPR	Surface plasmon resonance	
STEM	Scanning transmission electron microscopy	
TEM	Transmission electron microscopy	
THF	Tetrahydrofuran	
UV	Ultraviolet	
UV-vis	Ultraviolet-visible	
XRD	X-ray diffraction	

Greek Symbols

δ	Phase angle	rad s^{-1}
η	Viscosity	Pa·sec
γ	Interfacial tension	$N{\cdot}m^{-1}$
ω	Angular frequency	$rad{\cdot}s^{-1}$
ϕ	Oil volume fraction	-
ϕ_{cream}	Cream layer fraction	-
ρ_C	Mass density of continuous phase	$kg{\cdot}m^{-3}$
ρ_D	Mass density of droplet phase	$kg{\cdot}m^{-3}$
σ_s	Amplitude of applied stress	Nm^{-1}
τ	Tortuosity	-
ε	Porosity	-
φ_0	Amplitude of strain	-

Roman Symbols

A	Shell surface area	m^2
a	Acceleration due to gravity	$m{\cdot}s^{-2}$
C	Concentration	$mol{\cdot}m^{-3}$
C_D	Concentration (dissolved)	$mol{\cdot}m^{-3}$
D	Diffusion coefficient	$m^2{\cdot}s^{-1}$
d	Diameter	m
D_0	Unhindered active diffusion coefficient	-
D_a	Apparent diffusion coefficient	-
E^θ	Standard reduction electrode potential	V
F	Force	N
f	Friction factor	$N{\cdot}sec{\cdot}m^{-1}$

F_s	Drag force	N
F_B	Buoyancy force	N
$G''(\omega)$	Loss modulus	Nm^{-1}
$G'(\omega)$	Storage modulus	Nm^{-1}
$G^*(\omega)$	Complex shear modulus	Nm^{-1}
H	Partition coefficient	-
h	Thickness of capsule wall	m
J	Diffusion flux	$m^{-2}{\cdot}s^{-1}$
K	Partitioning coefficient	-
M	Molar concentration	$mol{\cdot}L^{-1}$
P	Permeability coefficient	-
p_L	Laplace pressure	Pa
R	Radius of curvature of droplet	m
r	Radius	m
S	Solubility (relative)	-
v	Linear velocity	$m{\cdot}sec^{-1}$
V_m	Molar volume	$m^3{\cdot}mol^{-1}$
v_S	Stokes velocity	$m{\cdot}sec^{-1}$

Contents

List of Figures

Chapter 1

Introduction

1.1 Scope of project

This project was originally designed to find a solution to increasing the longevity and preserve the volatile components in fragrance oils as directed by industrial sponsors. It would be desirable to create a perfume that would release some of the fragrance componants over time, so that the consumer is reminded of the 'true' smell of the perfume. Fragrances consist of a complex mixture of molecules with variable physicochemical properties such as solvent solubility, chemical reactivity and volatility. The controlled release of fragrances remains a challenge for industries as consumers are attracted to a perfume that provides a long lasting effect. The problem arises from the fact that fragrances are always comprised of some highly volatile species (the high/top notes in a perfume), which after application can often only be perceived for a short period of time.[100] The fragrance lifetime can also be limited due to loss by dissolution or degradation during storage. Due to the complexity of the fragrance, the components evaporate at different rates or dissolve to different degrees, which leads to a change in the overall fragrance over time. In particular the rapid loss of highly volatile molecules during storage and use has a great effect on the freshness and impact of the fragrance. Therefore, the consumer does not perceive them, which is of course undesirable.[205] Microencapsulation can provide protection of the fragrance, extended shelf life and offers a way of controlled release. Thus reminding the customers of what they are wearing 'in pulses' over a long period of time and enhancing their experience.

To make a perfume, fragrance oils are added to a mixture of alcohol and water. Generally perfumes use ethanol as the continuous phase, typically 95 -96% ethanol and 4-5% water. When the fragrance is placed in the hydroalcoholic solution an aging process begins. The fragrance materials can often react with the ethanol to form new compounds which is undesirable. For example, reactions between aldehydes and alcohol to form a hemiacetal commonly occur as solutions age.[99] Due to the small size of the ethanol molecule it is extremely challenging to keep fragrances encapsulated successfully. Mircocapsule systems traditionally used in industry are not suitable, hence why a new method has been developed here. The only likely option to provide a solution to this challenge is to encapsulate the fragrance oil using a capsule wall that can prevent the diffusion of very small molecules such as ethanol.

Though the primary focus was on the encapsulation of fragrance oils the research scope has broadened to encompass other potential applications. Microencapsulation of small chemical species on a more general level will be discussed as the challenges faced by the fine fragrance industry are applicable to other fields such as drugs, vitamins and flavour oils. For example, in the pharmaceutical industry targeted delivery at a specific site is desirable so that only the affected part of the body is exposed to the drug, therefore minimising potential side effects. These alternative applications have led to exploring other types of release mechanisms other than mechanical fracture.

1.2 Current challenge

Microencapsulation is a process in which solids, liquids or even gases may be enclosed by the formation of a shell wall around the core material. Microencapsulation of functional materials and chemically or biologically active ingredients is an area of interest due to its wide range of applications in a number of industries such as pharmaceuticals[179], cosmetics[110], home and personal care products, food and beverages[95], agrochemicals[244], textiles[177], printing[255], fragrances[165],[193], oil recovery[120], nanoreactors[136], functional coatings and paints, self-healing materials[227] and electronics.[211] For example, in the agrochemical industry biocides can be encapsulated to minimise evaporation, increase shelf life and control the

release of the active which may increase biological efficacy.[244] Microencapsulated eletrophoretic inks can be printed to form sheets of electronic paper and can reduce the sensitivity of the transistors to the environment (e.g. they were still able to perform when submerged in various solvents).[211] Microencapsulated healing agents can be embedded in composite polymer materials containing a catalyst capable of polymerising the healing agent which leads to bonding of the crack faces.[227] Microencapsulation is able to both improve and provide new functionalities for these products.

The main roles of encapsulation are to isolate the active material from its surroundings, act as a form of protection from exterior environments and provide a mechanism for controlled release. Encapsulation can increase the stability and life of the product. For example, active ingredients in the food and pharmaceutical industries can be protected from oxidation or moisture. Encapsulation can facilitate the manipulation of the product during processing. Liquid active components can be converted into a dry solid system and handling properties of sticky materials can be improved. Incompatible components can be separated, which can be beneficial to the food and beverage industries as loss of ingredients during processing can be reduced or avoided and reactive compounds can be separated.[141] Volatile compounds can be encapsulated to retard the release, such as fragrance oils which tend to evaporate quickly.[232] Pesticide formulations can be encapsulated to make it safer for applicators to mix and apply highly toxic materials.[257] Encapsulation can provide many added benefits to a product, however the process can be expensive so is only suitable for formulations where the overhead for the formulation is high, the material to be encapsulated is expensive or the safety of a product can be improved, e.g. encapsulation of some drugs can avoid damage to healthy tissue and therefore reduce unwanted side effects.

When successful active protection and retention within the designed capsule is obtained, the active release can be sustained over a period of time or triggered by an external stimuli such as change in pH, temperature, light intensity, pressure, chemical or biological environment, electrical or magnetic field etc.[74] Generally there are three different release mechanisms by which the core can be released; mechanical rupture of the shell wall, dissolution or melting and diffusion through the wall. Biodegradation and slow erosion of the shell are also

utilised.[70] The release mechanism depends on the nature of the application. For example, triggered release can be implemented by electric field release for delivering anti-corrosive materials only when a metallic surface is compromised and may be useful in battery materials which experience high voltages. Antiperspirant and deodorant materials can be released when they reach a target temperature, allowing the active to be delivered only when the person perspires.[74] The detergent industry utilises the dissolution of the shell wall of powder detergents to release enzymes which remove bloodstains from clothing.[16] Pesticides can be encapsulated to be released over time, so that application can be carried out less often rather than an initial highly concentrated and toxic application. The sustained release of fragrance molecules in a perfume is desirable in order to prolong the sensory experience and longevity of the perfume.[105] One important diffusion controlled application is novel clothing fabric, which contains chemical decontaminants encapsulated within semi-permeable polymers. The polymer is selectively permeable, allowing toxic chemicals to diffuse into the microcapsules where they undergo irreversible detoxifying chemical reactions.[50] Sustained release can be useful in pharmaceutics where it is desirable to release a drug in the body over and extended period of time to sustain therapeutic levels. Rapid adsorption of some drugs can be harmful, however the risk can be reduced by formulating the drug as sustained-release, where the adsorption will be slower.[7] It can be particularly difficult to combine sustained and triggered release, i.e. a capsule that prevents diffusion of the active and releases at a steady rate once triggered. For example, microcapsules which can release their payload at a particular location in the body once triggered, by either *in vivo* stimuli such as change in pH or the presence of certain chemicals or external stimuli, and then release steadily would be advantageous in drug delivery.

There are various physicochemical factors which affect the microcapsule stability and release. For example, molecular weight of the active agent has an impact on release; as the molecular size increases, the diffusion decreases exponentially. The functional moiety and surface charge of the active ingredient can play a role in reducing the rate of diffusion. Changing the ionic properties can result in a change of solubility of the active ingredients. Thermodynamic properties such as temperature, solubility, concentration, wettability and interfacial properties

can all affect microcapsule stability and release. As the concentration gradient between the inside of the microcapsule increases, compared to the outside surroundings, the rate of diffusion increases. Actives in a solubilised state can be expected to release faster than those in a dispersed state. The wettability of the active ingredient impacts the dissolution and subsequent release rate. Release will not occur if the aqueous media cannot wet the surface of the active ingredient. Wettability can be quantified by the hydrophilic-lipophilic balance (HLB), which relates to how wettable the active is with water. This is one of the parameters often considered during microcapsule design. Temperature is the most critical factor influencing the rate of release as diffusion is enhanced at higher temperatures. As a result, capsules stored at elevated temperatures tend to be less stable than those stored at room temperature or under refrigeration. Therefore the microcapsule materials, manufacturing process and storage conditions all must be considered when designing a microcapsule system.[88]

The rate controlling step for diffusion depends on the choice core material, morphology, physicochemical properties of the active and the shell material and the system in which the microcapsule is placed. Diffusion models are typically used and there are various kinetic release profiles to consider, however the release rates that are achievable from a single microcapsule are generally "zero order", "half order" and "first order". Zero order occurs in a core-shell system where the active ingredient (core) is a pure material and releases through a microcapsule as a pure material. The rate is independent of the concentration of the active ingredient and the amount released can be described as directionally proportional to time and release is slow. First order release occurs when the core is a solution. The concentration of the solute material in the solvent decreases as the solute material is released from the capsule. First order release is concentration dependant.[88],[166] Fickian diffusion models can be used to describe the diffusion rates of active ingredients permeating across a membrane. In the terms of one-dimensional spherical coordinated relating to a microsphere morphology, Fick's Law can be defined in Equation 1.1 as published by Gaonkar et al.[88];

$$J = \frac{1}{A} \cdot \frac{dC}{dt} = -D\frac{dC}{dr} \tag{1.1}$$

where J is the diffusion flux (the amount transferred per unit area per unit time or mass flow of the active under the assumption of steady state), C is the concentration outside of the microsphere, t is time, D is the diffusion coefficient, r is the radius of the microcapsule, and A is the surface area of the capsule. This equation is consistent only for an isotropic homogenous medium where the diffusion properties do not change in other spherical coordinates.

The diffusion rate from a microcapsule, dC/dt, across a capsule membrane can also be thought of empirically by considering Equation 1.2

$$\frac{dC}{dt} = A \cdot H \cdot D_a \cdot \frac{C_{in} - C_{ext}}{h} \tag{1.2}$$

where A is the exposed shell surface area, H is the partition coefficient, D_a is the apparent diffusion coefficient, C_{in} is the concentration inside the microcapsule, C_{ext} is the concentration outside of the microcapsule and h is the thickness of the capsule wall. In this case the apparent diffusion coefficient, D_a, can be defined by Equation 1.3

$$D_a = D_0 \frac{\varepsilon}{\tau} K \tag{1.3}$$

where D_0 is the unhindered active diffusion coefficient, ε is the shell porosity (cross sectional area available for diffusion), τ is the tortuosity (relative trajectory relative to end-to-end distance in the diffusive direction) and K is the system constant dependent on the ratio of active size to pore size. According to Equation 1.2, the diffusion rate can be greatly reduced by minimising the relative solubility of the dispersed phase within the continuous phase or reducing the diffusion coefficient. One of the prominent challenges of encapsulating small compounds arises from the fact that most microcapsule membranes no not provide a sufficient barrier against diffusion and current shell materials (polymeric/lipid based membranes/ particulate) have relatively high diffusion coefficients, D. Leaching of the encapsulated active ingredient may occur over time which is undesirable as premature release can cause side effects and waste the active ingredient. This is particularly prominent for small actives such as those found in drugs, vitamins, fragrance and flavour oils.

A large number of microcapsule synthesis methods exist, some of which will be reviewed in the next chapter. Most will result in a core-shell structure where the shell consists of a polymer film, which typically would result in short retention times when the capsules are dispersed in challenging environments. These challenging environments can range from high pH or surfactant concentration to continuous phases that can dissolve the active ingredient. As a result, efforts have been made to significantly decrease the diffusion of actives from the microcapsule shells using several methods. For example, increasing wall shell thickness can result in slowing down the release of the active but, this option often reduces the payload of the capsule core[188] (Figure 1.1). Furthermore, it can lead to enhanced specific interactions between the active and the microcapsule shell, which can later hinder full release of the active. Other methods of reducing diffusion such as annealing a layer of particles forming the wall of the microcapsules have been used. For example, Thompson et al.[235] showed that cross linked colloidosomes failed to retard dye release during tests due to interstitial pores between adjacent latex particles. The colloidosomes were internally crosslinked to provide stability to the colloidosomes. No improvement was observed when annealing was conducted in an attempt to close the pores. Some improvement was observed when the cross-linked colloidosomes were coated with a layer of polypyrrole, with thicker coating leading to slower release. These issues highlight that none of these methods provide a practical means of encapsulating small molecules over relevant time scales and shows a gap in existing literature and technology.

1.3 Approach to solution

Theoretically it would be desirable to synthesise a shell with low to no diffusion of the active. As discussed previously this is currently challenging as employing tactics such as increasing shell thickness are not feasible as several orders of magnitude of difference would need to be attained to accomplish this. This is only possible by altering diffusion coefficients and wetting properties of the shell.

Metal coated microcapsules are of particular interest as they can offer an improved barrier to diffusion. Additionally, there is potential opportunity to

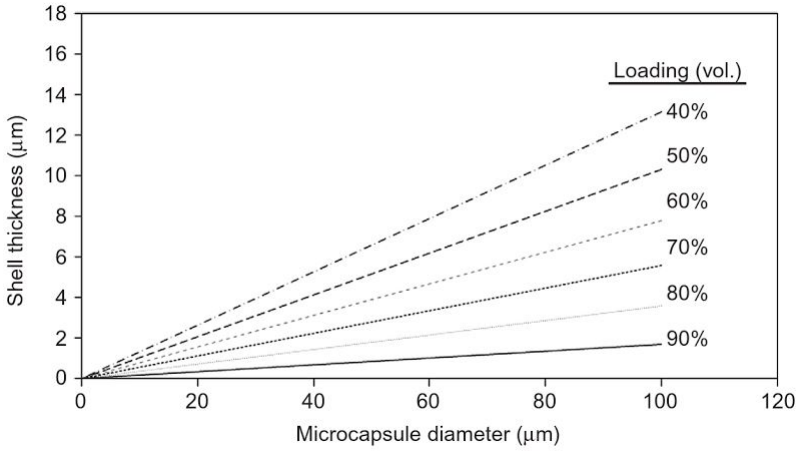

Figure 1.1: Payload comparison at a function of shell thickness[188]

exploit electrical, mechanical, optical and magnetic properties of the metallic shell for more capsule functionality. In particular metal shells can be remotely triggered to release their contents by methods such as ultrasound and IR irradiation. This offers potential for drug delivery methods in the pharmaceutical industry. Metal encapsulated compounds can have improved shelf life, especially those that are sensitive to water and oxygen. A continuous metal shell can also provide reduced diffusion of the core material compared to just a polymer shell and can prevent the escape of volatile encapsulated compounds.[191] These capabilities arise from the greatly improved barrier properties of metals as compared to those of polymers. The relatively rapid diffusion through polymers is governed by the size and shape of pores available. Free volume, due to gaps created by thermally induced chain segment rearrangement or inefficient packing of chains provides low resistance pathway for diffusing molecules.[253] Diffusion coefficients, as described by Ficks Law, for polymers are closer to those for liquids than those of solids, even in crystalline polymers. These coefficients vary strongly with concentration.

The rate of diffusion of gases through metals is reduced compared to that of polymers due to their crystalline structure and porosity.[204] Diffusion of gas molecules through metals only occurs via interstitial hopping, grain boundary diffusion or vacancy diffusion. Therefore, metal films are able to prevent the

permeation of small organic molecules.[191] Diffusion for solids, such as metals and crystals is much smaller than those of polymers (typically 10-40 orders of magnitude lower). In fact the values are so small that it is thought that all significant transport occurs through gaps and flaws in the solids, especially along grain boundaries. However thin film diffusion is difficult to understand due to problems arising with adapting the mathematics to the widely varying situations with different chemical and physical effects.[52] With the challenge of encapsulating small species in mind, a metal film provides a promising solution to our encapsulation needs.

Metallic encapsulation has successfully been demonstrated within the group[101] however the process uses a solvent evaporation method to form a polymeric capsule on which the metal film is deposited. This process involves emulsifying an oil phase containing a polymer, a volatile solvent and a non-volatile solvent. As the volatile solvent evaporates the polymer is forced to precipitate at the oil-water interface, creating a core shell structure. Various washing stages are involved which is time consuming and wasteful. Some of the steps in the process may be difficult to scale up. The solvent extraction method involves using a large proportion of volatile solvent within the core of the emulsion template, which drastically reduces the encapsulation template. This method has relatively low encapsulation efficiency, whereby encapsulation efficiency (EE) is defined as 'the percentage of core material incorporated into the microcapsules relative to the total amount of the core material added during encapsulation process'.[197] Indeed, the oil to be encapsulated is only present up to 15% and is limited to a number of oils and stabilisers due to restrictions in the methods as a result of complex wetting and solubility requirements. As shown in Figure 1.1 it is challenging to synthesise a polymer capsule that has a high loading volume, particularly at higher shell thickness which would be required to significantly reduce diffusion. Therefore a polymer shell on its own does not seem capable of preventing the release of small compounds efficiently. Even with the addition of a metallic film on a polymer capsule the payload of the capsule is limited, so alternative solutions have been explored.

1.4 This work

Here, a method where the metallic film is deposited directly onto an emulsion droplet, hence allowing for up to 100% EE if all the oil is emulsified (potentially corresponding to 100% of the active material depending on conditions) and eliminating waste solvent from the previous method is proposed. A metallic nanoparticle (NP) emulsifier is used as the catalyst for the growth of a secondary metallic film directly on the droplet interface via electroless deposition. The catalyst is localised at the emulsion interface allowing metallic growth to only occur on the droplet, so that only negligible growth occurs in the bulk. This work aims to simplify the previous fabrication process, demonstrate control over the method, demonstrate that full retention of the oil core is possible in challenging environments, such as mediums in which the core readily dissolves, and show the possibility for remote triggered release of the encapsulated active. This provides many benefits for potential future applications. Figure 1.2 details the stages of the fabrication process.

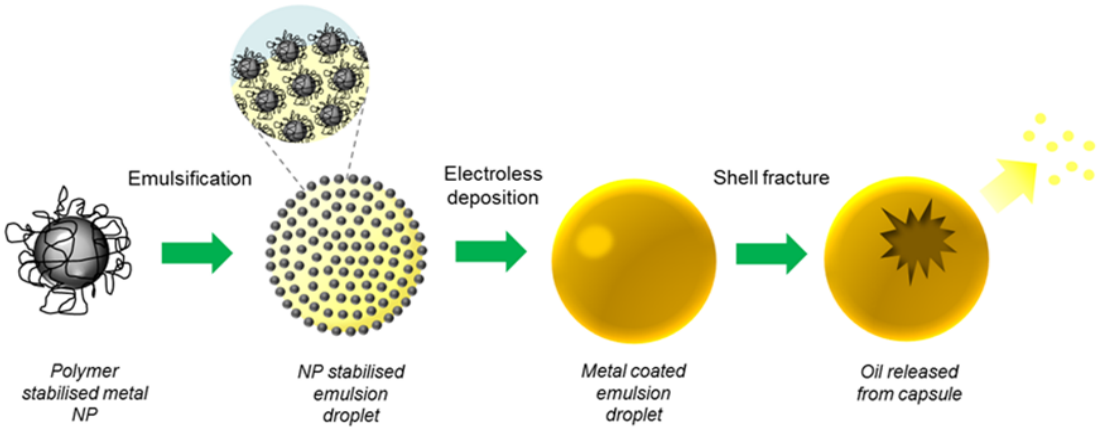

Figure 1.2: Schematic illustrating fabrication of metal capsules using metallic nanoparticle emulsifiers.

1.5 Thesis structure

Chapters 1-2 cover the introduction, background theory and literature review which sets the aims and objectives and the reasoning behind the approach taken. Chapter 3 describes the materials and methodology used to synthesise and characterise the nanoparticles, emulsions and capsules. Figure 1.2 summarises the steps involved in the formation of the capsules, which is covered in Chapters 4-7. Chapter 4 details the platinum nanoparticle synthesis, in particular the variables which effect their size and designing particles suitable for our application as both an emulsifier and catalyst. Chapter 5 investigates the viability of these particles acting as emulsifiers and their characterisation and the oil-water interface. Chapter 6 focusses on the emulsification step and optimising this for the subsequent step. Chapter 7 examines the secondary metal coating on the emulsion template via electroless deposition and how this coating can be optimised and controlled. Different release mechanisms for the encapsulated oil are also introduced. Finally Chapter 8 concludes the main findings and discusses potential future work that could be carried out.

Chapter 2

Background theory and review of the relevant literature

2.1 Synopsis

As proposed previously this project aims to improve the retention capability of microencapsulation systems for the controlled delivery of small actives by utilising a metallic shell on an emulsion template. This chapter will review the previous literature, which has led to the choice of encapsulation method in this work. It will examine the advantages and drawbacks associated with other methods, their suitability for the encapsulation of small actives and how the metallic encapsulation addresses challenges with current methods. Additionally it will look at the theory behind the properties that govern emulsion formation generally and the chosen encapsulation process.

2.2 Background theory

There is a wide variety of both physical and chemical routes to microencapsulation used both in industry and academia. The choice of appropriate encapsulation technique typically depends on the end use of the product and the processing conditions involved in making the product. For example, with some encapsulation techniques, the product can be designed to trigger the release of the active at a

certain point or for other applications sustained release is used where the payload is released slowly over time. The controlled release and environmental factors will impact the shelf life of the product which is an important consideration in industry.

This section will focus on the different ways in which capsules can be formed and the factors that affect and dictate their ability to encapsulate actives. Firstly, the section will focus on non-emulsion based methods, which are unlikely to lead to microcapsules with the ability to retain small molecules, however they are frequently used in industry. These methods often use high temperatures, limited materials can be used and the processes can be hard to control. Here the drawbacks of these methods and why they are not suitable for the intended purpose will be reviewed. Subsequently, the chapter will review in detail emulsion based methods and how such methods have been adapted and developed to retain small molecules.

2.2.1 Non-emulsion based methods of microcapsule production

2.2.1.1 Spray Drying

In the spray drying process the substance to be encapsulated is dispersed in a slurry, often referred to as the carrier material. This is followed by atomisation and spraying of the mixture into a hot chamber. The resulting microcapsules are then transported into a cyclone separator for recovery (Figure 2.1).

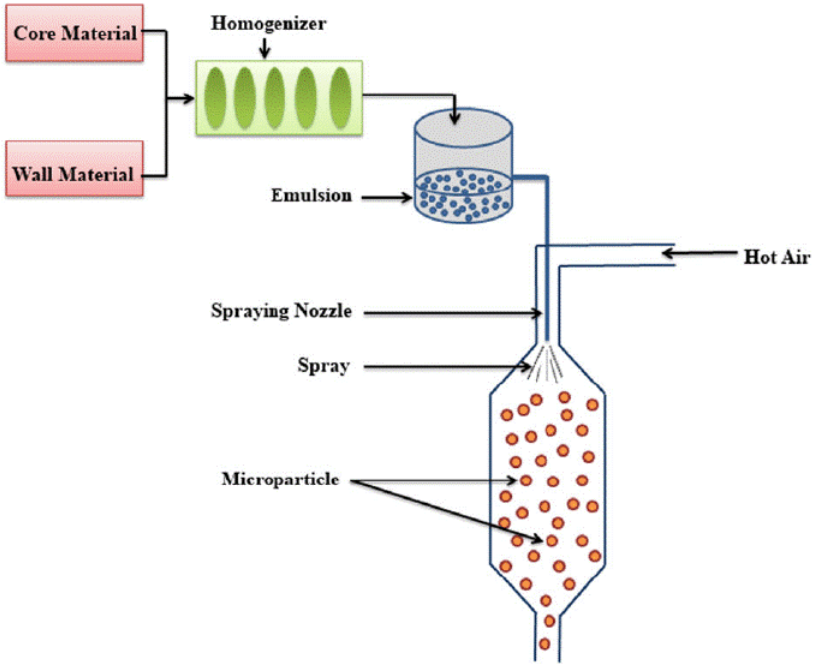

Figure 2.1: Schematic of spray drying process.[14]

The rate of evaporation and diffusion of the solute to the interior of the drying particles can result in different morphologies of the formed capsule (Figure 2.2).[43] Therefore the particles produced often have porous and irregular surface due to solvent evaporation. Another disadvantage with this method is that some low-boiling point aromatics can be lost and the intended core material can also be on the surface of the capsule, which could encourage oxidation (often anti-oxidants are added), greatly affect the release rates and affect the ability of retaining the active.[159],[254] Additionally the control of particle size and composition is difficult and results in a broad distribution of the particle properties, including dissolution and release rate. This is a result of differences in drying rates and the size of the droplets produced by the nozzles. The technique also produces a fine powder which needs further processing, such as agglomeration. However this method is suitable for applications where a narrow size distribution and heat sensitive materials are not required and the particles can be made on a large scale continuously at a low cost. Microencapsulation efficiencies can exceed 90%

in some cases. Microencapsulation efficiency can be increased by increasing the concentration of wall material which can be related to the formation of a shell around the core material.[14]

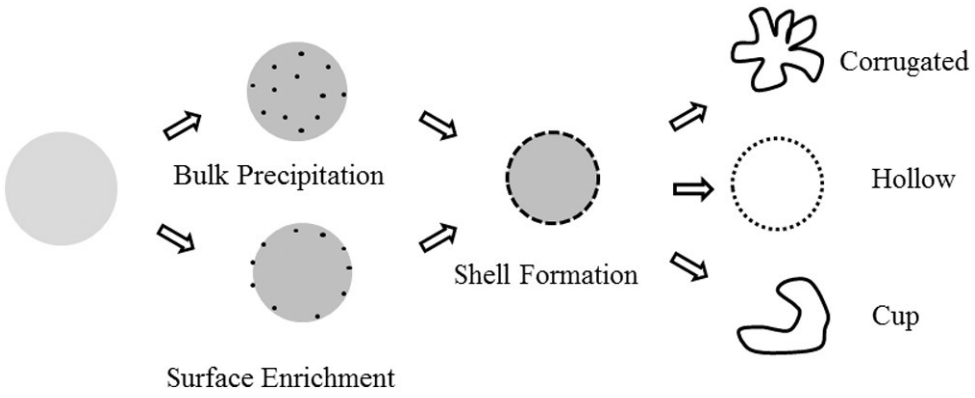

Figure 2.2: Schematic of particle formation via spray drying.[43]

2.2.1.2 Spray cooling/chilling

Spray cooling/chilling (Figure 2.3) offers an inexpensive method of encapsulation and is often used for the encapsulation of aroma compounds to convert liquid flavour into a powder, to improve heat stability and to delay release in a wet environment. It is a low-cost continuous process which is easy to scale up. These methods are similar to spray drying where the core material is dispersed in the liquid coating material and then atomised to disperse the droplets from the feedstock. The incorporation of the active into the carrier material is usually performed by either dissolving or mechanically dispersing the material. After the atomisation of the molten material, the droplets are immediately cooled and solidify into powder form.[95], [186] The particles produced by spray chilling are typically matrix type particles. The atomisation of the molten mixture and solidification process are considered to be critical steps and can greatly affect the resulting particles. For example, disintegration of the molten mixture into small particles can occur during the atomisation process and insufficient cooling can lead to agglomeration of droplets and/or adhesion of these droplets to the surface of the chamber, which in turn affects the morphology and other proper-

ties of the particles. The main limiting factors of the active loading are process limitations and barrier properties of the matrix. Higher solid loading in the melt feed increases the viscosity, which is a vital parameter in the successful operation of spray chilling to produce particles of a certain size. Loading levels of 20-30% are common, though higher loadings can be obtained using gels. However the disadvantage of higher loadings is a decrease in effectiveness of the barrier. All microspheres will have a small amount of active material at or near the surface and as loading increases the amount of matrix material protecting the active decreases. So often loading has to be reduced in order to achieve suitable protection.[90] Other drawbacks include, poor shelf life due to the possibility of the expulsion of the active from the matrix, limited choice in encapsulant due to temperatures used in processing, rapid cooling rates can lead to unstable crystallisation forms and hence lower barrier properties, capsules prepared from lipids are insoluble in water and the matrix structure obtained can lead to dispersion of the active so that it is not protected on the surface of the particle.[186]

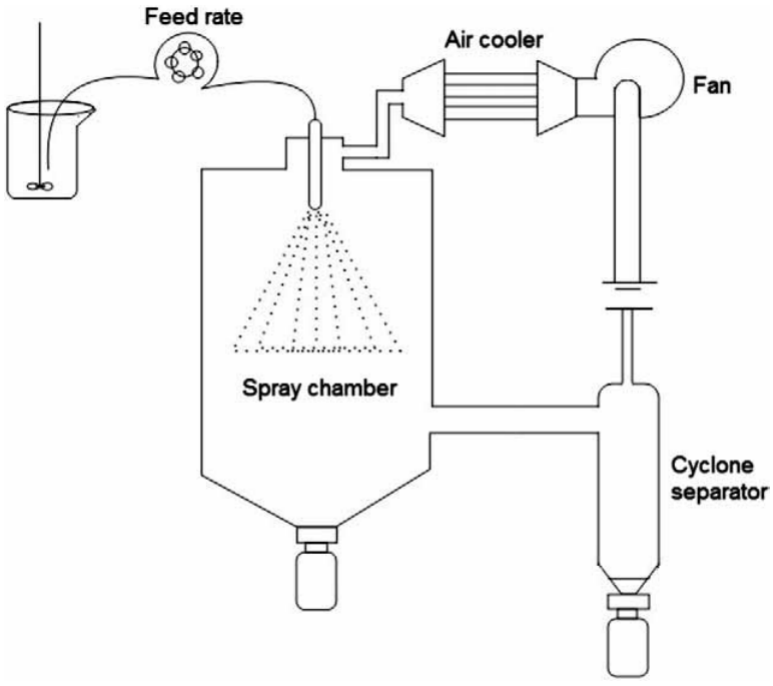

Figure 2.3: Schematic of spray chilling equipment.[186]

2.2.1.3 Fluid bed spray coating

Fluid bed spray coating consists of three steps. Initially the particles to be coated are fluidised in a coating chamber by suspending particles of the core material by an air stream under controlled temperature and humidity. Subsequently, the coating material is sprayed through a nozzle onto the particles where film formation is initiated. Then a series of wetting and drying stages occurs. Droplets of the sprayed liquids coalesce on the surface and the solvent or mixture is evaporated off in hot air, leaving the coating material adhered to the particle (Figure 2.4).[159]

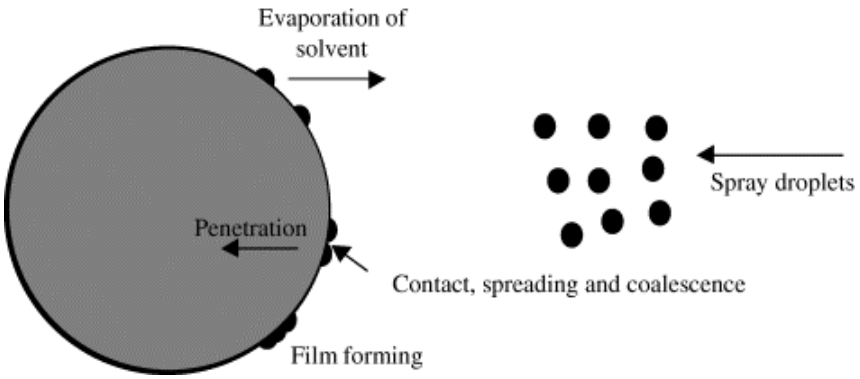

Figure 2.4: Schematic showing film formation during fluid bed coating process.[159]

There are various methods including top, bottom and tangential-spray fluid bed coaters, as shown in Figure 2.5. This technique offers the advantage of being able to mix, granulate and dry ingredients in the same vessel, which reduces the material handling and processing time. Additionally it is a low cost procedure. However thin coatings are hard to control, a post cure is often needed, the substrate must be heated above the plastic melting or fusion temperature and the surface finish may be uneven.[146]

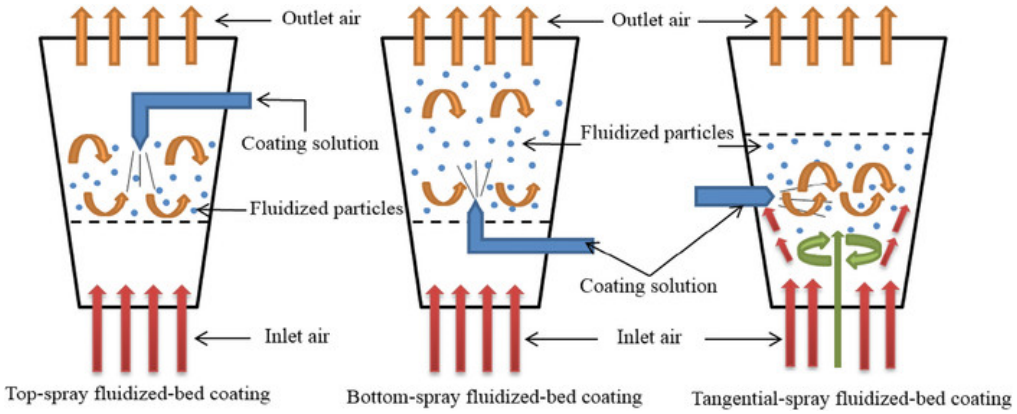

Figure 2.5: Schematic showing top, bottom and tangential-spray fluidised bed coating.[14]

2.2.1.4 Extrusion

Encapsulation by extrusion was first patented by Swisher and co-workers in 1957.[71] Simple extrusion involves the dispersion of a volatile compound in a matrix polymer at high temperatures. The mixture is then forced through a die and then plunged into a desiccant liquid which hardens the extruded mass and thereby traps the active substance. There are three main processes; (i) melt injection, (ii) melt-extrusion and (iii) centrifugal extrusion, as shown in Figure 2.6.

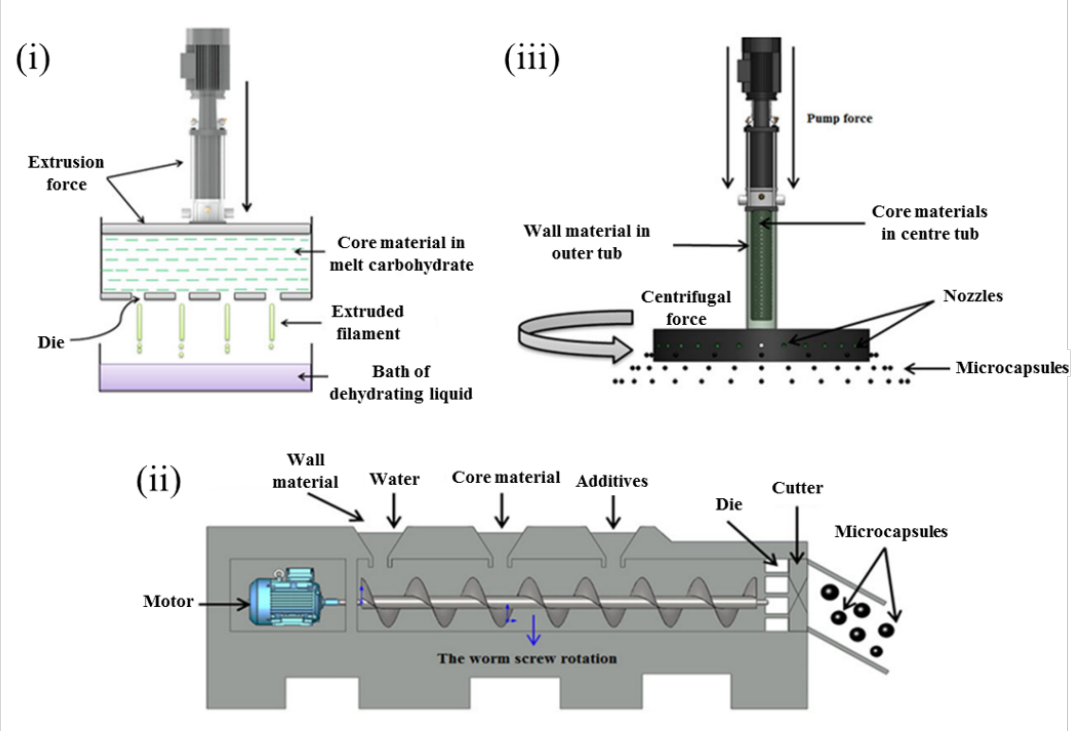

Figure 2.6: Schematic of (i) melt injection, (ii) melt extrusion and (iii) centrifugal extrusion process.[14]

The system is viewed as a dispersion of the oil phase in the form of small inclusions in the matrix. Different morphologies are attainable, as shown in Figure 2.7.

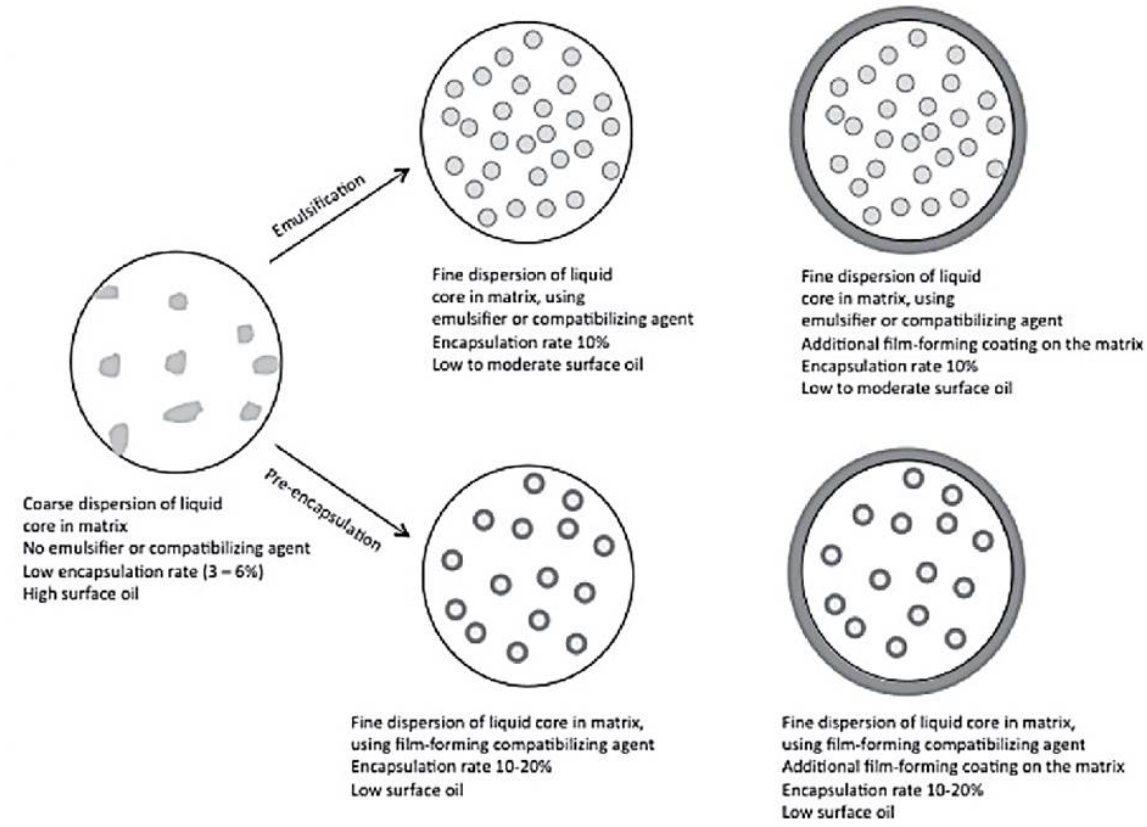

Figure 2.7: Schematic of possible encapsulation morphologies obtained using extrusion microencapsulation.[35]

This method offers the advantage of being stable against oxidation and has a prolonged shelf life compared to spray drying, though it is a more expensive process. The process also offers lower energy consumption during operation and minimal contaminated exhaust air compared to spray drying.[35] However diffusion of the encapsulated material through structural defects such as thin walls, cracks or pores formed during or after processing can be problematic.[159] Active loading is limited and does not usually exceed 15-20%, however higher loadings are possible. This technology typically produces fairly large capsules (typically 500 - 1000 μm, which can limit its applications, for example in the food industry where mouth feel is a crucial factor in encapsulated flavours. There is also a limited range shell materials available for extrusion encapsulation.[95]

2.2.1.5 Co-crystallisation

This technique offers an economical and flexible approach to microencapsulation as the method is relatively simple. A crystal structure, such as sucrose, is modified from a perfect crystal to a conglomerate. This produces a porous structure which can accept the addition of a second ingredient. The process involves the heating of the crystalline substance followed by a reduction in temperature in a low moisture environment.[159],[20] It is important to properly control the rates of nucleation, crystallisation and the thermal balance during the process. Aroma and flavouring compounds can be added at the time of spontaneous crystallisation. For example, Beristain et al.[20] were able to show that co-crystallisation offered similar volatile oil retention as spray drying and extrusion. The procedure is relatively simple and requires an inexpensive encapsulation medium.[113] The addition of an anti-oxidant is often required to retard oxidation during storage. This method is not widely commercially used as it is not economically feasible. Additionally the high temperatures required to maintain the supersaturated sucrose solution make this technique unsuitable for encapsulating heat sensitive materials such as probiotic bacteria.[132]

2.2.1.6 Layer-by-layer polyelectrolyte deposition

This technique utilises electrostatic attraction and complex formation between oppositely charged polyions to form a polyelectrolyte shell to encapsulate the core material, as illustrated in Figure 2.8. Initially, charged particles are placed in a dilute solution of oppositely charged polyelectrolytes. Electrostatic interactions provide the driving force for the polymer to adsorb and relax onto the particle surface, hence inverting its apparent charge. Excess polyelectrolyte is removed by subsequent cycles of centrifugation and washing. Deposition is then repeated with a polyelectrolyte solution of opposite charge and the process is repeated as many times as required to achieve the desired shell thickness. Finally the core is dissolved to attain a hollow core.[261] In some cases the polyelectrolyte shell is formed around a solid active, in order to reduce the dissolution of the active. For example, crystalline vitamins and insulin can be encapsulated in this way, and the dissolution of the shell can be triggered to deliver the active.[55] The

technique is more common with aqueous cores due to the electrostatic driving force. It is possible to encapsulate biological species due to the use of non-harsh solvents and the shells can be fabricated with controlled chemical and physical properties. Additionally different species can be incorporated into the shell, such as catalysts, giving them unique tailorable properties.[64] The disadvantage of this technique is the time consuming multiple deposition steps and the various cleaning stages involved, which makes this method unsuitable for industrial-scale manufacture. Moreover, there is also a high tendency for polyelectrolyte induced particle flocculation, therefore low particle concentrations are used which affects the production rate. The polyelectrolyte shells are able to maintain their shape, even after the removal of the template however the long term stability of the microcapsules are highly dependent on the surrounding medium.

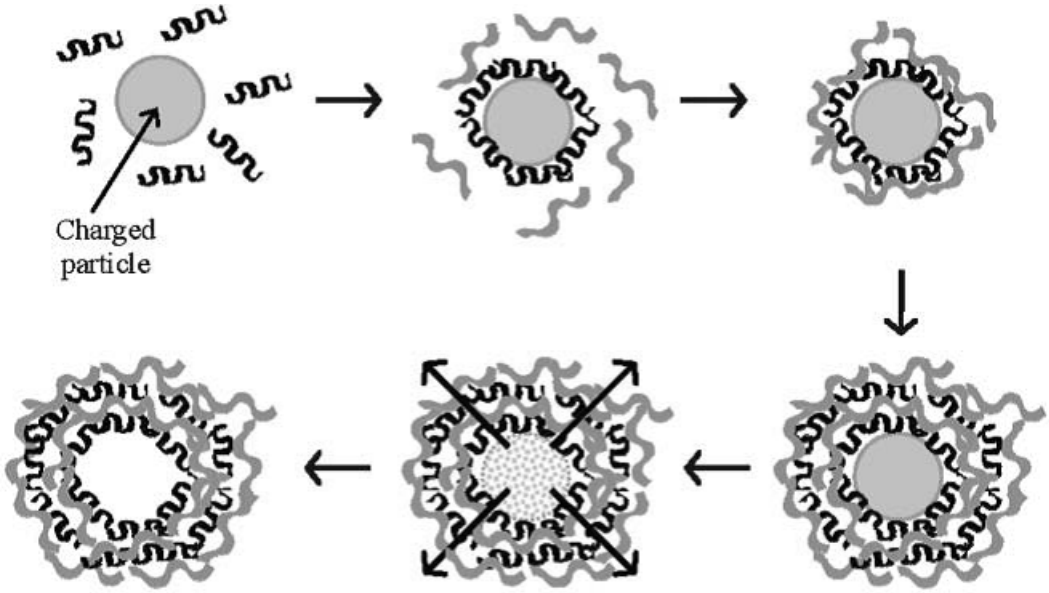

Figure 2.8: Schematic of layer-by-layer polyelectrolyte deposition.[261]

2.2.1.7 Copolymer and lipid vesicles

Copolymer vesicles, often referred to as polymersomes, are formed by the self-assembly of amphiphilic block copolymers around a core to form a thin molecular membrane (Figure 2.9). Similarly lipid vesicles are the result of the self-assembly of amphiphilic lipid molecules, such as phospholipids, with at least one

bi-layer and are known as liposomes.[130] The self-assembly is mainly driven by non-covalent interactions of the hydrophobic block, as they are normally formed in aqueous solutions. In general they can be prepared by methods such as film rehydration, double emulsion, direct injection, electroformation or dissolution.[98], [152], [215] , [62] Polymersomes and liposomes can be generated in sizes ranging from tens of nm to μm. The size is influenced by parameters such as amphiphilicity of the polymers and the preparation method used to self-assemble the polymersomes. Polymersomes offer potential as capsules for cosmetics, nutrients and drugs. Polymersomes and liopsomes are often used in biomedical applications due to their biocompatibility, biodegradability, and can help to reduce the toxicity of encapsulated drugs. Liposomes offer the flexibility to couple with site specific ligands for active targeting. However they often have low solubility, a short half-life, oxidation and hydrolysis-like reactions can occur and suffer from leakage and fusion of encapsulated molecules. Additionally production cost is high. Polymersomes are generally more robust than liposomes, and this can be further enhanced by crosslinking. Despite their simple synthesis, the formed microcapsules are typically polydisperse and coexist with other ordered structures. However they can be formed in microcapillary devices, which enables the formation of uniform capsules with high encapsulation efficiencies and control over particle size and architecture. The number of vesicles formed is limited by the droplet frequency of the device. Another drawback of polymersomes is the slow release due to the robust and stable nature of the bilayer membrane.[265], [2], [261]

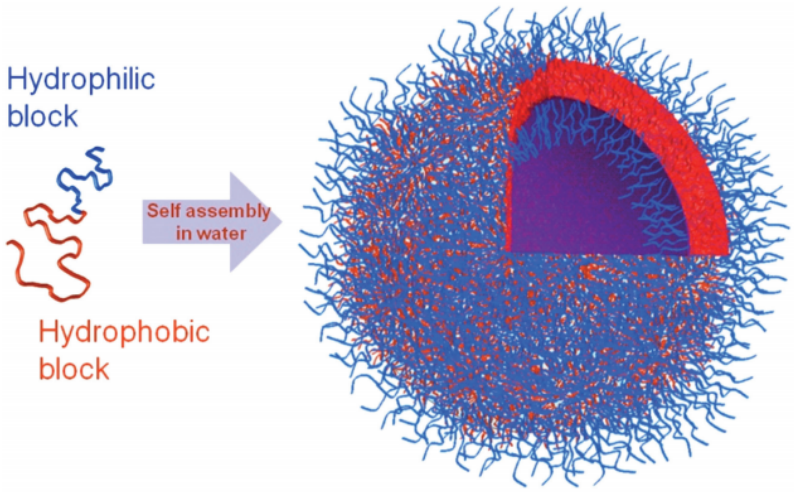

Figure 2.9: Schematic of a polymersome.[150]

2.2.2 Emulsion based methods of microcapsule production

The chapter will now focus on emulsion based techniques and their potential for encapsulating small actives. First the theory behind emulsion formation and stability will be briefly reviewed as the characteristics of the emulsion plays a significant role in the subsequent mechanism used for encapsulating the core.

2.2.2.1 Emulsion formation

To form an emulsion, generally an oil phase, a water phase, an emulsifier and energy are needed. The composition of the system and the manufacturing route have implications on the characteristics of the resulting emulsion; in particular they control the emulsion droplet size distribution and the emulsion type (oil-in-water or water-in-oil). The latter, is primarily determined by the behaviour of the emulsifier at the oil-water interface and its concentration, and the volume fraction between the two immiscible phases.[228] The energy required to expand the interface, $\triangle A\gamma$ (where $\triangle A$ is the increase in interfacial area when the bulk oil with area A_1 produces a large number of droplets with area A_2 ; $A_2 \gg A_1$, and γ is the interfacial tension) must be considered. As γ is positive, the energy

required to expand the interface is large and positive. The energy term cannot be compensated by small entropy of dispersion, T△S (also positive) and the total free energy of formation of an emulsion △G is positive (given by Equation 2.1, from the second law or thermodynamics)

$$\triangle\ G^{form} = \triangle\ A\gamma_{12} - T\ \triangle\ S^{conf} \tag{2.1}$$

Therefore emulsion formation is nonspontaneous and energy is required to produce the droplets. The system is thermodynamically unstable and in the absence of a stabilisation mechanism, the emulsion will break up.[228] These destabilisation processes will be discussed later in the chapter.

The emulsification process is very complex and involves multiple processes occurring at the same time, typically on different scales. Energy input can occur at different frequencies depending on the source of the energy input. For example, for shear processes, such as high speed stirrers, the process is slower than for cavitation driven processes, such as ultrasonication. The adsorption of the emulsifier can have different frequencies depending on their type and associated diffusion. Generally higher energy is required for the formation of smaller droplets. The energy required to form a droplet can be understood from the consideration of the Laplace pressure, p_L, which is defined as the difference in pressure inside and outside of a droplet and is given by Equation 2.2

$$p_L = \gamma(\frac{1}{R_1} + \frac{1}{R_2}) \tag{2.2}$$

where γ is the interfacial tension between the oil and water phase and R_1 and R_2 are the principle radii of curvature of the droplet. For a spherical drop $R_1 = R_2 = d/2$, where d is the diameter. In order for droplet break up to occur, it must be strongly deformed which requires external stress to be applied. This implies a large pressure gradient and hence and increase in p_L.[248] The stress needed to deform a drop is higher for a small drop. The stress can be due to a pressure difference (chaotic motion of the liquid or due to a velocity gradient (shear stress)). In general, stress is submitted to the surrounding liquid by agitation. Higher stresses need more vigorous agitation and therefore more energy.

If the interfacial tension is low, due to the addition of a suitable surfactant, the Laplace pressure will be lower and thus emulsification will require less energy.

The type of emulsion formed (w/o or o/w) is determined by the type of emulsifying agent used, the concentration of emulsifying agent, the ratio of the constituent immiscible liquids and the temperature. In particular the temperature affects the miscibility of the emulsifier into both phases and its behaviour at the interface. Another important factor when determining the type of emulsion is Bancrofts rule[15] which states that the phase in which an emulsifier is more soluble typically constitutes the continuous phase of the produced emulsion. Therefore water soluble emulsifiers tend to give oil in water emulsions and oil soluble emulsifiers preferentially form water in oil emulsions.

2.2.2.2 Methods of emulsification

A number of different homogenisation devices can be employed to produce emulsions. Consideration needs to be taken for both scientific requirements and practical engineering limitations. On a fundamental level the desired droplet size, physicochemical properties and type of starting materials must be considered. From an engineering point of view the method will be dependent on the scale of production, the equipment available and the costs involved with purchasing and running the equipment. Several procedures with a variety of energy inputs can be considered ranging from simple pipe flow (low agitation energy), static mixers and general stirrers (low to medium energy), high speed mixers (medium energy), colloid mills and high pressure homogenisers (high energy) and ultrasound generators (medium to high). The methods can also be batch-wise or continuous.

2.2.2.2.1 Comminution methods of emulsification involve the disruption of a large volume into smaller units, which requires sufficient energy to cause one phase to break into droplets dispersed in the second phase. In most comminution methods turbulent flow is involved. In all comminution methods, droplet re-coalescence is occurring as well as break up. Comminution can be performed by a variety of methods ranging in energy input. Some common types of homogenisation devices are discussed below.

1. **Static mixers** consist of motionless structured inserts called elements placed in cylindrical pipes. Complex flow is induced by redistributing fluids in the directions transverse to the main flow. This process has advantages such as being able to work continuously, have no moving parts, small space requirements, little or no maintenance, enhanced heat transfer and low power requirements. However this method is less suitable for creating fine emulsions, blending liquids of widely different viscosities and has high pressure drops. Additionally selection of static mixers is also difficult due to the limited information on their performance in open literature.[51], [234]

2. **High speed blenders** are commonly employed to directly homogenise oil and aqueous phases. The liquid phases are placed in a suitable vessel, for which the scale of production dictates their size, and are then sheared at high speeds (typically 20-2000 rev min^{-1}) using a rotor stator. The rapid rotation of the blade results in a velocity gradient which consequently disrupts the interface between the water and oil phases, causing large droplets to break up into smaller ones. The droplet size tends to decrease with increased time or rotation speed of the stirrer, until a lower limit is achieved. This is dependent on the concentration and nature of the starting materials used. This method is useful for emulsions with low or intermediate viscosities. In general, droplets produced using this method are in the size range of about 2 to 10 μm in diameter.[163], [3]

3. **Colloid mills** reduce the size of a coarse emulsion rather than homogenising two separate phases. In this case, the coarse emulsion is fed into the homogeniser and flows through a narrow gap between two disks.[219] Colloid mills are more suitable than most other types of homogenisation for emulsifying intermediate or high viscosity fluids and typically produce emulsion with droplet diameters between 1 and 5 μm.[3], [163].

4. **High pressure valve homogenisers** are commonly used in industry to produce fine emulsions. Similarly to colloid mills, they are more effective at reducing the droplet size of an existing emulsion than creating a primary emulsion. The coarse emulsion is pulled into a chamber by a pump on

its back stroke and then forced through a narrow valve at the end of the chamber on its forward stroke.[189] Smaller droplets can be produced by decreasing the size of the orifices and therefore increasing the pressure. However the throughput is reduced and more energy is required. This method is suitable for a wide range of materials ranging from low viscosity to viscoelastic pastes and can produce droplets with diameters as small as 0.1 μm.[3]

5. **Ultrasonic homogenisers** utilise high intensity ultrasonic waves to generate pressure gradient and shear to disrupt the droplets. A two-step mechanism has been proposed for the emulsification via ultrasound. Firstly, a combination of instabilities and interfacial waves leads to the disruption of dispersed phase droplets into the continuous phase. This is followed by the breaking of these droplets through cavitation near the interface.[160] Liquid jet generator and piezoelectric transducers are most commonly used to create high-intensity ultrasonic waves.[222] The technique can either operate as batch or continuously by pumping the suspension through a flow cell. Ultrasonic transducers are more commonly used in benchtop scale in a laboratory and are ideal for preparing small volumes (few millimetres to few hundred millimetres). Ultrasonic jet homogenisers are used mainly for industrial applications, where a stream of fluid is made to impinge on a sharp edge blade, which causes rapid vibrations of the blade. This generates an intense ultrasonic field which breaks up the droplets in its immediate vicinity. This device offers the advantages of being capable of continuous production, generation of small droplets and is more energy efficient than high-pressure valve homogenisers (less energy is needed to create a droplet of the same size).[3] It has been established that ultrasound is very effective in producing fine emulsions and nano-emulsions, though it may have an effect on biochemical properties of both dispersed and continuous phases[51]. On a small scale ultrasonication may be a valid cheaper alternative to high pressure homogenisers; however industrial applications are limited by scale up issues concerning sonicator devices and treatment chambers.

2.2.2.2.2 Microengineering techniques have been developed for the production of droplets individually. Unlike traditional bulk homogenization methods, drop-by-drop emulsification results in droplets being formed by bringing into contact at least two or more immiscible liquids. At least one of these liquids is injected through a micro-channel or pore so that droplets are formed as they exit the channel/pore.[228]

1. **Microfluidisation** brings together the oil and aqueous phase at high velocity, causing the mixing of the liquids and the disruption of the droplets. This method allows the production of very small emulsion droplets (<0.1μm) by recirculating the emulsion through the microfluidiser a number of times.[225] Microfluidisation produces emulsions with narrow droplet size distributions and can be used to make nano emulsions. Additionally lower emulsifier concentrations are often required. However this method can be unfavourable in some circumstances such as higher pressures and longer emulsification times. As a result of the high turbulence intensity in many cases re-coalescence of newly formed droplets is inevitable, so careful optimisation of factors such as emulsifier type and concentration is necessary.[115] Operation of a microfluidiser is not as convenient as some other techniques as there is no easy way to establish whether the interaction chamber is contaminated or deteriorated. Additionally scale up is not straight forward and may involve much more expensive equipment.[158]

2. **Membrane emulsification** forms an emulsion by forcing of an immiscible liquid into another through a microporous membrane which contains pores of uniform sizes. This technique can be employed as either a batch or a continuous process. The technique is highly energy efficient as less energy is lost due to viscous dissipation. Droplets sizes between 0.3 and 10s of microns can be produced in this way. Similarly to microfluidic techniques emulsions can be created with uniformly sized droplets of a controlled size, shape and internal morphology. One of the main limiting factors with regards to industrial scale up for membrane emulsification is the low level of dispersed phase flux through the membrane, especially for small droplets, which results in low productivity. At higher fluxes, the average droplet size

and distribution tend to increase due to increased droplet coalescence at the membrane surface.[39] There is a strong dependence of emulsion uniformity on viscosity of the dispersed phase and on size distribution of the membrane pores, so often premixing is required to overcome these issues.[216] Additionally many process parameters such as membrane type, pore size and porosity, transmembrane pressure and crossflow velocity must be considered for successful emulsification.

The methods reviewed here have advantages and disadvantages for different applications and material requirements as discussed above. The choice of emulsification method is dependent on various factors including the desired droplet size, volume to be emulsified, nature of the sample, energy requirements, equipment available and desired throughput. Here the focus will be on lab scale batch production as a starting point, though this is not to say that the process could be scaled up at a later point and even a different method of emulsification used, as for the commercial viability scale up needs to be possible. For fundamental studies, often small volumes are used. There are scaled down versions of industrial homogenisers that can be used on a laboratory scale and ultrasonic piezoelectric transducers also only require small sample volumes so would be suitable. Small sample volumes are also desirable when the materials used are expensive or limited in availability. When monodispersity is important, membrane emulsification offers a suitable method. To create an emulsion with small droplets colloid mills, high pressure valve, ultrasonic or microfluidisation homogenisers can be utilised depending on the viscosity of the liquids.

2.2.2.3 Emulsion stability

The stability of an emulsion is paramount to the shelf life of emulsion-based products. Emulsions are inherently thermodynamically unstable systems, which will inevitably lead to complete break-down of the emulsion into two separate phases. This breakdown occurs via various physical processes as illustrated in Figure 2.10 and include sedimentation, creaming, flocculation, coalescence, Ostwald ripening (disproportionation) and phase inversion.[228], [201]

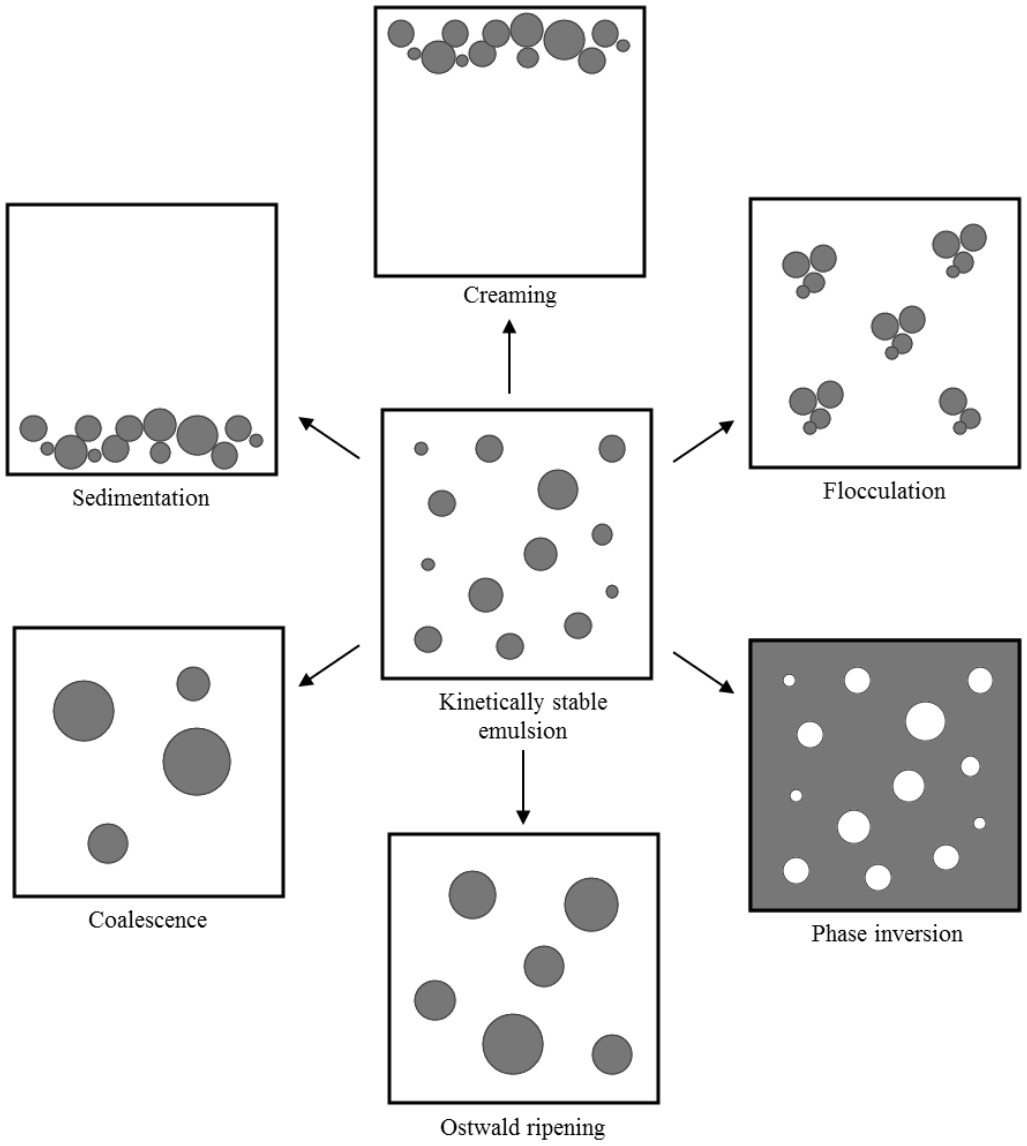

Figure 2.10: Emulsion destabilisation processes.

2.2.2.3.1 Creaming and sedimentation occur due to differences in density between the emulsion droplets and the continuous phase that surrounds them. In the creaming process, buoyant emulsion droplets rise to the top of the container. In sedimentation, the droplets sink to the bottom. These phenomenon do not

directly lead to phase separation, rather the emulsion separates into two, one of which is richer in the dispersed phase. They can often act as a precursor to coalescence. Sedimentation and creaming result from external gravitational or centrifugal forces. When such forces exceed the thermal energy of the droplets responsible for Brownian motion, a concentration gradient builds up, where larger droplets move to the top (if their density is less than that of the medium) or to the bottom (if their density is more than that of the medium) of the container.[228] According to Archimedes, the buoyancy force F_B acting on a submerged sphere can be defined by Equation 2.3

$$F_B = \frac{1}{6} a \pi d^3 (\rho_D - \rho_C) \tag{2.3}$$

where ρ_D is the density of the droplet phase, ρ_C is the density of the continuous phase, a is the acceleration of the sphere (due to gravity or centrifugation) and d is the diameter of the sphere. If $\rho_D - \rho_C = \Delta\rho \neq 0$ the droplet will move through the liquid and will experience a drag force, F_S. According to Stokes this can be defined as Equation 2.4

$$F_S = fv = 3\pi d \eta_C v \tag{2.4}$$

where f is the friction factor, η is the dynamic viscosity and v is the linear velocity of the droplet. If both forces are equal and opposite the system will be at equilibrium and Stokes velocity, v_s, can be given as Equation 2.5

$$v_S = \frac{F_B}{f} = \frac{a \Delta\rho d^2}{18 \eta_C} \tag{2.5}$$

This equation is based on many assumptions about the droplet, the continuous phase and how they interact. For example, for the equation to be valid the droplets should be perfect, homogenous spheres, the interface of the droplet should be immobile, Brownian motion should not disturb sedimentation, there should be no disturbance due to convection currents, the sedimenting droplets should be surrounded by a volume of continuous phase very much larger than the droplet and there should be no colloidal interactions. However, in a real system droplets are likely be affected by other droplets in the system. Further complications arise from accounting for the size distribution of the droplets.[17] Creaming

and sedimentation can be prevented in various ways such as matching the density of oil and aqueous phase, reduction of droplet size and use of thickeners.

2.2.2.3.2 Flocculation is a process of contact and adhesion whereby dispersed particles form larger sized clusters. It is a result of van der Waals attractions when the repulsive interactions between approaching droplet surfaces are not large enough to keep the droplets apart. Flocculation may be strong or weak depending on the attractive forces involved. The presence of some additives, such as surfactants or polysaccharides can induce flocculation in emulsion systems.[11], [59] However flocculation can be reduced with the addition of additives that stabilise the emulsion. To overcome the van der Walls attractions emulsions can be stabilised by electrostatic stabilisation using ionic surfactants. This results in the formation of an electric double layer that induces repulsive energy that overcomes the attractive forces. However emulsions stabilised in this way become flocculated at intermediate electrolyte concentrations. Alternatively steric stabilisation can be employed, whereby non-ionic surfactants or polymers are adsorbed to the interface. For example, if two droplets are provided with a layer of protruding molecular chains and come into close approach, there will be a strong steric repulsion between the droplets.[228] The use of emulsifiers will be discussed further later in this chapter.

2.2.2.3.3 Coalescence occurs when droplets collide with each other and form a larger droplet, therefore the average droplet size increases over time. Coalescence is driven by the thinning and disruption of the liquid film between the two approaching droplets. The liquid film between the droplets undergoes fluctuations when they approach each other closely. These fluctuations are due to the interfacial tension or surfactant concentration gradient across the thin film. When the film thickness reaches a critical value it ruptures resulting in its collapse. The Laplace pressure differences then cause the droplets to rapidly fuse into one droplet. The limiting case for coalescence is the complete separation into layers of the two liquid phases. The coalescence process usually follows flocculation.[262] To produce a stable film and therefore prevent coalescence a combination of two mechanisms can be utilised: (i) increasing repulsion (both electrostatic and

steric) and (ii) dampening of the fluctuations by enhancing the Gibbs elasticity. Several methods can be applied to achieve these effects such as the use of mixed surfactant films and formation of lamellar liquid crystalline phases at the oil-water interface.[228]

2.2.2.3.4 Ostwald ripening is the phenomenon in which small particles/ droplets in solution dissolve and redeposit on larger particles/droplets by molecular diffusion across the intervening continuous phase and occurs when the dispersed phase is partially soluble in the continuous phase. It is a thermodynamically driven process which occurs because larger droplets are more energetically favourable than smaller droplets due to the fact that molecules on the surface of a particle are energetically less stable than the interior molecules. Large particles have a lower surface to volume ratio and thus a lower energy state. The driving force of Ostwald ripening is the difference in Laplace pressure (pressure inside the droplet) between large and small droplets. The Laplace pressure, Π, for a droplet with radius of curvature r can be defined in Equation 2.6[36];

$$\Pi = \frac{2\gamma}{r} \tag{2.6}$$

Droplet stability increases with size due to a decrease in Laplace pressure, and therefore solubility. In smaller droplets the Laplace pressure difference is higher, forcing the oil phase out of the small droplets to add on to larger ones.

Small emulsion droplets have larger solubility than large emulsion droplets due to a decrease in radius of curvature. This leads to the disappearance of the smaller droplets into the bulk and the redeposition of their constituent molecules onto larger droplets leading to a shift of the size distribution to larger values.[228] Equation 2.7 shows how the solubility of the material in a spherical droplet increases as the size of the droplet decreases (which is related to the radius of curvature)[163]:

$$S(r) = S(\infty)exp\left(\frac{2\gamma V_m}{RTr}\right) \tag{2.7}$$

where $S(r)$ is the solubility of the solute when contained in a spherical droplet of radius r, $S(\infty)$ is the solubility of the solute in the continuous phase for a

droplet with infinite curvature (a planar interface), V_m is the molar volume of the solute, γ is the interfacial tension, R is the gas constant and T is the absolute temperature. There is a higher concentration of solubilised material around a small droplet compared to a larger droplet. Due to this concentration gradient the solubilised molecules therefore move from the smaller droplets to the larger droplets.

2.2.2.3.5 Phase inversion occurs when there is an exchange between the dispersed phase and the continuous phase. For example, with change of time or conditions, an o/w emulsion may change to a w/o emulsion or vice versa. Often, during phase inversion, the emulsion passes through a transition state where multiple emulsions are produced.

2.2.2.4 Emulsifiers

An emulsifying agent can provide kinetic stability via two mechanisms; by lowering the interfacial tension and by providing stability against coalescence. When water and oil are mixed they separate into two layers, as this represents the most thermodynamically stable state. This layer position minimises the contact area between the two phases and minimises their free energy. In order to create an emulsion, energy is required to be input to the system. The efficiency of disruption of the emulsion droplets is dependent on the oil-water interfacial tension. Droplet break up is facilitated when the interfacial tension is low. The presence of an emulsifier may help to decrease interfacial tension and hence minimise the effects of interfacial forces. By adsorbing to the oil-water interface, the emulsifier is able to act as a shield between the water and oil molecules. The unfavourable direct contact between the oil and water molecules is replaced by interactions between the polar segments of the emulsifier and the water molecules and the non-polar segments of the emulsifier and the oil. Additionally, emulsifier molecules tend to have both polar and non-polar segments, which when dispersed in the bulk water some of the non-polar regions come into contact with the water. This is energetically unfavourable due to the hydrophobic effect. By adsorbing to the interface, these unfavourable interactions are minimised, whilst increasing the number of favourable interactions between polar segments and water. The

emulsifier may also form a protective layer around the droplets and prevent coalescence.[145], [163] Surfactants, particles and polymers are often used as emulsifiers. The nature of the emulsifier is crucial to the formation of the emulsion and its long-term stability.

There are a variety of types of emulsifiers, with the simplest being an ion such as OH^-, which can be adsorbed to the droplet surface and thus create a charge. The electrical double layer produced provides a route to repulsive interactions in the system that may compensate the attractive van der Waals forces.[228]

Surfactants (surface active agents) are often more effective as they are able to stabilise both o/w and w/o against flocculation and coagulation. Surfactants have a characteristic molecular structure consisting of a lyophilic part, which has an affinity for the solvent and a lyophobic group, which is poorly soluble in the solvent (Figure 2.11). These can be classified depending on the nature of the head group and can be anionic, cationic, zwitterionic or non-ionic. The head of an ionic surfactant has a net charge. Anionic surfactants, such as alkylbenzene and alkyl sulfates, have a negative charge. Cationic surfactants, such as quaternary ammonium alkyl salts, bare a positive charge. Zwitterionic surfactants contain both positive and negative charges; examples include long chain amino acids and sulfobetaine. Non-ionic surfactants include polyoxyethlenated alkylphenols, polyoxyethlenated alcohols and monoglycerides of long chain fatty acids and have no ionic charge.[213]

Surfactant mixtures, such as ionic and non-ionic, can often be more effective in emulsification and stabilisation of the emulsion as they can create conditions where a tighter surfactant packing at the interface is achieved. Non-ionic polymers, often referred to as polymeric surfactants, are effective emulsion stabilisers but require a high amount of energy to produce small droplets. Polyelectrolytes such as polymethacrylic acid can also be employed as emulsifiers. Mixtures of surfactants and polymers are often used to achieve optimal stabilisation.[228]

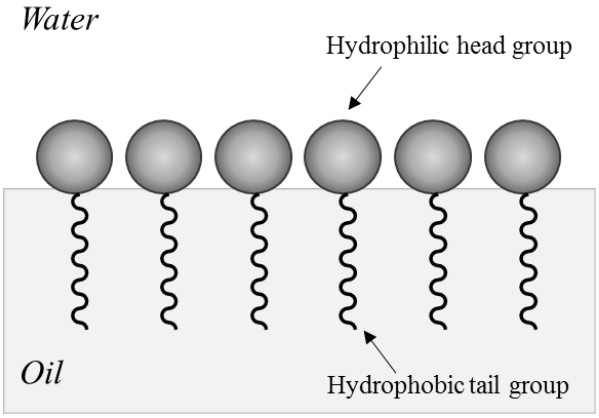

Figure 2.11: Schematic illustrating the conformation of surfactants at the oil-water interface.

2.2.2.4.1 Polymer Emulsifiers Polymeric surfactants offer a great degree of flexibility and diverse functionality. To effectively provide steric stabilisation a polymeric emulsifier must have particular physicochemical properties. It must have some segments that bind strongly to the droplet interface and other segments (strong enough to prevent the emulsifier from desorbing from the droplet surface as the droplets approach each other) which protrude into the surrounding liquid to prevent the droplets coming too close together. Therefore, for an oil and water system, the polymer must be amphiphilic, with both hydrophobic and hydrophilic segments to meet this criterion. Secondly, the continuous phase for the dispersed droplet must be a good solvent for the protruding segment of the polymer so that the mixing contribution to the overall interaction energy is repulsive. The repulsive polymeric interactions must act over a distance that is comparable (or preferably larger) to the range of attractive van der Waals forces. Additionally, there must be a sufficiently high concentration of polymer on the surface. If there is an insufficient concentration of polymer then one polymer segment may adsorb to more than one droplet, causing bridging between emulsion droplets which leads to flocculation, and subsequently coalescence. Hydrophobic interactions can also arise from some of the non-polar regions being exposed to the aqueous phase. Many polymeric stabilisers are charged, so are able to stabilise emulsion droplets

both sterically and electrostatically.[163], [47]

2.2.2.4.2 Pickering Emulsifiers Solid particles adsorbed at the interface (See Figure 2.12) between the two phases can be used as emulsifiers and are referred to as Pickering emulsifiers, named after S.U. Pickering who described the phenomenon in 1907. The particles are partially wetted by the oil phase and partially by the water phase.[198] Once sufficiently packed at the oil-water interfaces, they provide approaching droplets with a steric (physical) barrier to coalescence. In general the particles have a preference for one of the two liquids, and this wettability can often determine the type of emulsion. The interface bends in the direction of the more poorly wetting liquid as a result of the particles assembling at the oil-water interface thereby enabling emulsification.

The size of the resulting droplets can be limited by the size of the stabilising particles. Solid particles in the nano-size range (or sub-micron, $\sim$ 100 nm) allow the stabilisation of droplets down to a few micrometers in diameter, though larger droplets can also be stabilised. Micron size particles can stabilise larger droplets, possibly up to a few millimetres. Adsorption is strongest, and in most instances stability is highest, when the contact angle in 90°. Larger particles have a larger surface area in contact with the interface, hence have a larger absorption free energy. However, even small nanoparticles (at the lower limit of the range) have an adsorption energy in high excess in relation to thermal energy. There is no lower limit of particle size according to theory.[46] Colloidal particles, and in particular nanoparticles can add functionality at the interface which can lead to a wider range of applications.[22]

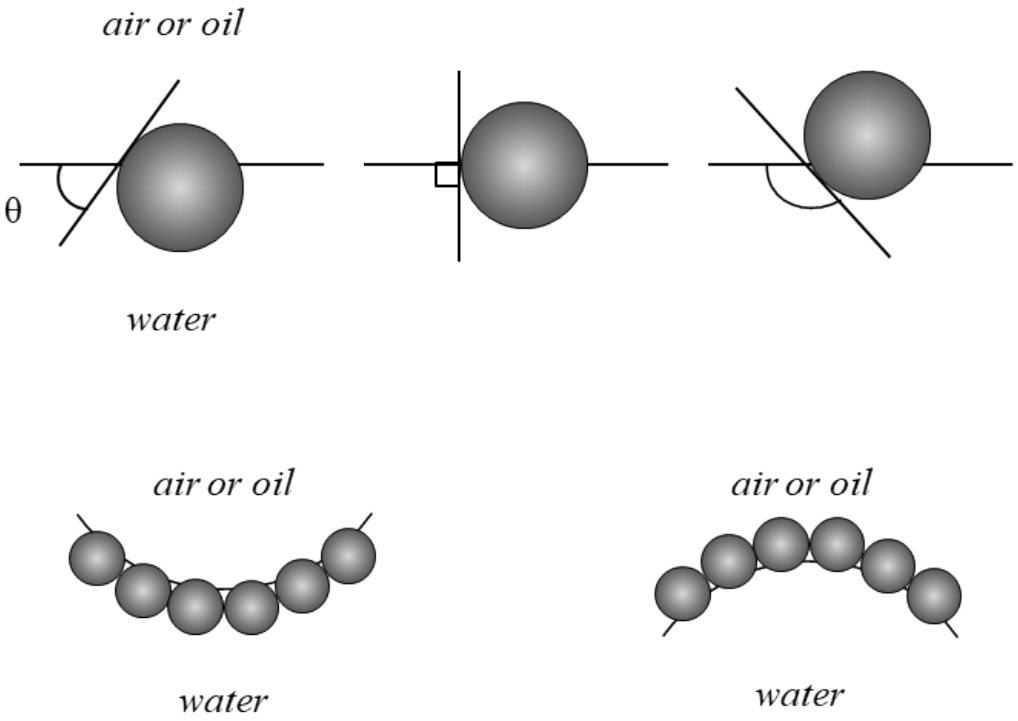

Figure 2.12: (Top) Position of a small spherical particle at a planar fluid-water interface for a contact angle; less than 90° (left), equal to 90° (centre) and greater than 90 (right). (Bottom) Position of particles at a curved fluid-water interface: for $\theta < 90°$, oil-in-water emulsions may form (left), for $\theta > 90°$ water-in-oil emulsions are preferred (right). Adapted from Binks et al.[24].

2.2.2.5 Existing encapsulation techniques based on emulsification

2.2.2.6 Colloidosomes

Colloidal particles can stabilise emulsions by arranging themselves at the interface of the two immiscible liquids. The colloidal particles on the resulting Pickering emulsions can be joined together to form porous microcapsules termed colloidosomes.[61] A typical fabrication process can be seen in Figure 2.13.

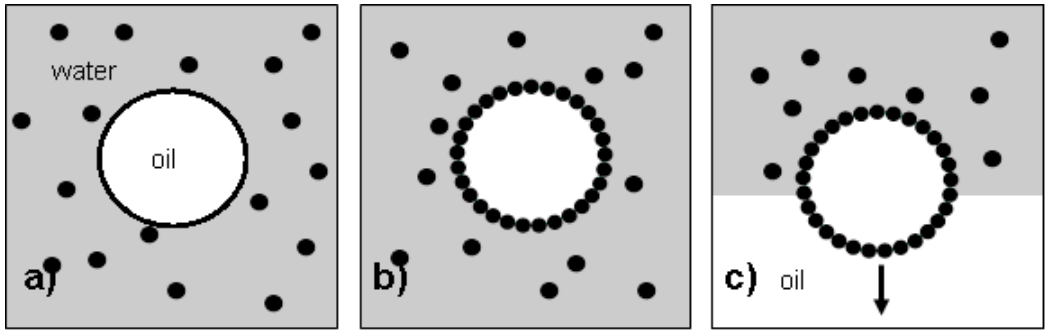

Figure 2.13: Schematic illustration of self-assembly formation of colloidosomes. a) Oil is added to aqueous solution containing colloidal particles. Oil droplets are formed by shearing for several seconds. b) Particles adsorb to surface of oil droplets to reduce the total surface energy. The particles are then locked together to form an elastic shell. c) The droplet is transferred to oil by centrifugation. The same approach can be applied to encapsulate a water droplet in an exterior oil phase.[61]

The method was originally reported by Velev et al.[245] in 1996 but was not coined until six years later by Dinsmore et al.[61] Cayre et al.[37], Noble et al.[180] and Duan et al.[69] employed a gel trapping technique to create colloidosomes with a solid-like core as a result of gelling the aqueous sub-phase and the formation of a particle monolayer at the interface. This technique provided better support for the shell and improved structural integrity for the colloidosomes to survive their transfer into the aqueous phase. Permeability and rupture stress can be controlled through particle size and postproduction treatments, such as sintering or the deposition of a further layer of particles/polymer. Colloidosomes that can break down in response to external stimuli such as stress, pH and temperature can also be fabricated. This allows controlled release of the colloidosomes contents.[124] Although this method has many advantages, a further shell stabilisation stage is required to produce a robust structure. This is often done by heating the dispersion above/close to the glass temperature of the polymer/particles forming the shell to lock them together and form a continuous shell. Alternatively, coagulants or the adsorption of polymers can be used to lock the shell once stabilised.[261]

Additionally there is the risk of incomplete shell formation, which can lead to core contamination and/or leakages.

2.2.2.7 Polymer precipitation by phase separation

Hollow microsphere microcapsules can also be formed by phase separation and precipitation of a polymer. There are two different approaches to microcapsules formed in this way; (i) polymerisation induced phase separation and (ii) solvent extraction and evaporation.[261]

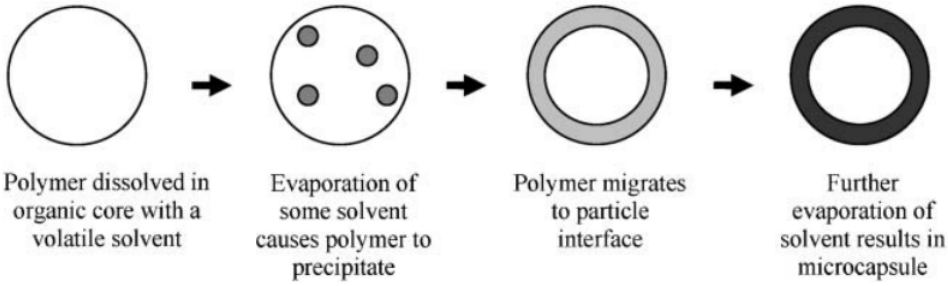

Figure 2.14: Schematic of steps involved in solvent extraction and evaporation[261] (adapted by Loxley and Vincent[154]).

1. In polymerisation induced phase separation a monomer is dissolved in precursor emulsion droplets. After initiation of the polymerisation reaction, the propagating polymer chains become immiscible within the dispersed phase leading to precipitation at the interface and shell formation. This most commonly occurs in a system using an oil core and an aqueous continuous phase.

2. In the solvent extraction method, an oil-in-water emulsion is used as a precursor to the microcapsules. The oil phase comprises a shell forming polymer, a volatile good solvent and a non-volatile poor solvent. As the good solvent evaporates, the polymer is forced to precipitate and forms small droplets of polymer rich liquid within the emulsion droplets. Under

suitable conditions these droplets migrate to the surface and encapsulate the droplet, forming a shell (Figure 2.14).

Though capsules with relatively thick shells and narrow size distributions can be obtained there are many disadvantages associated with the method including the use of an organic solvent is required, the right wetting conditions are critical for capsule formation and there is less than 100% release of active ingredients. It can be difficult to remove all of the organic solvent during evaporation so there is often residual solvent in the capsules. Additionally it has been seen that thin polymer shells can be hard to obtain using this method.

2.2.2.8 Coacervation

Coacervation was patented by the National Cash Register in the 1950s for carbonless paper and is often regarded as the original method of encapsulation. The method relies on the separation from solution of colloidal particles which then agglomerate into a separate liquid phase called coacervate.[159] The process consists of three steps; (i) the formation of three immiscible phases (a liquid phase, a core material phase and a coating material phase), (ii) deposition of the liquid polymer coating on the core material and (iii) solidification of the coating material.[179] In general the core material used must be insoluble (or scarcely soluble) in the coacervation medium and compatible with the polymer[159]. Simple coacervation involves the use of only one polymer with the addition of a strongly hydrophilic agent to the colloidal solution; whereas complex coacervation involves two or more types of polymer.[159] Figure 5 shows an example using gelatine and gum Arabic.

Limitations of this method include evaporation of volatiles, oxidation of the product due to residual core materials often adsorbing onto the exterior of the capsule wall and dissolution of the active compound into the processing solvent.

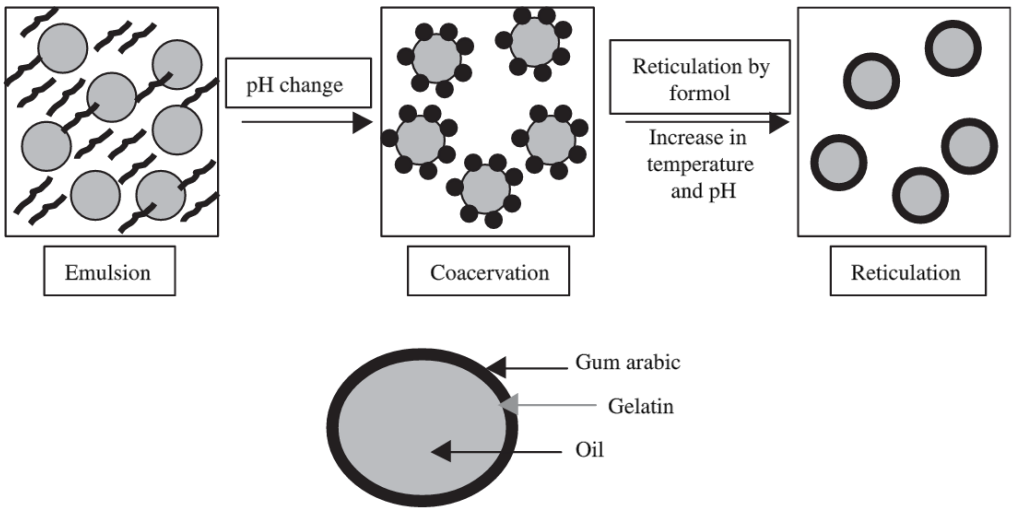

Figure 2.15: Principle of the complex coacervation method: Coacervation consists of the separation from solution of colloid particles which then accumulate in a separate liquid phase.[159]

2.2.2.9 Polycondensation interfacial polymerisation

This technique, shown in Figure 2.16, involves dissolving a monomer and initiator in two incompatible phases. Subsequent emulsification of these phases allows these components to meet at the interface, where they react to form a shell. The reaction rate decreases as diffusion of the monomer to the interface becomes restricted by the growing polymer shell. Both oil-in-water and water-in-oil microcapsules can be formed using this method.[261] This method offers a simple fabrication process and ease of control over final shell thickness; however shell formation is diffusion controlled and hence slow.[218], [205]

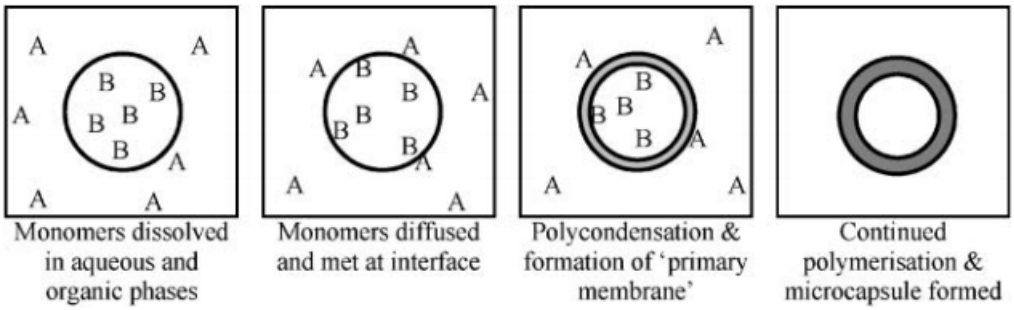

Figure 2.16: Illustration of polycondensation formation of shells around emulsion droplets.[30]

Though these methods are suitable for many applications they have drawbacks which make them less ideal for the encapsulation of small chemical species. This is illustrated in Table 2.1. As mentioned before side reactions, incomplete shell formation, limited formulation parameters and use of solvents make these methods undesirable. This highlights the gap in the current technology and the requirement for a new method to meet the needs of encapsulating small compounds. The next section will look at reviewing in more detail the challenges and possible solutions to the problem.

2.3 Literature Review

2.3.1 Challenges with current methods

Though many of these, and other methods are used for encapsulation in industry, few are suitable for encapsulating small actives as there are drawbacks associated with many of the aforementioned techniques such as harsh processing conditions, loss of active ingredients while processing and unwanted side reactions. In some methods, such as spray drying, the processing conditions such as heating make it an unsuitable procedure for the encapsulation of small species such as vitamins, drugs, and flavour and fragrance oils. Drawbacks of methods such as polycondensation, interfacial polymerisation and coacervation include a large degree of

Table 2.1: Pros and cons of different emulsion based encapsulation methods

Method	**Pros**	**Cons**
Colloidosomes	Permeability and rupture stress can be controlled. Can break down in response to external stimuli.	Further shell stabilisation required to produce robust. structure. Risk of incomplete shell formation. Pinhole defects are always present.
Polymer precipitation by phase separation	Thick shells and relatively narrow size distributions can be obtained.	Organic solvents (often chlorinated) required. Correct wetting conditions are critical. Less than 100% release of actives. Difficult to remove all of the organic solvent during evaporation. Thin shells hard to obtain.
Coacervation	Simple, low cost process. Does not require high temperatures.	Evaporation of volatiles. Oxidation of product can often occur. Dissolution of active compound in processing solvent possible. Only occurs within limited pH ranges, colloid concentrations and/or electrolyte concentrations.
Polycondensation interfacial polymerisation	Simple fabrication process. Control over final shell thickness. o/w and w/o microcapsules can be formed.	Shell formation is diffusion controlled and hence slow. Risk of monomer hydrolysis.

partitioning of fragrance components between the core of the capsule and aqueous phases during membrane formation and upon further processing or storage. This can lead to the loss of highly volatile molecules and water-soluble species can alter the character of a fragrance profile. The partial solubility of many essential oils leads to instability by interfacial reactions due to change in hydrolytic stability during the polymerisation reaction. Additionally reactive species such as aldehydes can take part in the polymerisation by side reactions with monomers and can be partially lost. This can also lead to alteration of the encapsulated product. To avoid such problems harmful phenol-formaldehydes are often used. A small amount of monomer will always remain in the droplets and may cause odour or toxicity problems.[218], [205] Other methods, such as layer-by-layer construction of a polyelectrolyte shell, contain many steps and are time consuming, and hence are not suitable for large scale production.

Most methods reviewed above produce capsules, which in the conditions mentioned will be unable to retain their core material efficiently. Attempts have been made to reduce permeability of the shells. For example Dowding et al. showed that an increase in the thickness of polymer capsule retards the release of 4-nitroanisole, however after 20 hours over 60% was still released (Figure 2.17).[66] They prepared the capsules via polymer phase separation and were able to control the thickness by altering the mass of polymer dissolved in the oil. They also found that crosslinking the polymer shell after formation reduced the release rate. There were other factors in the capsule formation method which influenced the release rate such as the rate at which the volatile solvent was removed, as this effected crack size.

Thompson et al. showed that cross linked colloidosomes failed to retard dye release during tests due to interstitial pores between adjacent hydroxyl-functionalised sterically stabilised latex particles. No improvement was observed when annealing was conducted in an attempt to close the pores (Figure 2.18[235]). They also coated the cross-linked colloidosomes with a thin layer of polypyrole which showed significant improvement with regards to release however none of these methods were able to retain the dye over relatively long time scales and offers more potential for retaining larger actives.

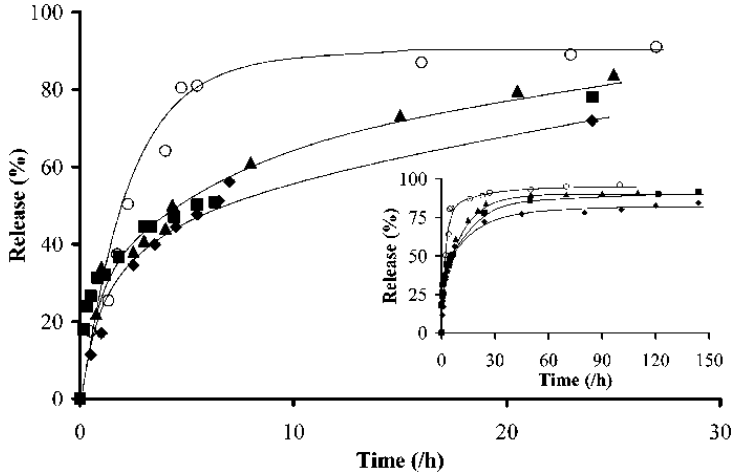

Figure 2.17: Effect of variation in the mass (grams) of polystyrene present, and hence the shell thickness, on the release profile of 4-nitroanisole: (◯) 1.75 g; (▲) 3.8 g; (■) 5 g; (♦) 8 g. The lines are drawn to guide the eye. The inset shows the release of 4-nitroanisole over a longer time scale (up to 150 h).[66]

Zieringer et al. demonstrated that a high percentage of aqueous cargo could be retained in perfluoropolyether (PFPE)-based microcapsules for over 25 days (Figure 2.19 a)) which were synthesised using a double emulsion template via microfluidic fabrication. The contents of the capsules could be released via osmotic stress. When encapsulating Nile Red, an organic dye, in different solvent the PFPE membranes were found to be more permeable (Figure 2.19 b). However the double emulsion microfluidic fabrication utilised has a low production rate rendering it unsuitable for many applications.[269] Lee et al. also exploited a combination of bulk and microfluidic emulsification to encapsulate a fragrance in a polymeric shell at a fairly high efficiency, however after 5 days over 50% was released. They were able to exhibit control over microcapsule size and shell properties such as crosslinking density, polarity and thickness.[133]

Shi and Caruso encapsulated a fluorescent probe, pyrene, in polyelectrolyte multilayer capsules. Though increasing the number of polyelectrolyte layers retarded release, after 300 minutes 100% of the active was lost (Figure 2.20).[223] Further control over the permeability of the capsules was introduced by a pre-layer being deposited onto the microcrystals. The layer-by-layer deposition method can

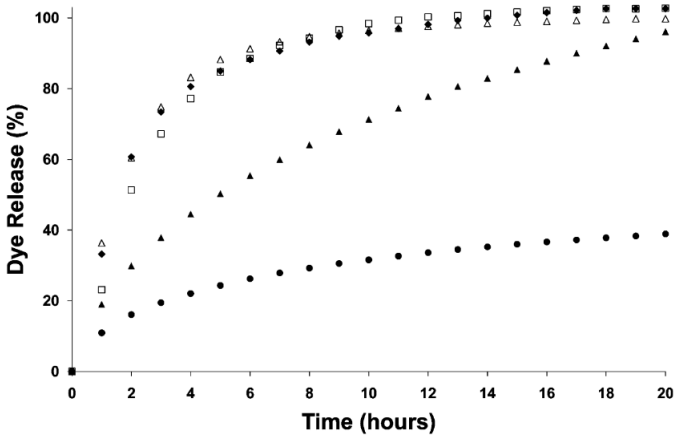

Figure 2.18: Release curves obtained at pH 9 for fluorescein dye diffusing from: sunflower oil control (closed diamonds), uncoated cross-linked colloidosomes prepared with 1188 nm PGMA50-PS particles (open squares), cyclohexane annealed colloidosomes (4:1 n-dodecane/cyclohexane oil phase, open triangles), cross-linked colloidosomes after coating with 0.66 wt % polypyrrole (closed triangles) and cross-linked colloidosomes after coating with 1.32 wt % polypyrrole (closed circles).[235]

often be time consuming. These issues highlight that none of these methods are entirely suitable for the encapsulation of small molecules and shows a gap in existing literature and technology.

One of the most challenging requirements of this work relates to the application for the intended microcapsules. These capsules are to be used in high-end perfume products, in which the continuous phase is typically composed of 70% ethanol. This means that a successful retention of the perfume oils within the capsule cores over the shelf life of these products will involve stopping i) penetration of ethanol through the formed capsule membrane, ii) release of the fragrance oils (that are very soluble in ethanol) in the continuous phase and iii) control the mechanical strength of the capsules to enable shear-driven breakage of the capsule shells and release of the perfume oils.

The sustained release of the active from the the microcapsule is determined by its ability to diffuse through the shell. Release can also occur by erosion of

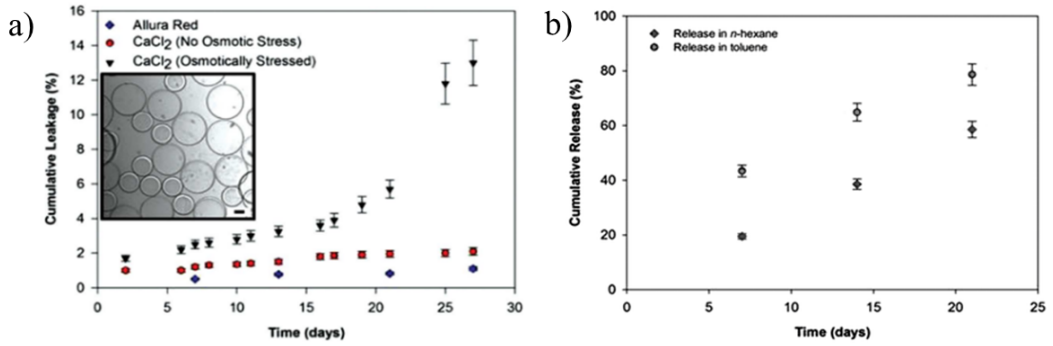

Figure 2.19: a) Graph showing the leakage of encapsulated model compounds in water. Percentage of Allura Red leaked over four weeks (blue diamonds). Percentage of $CaCl_2$ ions leaked as a function of time for capsules under osmotic stress (black triangles) and capsules under no imposed osmotic tensile stress (red circles). Inset: Optical image of mixed population of microcapsules either under osmotic stress (large capsules) or ruptured (small capsules) at t = 25 days; scale bar = 100 μm; b) Graph showing cumulative release of low MW hydrophobic cargo molecules over three weeks. Percentage of Nile Red released in toluene and in hexane.[269]

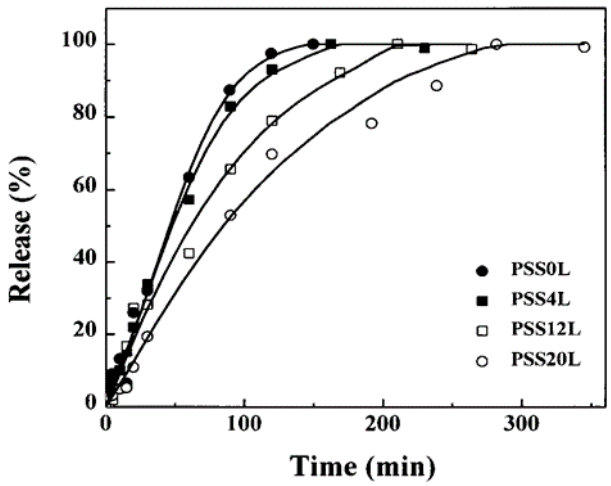

Figure 2.20: PYR release-time profiles for microcrystals coated with a different number of polyelectrolyte multilayers. The solvent used was 100% ethanol.

the shell wall. The permeation of the active through this barrier is dependent on both kinetic and thermodynamic parameters. The mass rate of permeation (dM/dt) of an active through a capsule wall can be describes by Fick's law under sink conditions (Equation 2.8);

$$\frac{dM}{dt} = \frac{DKAC_D}{h} \tag{2.8}$$

where D is the diffusion coefficient of the active, K is the partitioning coefficient of the active between the shell and the capsule core, A is the surface area, C_D is the concentration (if dissolved) or solubility (if solid) of the active inside the capsule and h is the thickness of the capsule wall.

In order to compare various systems, the permeability coefficient, P is often used as it is independent of the concentration, C_D, and the surface area. For a polymer shell permeability is described in Equation 2.9;

$$P = \frac{DK}{h} \tag{2.9}$$

Asides from any degradation, diffusion governs the release process of an active from a microcapsule.[10] Therefore the shell wall material is particularly important when it comes to retarding diffusion. Diffusion coefficients for polymers are orders of magnitude higher than those of metals as the diffusion coefficient for polymers is closer to those of liquids, even for crystalline polymers.[52] The majority of capsules are polymer based and due to the diffusion constraints in current systems a sufficient barrier is required. Metallic encapsulation can offer a suitable barrier.

2.3.2 Metallic encapsulation

As discussed previously the encapsulation of small species over relevant time scales requires an appropriate physical barrier to limit diffusion. Metal coated microcapsules are of particular interest as they can offer improved protection. Additionally, there is potential opportunity to exploit electrical, mechanical, optical and magnetic properties of the metallic shell for more capsule functionality. Metal encapsulated compounds can have improved shelf life, especially those that are sensitive to water and oxygen. A continuous metal shell can also provide reduced diffusion of the core material compared to just a polymer shell and can prevent

the escape of volatile encapsulated compounds.[191] These capabilities arise from the greatly improved barrier properties of metals compared to polymers.[204] The diffusion of actives through polymers is governed by the size and shape of pores available. Free volume, due to gaps created by thermally induced chain segment rearrangement or inefficient packing of chains provides low resistance pathway for diffusing molecules.[253] Whereas diffusion of gas molecules through metals only occurs via interstitial hopping, grain boundary diffusion or vacancy diffusion. Therefore, metal films are able to prevent the permeation of small organic molecules.[191] Diffusion coefficients, as described by Ficks Law, for polymers are closer to those for liquids than those of solids, even in crystalline polymers. These coefficients vary strongly with concentration. Diffusion for other solids is much smaller. In fact the values are so small that it is thought that all significant transport occurs through gaps and flaws in the solids, especially along grain boundaries. This is especially applicable to metals and crystals. However thin film diffusion is difficult to understand due to problems arising with adapting the mathematics to the widely varying situations with different chemical and physical effects.[52] Metallic coating of colloidal objects has been previously shown; however these are mostly applied to solid objects and they often involve complex methods.

Metallic encapsulation has successfully been demonstrated within the group[101] however the process uses a solvent evaporation method to form a polymeric capsule on which the metal film is deposited via electroless deposition. This process involves emulsifying an oil phase containing a polymer, a volatile solvent and a non-volatile solvent. As the volatile solvent evaporates the polymer is forced to precipitate at the oil-water interface, creating a core shell structure (Figure 2.21). Various washing stages are involved which as time consuming and wasteful. Often harmful solvent such as dichloromethane (DCM) are used. DCM is a harmful chemical so adequate ventilation is required, which can be expensive. This technique tends to start with an oil phase mixture where the oil to be encapsulated is only present up to 15% and is limited to a number of oils and stabilisers due to limiting wetting characteristics. It involves several steps, some of which may be difficult to scale up. Using an emulsion template offers a solution to some of these problems as the metallic film is deposited directly onto an emulsion droplet,

hence allowing 100% of the emulsion core (potentially corresponding to 100% of the active material depending on conditions) to be encapsulated and eliminates waste solvent from the previous method.

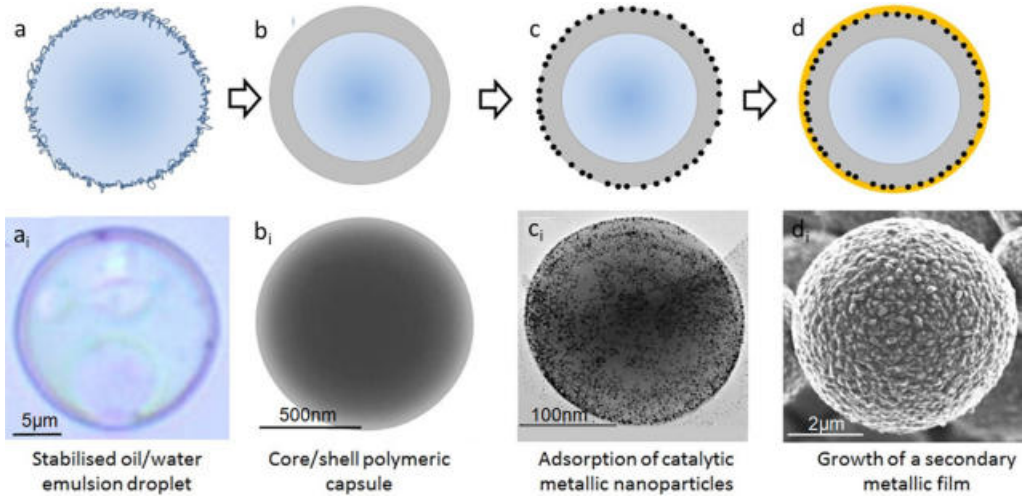

Figure 2.21: (a-d) Schematic diagrams and corresponding optical and (a_i - d_i) electron microscopy images of the different phases from emulsion droplet to metal coated capsule: (a) emulsion droplet, (b) capsule, (c) capsule with adsorbed NPs, (d) metal (Au) coated capsule, (a_i) emulsion droplet (optical microscopy), (b_i) capsule (TEM), (c_i) capsule with adsorbed NPs (TEM), and (d_i) metal-coated capsule (SEM). The micrographs correspond to different samples and are chosen to illustrate the evolution of the systems over the different steps[101].

Though there are drawbacks associated with this method it highlights the merits of metallic encapsulation. As mentioned electroless metal plating is an efficient way of applying a metallic layer to a substrate. The next section will look in depth at this process.

2.3.3 Electroless metal plating

An additional metallic coating can be applied to microcapsules to reduce the diffusion of the active through the shell and therefore retain the core for longer periods of time. Electroless plating (ELP) is widely used due to its low cost, low

energy and capability to deposit a thin metal film. The metal coating can be applied to non-conducting substrates such as glass, plastics and ceramics.[102] ELP is the process of depositing a coating to a surface with the aid of a reducing agent in solution, without the application of an electric current from an external source. The electrochemical deposition of a metal from a solution of the salt of said metal occurs via an electrochemical redox reaction, where electrons are transferred between the reacting chemical species. The simplest form of chemical plating is the metal-displacement reaction.[161] Electroless deposition also offers the advantages over electrodeposition as it allows the metallisation of non-conducting surfaces, it has the ability to deposit on targeted sites on the substrate, complex shapes and holes can be plated and an external current force is not required. Films obtained from ELP tend to be denser and have improved properties for corrosion and electronics applications.[63]

ELP has been used to deposit a broad range of metals, such as iron[60], nickel[191], copper[176],[83], gold[102], silver, platinum[161] and palladium[183]. Electroless alloy metal coatings have also been reported in a number of papers. Metal alloy deposition allows the physicochemical properties to be tuned, thereby extending the range of possible applications[182]. There is an extensive range of alloy combinations, for example gold alloys such as Au-Ni and Au-Co have been successfully deposited[233]. Gao et al. studied the permeation properties of Pd-Cu membranes synthesised via ELP.[85] Tertiary alloy coatings such as Ni-W-P have also been documented. Du et al. were able to deposit Ni-W-P coatings onto a metal substrate using $H_2PO_2^-$ as a reducing agent.[68]

ELP is an electrochemical process involving donor/acceptor electron reactions whereby metal ions in an aqueous solution react with a reducing agent to form a metallic coating. A chemical reducing agent provides electrons in solution for the conversion of metal ions to the metal form (Equation 2.10). Chemical reducing agents commonly used include NaH_2PO_2, borohydrides, formaldehyde (especially for Cu), hydrazine, amine boranes, and some of their derivatives.

$$M^{2+} + 2e^- (\text{supplied by reducing agent}) \xrightarrow{\text{catalytic surface}} M^0 \tag{2.10}$$

The catalytic surface is the only place that this reaction can occur. Once the deposition has begun, the deposited metal must also act catalytically for the

deposition to continue. As deposition progresses, islands are formed around the nucleation sites and grow until they form a continuous film. The growth rate of film thickness is linear in time once a continuous film has been reached.[220]

This study will focus predominately on the ELP of gold metallic films. Gold has a high chemical and thermal stability, is resistant to oxidation and mechanically robust. This allows for a broad range of applications including use in biochemistry.[92]. There are many industrial processes that involve the use of cyanide containing solutions ($KAu(CN)_2$) and borohydride or dimethylamine borane as the reducing agent in gold film deposition, but there are issues associated with the toxicity, plating rate, contamination with minute amounts of nickel ions, high pH is required and stability of such solutions.[184] Efforts have been made to improve the stability and plating rate, however these baths have certain incompatibilities with many current technologies and the toxicity is undesirable. Cyanide free methods have been developed utilising other gold salts in the formulation including chloroaurate (III), Au(I)-sulfate complex, Au(I)-thiosulfate complex and Au(I)-thiomalate. One such example of a cyanide free bath uses catalytic platinum colloids, a gold salt and hydrogen peroxide as the reducing agent, which reduce chloroauric acid (Equation 2.11).[102] This method will be the basis for the gold coating work in this project.

$$2HAuCl_4 + 3H_2O_2 \xrightarrow{\text{Pt}} 2Au + 3O_2 + 8HCl \tag{2.11}$$

However as previously mentioned there are other metal combinations possible such as silver catalysed by gold particles[44] and gold catalysed gold growth[172], which would be particularly favourable as gold is suitable for use in biochemistry. Though using gold and platinum is expensive, so not suitable for many applications, it provides a good model system and is known to be prepared easily. This allows us to focus on optimising both this stage and the emulsification stage. As stated above a nanoparticle catalyst is required for this process so the next two sections will focus on synthesising said particles and their use as catalysts.

2.3.4 Metal nanoparticle synthesis

There are two general approaches to colloidal nanoparticle synthesis; top down and bottom up. The top down approach involves the subdivision of a bulk material into nanosized material and subsequent stabilisation. These are generally physical methods such as mechanical crushing, sputtering, pulverisation of bulk metal, arc discharge between metal electrodes, pulse laser deposition etc. The particles produced tend to be large in size and have a broad size distribution. Whereas the bottom up approach relies on building up nanoclusters from zero valent metal atoms which group together to form a stable nucleus and are then stabilised. Chemical methods include sol-gel, co-precipitation, chemical vapour synthesis, hydrothermal and reduction of metal ion precursors by a chemical reductant (such as $NaBH_4$). Nanoparticles prepared by chemical methods tend to have a narrower size distribution.[170], [237]

A commonly used method is the reduction of metal salts in the presence of a stabilising agent. It is thought that the mechanism occurs via the metal salts being reduced to zero-valent metal atoms in the initial stage of nucleation. These can subsequently collide with other metal ions, metal atoms or clusters to form an irreversible seed of stable metal nucleus. The diameter of the seed nucleus is determined by the difference in redox potentials of the reducing agent and metal salt used and the strength of the metal-metal bonds. The relative rate of nucleation and particle growth determines the final size of the metal colloid.[207]

A wide range of stabilisers are used such as polymers, surfactants and donor ligands which control the growth and prevent agglomeration. There are two main modes of stabilisation, electrostatic and steric. Electrostatic stabilisation relies on repulsion between particles due to the electrical double layer which is formed by ions and counterions adsorbed at the particle surface. Steric stabilisation is provided by coordinating molecules that act as a protective shield at the surface. They separate the nanometallic cores and hence prevent agglomeration. Some such protective groups are polymers and block copolymers, P, S and N donors (e.g. phosphines, thioesters, amines), long chain alcohols, surfactants, organometallics solvents such as THF or propylene carbonate. The solubility of the stabilising group tends to influence the solubility of the resulting colloid. So hydrophilic

stabilisers produce water-soluble colloids and lipophilic protective agents give colloids that are soluble in organic solvents.[208]

2.3.5 Catalytic activity of metal nanoparticles

Nanoparticles have attracted interest for their catalytic uses as there has been reported enhanced reactivity and selectivity compared to their bulk counterpart. Metal based catalysts are generally expensive and can often be toxic; therefore it is desirable to reduce the amount of these compounds used. They offer the advantage of a high surface-to-volume ratio and have better dispersion ability due to their small size, which enhances their effectiveness compared to larger crystals of the same mass.[212],[109] Lower loading can be equally effective during reactions, due to the high area-to-volume ratios, making the reaction more economical. Colloidal dispersions of metal nanoparticles are able to operate as catalysts at low temperatures.[170] The size of the nanoparticle is pivotal in establishing its catalytic reactivity. Small particles lead to more active sites on the surface. Surface defects of the catalyst have an effect on the catalytic activity. Smaller particles tend to have more kinks and edges compared to larger particles and this increased surface energy can provide lower activation energy pathways. The size of the nanoparticles can also affect the selectivity of the catalyst.[237] More recently work has been done into how the shape of nanoparticles effect the catalytic activity, with some studies showing structure sensitive behaviour[212]

One of the major challenges to the performance of the NP catalyst is the tendency for nanoparticles to aggregate. This can be overcome by using a medium for dispersion or a support to maintain a high surface area. The maximum dispersion of the NPs is critical for catalytic behaviour.[170] Since Faraday's[77] first preparation of metal nanoparticles in an aqueous medium a large number of methods have been established and developed for the synthesis of metal nanoparticles involving the use of different supporting agents such as polymers, citrate ions, borohydride ions, gelatine and organometallic ligands.[190] Without stabilisers it can be difficult to obtain a stable colloidal dispersion.

Metal NPs are also able to form catalytic nuclei on a variety of surfaces such as polymers and ceramics.[268] This makes them suitable for applications in ELP.

NPs facilitate ELP by providing active nuclei sites on the desired surface which can catalyse the electrochemical reaction. It has been shown that metal NPs are able to preferentially direct the growth of a metal. Horiuchi et al.[102] illustrated that polyvinylpyrrolidone (PVP) could be used to stabilise platinum nanoparticles which were then used to catalyse the growth of a polymer film (see Figure 2.22). Other polymer stabilisers such as poly(diallyldimethylammonium chloride) (PDDA)[264], poly(N-isopropylacrylamide) (PNIPAAm)[40] and polyethylene glycol (PEG)[45] have been shown to stabilise platinum nanoparticles. However these methods often require more complicated synthesis such as multiple steps, reflux conditions or high temperatures and high pressure, whereas PVP stabilised nanoparticles can be prepared at room temperature in one step. Additionally some of these polymers may not be suitable for stabilising an oil-water interface as required.

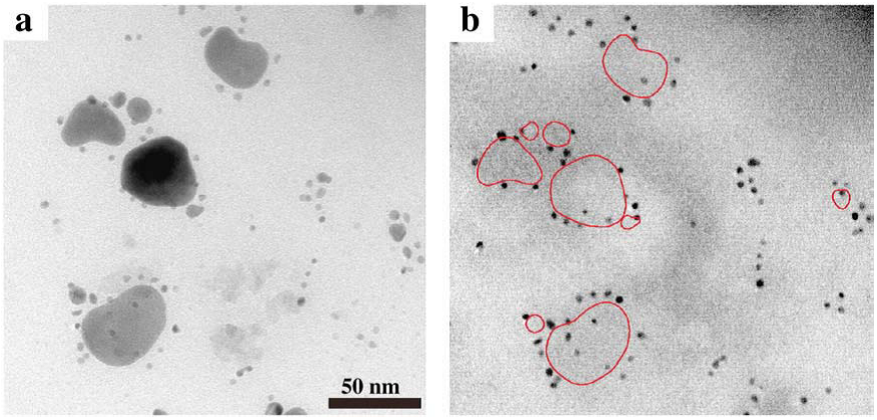

Figure 2.22: (a) TEM micrograph showing the gold depositions on the Pt colloidal particles on a carbon thin foil. The Pt colloidal particles were immobilized by dipping the substrate into the colloidal solution for 10 s, and the gold deposits were produced by ELP for 10 s. (b) shows the same position of (a) after the removal of gold deposits by bromine/tetraethylammonium bromide/acetonitrile solution[102].

It has also been shown that in the absence of the activated catalyst the metal films would not adhere to the desire substrate (e.g. on the glass beaker) or the plating reaction would not occur at all.[191] It has been found that the uniformity

of the deposition of the NPs for electroless plating can affect the coverage of the metallic film. A uniform and relatively dense distribution of seed nanoparticles is necessary for good film growth.[144]

2.3.6 Electroless deposition on to colloids

There has been significant research on electroless deposition onto planar solid substrates, however much less on colloidal particles. There has been work on the metal coating of solid colloidal particles for applications such as processing of metal matrix composites to improve wetting characteristics[89], improving opto-electric properties of functional surfaces[134], providing electrical conductivity[82], molecular sensors[125], providing magnetic properties[251], anisotropic conductive films for surface mount technology[157], bioseparation[249] and many more.[139] The metal coating is often applied to a polymer particle, such as polystyrene[157],[139] or PMMA[140], or a ceramic powder[89], where the outer material provides functionality. There is however, much less work on encapsulating a liquid core with metal. Nocera et al. coated an o/w emulsion with a silver coating, however the diffusion of the core through the shell was not tested as the silver layer was providing fluorescent properties rather than encapsulating an active.[181] Additionally the method they described used many steps and many different chemicals were involved. Routh and Sun successfully encapsulated Allura Red dye in a colloidosome with a silver shell for up to 500 hours with negligible release over that time period. However when nitric acid was added to trigger the release of the contents, the maximum release yield was around 20% at 84 hours[226]. This exemplifiers that there is a need for an encapsulation system that is able to encapsulate and release with high efficiencies.

2.4 Aims and objectives

After reviewing the challenges and limitations with current techniques for encapsulation of small species, the aim of this work is to develop a simple emulsion-based methodology that allows for the rapid and efficient production of metal-shell microcapsules capable of retaining small species and of remotely delivering the

core contents when triggered. An encapsulation system based on the electroless deposition of gold onto platinum nanoparticles has been chosen as it is a good model system which is known to be easily prepared at room temperature, which will allow us to optimise the emulsification and metal plating step. The following objectives will be set out in order to meet this aim:

1. Study the ability of synthesised platinum nanoparticles to efficiently stabilise emulsion droplets
2. Simplify previous fabrication processes
3. Study the ability of directly depositing a secondary metal film at the oil water interface
4. Demonstrate that retention of the active is not compromised
5. Study the ability of IR laser and ultrasound energy devices to induce metal shell fracture of the microcapsules

Here, a method where the metallic film is deposited directly onto an emulsion droplet, hence allowing 100% of the emulsion core (potentially corresponding to 100% of the active material depending on conditions) to be encapsulated and eliminating waste solvent from the previous method is proposed.

The proposed method will be based upon electrolessly plating a metal film (as described in Section 2.10) onto an emulsion droplet which is stabilised by catalytic metal nanoparticles (as described in section 2.3.5). After reviewing the literature and theory a platinum catalyst and gold as the secondary plating metal were chosen as a model system due to the inertness and biocompatibility of gold and the previous success of the platinum and gold combination.

Initially the synthesis of the platinum nanoparticles will be studied and optimised for their use as an emulsifier. The parameters that affect the emulsification of these nanoparticles in order to create a system where the reduction of a gold salt can be isolated at the oil-water interface (and not in the bulk) will then be examined. Finally, the ability of the shell to act as an efficient barrier against diffusion of the core into the continuous phase will be tested and the methods of rupture and release explored.

Chapter 3

Materials and Methodology

3.1 Materials

The following chemicals were used as received: Polyvinylpyrrolidone (PVP, 40kDa, Fluka Analytical, CAS: 9003-39-8), Sodium borohydride ($NaBH_4$, Sigma Aldrich, $\geq$ 98.0% (assay (hypochlorite)), CAS: 16940-66-2), hexachloroplatinic acid hydrate ($H_2PtCl_6 \cdot xH_2O$), Sigma Aldrich, $\geq$ 99.9% trace metals basis, CAS: 26023-84-7), Gold (III) chloride hydrate ($HAuCl_4 \cdot 3H_2O$), Sigma Aldrich, $\geqslant$99.9% trace metals basis, CAS: 16961-25-4), Hexadecane ($CH_3(CH_2)_{14}CH_3$), Sigma Aldrich, 99%, CAS: 544-76-3), Hydrochloric acid (fuming HCl, Merck, 37% HCl, CAS (water): 7732-18-5, (HCl): 7647-01-0), Hydrogen peroxide (30.5wt% H_2O_2, P-code:101152527)

Water used in the experiments was purified Millipore Milli-Q water (18.2 M Ω cm resistivity at 25°C). Experiments were carried out under ambient temperature.

3.2 Methodology

3.2.1 Synthesis of platinum nanoparticles

Pt nanoparticles were synthesised by the reduction of a metal salt in the presence of a reducing agent at room temperature. $H_2PtCl_6 \cdot 6H_2O$ (0.23g, 5.61 mM) was dissolved in a 0.0067 wt% PVP solution (100 ml). Under vigorous stirring at 750 rpm ((250 ml conical flask, 2.5 cm stirrer bar) $NaBH_4$ (2 ml, 1.1 mM) was rapidly

added into the mixture, producing a dark brown solution. After stirring for 20 minutes the nanoparticle suspension was filtered with a 0.2 μm PTFE filter then stored in the fridge.

3.2.1.1 Effect of varying concentration of PVP

Nanoparticles were synthesised as above with $H_2PtCl_6 \cdot 6H_2O$ (0.56 mM), $NaBH_4$ (1.11 mM) and PVP (0.2 wt % to 0.005 wt %)

3.2.1.2 Effect of varying concentration platinum salt

Nanoparticles were synthesised as above with PVP (0.0067 wt%), $H_2PtCl_6 \cdot 6H_2O$ (0.56 - 5.6 mM) and 2 x molar excess of $NaBH_4$ (1.11 - 11.12 mM).

3.2.1.3 Effect of varying concentration of reducing agent

Nanoparticles were synthesised as above with PVP (0.0067 wt%), $H_2PtCl_6 \cdot 6H_2O$ (5.6 mM) and $NaBH_4$ (11.12 - 27.78 mM).

3.2.2 Emulsification of platinum nanoparticles with hexadecane

Hexadecane and a Pt-PVP nanoparticle dispersion were homogenised using a sonic dismembrator ultrasonic processor (Fisher Scientific) for 1 min (40% amplitude, 3.1 mm microtip, in 40 ml glass vial) in a water bath. The resulting emulsion was agitated on a carousel for 30 mins and then washed with Milli-Q water once a fully creamed emulsion was obtained.

3.2.2.1 Effect of the addition of excess PVP before emulsification

For the emulsions in Section 6.4 PVP (0.5 ml) was added to Pt-PVP NP dispersion (9.5 ml). PVP solutions were added from concentrations of 0.05 wt% to 2 wt%, giving overall PVP concentrations of 0.0025 wt% to 0.1 wt%. The resulting NP dispersion was homogenised with hexadecane (0.75 ml) using the method above.

3.2.2.2 Effect of oil fraction

For emulsions in Section 6.5 Pt-PVP NPs (10 ml) were homogenised with hexadecane using the method above. The volume of oil was varied from 0.1 ml to 4 ml, corresponding to an oil volume fraction (ϕ) from 0.01 to 0.29.

3.2.2.3 Effect of the addition of excess salt to system before emulsification

In order to remove any excess salt from the system the particle were dialysed (8000 MW) with MilliQ water until the conductivity of the dialysis water was constant. Conductivity was measured with a Mettler Toledo Seven2Go S3 conductivity meter.

For emulsions in Section 6.6 NaCl (0.5 ml) was added to dialysed Pt-PVP NP dispersions (9.5 ml) and subsequently emulsified with 0.75 ml of hexadecane using the method above. NaCl solutions ranging from 5-2 x 10^{-4} M were added resulting in overall concentrations of 0.25- 1 x 10^{15}M NaCl.

3.2.3 Gold film growth at emulsion interface

3.2.3.1 Demonstrating permeability

Capsules were prepared from a hexadecane (0.75 ml) and Pt-PVP NP (10 ml) emulsion homogenised with an ultrasonic probe at 40% amplitude for 1 minute (40% amplitude, 3.1 mm microtip, in 40 ml glass vial). Following washing cycles the emulsion (0.5 ml) was placed in a plating solution consisting of PVP (5 ml, 0.2 wt%), water (10 ml), gold (III) chloride hydrate (2 ml, 180 mM) and hydrogen peroxide (1 ml, 1620 mM) as a reducing agent in a 40 ml vial. The capsules were mixed (by inverting) for 30 minutes and subsequently washed after sedimentation by removing the supernatant and replacing with Milli-Q water.

3.2.3.2 Effect of polymer stabiliser

A hexadecane and Pt-PVP NP emulsion was prepared as described above. The emulsion (0.5 ml) was added to a plating solution of water (10 ml), polymer stabiliser (10 ml, 0.05 wt%; 40 kDa PVP, 35 kDa PEG, 67 kDa PVA), gold (III)

chloride trihydrate (2 ml, 180 mM). Subsequently hydrogen peroxide (1 ml, 1620 mM) was added to initiate the electroless deposition process. The ratio of gold salt and reducing agent remained constant for each sample (4.5 x molar excess to ensure full reduction of the metal salt in the process). Upon the addition of the H_2O_2 the samples were agitated for 30 minutes on a carousel and then left to sediment.

3.2.3.3 Effect of gold salt concentration

A hexadecane and Pt-PVP NP emulsion was prepared as described above. The emulsion (0.5 ml) was added to a plating solution of water (10 ml), PVA (10 ml, 0.05 wt%, 67 kDa), gold (III) chloride trihydrate (2 ml). Subsequently hydrogen peroxide (1 ml) was added to initiate the electroless deposition process. The concentration of gold (III) chloride trihydrate added was varied from 180 mM to 12.5 mM. The ratio of gold salt and reducing agent remained constant for each sample (4.5 x molar excess to ensure full reduction of the metal salt in the process). Upon the addition of the H_2O_2 the samples were agitated for 30 minutes on a carousel and then left to sediment or cream.

3.3 Characterisation methods

3.3.1 Characterisation of polymer and nanoparticles

3.3.1.1 Transmission electron microscopy (TEM)

Pt-PVP NP samples were analysed using a FEI Tecnai TF20 field emission transmission gun electron microscope (FEGTEM) fitted with a HAADF detector and Gatan Orius SC600A CCD camera. An Oxford Instruments INCA 350 EDX (energy dispersive x-ray) system/80mm X-Max SDD detector was used for elemental mapping. Prior to analysis, samples were dispersed on a plasma cleaned TEM grid (holey carbon film, 400 Cu Mesh from Agar Scientific) and allowed to dry. The TEM grids were plasma cleaned prior to sample deposition in order to ensure the surface was suitably hydrophilic in order for the particles to adhere.

Particle sizes were then determined using ImageJ software. This gives the size of the nanoparticle metal core (not including polymer stabiliser.)

High resolution images for lattice spacings were recorded using an FEI Titan^3 transmission electron microscope and a Gatan One-View CCD.

3.3.1.2 UV-Vis spectroscopy

Pt-PVP NP samples were analysed with a Perkin Elmer Lambda 950 UV-Vis spectrophotometer in order to detect characteristic platinum salt peaks. Samples were analysed from 190-800nm. The disappearance of the platinum salt peak at 257 nm indicated the reduction of the Pt (IV) to Pt(0).

3.3.2 Characterisation of oil-water interface

3.3.2.1 Pendant drop tensiometer

The pendant drop method offers a convenient way to measure the interfacial tension (IFT) between two liquid phases. Interfacial tensions of the Pt-PVP dispersions in hexadecane were recorded using a Theta Optical tensiometer with a USB3 digital camera and LED based background lighting (Figure 3.1). The surface tension measurements were taken using the pendant drop method by injecting a droplet of the Pt-PVP dispersion into hexadecane and obtaining the largest drop possible. The surface tension was then calculated based on the Young-Laplace equation. The IFT for water in air and water in hexadecane was checked before each experiment to ensure the system was clean. A 22 GA needle was used for the measurements.

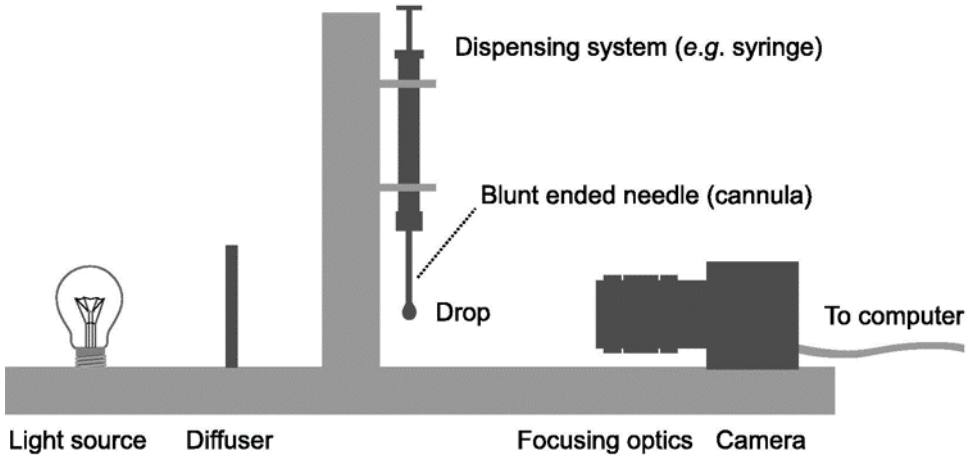

Figure 3.1: Typical set-up for pendant drop tensiometry experiment.[21]

The shape of a drop hanging from a syringe is determined from the balance of forces, including the surface tension of that liquid. The interfacial tension can be related to the drop shape through Equation 3.1

$$\gamma = \frac{\triangle \rho \cdot g \cdot R_0}{\beta} \tag{3.1}$$

Where γ is the surface tension, $\triangle \rho$ is the difference in density between fluids at interface, g is the gravitational constant, R_0 is the radius of drop curvature at apex and β is the shape factor.

The shape factor, β, can be determined using the Young-Laplace equation expressed through three dimensionless first order equations which are shown below (Figure 3.2);

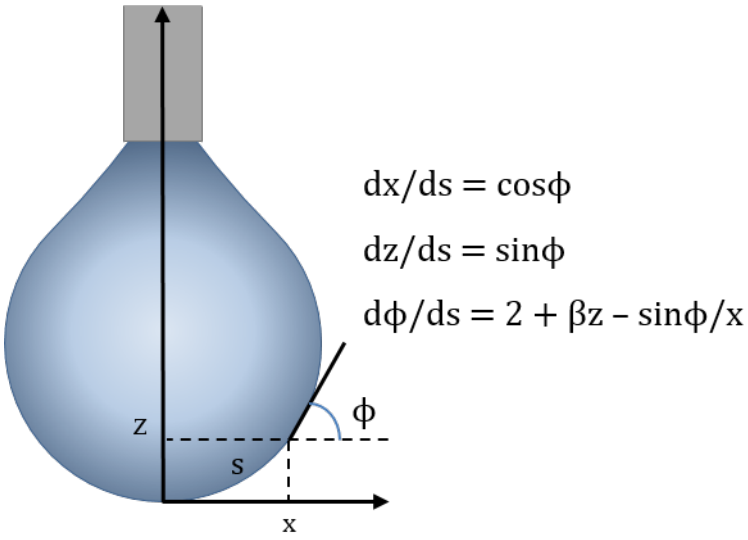

Figure 3.2: Schematic of pendant drop below a needle with associated variables used to determine the shape factor, β.

Computational methods using iterative approximations allow the analysis of the shape of a drop and then fit it to the Young-Laplace equation to calculate interfacial tension. Therefore if the densities of the two liquids are known the surface tension can be calculated.

3.3.2.2 Interfacial rheology

Interfacial rheology of the oil-water interface was studied over time using a TA Discovery HR2 Rheometer with a double wall ring geometry (DWR) (Figure 3.3). The DWR geometry has advantages over other geometries such as the bi-cone and Du Noüy ring for characterising thin liquid layers as it has good intrinsic sensitivity due to small area in contact with the bulk phase compared to the perimeter in contact with the interface. The square edge cross section shown in Figure 3.3, provides improved ability to pin the interface. Additionally it has well defined flow fields, enabling the bulk and surface contributions to be separated. [80]

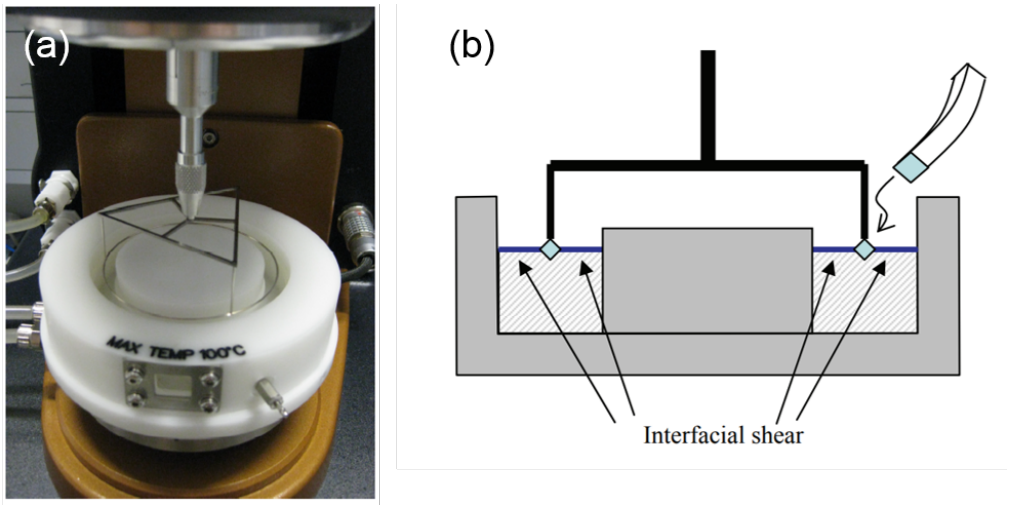

Figure 3.3: (a) DWR set up on TA rheometer, (b) schematic representation of DWR configuration.[80]

The nanoparticles used here were synthesised with 5.56 mM (0.23 wt%) $PtCl_6H_2$, 0.0067 wt% PVP and 22.25 mM $NaBH_4$ as concluded at the end of Chapter 4 to be optimal for emulsification. The nanoparticle 2D film was prepared in situ as follows; The aqueous nanoparticles (the dense phase) were loaded into the channel up to the step in the wall. The DWR geometry was flame cleaned and positioned to pin the air-water interface. Finally a layer of hexadecane was deposited on top carefully so not to disrupt the liquid-liquid interface. The temperature of the interface was maintained at 20.5 °C. Strain amplitude sweep experiments were conducted in oscillation mode at a fixed angular frequency ($\omega = 0.5$ rad$\cdot s^{-1}$) and the strain was varied from low to high and correspondingly the stress was changing. The strain sweep corresponds to progressively increasing the deformation in the system and monitoring the effect this has on the complex modulus monitored in the measurement. As the experiments were done in the linear region the structure of the film was not disturbed by the shear stress, thus droplets were not formed at the interface. Measurements were taken over several days, and stress was applied to the dispersion each time when the measurement was taken. The lag between the strain measured and the stress applied is characteristic of the storage (elastic) and loss (viscous) and moduli.

3.3.2.3 Cryo-TEM/STEM

Cryo-TEM was conducted on a FEI Titan^3 Themis G2 operating at 300 kV fitted with 4 EDX silicon drift detectors running Bruker Esprit software, and a Gatan One-View CCD. For cryo-STEM-EDX imaging, conditions were set at dwell time 25 μs and probe current of 40 pA.

Cryo-TEM sample preparation was carried out using a FEI Vitrobot. A continuous carbon TEM grid (EM Resolutions) was plasma cleaned and then held within the Vitrobot before a 3.5 μl drop was pipetted on the grid. The grid was then blotted and plunged into liquid ethane, after which it was maintained under liquid nitrogen before being transferred to a Gatan 914 TEM cryo-holder.

Scanning transmission electron microscopy (STEM) mode combines transmission electron microscopy and scanning electron microscopy. The technique scans a very finely focussed beam across the sample, like in SEM. The resulting interactions between the sample atoms and the beam electrons.

3.3.2.4 Cryo-SEM

Cyro-SEM was conducted on a Hitachi SU8230 cold field emission SEM with a Quorum PP3010T cryo transfer unit at an accelerating voltage of 1.0 kv. Images were collected using the upper secondary electron detector (SE(U)).

Cryo-SEM-EDX imaging was carried out with an Oxford Instruments XMax 80mm SDD spectrophotometer on a frozen sample.

3.3.3 Characterisation of emulsions

3.3.3.1 Benchtop C70 FlowCAM

Droplet size distribution was measured using the Benchtop C70 Series FlowCAM imaging flow cytometry instrument which measures particle size and shape using image analysis. The FlowCAM analyses the samples in suspension in real time, therefore allowing information on parameters such as particle size distribution and shape parameters to be calculated simultaneously. The sample is drawn into the flow chamber by a syringe pump and then deposited into an outflow

collection. A flash LED light illuminates the chamber, which is then imaged with the objective onto the high resolution digital camera.

Experiments were recorded in AutoImage mode using a 20x objective, FC50 flow cell in a reverse flow configuration (Figure 3.4). The reverse flow set up allows the emulsion sample (A) to flow up into the cell (B), thereby insuring larger droplets, which would cream quickly are measured. Post capture, the particles can be filtered using several parameters such as edge gradient, circularity and circle fit to ensure that the particles sizes are in focus. In particular the diameter (ABD), which is the diameter based on a circle with an area that is equivalent to the ABD area can be determined. The ABD area is defined as the combined area of all the pixels that are deemed part of the particle, so the ABD diameter is the diameter of the circle obtained by arranging these pixels in a solid circle.

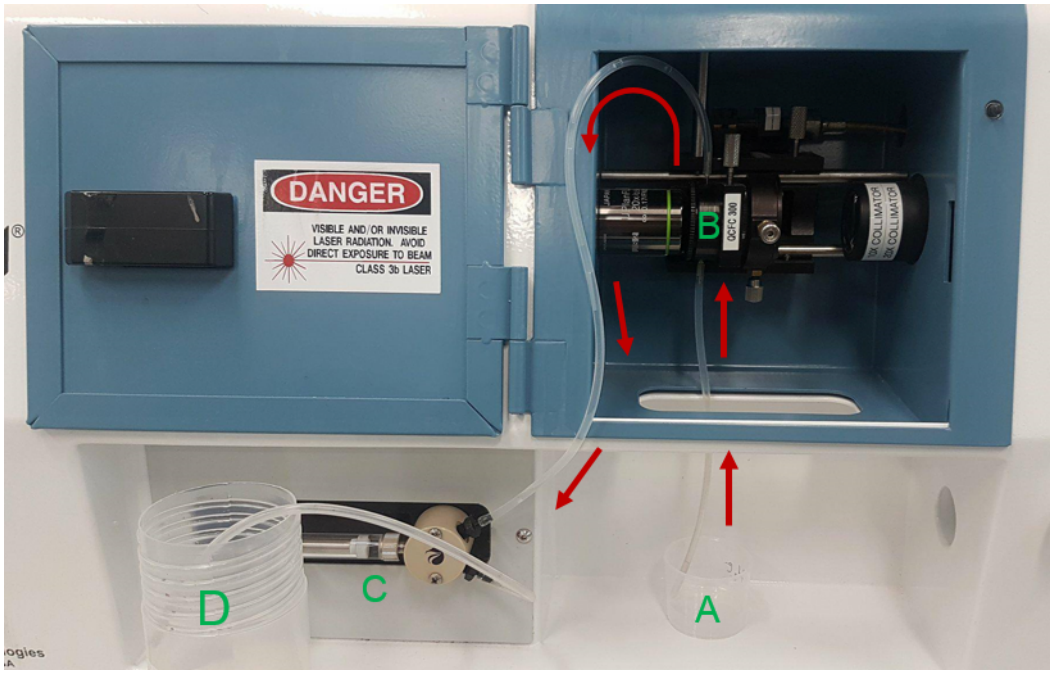

Figure 3.4: Reverse flow set-up for FlowCAM. Arrows indicate direct of flow. A; sample, B; flow cell, C; syringe pump, D; outflow collection.

The advantage of using the FlowCAM for image analysis is that refractive index properties are not required as with light scattering methods. Therefore

assumptions do not need to be made about the refractive index of the emulsion droplets. It also uses low flow rates so the emulsion is not subject to high shear forces which would potentially break down the emulsion.

3.3.3.2 Optical Microscope

The emulsions were visualised using an Olympus BX51 optical microscope with a Colorview 2 digital camera. Cell D imaging software was used to record the image. The gold coated microcapsules were also visualised using the optical microscope with both transmitted and reflected light. In this case a GXCAM HiChrome-MET camera was used.

3.3.3.3 LUMiSizer

LUMiSizer Dispersion Analyser employs STEP-Technology (space and time resolved) which allows the intensity of the transmitted light to be measured as a function of time and position over the full sample length simultaneously while under centrifugation (Figure 3.5). The data is displayed as a function of radial position, as a distance from the centre of rotation. The transmission profiles are representative of variation in particle concentration in the sample (low transmission means high particle concentration and high transmission means low particle concentration).

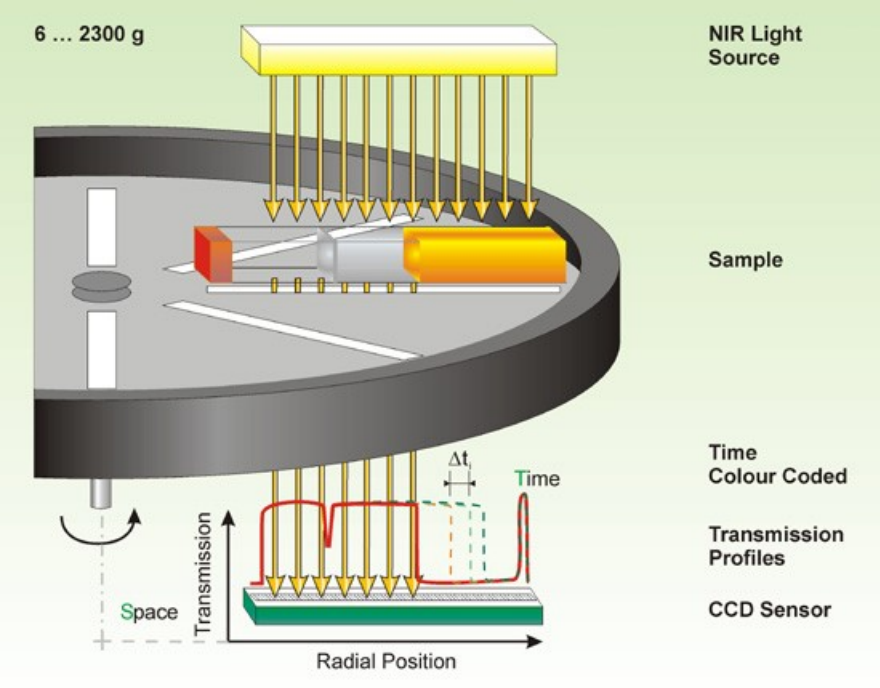

Figure 3.5: Schematic of LUMiSizer set up. The transmitted light is passed though the sample and picked up by thousands of detectors.

After creaming the aqueous phase of the emulsion was replaced by milliQ water. Samples of the lower aqueous phase was subsequently centrifuged on an Eppendorf Mini Spin plus at 10,000 rpm for 1 minute to separate any remaining oil. Measurements on the LUMiSizer were carried out at 25 °C at 300 rpm using 2mm PC 110-131XX cells at 865 nm. Transmission (T) measurements were used to analyse the concentration of Pt-PVP NPs remaining in the aqueous phase after emulsification, and thus the amount at the oil-water interface, using a calibration of Transmission against NP concentration (Figure 3.6). Values were obtained from the average T across a fixed position range in the cell.

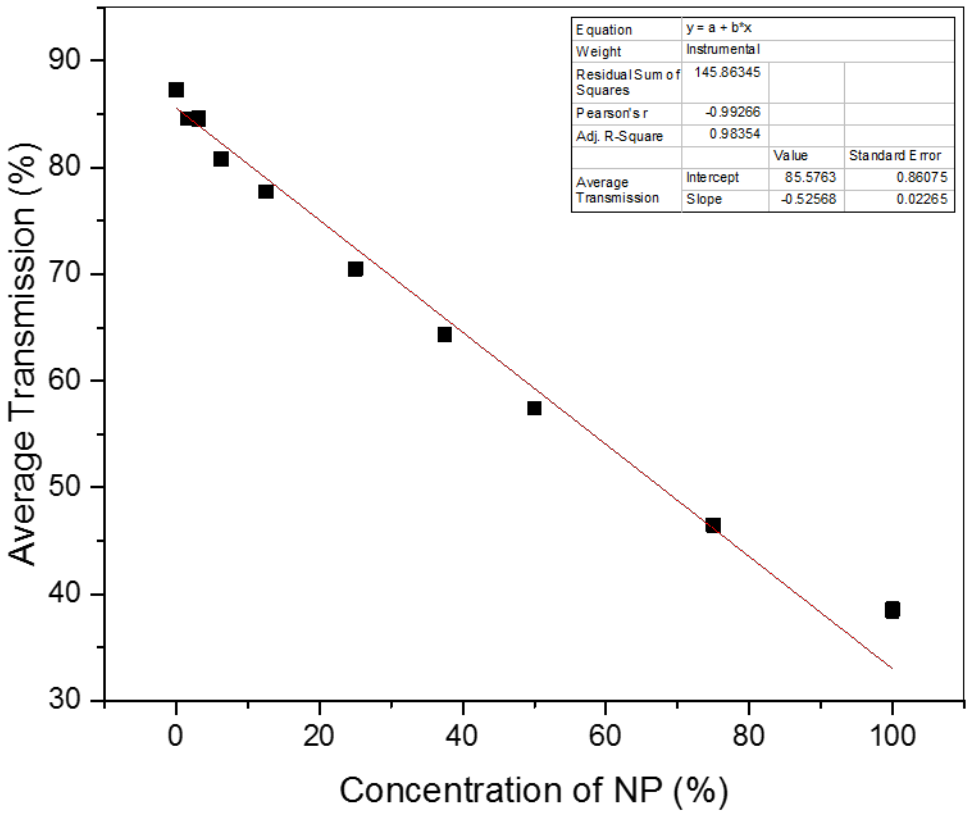

Figure 3.6: Transmission as a function of NP dilution. 100% represents undiluted NPs.

Experiments were also carried out under the same conditions to establish creaming rates. In this case the emulsion was inverted to homogenise and a sample was taken. Front tracking analysis was undertaken whereby the transmittance at a threshold of 10% was monitored over time to determine creaming rates. Figure 3.7 shows an example of a creaming profile for an emulsion.

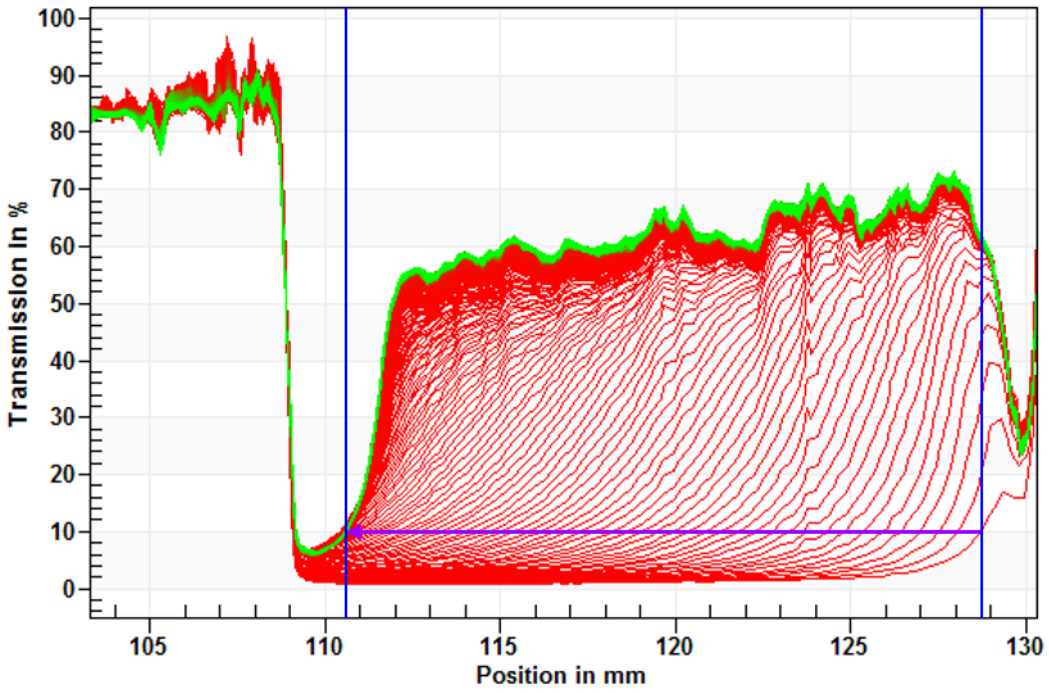

Figure 3.7: Example of a creaming profile of hexadecane in oil emulsion. Experiment was run at 300 rpm. Transmission measurements were taken initially every 5 s (for 1250 s) then every 25 s (for 18750 s). The purple arrow indicates the settling direction (creaming) at the threshold used for front tracking measurements. Front tracking plots position against time, from which creaming velocities can be obtained.

3.3.4 Characterisation of metallic capsules

3.3.4.1 Gas chromatography (GC)

Release of hexadecane from the gold coated capsules was analysed using gas chromatography. The gold coated capsule solution (2 ml) was added to absolute ethanol (8 ml). The capsules were redispersed and 1.5 ml sample (x2) was centrifuged on an Eppendorf Mini Spin plus at 7000 rpm for 1 minute to remove the capsules. The supernatant was added to a GC sample vial for GC analysis. The remaining sample was placed in a water bath at 40 °C. A 1.5 ml sample was

taken at various time intervals and the previous sampling method repeated.

Samples were run on a Perkin Elmer Clarus 580GC using the following method and column. GC column: Elite-1 capillary column, length 30 m, internal diameter 0.25 mm. The column temperature was programmed from 50°C to 300°C at 20°C/min at a flow rate of 2 ml/min. Data was compared to a calibration curve of the encapsulated oil to determine the concentration on oil.

3.3.4.2 SEM

Dried microcapsules were visualised using the Hitachi SU8230 high performance cold field emission (CFE) SEM with 80mm X-Max SDD detector, operating at 2kV.

Dried microcapsules were also imaged using the TM3030 Tabletop SEM at 15 kV under normal observation conditions.

3.3.4.3 Cryo-SEM FIB

Cryo-SEM was used to visualise the metal coated emulsions in order to study the surface morphology and shell thickness (via Focussed ion beam (FIB)). Freezing the samples prevents the shell collapse. The FIB can directly mill the frozen sample surface, via the sputtering of ions.

Cryo-SEM was conducted on a FEI Helios G4 CX at 2 kV and FIB was run at 30kV. Sample preparation was carried out using a Quorum Technologies, PP3010T Cryo-FIB preparation system. The samples was held at -140°C with the anticontaminator at -175°C. Samples were plunged into slushed nitrogen instead and transferred over under vacuum. All the samples were coated in Pt 5μA for 45s. EDX was carried out with an Oxford instruments XMax 150mm^2 at 15 kV with a 3.2 nA probe current.

3.4 Calculations

3.4.1 Number of NPs per unit volume

The number of nanoparticles per unit volume is calculated from the mass of platinum used and average size of the nanoparticles. This calculation is based on

the assumption that all of the platinum salt was reduced to metallic nanoparticles in the reduction reaction. As described in section 3.2.1, 0.23 g of platinum salt ($H_2PtCl_6 \cdot 6\,H_2O$) has been used in the synthesis of the nanoparticles. The mass of platinum produced in the reaction can be calculated from the ratio of the molar mass of platinum and that of chloroplatinic acid hydrate (Equation 3.2).

$$\text{Molar mass ratio} = \frac{\text{molar mass Pt}}{\text{molar mass } H_2PtCl_6 \cdot 6H_2O} = \frac{195.084}{409.81} = 0.476 \tag{3.2}$$

The total mass of Pt produced, M_{total}, is given by Equation 3.3,

$$M_{total} = 0.476 \text{ x } 0.23\text{g} = 0.109 \text{ g} \tag{3.3}$$

The total number of particles (N_{total}) in the suspension can be calculated using Equation 3.4

$$N_{total} = \frac{M_{total}}{M_p} \tag{3.4}$$

where the mass of one particle, M_p, (Equation 3.6) is determined using the volume of one particle, V_p, (Equation 3.5), which is based on a Pt core diameter of 3.3 nm and the density of Pt, ρ_{Pt} (2145000 g m^{-3})

$$V_p = \frac{4}{3}\pi r^3 = 1.41 \text{ x } 10^{-26} m^3 \tag{3.5}$$

$$M_p = \rho_{Pt} V_p = 3.03 \text{ x } 10^{-19} g \tag{3.6}$$

Therefore the total number of particles in 102 ml synthesis (2 ml of reducing agent) is 2.71 x 10^{17} which gives 2.65 x 10^{15} NPs ml^{-1}.

3.4.2 Ratio of polymer chains to nanoparticles

Using the number of NPs and number polymer chains in a set volume the ratio between the two can be established. For the nanoparticle synthesis 0.0067 wt% PVP was used (0.0067 g in 100 ml). The number of polymer chains (N_{PVP}) can be calculated from the following equation

$$N_{PVP} = \frac{M_{PVP}}{M_W} \cdot N_A \tag{3.7}$$

where M_{PVP} is the mass of PVP used (g), M_W is the molecular weight of PVP (g mol^{-1}) and N_A is Avogadro's constant which has the value of 6.022140857 x 10^{23} mol^{-1}. This gives a value of 9.90 x 10^{14} chains ml^{-1}.

Using the method calculated above the number of NPs can be calculated from 2.3-4.3 nm (the error associated with the NP size). The ratios are summarised in Table 3.1.

Mean core diameter of Pt NP (nm)	Number of NPs per ml (x 10^{17})	Ratio PVP:Pt NPs
2.3	8.01	7.9
3.3	2.71	2.7
4.3	1.22	1.2

Table 3.1: Ratio of PVP molecules to Pt NPs at different Pt NP mean core diameters

As expected the ratio decreases for a larger NP diameter. All of the values suggest that there is no excess PVP in the system.

3.4.3 Nanoparticle density at the interface

The transmission of the aqueous phase, measured by the LUMiSizer, can be used to determine the number of particles remaining in the bulk aqueous phase through comparison with calibration work where the transmission of Pt NP suspensions of a broad range of nanoparticle concentrations was measured. By using the total oil-water interfacial area in the system and comparison between the number of particles remaining in the emulsion continuous phase versus particles present

before emulsification, the adsorbed Pt NP density on the oil droplet surfaces can be estimated (NPs per area (NP m^{-2}) or mass per area (g m^{-2}).

A theoretical surface area that the particles can cover can be determined by assuming hexagonal close packing and calculating the area that one (partially wetted) particle would occupy. The area occupied theoretically by a single particle can be expressed by the area of a hexagon including the particle (Equation 3.8) [107]

$$A_H = \frac{\sqrt{3}}{2}x \tag{3.8}$$

where x is the average particle cross section area as detailed in Equation 3.9

$$x = \pi r^2 \tag{3.9}$$

and r (Equation 3.11) is comprised of the diameter of the core NP (as determined by TEM) and the spacing created by the polymer, z. The interparticle spacing, s_{IP} is the space between two particle cores and is equal to $2z$ (Equation 3.10), as illustrated in Figure 3.8.

$$s_{IP} = 2z \tag{3.10}$$

$$r = \frac{s_{IP} + d_{NP}}{2} \tag{3.11}$$

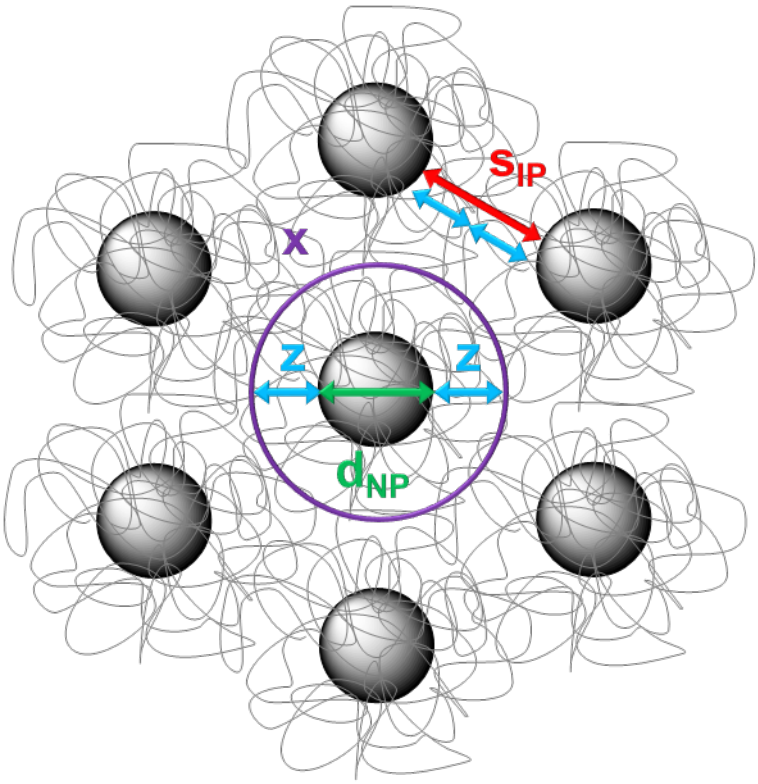

Figure 3.8: Schematic showing hexagonal close packing of particles, where d_{NP} is the NP core diameter, z is the spacing caused by the polymer, x is the average particle cross section area and s_{IP} is the interparticle spacing.

Once the area that one particle occupies is obtained this can be multiplied by the number of particles in the system at the interface ($NP_{interface}$) to provide the area that the particles can cover (A_{total}) at a given particle diameter and spacing (Equation 5.2).

$$A_{total} = A_H \cdot NP_{interface} \tag{3.12}$$

If the number of particles adsorbed at the interface (from transmission data) and the interfacial area of the emulsion (from size distribution data) is known, the interparticle spacing, s_{IP}, as shown in Figure 3.8 can be back calculated. This is achieved using the Goal Seek function on Excel where A_{total} is set to the total

interfacial area obtained from the size distribution of the emulsion by changing the interparticle spacing (s_{IP}).

Chapter 4

Nanoparticle Synthesis

4.1 Synopsis

This chapter will focus on the synthesis and characterisation of polyvinylpyrrolidone stabilised platinum nanoparticles (Pt-PVP NPs) which will subsequently act as an emulsifier and a catalyst in the secondary metal plating. In particular the parameters that influence synthesis shall be discussed and adapted to optimise the resulting nanoparticles for their use as efficient Pickering emulsifiers. This chapter will lead us to understand that minimising the excess polymer in the nanoparticle dispersion while still creating stable nanoparticles will be paramount to achieve this objective.

4.2 Preparation of polyvinylpyrrolidone stabilised platinum nanoparticles (PVP-Pt NPs)

Metal nanoparticles have been widely reported for their use as catalysts. They offer the advantage of a high surface-to-volume ratio and have better dispersion ability and long term stability due to their small size, which enhances their effectiveness as catalysts compared to larger crystals of the same mass.[212],[109] Lower loading, compared to larger particles can be equally effective during reactions, due to the high area-to-volume ratios, making the reaction more economical. The original approach was to use finely dispersed colloidal particles in aqueous

or organic solutions or a solvent mixture. However these colloidal dispersions required stabilisation from a capping agent to prevent aggregation or facilitate recycling. One of the disadvantages of soluble metallic colloidal dispersions is recovery from the reaction products. Often this is overcome by using immobilisation systems such as thin films of liquids on porous supports, fluorinated solvents or using aqueous/organic biphasic condition.[214] Therefore the interfacial activity of the nanoparticles synthesised here is both important for this project but for their general use as catalysts.

Colloidal dispersions of metal nanoparticles are able to operate as catalysts at low temperatures.[170] This is useful for our use as an emulsifier as high temperatures would alter the behaviour of the emulsion on which the nanoparticles will be adsorbed. Additionally, applying heat in a process increases costs. In particular it has been shown that metal NPs are able to preferentially direct the growth of a metal from their surface through a process known as electroless deposition. Horiuchi et al.[102] demonstrated the growth of a gold film on platinum nanoparticles. This is interesting for our application as when adsorbed onto a solid (and potentially liquid droplet) surface, platinum nanoparticles can catalyse the growth of a secondary gold film onto that surface.

It is well known that PVP acts as an effective steric stabiliser for the dispersion of metallic nanoparticles.[87], [246], [239], [127] For example, there are several cases in the literature of the reduction of metal salts with $NaBH_4$ in the presence of PVP, leading to the formation of stable nanoparticle suspensions.[190], [28] In particular, it has been shown that platinum nanoparticles can be obtained from this method at room temperature.[102] The platinum nanoparticles discussed in this chapter are synthesised via this method, where reduction of the metal salt is carried out in the presence of PVP, which stabilises the synthesised nanoparticles. By controlling the ratio of concentrations between the PVP stabiliser and the metal ions added into the system, one should be able to control the size of the nanoparticles and the extent of the excess polymer in the resulting suspension. In this particular project, excess polymer is undesirable, as it will likely compete with the nanoparticles to adsorb at the oil-water interface, which in turn will reduce the metal nanoparticle surface coverage on the resulting oil emulsion droplets (Figure 4.1). Gold is more

likely to grow in Pt rich areas, as these regions promote the formation of gold nuclei, therefore increase the deposition rate.

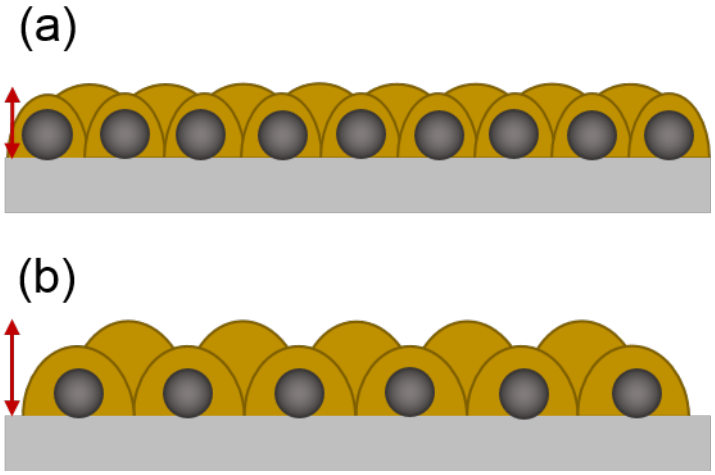

Figure 4.1: Schematic illustrating different packing density and subsequent secondary metal film growth; a) small separation distance between NP core, b) larger separation distance between NP cores.

The challenge here is to find optimal conditions to subsequently use these PVP-stabilised nanoparticles as stabilisers of oil emulsion droplets. The process will then aim to encapsulate the droplet within a metal film. In the next sections, the different variables influencing the final nanoparticle size and the amount of excess polymer stabiliser in the bulk will be explored.

4.2.1 Formation of Pt PVP NPs

It has been proposed by Van Rheenen that colloidal metal nanoparticle synthesis occurs through a two-step process; firstly the metal precursor is reduced to zero-valent metal atoms, and then the nanoparticles grow from the metal atoms. The chemical reduction of hexachloroplatinic acid by sodium borohydride proceeds via the following reaction in aqueous solution (Equation 4.1)[243]

$$NaBH_4 + H_2PtCl_6 + 3H_2O \longrightarrow Pt + H_3BO_3 + 5HCl + NaCl + 2H_2 \quad (4.1)$$

$$NaBH_4 + H_2O \longrightarrow H_2 + \text{boron hydrolysis products} \quad (4.2)$$

It can also be expressed as an ionic equation (Equation 4.3)

$$[Pt^{+IV}Cl_6]^{2-} + BH_4^- + 3H_2O \longrightarrow Pt^0 + H_2BO_3^- + 6Cl^- + 4H^+ + 2H_2 \quad (4.3)$$

Van Rheenen claimed that the Pt NPs formed in the early stages could catalyse the hydrolysis of sodium borohydride (Equation 4.2) so an excess of sodium borohydride is required to ensure the completion of Equation 4.1.

There are various theories and models to describe particle formation mechanisms, though some of these are still not able to explain how synthesis parameters influence final particle size well. Theories have developed from nucleation based models to contrasting growth based models which states that for most synthesis the minimal particle size is determined by colloidal rather than thermodynamic stability, hence making nucleation irrelevant.

Nucleation describes the process of the first step in a first order phase transition and is a purely thermodynamic model. It describes the appearance of a new phase, the nucleus, in the metastable primary phase. The majority of work is based on classical nucleation theory (CNT)[18] however there have been adaptations of this theory for growth processes of NPs such as the LaMer theory.[164] The LaMer theory was developed in the 1950's and transferred the concept of CNT to NP synthesis by proposing the idea of burst nucleation. In burst nucleation nuclei are generated at the same time due to homogenous nucleation and then grow without additional nucleation. The NP formation concept is separate to nucleation and growth.[200] However these theoretical models are unable to describe or predict the particle evolution and size distribution. The LaMer theory only describes the nucleation process followed by growth of the stable nuclei, but the characteristics of the growth remain unspecific. Experimental studies by Zhang and co-workers have found that growth rate is dependent on the equilibrium of various interparticle interactions and not only diffusion as described by the LaMer model.[263]

More recently approaches to illustrate the growth process based on colloidal, rather than thermodynamic stability have been introduced.[259], [200] These growth

mechanisms are based on aggregation and subsequent coalescence of initial clusters of metal atoms forming unstable small nanoparticles, which merge with one another until surface coverage of a stabilising species becomes large enough to provide efficient repulsion between adjacent clusters, thus forming the final nanoparticles (Figure 4.2).

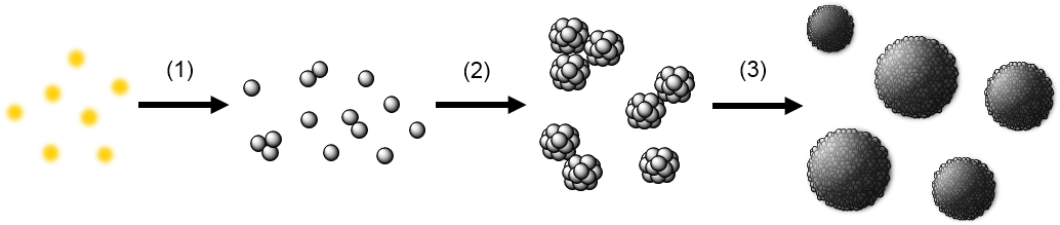

Figure 4.2: Schematic of generalised 3-step mechanism of nanoparticle growth due to coalescence: (1) reduction of metal precursor, (2) formation of initial clusters and (3) coalescence of clusters and nanoparticles. Adapted from Polte et al. [200]

Unlike the previous nucleation theories the size distribution is determined by the increase in colloidal stability, and therefore is independent of the nucleation process. For the reaction used here to synthesise the Pt NPs, the use of $NaBH_4$ as a reducing agent results in a reduction much faster than growth, therefore the reduction is separated from particle growth. [200] This growth based on colloidal stability is described by considering the stability as a result of attractive van der Waals and repulsive electrostatic forces between particles according to the theory by Derjaguin, Landau, Verwey and Overbeek (known as DLVO theory). The interaction energy between two identical spherical particles as a function of their distance is illustrated in Figure 4.3 (a). The minimum thermal energy of two interacting particles that is necessary to induce aggregation is represented by the maximum of the curve (aggregation barrier) (Figure 4.3 (b)). This aggregation barrier offers a measure of the colloidal stability and in most cases it increases with particle size. As illustrated in Figure 4.3 (c), as long as a system provides sufficient thermal energy, E_{kT}, where E_{kT} is greater than the aggregation barrier, two particles can overcome repulsive forces and aggregate or coalesce therefore enabling particle growth. This illustrates an increase of the aggregation barrier

(between two identical particles) with respect to particle size. The stability curve in Figure 4.3 (c) is separated into two sections by E_{kT} where in section I the thermal energy is higher than the aggregation barrier therefore particles can aggregate/coalesce and hence grow. Above E_{kT}, in section II the aggregation barrier cannot be overcome and further particle growth is inhibited, resulting in a stable colloidal solution. The minimal final particle radius of the particle is related to the intersection of E_{kT} of the stability curve. Consequently the final particle size is dependent on the available thermal energy, E_{kT}, and the stability curve which is reliant on the surface charge and chemical composition of the colloidal solution.

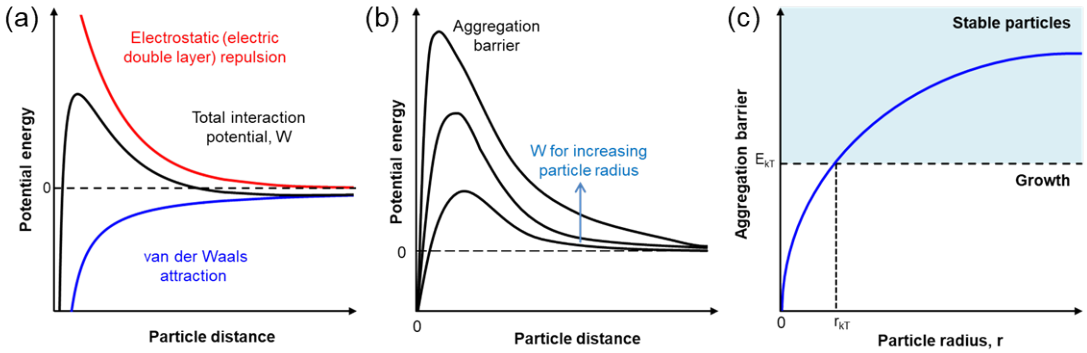

Figure 4.3: Concept of nanoparticle growth based on colloidal stability as described by DLVO theory; (a) Interaction potential between two spheres as a result of attractive and repulsive forces as a function of particle distance, (b) Total interaction potential (W) between two spheres as a function of particle distance for different particle radii, (c) Concept of nanoparticle growth with colloidally stable particles obtained at the intersection of E_{kT} and stability curve. Adapted from Wuithschick et al.[259]

The use of sodium borohydride as a reducing agent leads to very fast reduction of the metal precursor. During a metastable state, residual BH_4^- is converted to $B(OH)_4^-$ which initiates a second step of coalescence. The change in the solution's chemical composition in turn changes the surface chemistry and hence the colloidal stability decreases. As a result the particles aggregate a second time until reaching a stable size again. In this instance the presence of a steric stabilising agent such as a polymer or lowering the temperature can help increase the

stability and prevent further growth by increasing the distance of the stability curve of the system and E_{kT}.[259]

4.2.2 PVP as a stabiliser

In order for the Pt NPs to be used as emulsifiers for our application they must posess good colloidal stability in solution in order to be able to adsorb to the oil water interface during emulsification; this is the role of the PVP. Both the steric effects of the PVP and the specific interaction between the PVP chains and the metal contributes towards particle stability by preventing their agglomeration. PVP was chosen as a stabiliser as it is known to stabilise platinum and other nanoparticles.[102], [239], [29], [127] The PVP molecule has a hydrophilic component (pyrrolidone moiety) and a hydrophobic component (alkyl group) as seen in Figure 4.4. Water and many other non-aqueous solvents are excellent solvents for PVP. Additionally, PVP has biocompatibility, complexing stability, low toxicity, is relatively inert and resistant to thermal degradation making it a favourable candidate for the stabilisation of platinum nanoparticles.[221], [127]

To understand how PVP stabilises the NPs the interaction between the Pt NP surface and the PVP molecules (structure can be seen in Figure 4.4) must first be examined. The stabilising effect of PVP originates from the lone pairs on the nitrogen and carbonyl oxygen atoms. These lone pairs can be donated to the sp hybrid orbitals on the metal ions to form a complex. This specific bonding remains even when the metal is reduced, which eventually provides strong attachment of the polymer chains onto the resulting nanoparticles.[56]

Several research groups have investigated the protective mechanism of PVP on metal nanoparticles.[239], [28], [29], [147], [266], [260] The interaction of the PVP with metal precursors has been documented by various experimental means such as UV-vis spectroscopy[147], [148], [56], FTIR[239], [28], [29], UV-Raman[28], [29] and X-ray diffraction (XRD).[147], [104] For example Tu et al. used FTIR spectroscopy to examine peak shifts on the carbonyl groups between pure PVP, PVP and metal precursor mixtures and PVP and the metal species.[239] UV-Ramen spectroscopy has also been utilised to show interactions between polymer functional groups and surface metal atoms. Borodoko et al. observed selective enhancement of C=O,

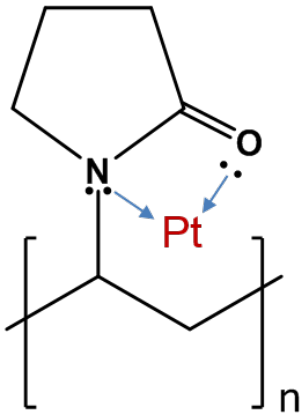

Figure 4.4: Structure of PVP, showing lone pairs on oxygen and nitrogen atoms complexing to Pt ion.

C-N and CH_2 vibrational modes as a result of interactions between surface metal atoms and the polymer functional groups.[29] Dandapat et al. reported a shift in the UV-vis absorbance peak of the $[PtCl_6]^{-2}$ ions in the presence of PVP.[56] Hossain et al. noted that the shifting and broadening of diffraction peaks in XRD diffraction patterns may be a result of the PVP stabiliser, which has the ability to donate electrons to the vacant d-orbital of the metal atoms, therefore increasing the electron density and leading to Pt-Pt bond expansion of the surface-near atoms.[104]

It is clear that the PVP polymer chains do adsorb through specific interactions with the electron-donor atoms in the PVP onto the final particle surface and provide a stabilising layer. Due to the polymer chain length, some of the polymer extends away from the particle stabiliser and thus acts as a steric stabiliser. Under both low and high particle surface coverage densities the polymer layers repel each other as they approach and interact.[33]

4.2.3 Effect of varying concentration of PVP

Initially, the concentration of PVP stabiliser in the synthesis was varied to manage the amount of excess PVP in the system and examine how this effects the resulting Pt-NP properties. As mentioned before, varying the concentration of PVP is

important in minimizing the amount of excess polymer in the NP dispersion to stop competition between excess PVP and NPs for adsorption at the oil-water interface. A system with minimal excess PVP would be preferable as this will allow a higher packing density at the droplet interface and potentially allow thinner, smoother coatings of the secondary metal, as illustrated in Figure 4.1. Pt nanoparticles were synthesised in-situ by the reduction of a platinum salt using $NaBH_4$. The method used is based on work by Horiuchi et al.[102]

PVP stabilised platinum NP dispersions were prepared for different PVP concentrations in the reaction medium, from 0.2 wt% to 0.005 wt%. The concentration of platinum salt and reducing agent was kept constant throughout experiments (0.56 mM (0.023 wt%) $PtCl_6H_2$, 1.11 mM $NaBH_4$). Transmission electron micrographs of the resulting samples in Figure 4.5 demonstrate that stable dispersions of particles of a few nanometres in size can be obtained for all stabiliser concentrations.

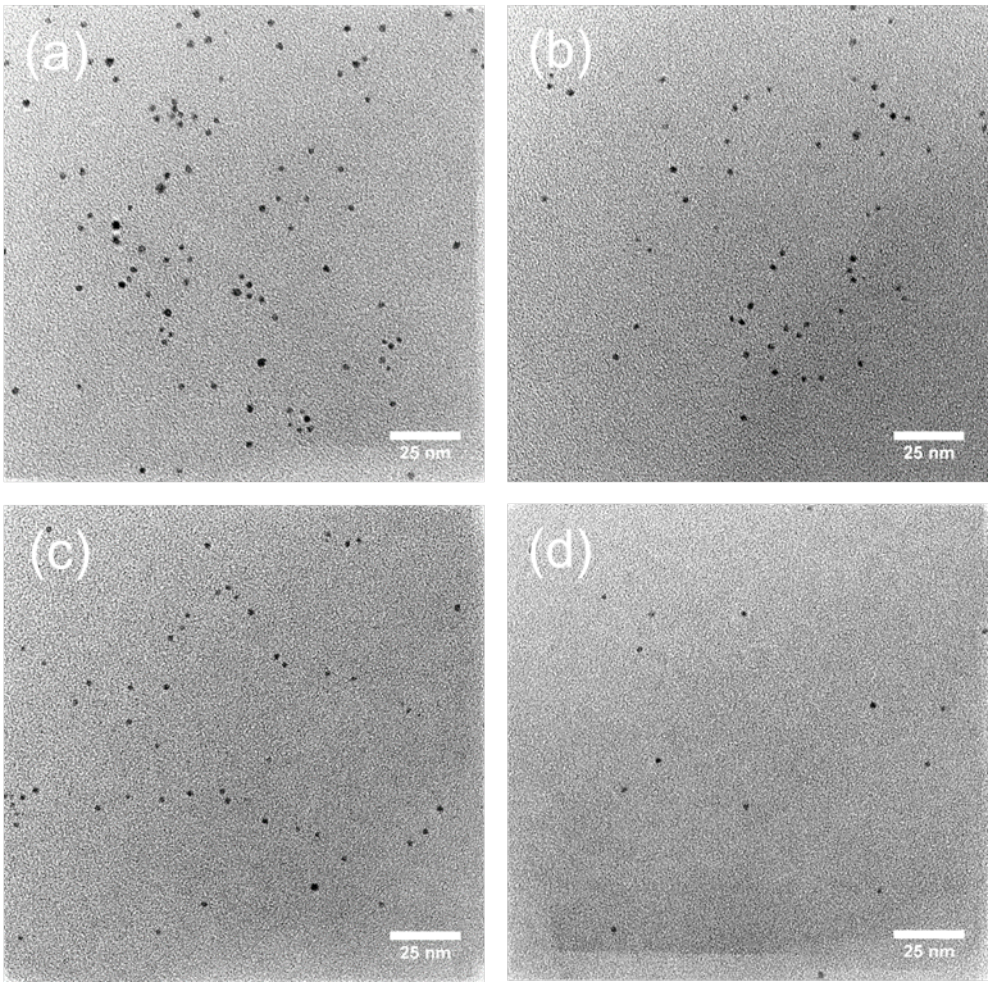

Figure 4.5: TEM micrographs of Pt-PVP NPs (2 weeks after synthesis) prepared with 0.56 mM (0.023 wt%) $PtCl_6H_2$, 1.11 mM $NaBH_4$ and different concentrations of PVP; a) 0.005 wt%, b) 0.05 wt%, c) 0.1 wt%, d) 0.2 wt%.

The nanoparticles were sized from the transmission electron micrographs using ImageJ. This procedure involved adjusting the brightness and contrast then applying a threshold to create a binary image. Finally the 'Analyse Particles' tool was applied to the binary image which provided particle areas. Particle diameters were calculated based on the equivalent circular diameter. From the transmission electron micrographs in Figure 4.5 nanoparticles around 1-3 nm are observed in all cases (Figure 4.6). This is similar to the 3 nm particles reported

by Horiuchi et al.[102] The size increases with decreasing concentration of PVP stabiliser. A coherent explanation for these results is derived from the current understanding of such nanoparticle synthesis in the literature as follows. As the same concentration of platinum salt is used in the synthesis, initially there will be the same amount of nuclei present. However aggregation and coalescence of these clusters is much faster and more efficient for lower concentrations of PVP, which results in a larger number of clusters forming each final particle, thus a smaller interfacial area being stabilised overall. Coalescence of initial clusters will be inhibited by a higher concentration of PVP and hence the final particle size will be smaller. When there is a lower ratio of PVP present there are less binding points from PVP molecules, so a decreased total interaction of PVP to the metal nanoparticles.

The TEM samples were taken two weeks after synthesis. Visually the dispersions appeared stable for months. This does not represent a quantitative proof of stability, however gives us a good indication whether the nanoparticles have aggregated enough to drop out of solution. As our aim is to reduce the amount of excess PVP in the dispersion going forward a minimal amount of PVP will be used.

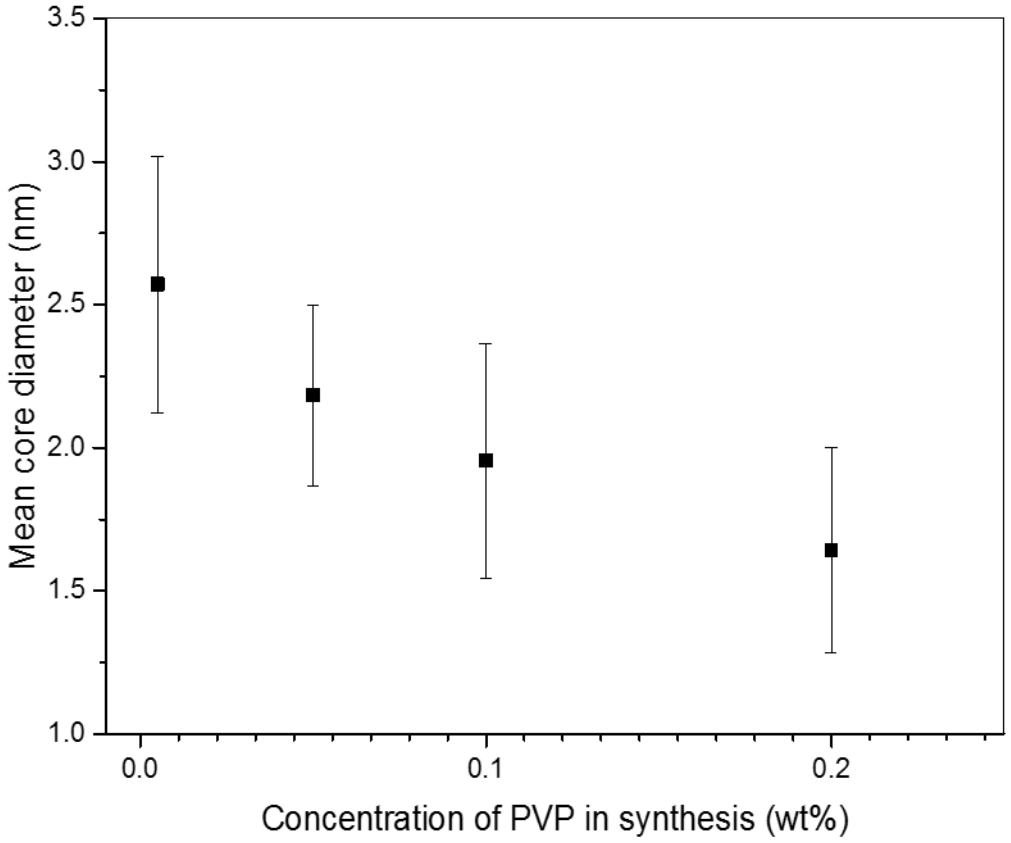

Figure 4.6: Mean core particle size obtained from ImageJ analysis at different concentrations of PVP used in synthesis (Numbers in brackets represent the coefficient of variation, CV (%)): (a) 0.005 wt% (17.4), (b) 0.05 wt% (19.3), (c) 0.1 wt% (20.8), (d) 0.2 wt% (21.8). Platinum salt and reducing agent concentration remained constant across different experiments (0.56 mM (0.023 wt%) $PtCl_6H_2$, 1.11 mM $NaBH_4$). Error bars represent the standard deviation of the mean.

4.2.4 Effect of varying concentration of platinum salt

In order to maximise the amount of Pt-PVP NP surface coverage at the oil-water interface the concentration of platinum salt in the nanoparticle synthesis was investigated. In order to reduce the excess PVP in the final nanoparticle concentration, a low concentration of PVP was used in this case. Based on the

previous study 0.0067 wt% was used as a slight increase on the minimum used in the previous study, to account for much higher ratios of platinum salt being used. The concentration of the reducing agent, sodium borohydride used was determined based on 2 x molar ratio of the platinum salt to ensure it was in excess, despite being stoichiometrically 1:1 (Equation 4.1) to try and reduce all of the platinum salt.

It has been previously proposed that increasing the concentration of H_2PtCl_6 in similar nanoparticle synthesis would result in larger nanoparticles.[230], [243] This is due to the proximity of nuclei to unreduced H_2PtCl_6 molecules being greater at higher concentrations. The probability of two particles aggregating in a collision process will increase with a higher concentration of platinum. The experimental results (Figure 4.7) agree with theoretical predictions and previous data from the literature. Visually in Figure 4.8 the particles appear slightly less spherical at higher concentrations of platinum. It is likely that with a higher ratio of platinum the initial formation of clusters is less well controlled as there is not sufficient PVP to well stabilise the smaller clusters, thus leading to less well controlled agglomeration of clusters. Borohydride is a strong reducing agent so will lead to fast reduction kinetics. In this set of experiments the ratio of reducing agent was kept constant with regards to the platinum salt concentration so changes will be predominantly due to the PVP: Pt-salt ratio.

As previously discussed, a low ratio of polymer to platinum core is desirable therefore using a high concentration of platinum is preferential. The ratio of polymer chains to Pt cores will increase for lower concentrations of platinum, which should allow for a better packing density at the oil-water interface so 0.23 wt% will be used from here on.

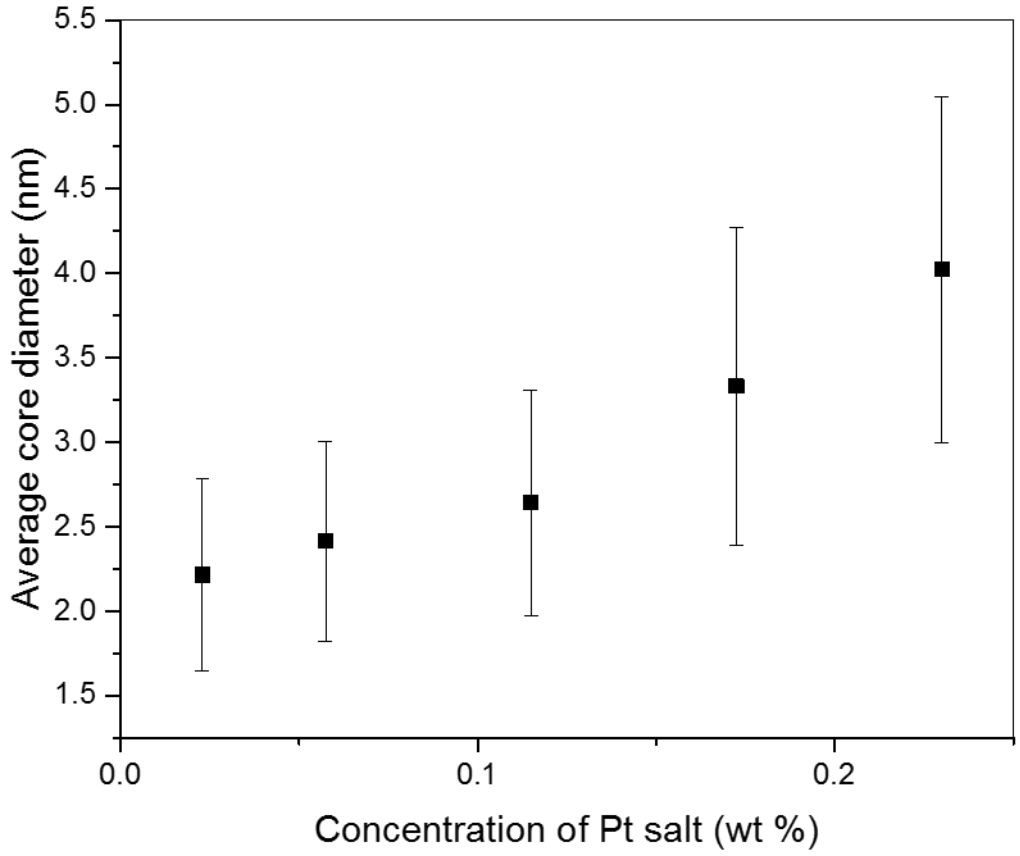

Figure 4.7: Mean core particle size obtained from ImageJ analysis of Pt NPs synthesised with 0.0067 wt% PVP and different Pt salt concentrations (Numbers in brackets represent the coefficient of variation, CV (%)); a) 0.023 wt% (25.7), b) 0.0575 wt% (22.9), (c) 0.115 wt% (25.2), d) 0.175 wt% (28.3), e) 0.23 wt% (25.5). A 2:1 molar ratio of $NaBH_4$ to Pt salt was used throughout. The error bars represent the standard deviation of the mean.

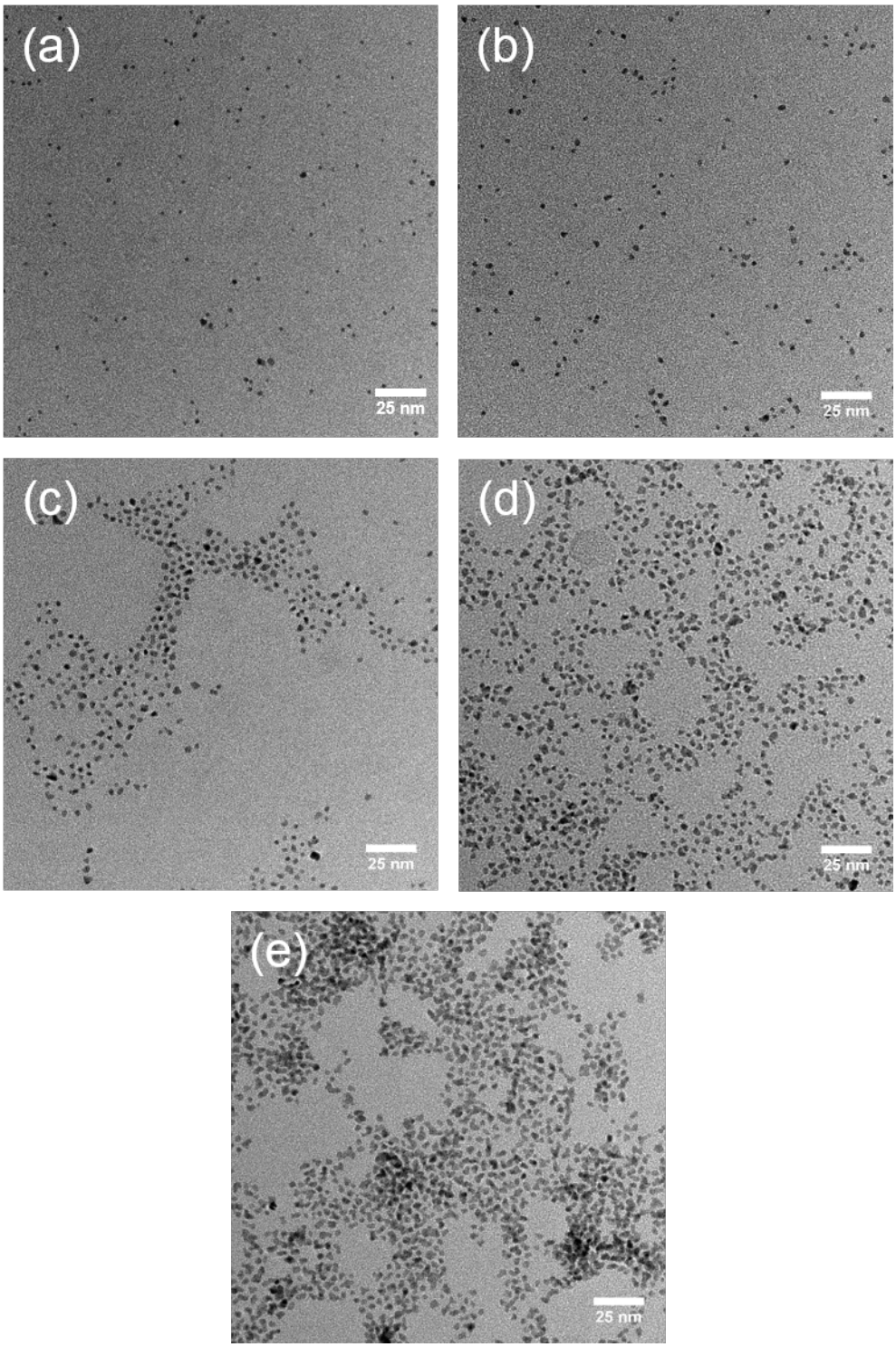

Figure 4.8: TEM micrographs of Pt NPs synthesised with 0.0067 wt% PVP and different Pt salt concentrations; a) 0.023 wt%, b) 0.0575 wt%, c) 0.115 wt%, d) 0.175 wt%, e) 0.23 wt%. A 2:1 molar ratio of $NaBH_4$ to Pt salt was used throughout. Scale bar = 25 nm.

4.2.5 Effect of varying concentration of reducing agent

It is beneficial to reduce as much of the platinum salt as possible in order to maximise the use of the material, which is expensive. Additionally, excess platinum in the continuous phase may cause unwanted side reactions. In order to ensure all of the platinum salt was reduced to platinum zero the effect of concentration of reducing agent used in the synthesis was investigated. Some studies have suggested that Pt-NPs formed in the initial stages of the reaction can catalyse the hydrolysis of sodium borohydride ions and therefore, a large excess of $NaBH_4$ (in Equation 4.1 there is a 1:1 ratio) is required to completely reduce the hexachloroplatinic acid.[243] Therefore the concentration of $NaBH_4$ was studied to try to maximise the amount of platinum salt being reduced to nanoparticles while still forming a stable dispersion. The platinum salt concentration was kept constant at 5.56 mM, as was the PVP concentration at 0.0067 wt %. The concentration of $NaBH_4$ was varied from 11.22 mM to 28.06 mM. This corresponds to a 1:2 ratio of Pt salt to $NaBH_4$ at the lowest concentration to a 1:5 ratio at the highest.

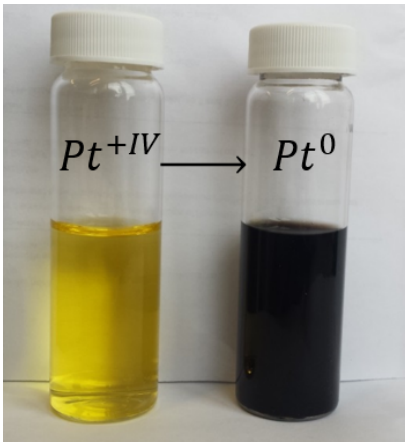

Figure 4.9: Right: platinum salt dissolved in PVP solution before the addition of reducing agent. Left: Pt-PVP NP dispersion.

During the reduction of the platinum salt (see Equation 4.1) a colour change from yellow to dark brown was observed (see Figure 4.9). This colour change is characteristic of the reduction of Pt(IV) to Pt(0). UV-vis spectroscopy can be used to study the transitions involved in the rearrangement of valence electrons

responsible for the colour change. The colour of metal salt solutions is dependent upon the metal, the metal oxidation state and the number of metal d-electrons. Colour in transition metal complexes arises from transitions in incompletely filled d-orbitals. The peak at 257 nm corresponds in this case to the absorption peak of the Pt (IV) species. The signal is due to the ligand-to-metal charge transfer transition of of $[PtCl_6]^{-2}$ ions. It can also be noted that a shift of the absorbance peak with the presence of PVP from ∼261 nm to ∼257 nm (Figure 4.10 (b)) confirms the interaction between the Pt ions and PVP. The ligand field splitting of the Pt 5d orbital expands the coordination of the N and/or O atoms of the PVP to the Pt^{4+} ions. This has been documented in the literature previously.[56], [147], [230] In addition to the UV-vis data, FTIR spectra were collected for PVP, H_2PtCl_6 in PVP and the Pt-PVP NPs. The FTIR peak of the amide C=O of pure PVP can be observed at 1652 cm^{-1}. A peak shift can be observed for the C=O peak of the polymer-salt to 1600 cm^{-1} suggesting that a complex is formed between the polymer and metal salt as the environment of the C=O bond has changed. Upon reduction of the metal salt and formation of the metallic platinum another peak shift to 1616 cm^{-1} can be observed. The red shift of the carbonyl frequency indicates the formation of a strong C=O-Pt bond. This supports the observations from the UV-vis of an interaction of the PVP with the metal salt and is also seen in literature.[239], [28], [29]

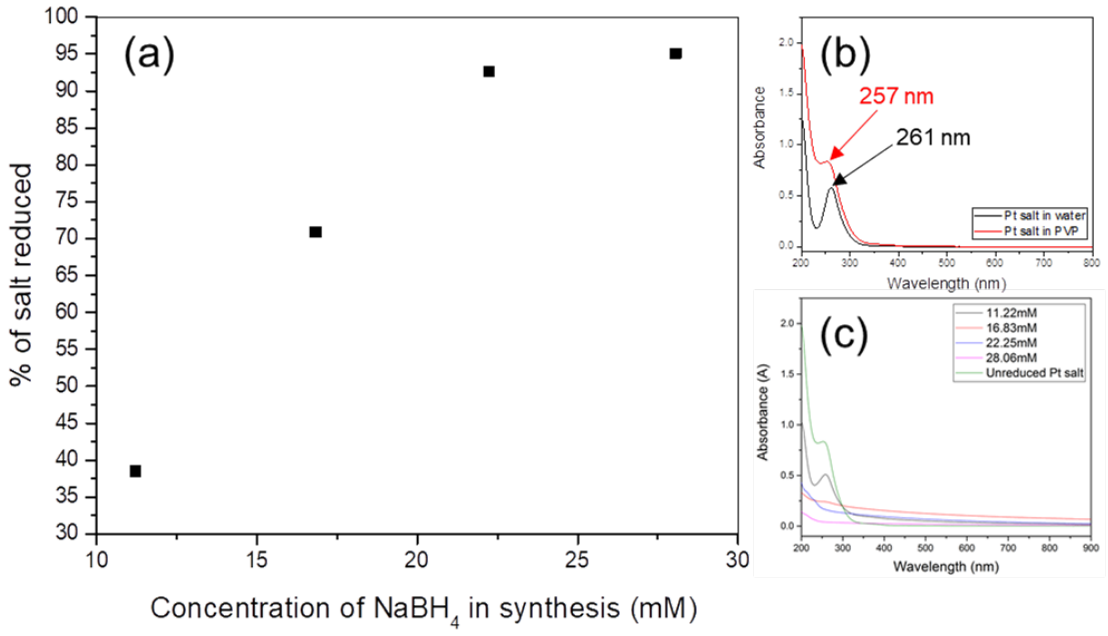

Figure 4.10: (a) Percentage of platinum salt reduced with different concentrations of reducing agent (from 11.22 mM to 28.06 mM), (b) absorption spectra for the unreduced platinum salt in water and the unreduced platinum salt in PVP, c) UV-vis spectra of platinum nanoparticles using different concentrations of reducing agent in the synthesis.

It can be observed that as the concentration of sodium borohydride is increased the Pt salt absorbance peak decreases and therefore a higher percentage of the salt is being reduced (Figure 4.10). Though the Pt salt peak completely disappears for 28.06 mM this produced an unstable dispersion as sedimentation could be observed in the sample vial. The TEM micrographs (Figure 4.11) also show larger, polydisperse aggregates compared to the samples where a lower concentration of reducing agent has been used. The TEM micrograph was taken a few days prior to the onset of the sedimentation, hence why even larger aggregates aren't present. Whereas for the other dispersions this was not evident. The explanation for this observation is that sodium borohydride is a very strong reducing agent[155], which leads to a fast reaction (which is accelerated with increase in concentration) where very small primary particles are produced. When

the platinum salt concentration is high, more interfacial area is created at the start of the process, which the PVP is unable to fully coat as its adsorption to the created surface is diffusion limited. This leads to a less stable, polydisperse dispersion as these primary particles have a tendency to aggregate into larger secondary particles. Additionally with higher concentrations of $NaBH_4$ there will be an increase in the amount of BH_4^- converted to $B(OH)_4^-$ which may cause destabilisation due to change in the surface chemistry of the particles.[259] In order to establish whether the instability is due to an increase in surface area and insufficient stabiliser or destabilisation due to change in surface chemistry of the particles further experiments would need to be carried out with higher concentrations of PVP.

In order to reach a compromise between stability and efficiency of the process the work from now on uses 22.25 mM $NaBH_4$ in the synthesis.

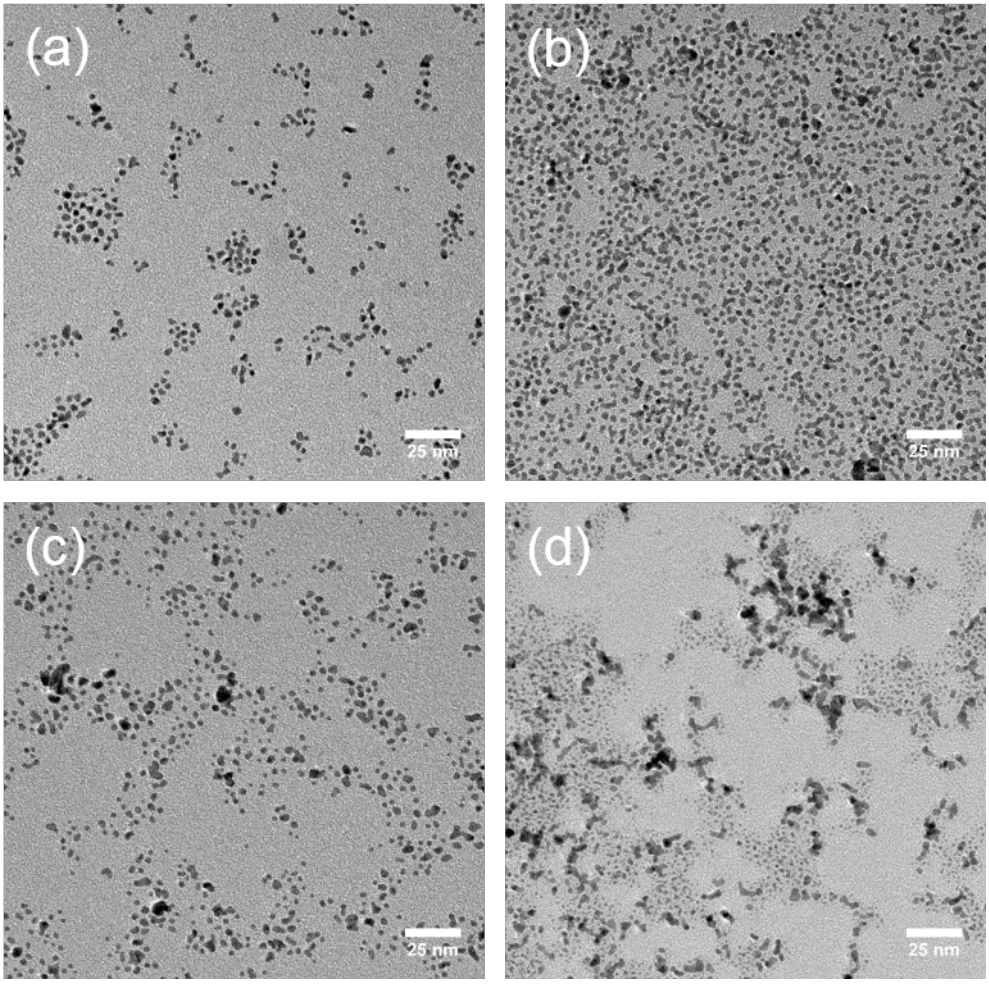

Figure 4.11: TEM micrographs of NPs synthesised with 5.56 mM (0.23 wt%) $PtCl_6H_2$, 0.0067 wt % PVP and different concentrations of $NaBH_4$; a) 11.22 mM, b) 16.83 mM, c) 22.35 mM, d) 28.06 mM.

4.3 In depth characterisation of optimised particles

The previous experiments have gone some way to optimise the nanoparticles for their use as catalytic emulsifiers. This section will examine the structure of the particles produced with the chosen synthesis conditions in more detail. The

particles studied here are made with 0.23 wt% $PtCl_6H_2$, 0.0067 wt% PVP and 22.25 mM $NaBH_4$. This produces particles with a Pt core diameter of 3.3 ± 1.0 nm as seen below in Figure 4.12.

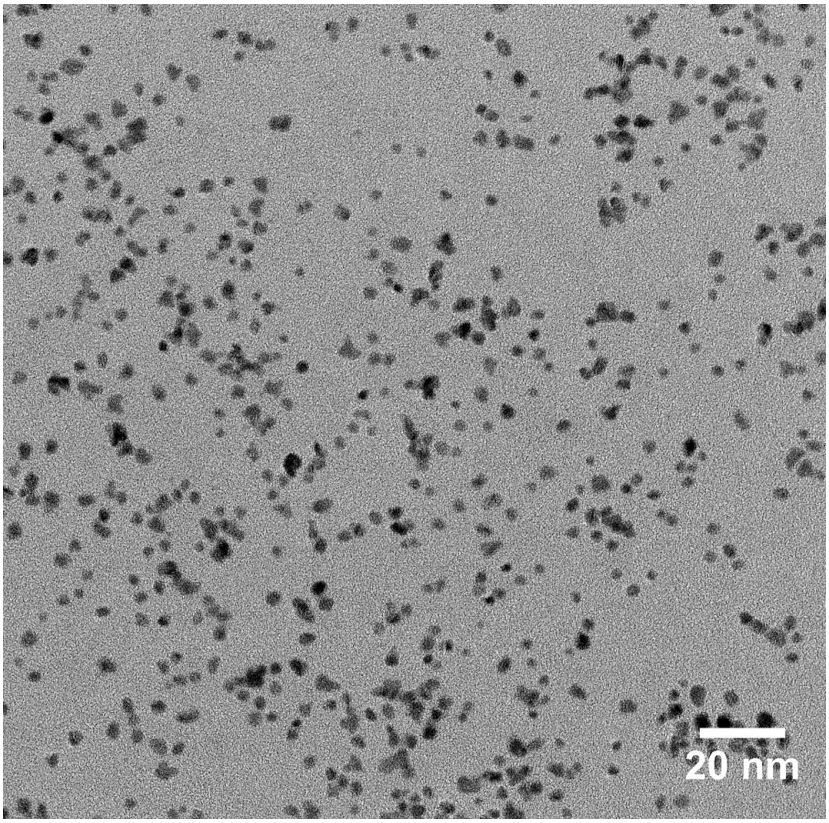

Figure 4.12: TEM micrograph of PVP stabilised Pt NPs synthesised with the following synthesis conditions: 5.56 mM (0.23 wt%) $PtCl_6H_2$, 0.0067 wt% PVP and 22.25 mM $NaBH_4$.

4.3.1 Electron microscopy techniques

Scanning transmission electron microscopy (STEM) is a type of transmission microscopy where unlike conventional TEM the electron beam is focussed on a fine spot which is then scanned over the sample in a raster, making it suitable for analytical techniques such as energy dispersive x-ray spectroscopy (EDX). EDX spectroscopy is a method used to identify the composition of a material using

x-ray excitation. It is able to characterise materials as each element has a unique atomic structure leading to unique electromagnetic spectrum peaks. In this case the EDX was carried out while the samples were being imaged by HAADF-STEM (High-angle annular dark-field scanning transmission electron microscopy)(Figure 4.13). The technique can also provide spatial distribution of elements through mapping. STEM microscopes can raster the beam over the sample to create a variety of transmitted electron images as well as x-ray maps. The individual elements can be identified and assigned a colour to differentiate them (Bottom right Figure 4.13). As can be seen in the spectrum in Figure 4.13 platinum exhibits three peaks. The other elements present are copper, oxygen and silicon which all originate from the TEM grid.

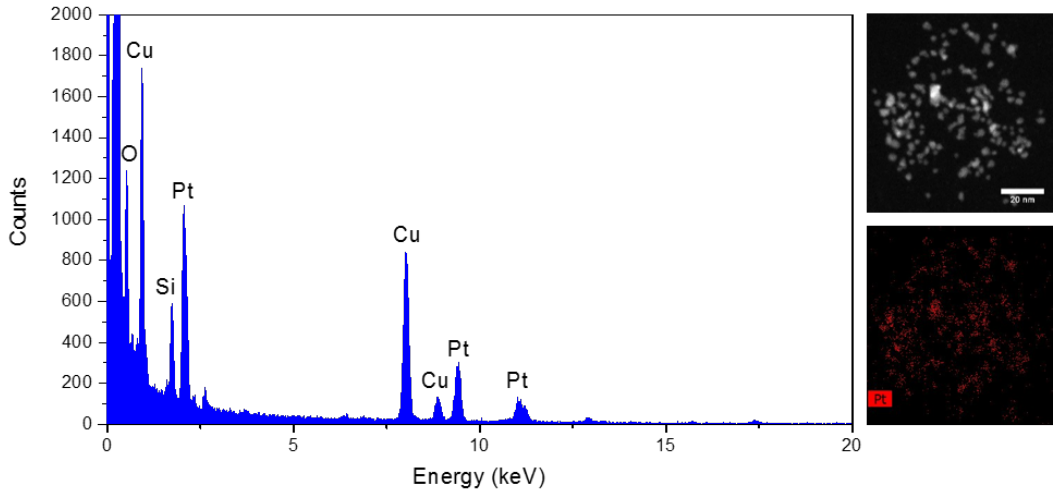

Figure 4.13: EDX spectrum imaged from HAADF-STEM. Top right HAADF-STEM image, bottom right corresponding false colour image showing Pt. Particles prepared under the following synthesis conditions: 5.56mM (0.23 wt%) $PtCl_6H_2$, 0.0067 wt% PVP and 22.25 mM $NaBH_4$.

From high resolution TEM (HRTEM) the crystalline microstructure of the nanoparticles can be determined. Selected area electron diffraction (SAED) patterns give information on the lattice structure of the nanoparticles (Figure 4.14.

The rings correspond to lattice parameters of platinum. Spots can be observed which correspond to a crystalline material. The radius of the diffraction rings is related to the miller indices that represent the crystallographic planes. The rings correspond to the {111}, {200}, {220} and {311} planes which represent a face-centred cubic (FCC) structure. This structure is well documented for platinum.[246], [32], [42]

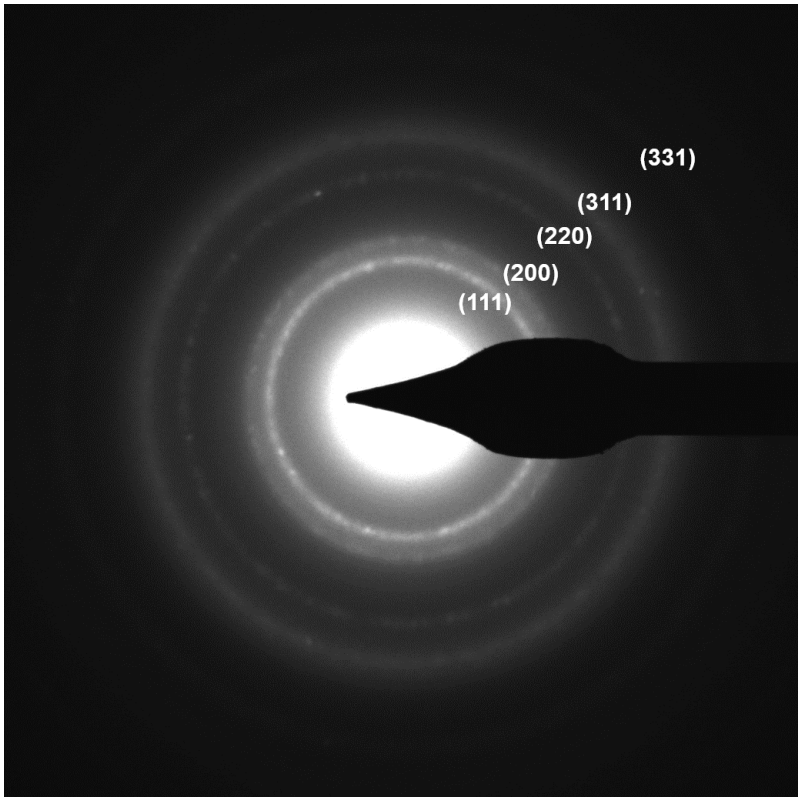

Figure 4.14: SAED diffraction pattern of platinum nanoparticles (NPs prepared with 5.56 mM (0.23 wt%) $PtCl_6H_2$, 0.0067 wt% PVP and 22.25 mM $NaBH_4$.)

HRTEM allows us to measure the interplanar spacing (d-spacing). The lattice image in Figure 4.15 (a) shows a d-spacing of 0.23 nm which corresponds to the Pt{111} plane. In Figure 4.15 (b) an interplanar spacing of 0.20 nm can be observed as it is orientated down a different zone axis. This corresponds to the Pt{200} plane. These values fit well with standard literature values[42], [57], [246]. The selected area diffraction pattern is over a larger area so will contain multiple

crystallites at different orientations, whereas these high magnification images are showing one crystal at a particular orientation.

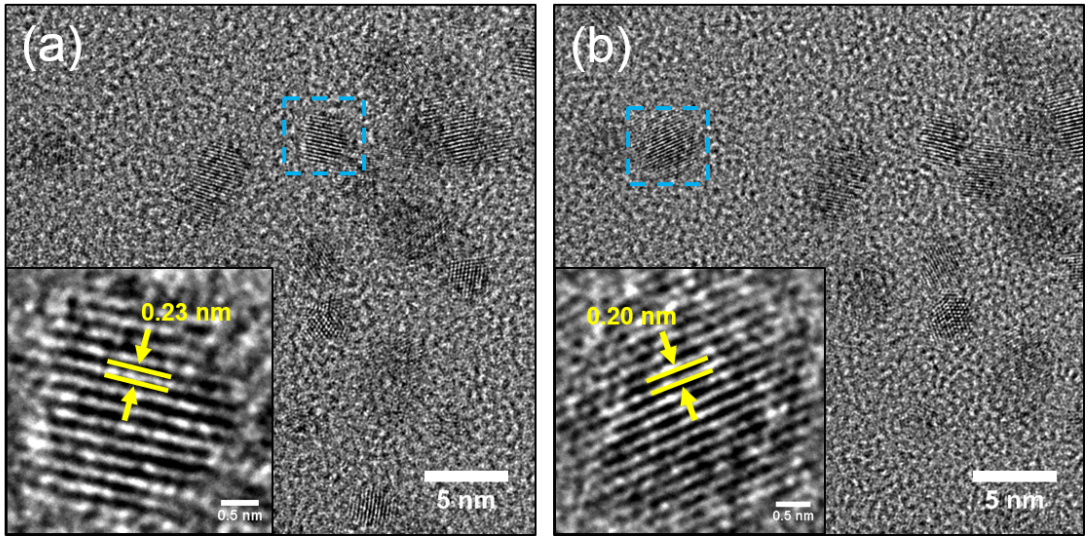

Figure 4.15: HRTEM micrographs of Pt-PVP NPs with insets showing lattice spacings of (a) 0.23 nm and (b) 0.20 nm. Both NP dispersions (a) and (b) were prepared with 5.56 mM (0.23 wt%) $PtCl_6H_2$, 0.0067 wt% PVP and 22.25 mM $NaBH_4$.

On the high resolution TEM particles that may appear to be larger NPs are in fact clusters of smaller NPs (Figure 4.16) as seen by the individual lattice patterns can be observed. This could be due to the way in which the particles dried on the TEM grid. It is also possible that the particles are aggregated in the suspension however no sedimentation is observed over several months. If there were aggregates present it would be likely that they would increase over time.

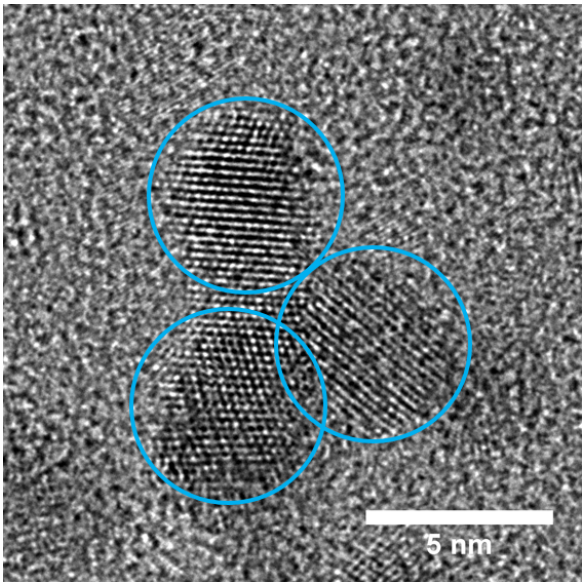

Figure 4.16: a) Lattice image of Pt-NPs showing individual particles (NPs prepared with 5.56 mM (0.23 wt%) $PtCl_6H_2$, 0.0067 wt% PVP and 22.25 mM $NaBH_4$.)

4.4 Conclusion

PVP stabilised platinum particles were successfully stabilised via the reduction of hexachloroplatinic acid hydrate with sodium borohydride. These particles were chosen for their ability to act as a catalyst for metal film growth via electroless deposition. Control over size was demonstrated by varying the ratio of stabilising agent to metal salt in the synthesis. As the aim was to use these particles as emulsifiers at an oil-water interface it was important that the amount of stabiliser was minimised in order to get a good coverage at the interface to facilitate even metal film growth. This was achieved by obtaining a stable dispersion using a ratio of 0.23 wt% : 0.0067 wt% of platinum salt: PVP. This is a drastically reduced amount of PVP compared to literature values.[102], [243] The amount of reducing agent was optimised to account for the catalytic breakdown of the sodium borohydride by the platinum microcrystals to that the maximum amount of platinum nanoparticles were produced. It was found that a 1:4 ratio (5.56 : 22.25 mM) of

platinum salt to sodium borohydride was most suitable as most of the platinum was reduced without compromising the stability. Higher amounts of $NaBH_4$ led to unstable dispersions. The overall method developed here has allowed us to synthesise NPs with a low excess of PVP in the continuous phase and the following chapter will go on to test how well these particles adsorb at the oil water interface.

Chapter 5

Characteristics of nanoparticle film at oil water interface

5.1 Synopsis

This chapter focuses on characterising the nanoparticles at the oil-water interface and on examining their viability as nano-Pickering emulsifiers for the oil droplets. The interfacial properties of the particles are characterised by pendant drop tensiometry and interfacial rheology. Additionally, techniques such as cryo-SEM and cryo-TEM will be used to directly visualise the nanoparticles on the droplet surface.

5.2 Interfacial tension

Interfacial tension (IFT) is a result of cohesive forces between two immiscible liquids. It can be described as the amount of energy required to increase the interface by one unit area of interface between two immiscible liquids, hence the units of Newtons per meter (Energy = N·m, Area = m^2 therefore Energy/Area = N·m/m^2 = N· m^-1). Determination of the IFT allows us to make deductions about the adsorption and desorption of surface active solutes as adsorbed species will decrease the interfacial tension by reducing the number of interactions between the immiscible liquids.[21] The presence of emulsifiers, such as surfactants

or polymers, at the oil-water interface can therefore lower the interfacial tension, and hence lower the amount of energy required to create more surface area, as droplet break up is facilitated when interfacial tension is low.

It is known that nanoparticles with suitable wettability and diameter will strongly adsorb at a liquid-liquid interface as this process lowers the total system energy. However, there is still no consensus on whether the adsorption of nanoparticles at the interface affects the interfacial tension.[76],[162] In some cases there is a dependence on the assembly at the interface[185] or surface chemistry of the particles including factors such as surface charge[217] as to the resulting measured IFT. Sometimes particles are found to decrease the IFT[93], though in some cases there is no significant impact.[247] However, when a significant reduction in interfacial tension is observed in previously published work on particle-stabilised interfaces, the effect is generally explained by the propensity of the particles to adsorb at the interface and their resulting adsorption energy at the interface.[76]

In the case of the Pt nanoparticles developed in this thesis for emulsion stabilisation, interfacial tensions of the NP aqueous suspensions with hexadecane were measured using a pendant drop tensiometer. The technique involves measuring the outline of the droplet and iterative fittings of the Young-Laplace equation to the recorded shape, as explained in the corresponding methodology in Chapter 3. The IFT of the droplets were measured over time to ensure equilibrium had been reached. IFTs were measured over 12,000 s in a covered cuvette, maintaining a constant temperature and humidity. Though in the emulsion the NPs are in the continuous phase, theoretically the IFT should be the same in both w/o drop or o/w drop. Due to the opacity of the Pt-PVP NP dispersion, hexadecane was used as the continuous phase for these measurements so that the drop outline could be distinguished accurately. When carrying out the measurements it was crucial that the droplet size was large enough to ensure that gravitational effects were non-negligible as this can lead to false fitting of the recorded droplet shape. Indeed the corresponding model relies on the influence of gravity forces on the droplet to balance interfacial tension.[21]

IFT measurements of water in hexadecane were first carried out and compared against literature values[138] to ensure that accurate readings could be obtained. The interfacial tension of hexadecane was found to be $\sim$49 mN m^{-1} and was

stable over a period of 30 minutes, indicating no significant polar impurities in the water or hexadecane. Subsequently, IFT measurements for PVP solutions in hexadecane and aqueous suspensions of the Pt-PVP nanoparticles with PVP in hexadecane were conducted. PVP solutions were added to Pt-PVP NPs after particle synthesis and the overall concentration compared to PVP solutions of the same concentration in the absence of the nanoparticles. The nanoparticles used were those described at the end of Chapter 4 (synthesised with the following reactant concentrations: 5.56 mM (0.23 wt%) $PtCl_6H_2$, 0.0067 wt% PVP and 22.25 mM $NaBH_4$)

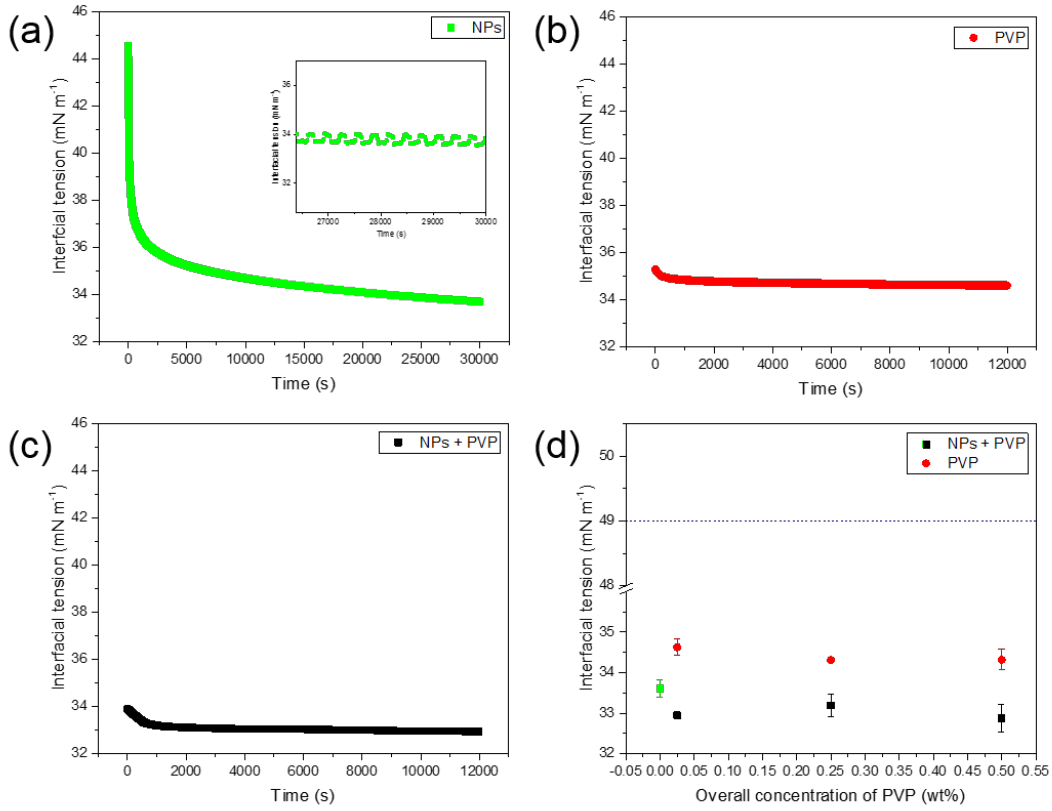

Figure 5.1: Interfacial tension as a function of time for; (a) NPs in hexadecane (inset shows last 3600 s), (b) PVP in hexadecane, (c) NPs + PVP in hexadecane. (d) Interfacial tension as a function of overall PVP concentration. Average from measurements over last 3600 s. The blue line represents the interfacial tension of hexadecane in water. The value at zero for NPs + PVP (green square) corresponds to the nanoparticles in the absence of excess PVP.

As can be seen from Figure 5.1 (d) that the presence of PVP lowers the interfacial tension compared to hexadecane in water as expected due to the polymer penetrating the interface and relaxing to maximise surface contact. However, an increase in PVP concentration does not lead to a decrease in interfacial tension as would be expected for a polymeric emulsifier, as emulsifier concentration is above the interface saturation concentration in this case. Literature values for

PVP show no change in surface tension over a wide range of concentrations and PVP molecular weights. Though there are some deviations at high concentrations of PVP, these are above the concentrations used in these experiments.[97], [27], [84] This cannot be directly correlated to the interfacial tension in this case, however it is clear the PVP has a limiting effect on the extent that it can reduce the interfacial tension, which is independent of PVP concentration. The nanoparticles in the absence of any excess polymer also exhibit a decrease in interfacial tension similar to that of the PVP. As the surface of the nanoparticles is stabilised by PVP a similar reduction in IFT might be expected. Reduction of IFT with polymer stabilised particles has been documented in literature by Alvarez et al. who investigated 20 nm silica nanoparticles grafted with poly(2-(dimethylamino)ethyl methacrylate) at both the xylene-water and air-water interface. They attributed the reduction in IFT to the polymer on the particles relaxing to a flatter conformation and hence maximising the surface contact.[5] Isa et al. also observed a reduction in IFT in the presence of nanoparticles with a PEG-shell at the n-decane/water interface.[112]

The dispersions containing both nanoparticles and excess PVP have a slightly lower IFT than the PVP in hexadecane. One possible reason for this is that when the free PVP adsorbs at the interface it relaxes and expands, whereas the PVP stabilising the NPs is not able to do so to as great an extent. Therefore it is possible that the combination of the polymer and nanoparticles leads to a denser layer at the interface. Compared to the PVP, the nanoparticles take a much longer time to reach equilibrium, as illustrated in Figure 5.1 (a) and (b). Additionally when PVP is added to the NP dispersion the kinetics are much more similar to the PVP on its own (Figure 5.1 (c)). This would suggest that the PVP is diffusing to the interface quicker. These results illustrate that any free PVP will be competing with the Pt nanoparticles required at the interface for the subsequent electroless deposition process, for the oil-water interface. Additionally, the dispersions containing nanoparticles and PVP have a lower IFT in hexadecane that the NPs on their own. Free PVP is able to rearrange more easily than the NPs at the interface and has a poor interfacial interaction (it only decreases the IFT by a relatively small amount compared to a surfactant). Therefore in the dispersion with NPs and PVP, the PVP may be able to fill gaps in the NP

interfacial layer and hence lower the IFT. This could be further studied by SANS and SAXS.

5.3 Interfacial rheology

Rheology is the study of flow and deformation of materials under applied forces. Generally, rheometers measure two parameters; stress and strain, where stress is the amount of force per unit area applied to the sample and strain is the degree to which a material deforms after the application of stress[41]. Bulk rheology deals with the 3D structure of materials and can for example be applied to the structuring of particles in suspensions. Materials can be divided into three categories with regards to rheological behaviour; viscous, elastic and viscoelastic. In elastic materials, deformation reverses spontaneously when an applied force is removed. In this case, energy is stored by the system and then released. In viscous materials, deformation ceases when the applied force is removed. Here energy performs work on the material to deform it without the material being able to regain its original shape.

The classic theory of elasticity deals with the mechanical properties of elastic solids in accordance with Hookes Law, where stress is directionally proportional to strain in deformations but is not dependent on the rate of strain. The theory of hydrodynamics deals with viscous liquids, which is in accordance to Newtons Law, whereby the stress is directly proportional to the rate of strain but independent of the strain itself. Viscoelastic materials exhibit both elastic and viscous behaviour.[174], [78]

Rheology allows us to determine both the relationship between viscoelastic properties and structure of the material and the relationship between stress, deformation and time. Predicting the rheological behaviour of colloidal dispersions can be challenging due to various factors that must be considered. Non-Newtonian effects can be observed due to interactions between the dispersed particles. As a result, predictive theories must consider the effect of colloidal forces on the spatial arrangement of the particles and must also take into consideration the effect of colloidal forces on the spatial arrangement in the externally applied flow field.[19]

Interfacial rheology involves the study of the two-dimensional systems formed at interfaces. Interfacial rheology (flow in two-dimensions) can be considered analogous to rheology (flow in three-dimensions).[195] The particle structuring, mentioned for bulk systems, which influences the response of the system to the stress applied, also exists when the particles are at a 2D interface. The deformation at the interface and the stresses exerted on it can be studied in a similar way. Rheometric measurements usually consist of strain or stress analysis at constant frequency in combination with frequency analysis. Such measurements typically give a complex shear modulus $G^*(\omega)$, where (ω) is the angular frequency, as an output. Subsequently this can be divided into component parts corresponding to the elastic and viscous contributions of the materials tested to their response to applied stress. The storage modulus, $G'(\omega)$, is a measure of the energy stored during a strain cycle, the real part of the complex shear modulus. It is also referred to as the elastic modulus. The loss modulus, $G''(\omega)$ is a measure of the energy lost during the strain cycle, the imaginary part of the complex shear modulus. It is also referred to as the viscous modulus. These are related by Equation 5.1.[41],[31]

$$G^*(\omega) = \frac{\sigma_s}{\varphi_0} e^{i\delta(\omega)} = G'(\omega) + iG''(\omega) \tag{5.1}$$

Where σ_s is the amplitude of the applied sinusoidal stress with frequency ω and φ_0 is the amplitude of the resultant strain at the same frequency ω that lags the stress by a phase angle $\delta(\omega)$.

In these experiments, interfacial rheology of the system was measured over time using a double wall ring (DWR) geometry at the oil-water interface. The DWR geometry is specifically designed for interfacial measurements and is detailed further in Chapter 3.3.2.2. The nanoparticles used here were synthesised with 5.56 mM (0.23 wt%) $PtCl_6H_2$, 0.0067 wt% PVP and 22.25 mM $NaBH_4$ as concluded at the end of Chapter 4 to be optimal for emulsification. The nanoparticle 2D film was prepared in situ as follows; the aqueous nanoparticles (the dense phase) were loaded into the channel up to the step in the wall. The DWR geometry was flame cleaned and positioned to pin the air-water interface. Finally a

layer of hexadecane was deposited on top carefully so not to disrupt the liquid-liquid interface. The temperature of the interface was maintained at 20.5 °C. Forming this oil layer allows us to study the oil-water interface, rather than the bulk properties. This will relate to the particle adsorption at the droplet surface during emulsification. Additionally the layer of oil on top prevents the evaporation of the aqueous phase which allowed us to study the system over long periods of time. Strain amplitude sweep experiments were conducted in oscillation mode at a fixed angular frequency (ω = 0.5 rad$\cdot s^{-1}$) and the strain was varied from low to high and correspondingly the stress was changing. The strain sweep corresponds to progressively increasing the deformation in the system and monitoring the effect this has on the complex modulus monitored in the measurement. As the experiments were carried out in the linear region the structure of the film was not disturbed by the shear stress, thus droplets were not formed at the interface. Measurements were taken over several days, and stress was applied to the dispersion each time when the measurement was taken. The lag between the strain measured and the stress applied is characteristic of the storage (elastic) and loss (viscous) and moduli.

Figure 5.2 shows the storage modulus (a) and loss modulus (b) over a range of oscillation strains at different times. Figure 5.3 shows the change in storage modulus, $G^{'}$, and loss modulus, $G^{''}$ over time for a specific oscillation strain. Over time an increase in both the loss and storage modulus can be observed. An increase in the storage modulus relates to an increase in elasticity, which is a result of film build up at the interface. $G^{'}$ dominates over $G^{''}$ which demonstrates that the film exhibits an elastic behaviour as the film is able to store energy and return to it's initial configuration to some extent after the application of stress. The increase in elasticity may relate to an increase in Pt-PVP NPs at the interface over time and the formation of a network of particles, possibly with an entanglement of the polymer stabilisers in between adjacent nanoparticles. This evidences that the particles are indeed adsorbing to the interface and forming a robust film, as these elastic responses would not be observed otherwise.

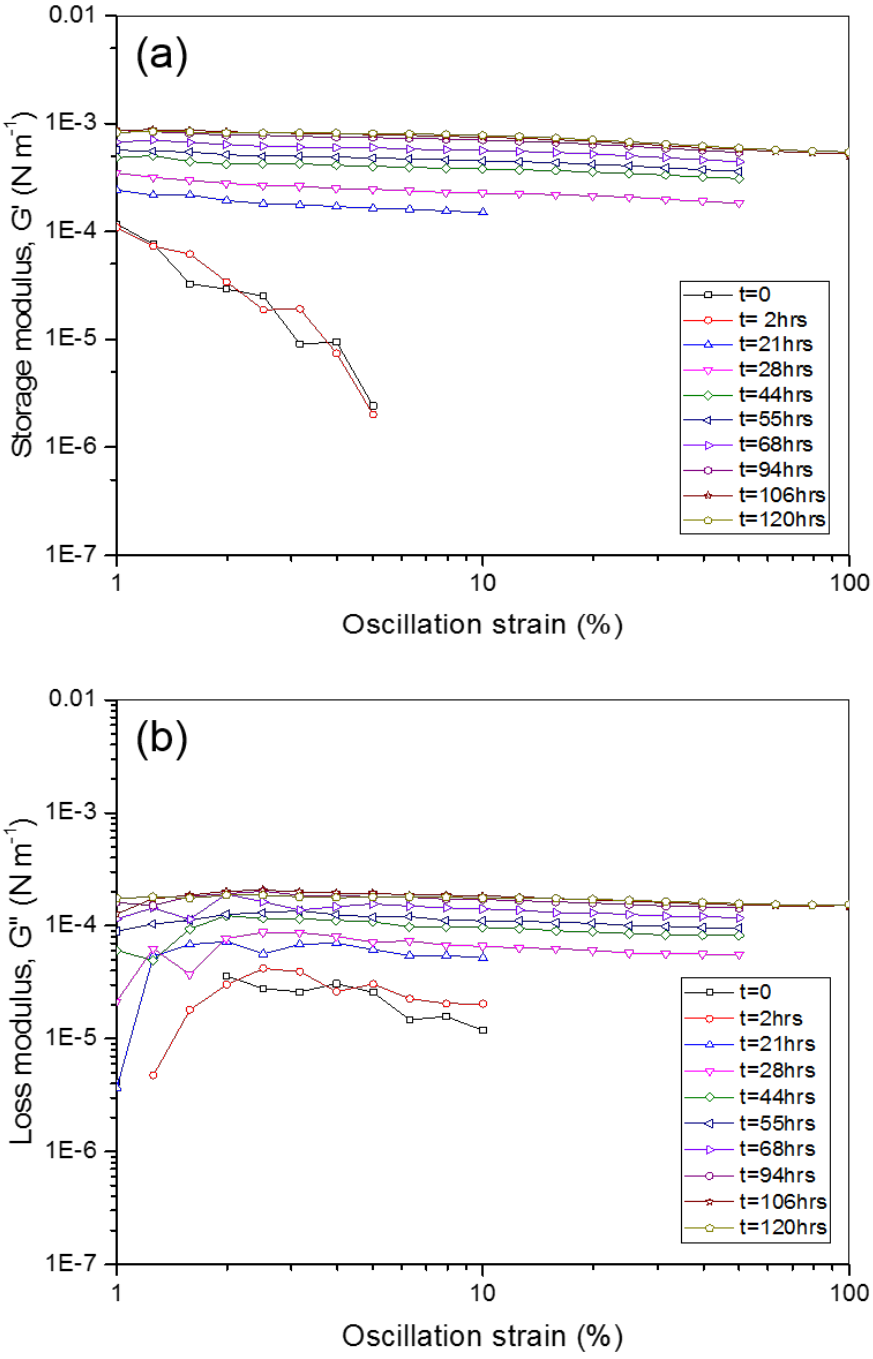

Figure 5.2: (a) Storage modulus, G', and (b) loss modulus, G'', over changing oscillation strain.

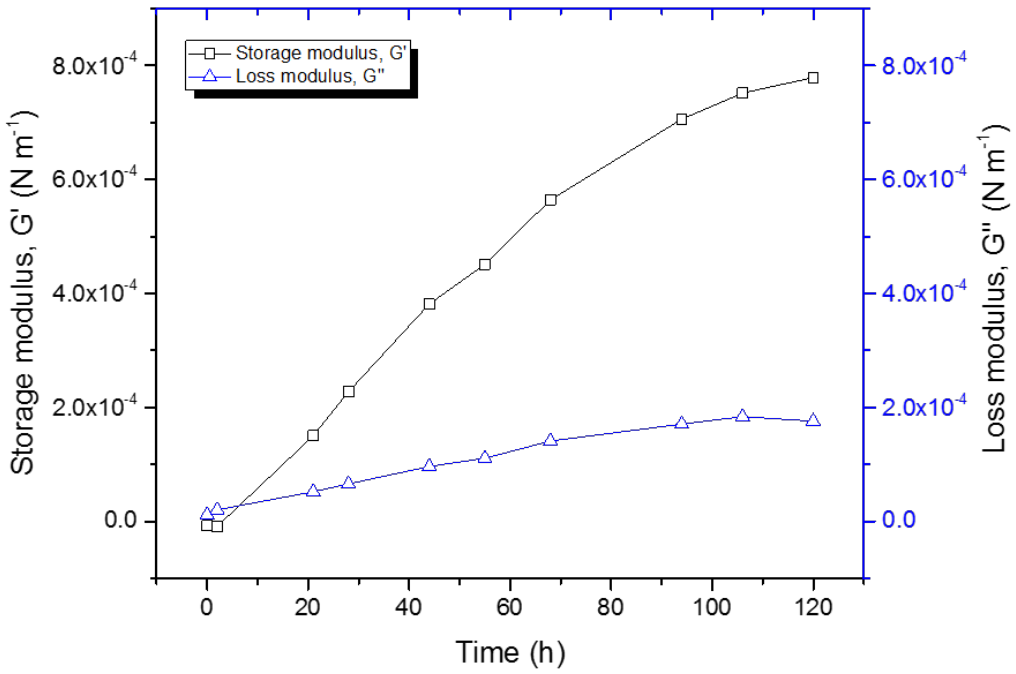

Figure 5.3: Storage modulus, G′, and loss modulus, G″, over time at oscillation strain = 10%.

Figure 5.3 shows the storage and loss modulus over time. The initial film (t=0) does not exhibit this elastic behaviour as G″ is slightly higher than G′. Additionally the storage modulus in Figure 5.2 (a) is not linear across the oscillation strain range for t=0 and t = 2 hrs. This demonstrates that the film is weak at this point. The particle film appears weaker at the beginning and builds over time. An increase in elasticity results from specific interactions leading to the particles strongly interacting with each other, in this case it is driven by interactions between adjacent polymer stabilisers on the surface of neighbouring particles. Here the solvency of the water phase for the polymer plays an important role in this process and is influenced by the electrolyte concentration of the suspension. Further rheological experiments would need to be carried out to determine the extent of the effect of electrolyte concentration on the film formation.

Because the focus of this thesis was on developing a method for deposition of an impermeable metal film on the surface of emulsions, several desired experiments to elucidate the behaviour and interactions of these nanoparticles at the oil-water interface were not conducted and will form the basis for future experiments in the research group. In anticipation of these results it might be expected that the elasticity would increase with increasing electrolyte concentration as PVP would have a decreased solvency for the bulk and hence polymer entanglement would be facilitated.

5.4 Visualisation of the Pt-PVP NP films at the oil-water interface

5.4.1 Cryo-SEM

In order to ensure that the secondary metal film deposition onto the surface of the droplets is successful, it is necessary to ensure the catalytic Pt nanoparticles form a strong, complete film on the droplet surface. Thus, observation of the nanoparticle film is an important step towards ensuring that an impermeable film can be successfully built on the surface of the droplet aimed to be encapsulated. Here, in addition to observing a drastic reduction in turbidity of the aqueous phase during emulsification (Figure 5.4) further evidence that the particles are adsorbing at the oil water interface can be obtained from EDX analysis on a sample observed under cryo-scanning electron microscopy (cryo-SEM). This allows us to observe the chemical composition of the adsorbed interfacial film without the droplets completely collapsing in the vacuum chamber of the electron microscope (Figure 5.5). The image has been taken in secondary electron mode which provides information on the surface and topological characteristics. Secondary electrons are emitted by atoms near the surface which leads to high resolution.

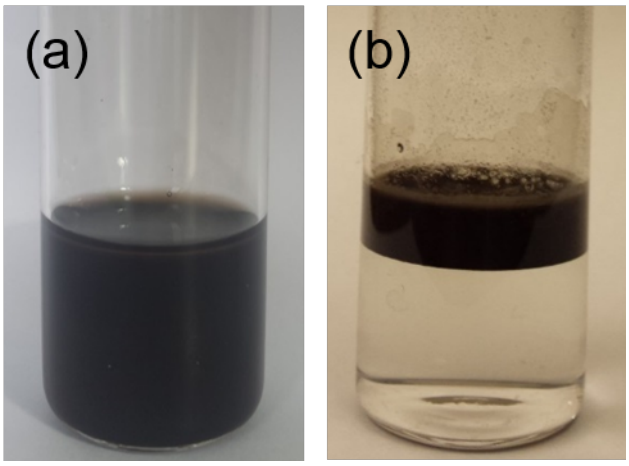

Figure 5.4: (a) Pt NP dispersion with layer of hexadecane before emulsification, (b) corresponding emulsion after homogenisation on ultrasonic processor. The emulsion has formed a cream layer due to hexadecane having a lower density than water.

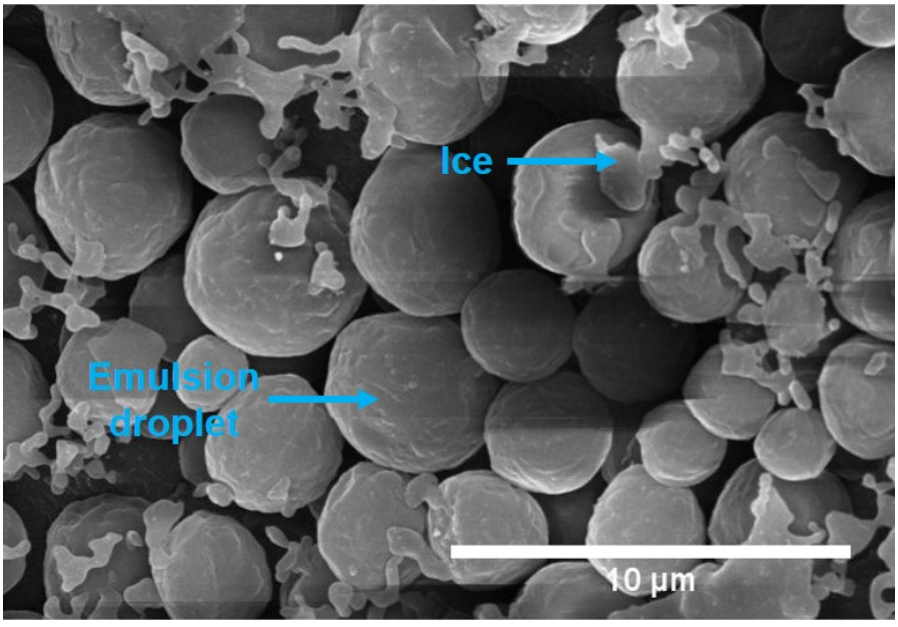

Figure 5.5: Cyro-SEM micrograph of Pt-PVP stabilised HD emulsion.

As can be observed in Figure 5.5 there is some wrinkling apparent on the

frozen droplet surface, which may be due to vacuum effects or slight changes during the freezing process. The non-spherical shapes are thought to be water (as labelled in Figure 5.5). Figure 5.6 shows a false coloured EDX map, where the red colour, representative of the presence of platinum is mainly situated on the surface of the observed droplets. Analysing the EDX further, it is clear that the oxygen in the sample appears to be present on the droplet interface, which is likely to be due to the presence of PVP. There is also a high concentration of carbon (Figure 5.6 (d)), which will be mainly derived from the hexadecane core. Additionally there will be some carbon from the PVP. The nitrogen present at the interface is due to the pyrrolidone moiety in the PVP. The high presence of O (and lack of Pt and C) in the non-spherical shapes back up the hypothesis that they are ice.

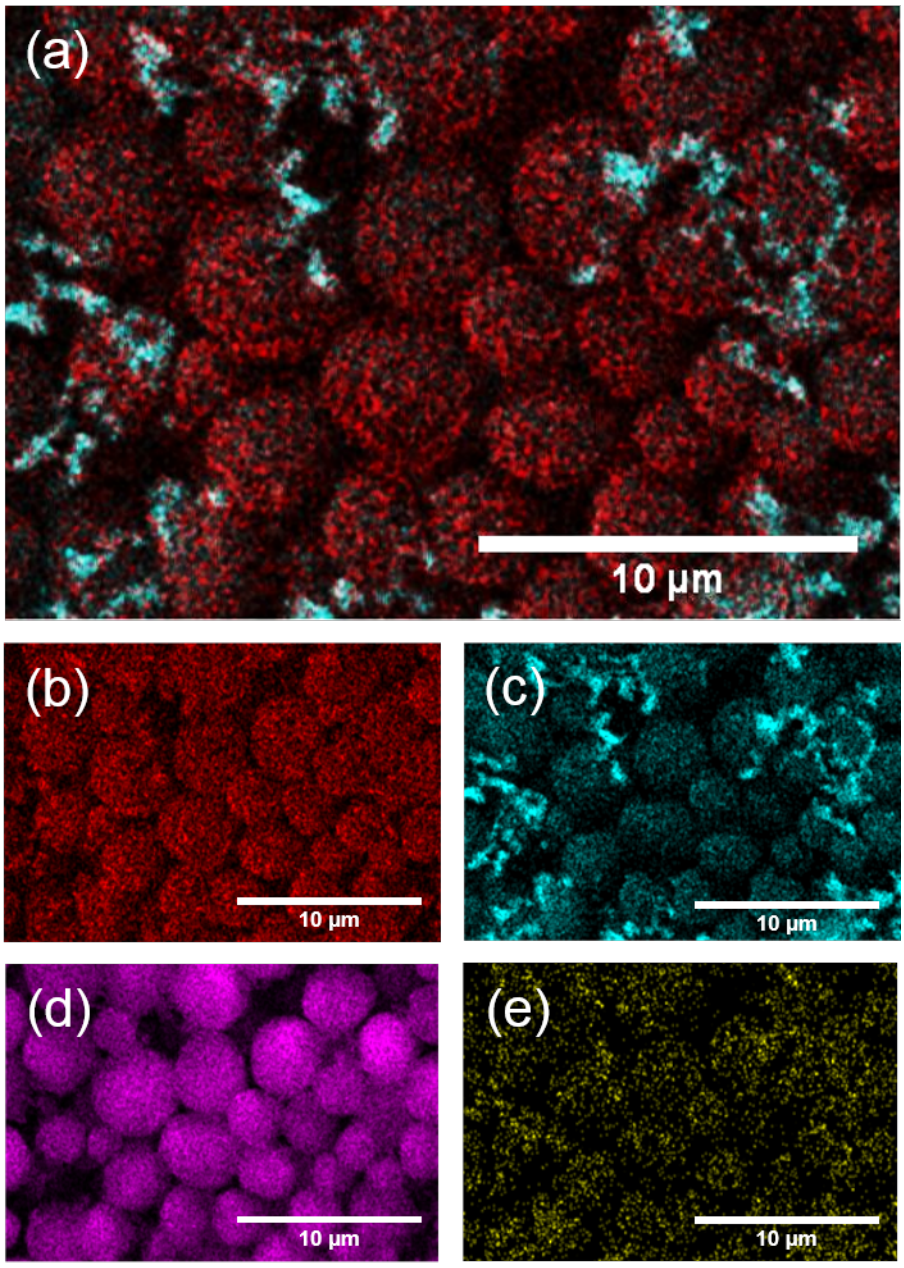

Figure 5.6: Cyro-SEM micrograph with EDX mapping. EDX false colour of (a) overlay of Pt and O, (b) Pt - red (Pt Mα map), (c) O - blue (O Kα map), (d) C - pink (C Kα map) and (d) N - yellow (N K α map)

5.4.2 TEM & Cryo-TEM

Drop casts of the emulsion droplets were observed on TEM. Here the emulsion droplets collapsed upon drying and the resulting 2D structures were imaged. The resulting 'deflated' droplet shapes could distinctively be observed, where the particle film is seen to buckle and fold, demonstrating the robustness of the particle film upon drying. This correlates observations made in the interfacial rheology experiments about the presence of a robust, entangled particle film at the interface. Here the particles seem closely packed, though as the droplets are collapsed both sides of the droplet can be observed. The particles in the background are most likely fragments of larger droplets, which are less structurally stable than the smaller ones.

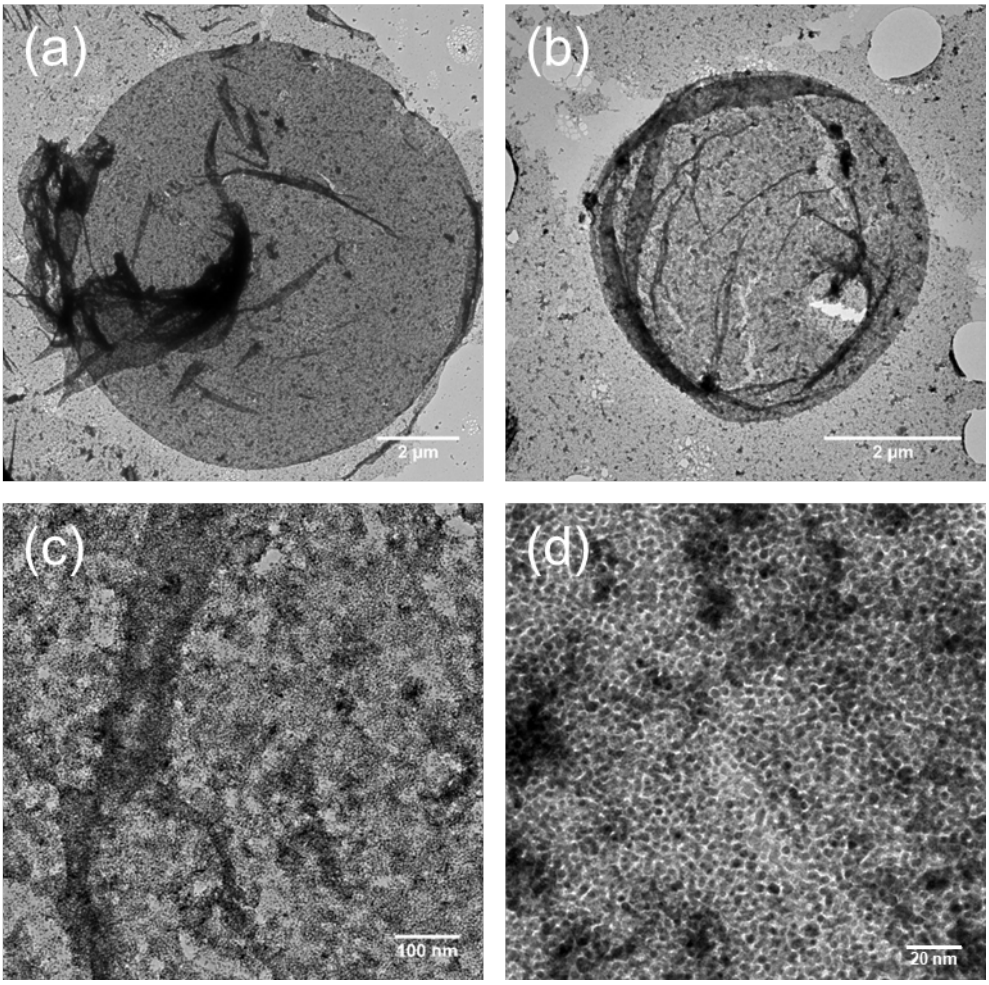

Figure 5.7: TEM micrographs of drop cast emulsion droplets. (a) and (b) show entire droplets, (c) and (d) show zoomed in region of droplet.

The emulsions were also observed on cryo-TEM (Figure 5.8) allowing us to visualise the nanoparticles at the interface of droplets frozen in their true environment. Indeed, by using cryo-TEM it was possible to preserve the structure of the droplets so that they do not collapse under the vacuum pressure. This enables the study of the packing density of the adsorbed Pt NPs at the interface. There are few reports in literature of Pickering emulsions produced from nanoparticles imaged using cryo-TEM techniques.[54],[196],[153] In this instance a holey carbon film was used, so what appears to be a hole in the droplet is in fact part of the

grid. The droplet is likely pinned on this hole which occurs during the freezing process. EDX mapping of the sample is possible while under STEM conditions. It can again clearly be observed that the platinum nanoparticles are localised on the droplet interface (red on the EDX mapping. The carbon comes from both the TEM grid, the hexadecane and the PVP.

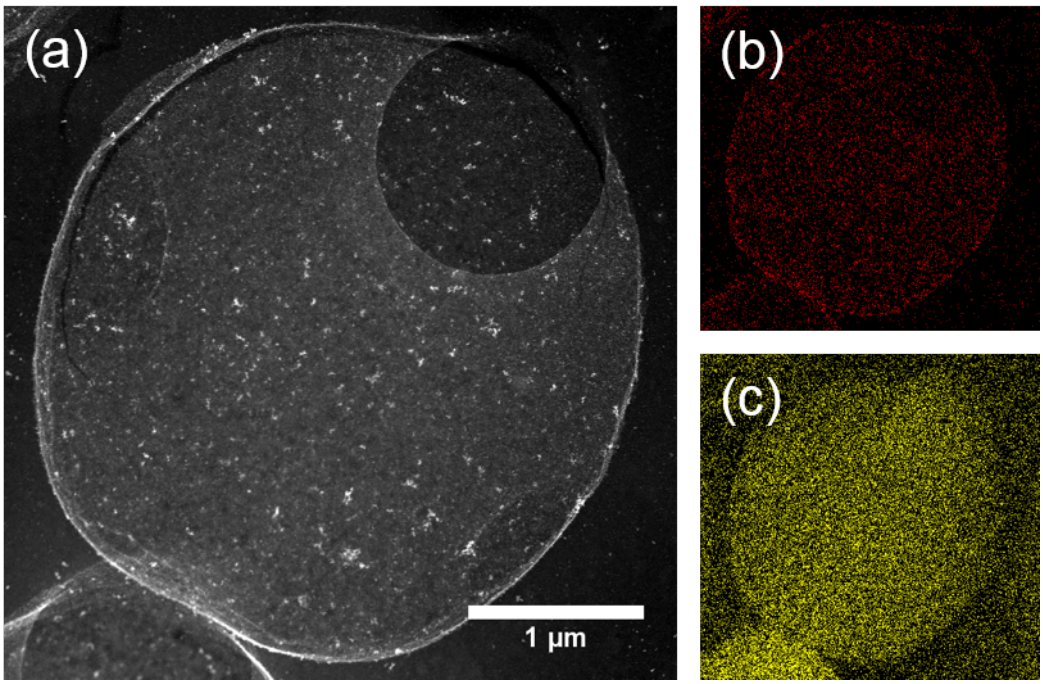

Figure 5.8: (a) Cryo-STEM micrograph of Pt-PVP stabilised emulsion droplet, (b) EDX false colour map of Platinum (red) and (c) Carbon (yellow)

5.4.2.1 Excess PVP

To initially investigate the importance of excess PVP in the Pt-NP suspension and its influence on the adsorption efficiency of these nanoparticles, an emulsion was prepared where excess PVP was purposefully added into the Pt-PVP NP dispersion after synthesis. This sample was compared to an emulsion sample prepared using the particles as synthesised to evaluate the differences in adsorbed nanoparticle density on the droplet surface using cryo-TEM. As described in the previous chapter, efforts have been made to reduce the amount of PVP used to

synthesise the nanoparticles in order to reduce competition of the free polymer in the bulk for the nanoparticle interfacial adsorption. Upon emulsification, due to the lower density of hexadecane, the emulsion creams, which allows for visual observation of the turbidity of the emulsion continuous phase. As can be seen from Figure 5.9 (a), where no excess PVP has been added, the aqueous phase appears colourless, providing evidence that most of the nanoparticles have adsorbed at the oil-water interface. Comparatively in Figure 5.9 (b), where excess PVP has been added, the aqueous phase of the emulsion appears very dark showing that not all of the NPs have gone to the interface and that the interface is likely populated with polymer in majority. Additionally the cream layer in (b) appears lighter, suggesting there are fewer Pt NPs present on the droplet surfaces. In emulsion (b) aggregates can be observed which is unfavourable. It is possible that aggregation is being driven by PVP diffusing to the interface first but not stabilising the interface as efficiently as the nanoparticles and the nanoparticles cannot easily substitute the adsorbed PVP.

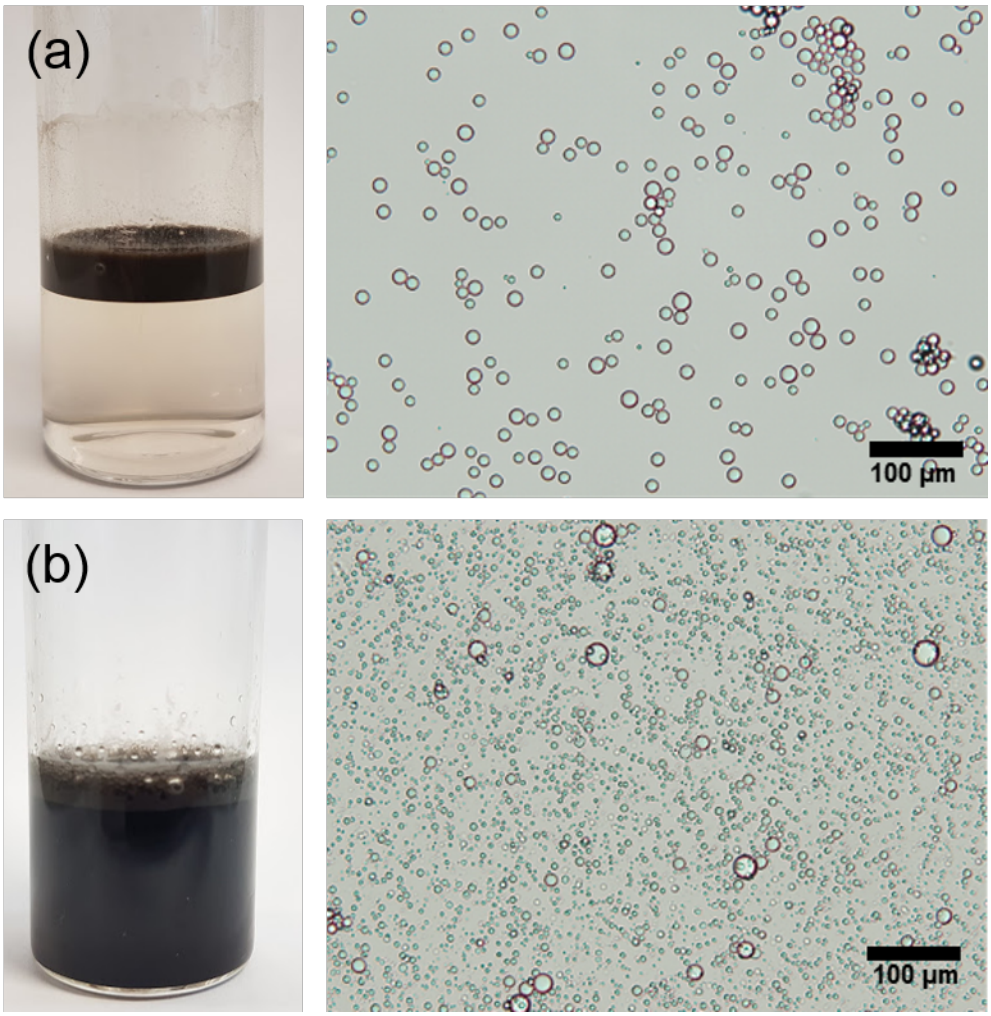

Figure 5.9: (a) Emulsion made with no excess PVP, (b) emulsion made with excess PVP.

The NP particle density at the interface for each emulsion can be calculated by using the size distribution (allowing for calculation of total surface area) of the emulsion and the number of NPs adsorbed. The transmission of the aqueous phase, measured by the LUMiSizer, can be used to determine the number of particles remaining in the bulk aqueous phase through comparison with calibration work where the transmission of Pt NP suspensions of a broad range of nanoparticle concentrations was measured. By using the total oil-water interfacial area in the system and comparison between the number of particles remaining

in the emulsion continuous phase versus particles present before emulsification, the adsorbed Pt NP density on the oil droplet surfaces can be estimated (in NP m^{-2}).

An average interparticle space, s_{IP}, as illustrated in Figure 3.8 (in Chapter 3), can be calculated by using the theoretical surface area that a set number of NPs can cover. This can be calculated from the area that one nanoparticle would occupy (A_H) on the assumption that the NPs form a hexagonal close packed array monolayer and is detailed in Chapter 3.4.3. Once the area that one particle occupies is obtained this can be multiplied by the number of particles in the system at the interface ($NP_{interface}$) to provide the area that the particles can cover (A_{total}) at a given particle diameter and spacing (Equation 5.2).

$$A_{total} = A_H \cdot NP_{interface} \tag{5.2}$$

If the number of particles adsorbed at the interface (from transmission data) and the interfacial area of the emulsion (from size distribution data) is known, the interparticle spacing, s_{IP}, as shown in Figure 3.8 can be back calculated as s_{IP} is a component of A_H. This is achieved using the Goal Seek function on Excel where A_{total} is set to the total interfacial area obtained from the size distribution of the emulsion by changing the interparticle spacing (s_{IP}). In this case a value of 3.3 nm for the core NP diameter has been used as calculated in Chapter 4.

The adsorbed Pt-NP density can also be measured using the cryo-TEM micrographs by processing the micrographs, focussing on the interface (using the image processing software ImageJ) to determine the number of particles for a given area. Though this is a transmission technique at high magnifications the focus is on particles likely to be on one side of the emulsion droplet due to relative height differences. Additionally it is possible to identify individual particles, whereas in the drop cast TEM micrographs this is more difficult as layers of the nanoparticulate films are being observed. Sizing is carried out on ImageJ by maximizing the contrast and brightness on the TEM micrograph followed by adjusting the threshold to obtain a black and white image. A good degree of contrast is required to differentiate the particles from the background. The binary image is then processed by the particle analyser tool, which provides information such as

size, shape and count. Parameters such as size and circularity can be defined when analysing the particles. An example of the image processing carried out for one particular micrograph is given in Figure 5.10.

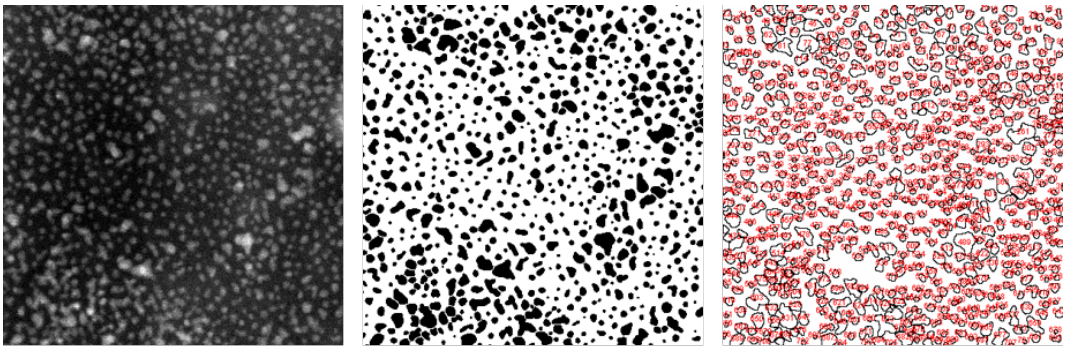

Figure 5.10: Steps involved in obtaining particle size and number from ImageJ software.

Using these techniques the particle density can be calculated and compared for the emulsions. Visually from Figure 5.11 a more densely packed interface for the emulsion with no excess PVP can be observed. For emulsion (a), using the transmission and interfacial area method described above, a value of 3.7 x 10^{16} NPs m^{-2} (1.5 x 10^{-2} g m^{-2}) is obtained for the particle density at the interface. Back calculating this gives a particle spacing of around 2.9 nm. These values fit with the measured average density from the cryo-TEM images of 3.4 x 10^{16} NPs m^{-2}. Going forward the transmission and interfacial area data can be considered a good representation of the density because they agree so well with each other in this case.

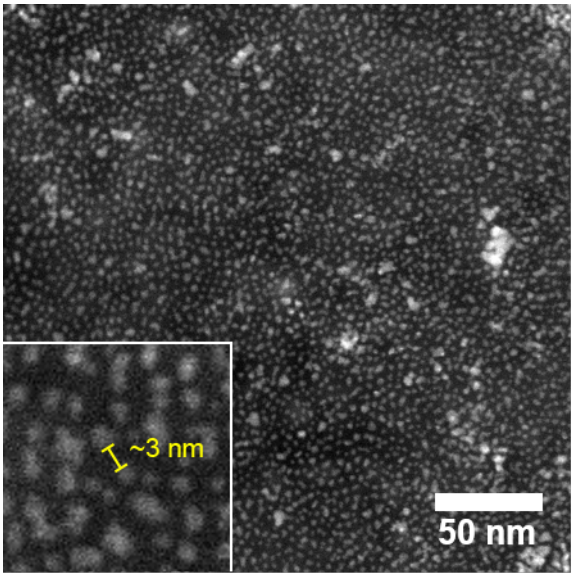

Figure 5.11: Cyro-STEM micrographs of Pt-PVP NP stabilised o/w emulsion with no excess PVP.

For the emulsion where excess PVP has been added before the emulsification process (Figure 5.9 (b)) the density is much lower, with a value of 5.26 x 10^{15} NPs m^{-2} being obtained from the aqueous phase transmission data and interfacial area. This produces a back calculated spacing of 13.0 nm. In the cryo-TEM images (Figure 5.12) particles that are more closely packed are observed, where some are in clusters and some are further away, therefore this number represents the average spacing of the particles. Due to the way the water has crystallised as it has frozen and high amount of ice (white haze on the image), the contrast on the cryo-TEM images was not good enough to obtain quantitative density values from the micrographs. Nonetheless, visually (Figure 5.12) the spacing values fit. This experiment illustrates the importance in reducing the amount of PVP in the system as excess PVP preferentially adsorbs to the interface and hence reduces the packing density of the catalytic Pt nanoparticles. Horiuchi et al.[102] emphasised the importance of having a high packing density in order to obtain a uniform metal film with high deposition rates. This will be discussed further in Chapter 6.

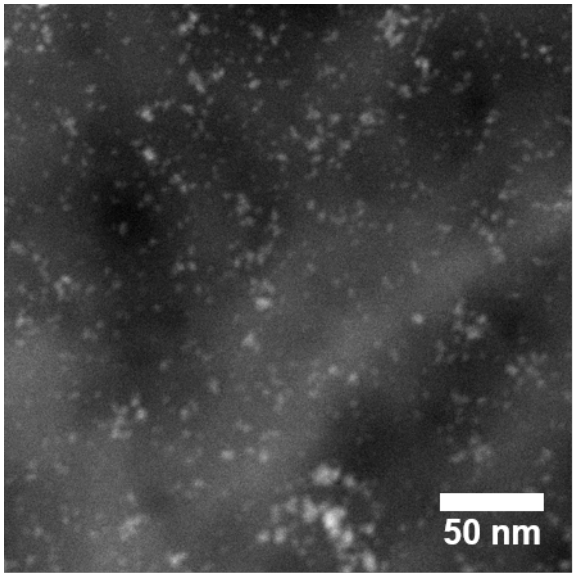

Figure 5.12: Cyro-STEM micrographs of Pt-PVP NP stabilised o/w emulsion with excess PVP added before emulsification.

5.5 Conclusion

As evidenced above via various techniques the Pt-PVP NPs are able to adsorb at the oil-water interface successfully. The presence of platinum at the interface was confirmed using EDX. As previously suggested excess PVP competitively adsorbs at the interface and prevents the NPs from adsorbing. A densely packed array of particles can be observed in the emulsions without excess PVP which suggests that they will provide a suitable interface for the growth of a secondary metal film.

Chapter 6

Emulsification of Pt-PVP nanoparticles

6.1 Synopsis

It has been previously demonstrated that the Pt-PVP NPs are able to adsorb at the oil-water interface. This chapter will examine the emulsification process, illustrated in Figure 6.1, and investigate some of the key parameters in order to optimise and demonstrate the control of the emulsion system. It has already been highlighted that PVP concentration in the aqueous phase is an important factor in the emulsification process and this will be discussed further. Additionally the effect on the resulting emulsion of oil fraction and electrolyte concentration of the nanoparticle dispersion will be investigated.

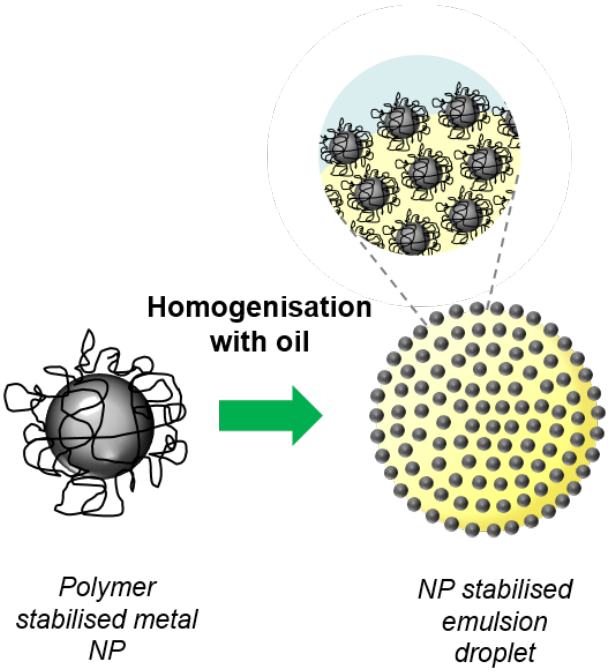

Figure 6.1: Schematic illustrating the formation of emulsion droplets stabilised by Pt-PVP NPs.

6.2 Emulsification of Pt-PVP with hexadecane

Pt-PVP stabilised hexadecane emulsions were prepared to act as a scaffold for metallic plating, in order to encapsulate the oil core. Hexadecane has been chosen as a model oil in this case as it has a relatively low molecular weight, has a simple structure so is easily identifiable on gas chromatography. The platinum NPs provide catalytic sites for the reduction of a secondary metal process to take place. In order to achieve a continuous metal film, a high density of nanoparticles at the interface is desirable. The particles can be considered as Pickering emulsifiers as the particles adsorb and stabilise the interface, where the self-assembly of colloidal particles at the liquid-liquid interface is driven by the reduction in the Helmholtz free energy, where the fluid-fluid interface is replaced by a fluid-particle interface. The tendency for the particles to adsorb and stay at the interface depends on various factors including the surface chemistry which affects the particles wetta-

bility and the particle radius.[142], [26] However, there are few reports in literature of sub 10 nm nanoparticles being used as emulsifiers.[196], [131], [26]

In Chapter 4 Pt-PVP NPs with a low ratio of PVP to platinum were produced in order to maximise the packing of the Pt cores at the interface and therefore maximise the catalytic activity. This will theoretically allow smoother, thinner coatings of the secondary metals to grow. The packing density at the droplet interface will be discussed later in the chapter. The nanoparticles used in this chapter are those detailed at the conclusion of Chapter 4 (5.56 mM (0.23 wt%) $PtCl_6H_2$, 0.0067 wt% PVP and 22.25 mM $NaBH_4$). In Chapter 5 it was evidenced that these nanoparticles are able to adsorb at the oil-water interface on both 2D and 3D systems.

6.3 Controlling limited coalescence of emulsions

The phenomenon of limited coalescence, whereby the droplets generated during emulsification will coalesce until they reach a coverage limit, defined by the emulsifier available in the system, has been documented for Pickering emulsions.[258], [9], [25], [175] To ascertain whether limited coalescence can be observed for this system, emulsion droplet size was studied over time. Hexadecane was homogenised with Pt-PVP NPs (10 ml) for 1 min at 40% amplitude on an ultrasonic processor. Oil volumes of 0.5 ml and 1 ml were used, corresponding to volume fractions (ϕ) of 0.05 and 0.9. One set of emulsions were agitated for 30 minutes (hence preventing the creaming process) then the size sampled at time intervals by inverting so that a homogeneous sample was taken. Another set of emulsions was left to cream immediately after emulsification and the same sampling process was undertaken.

As can be observed in Figure 6.2 the mean droplet diameter evolves over time and then plateaus when the emulsion is not agitated (as does the coefficient of variation, CV). This suggests that limited coalescence is occurring as the droplet diameter is changing until a coverage limit is reached. Whereas for the emulsions that were agitated on the carousel, Figure 6.3, the mean diameter remains stable over time. The CV does not change much over time and for both volumes is lower than the emulsions without the agitation step. In this case the limited

coalescence process is controlled during the agitation stage. Additionally, the final mean droplet size is slightly larger and the size distribution of the emulsion is narrower for the emulsions subject to agitation. This may be as result of increased droplet collisions during agitation, some of which lead to coalescence and hence larger droplets. The agitation on the carousel also allows time for the nanoparticles to distribute themselves across the droplets more evenly. The interfacial rheology experiments (Chapter 5) showed weaker films were formed initially, which increased in elasticity and became more robust over time. By preventing the emulsion from creaming immediately the particles are able to build a film at the interface and controlling this process results in a more stable system. The time scales for film build up are not comparable as there is no energy input to the interfacial rheology system, whereas large amounts of energy are input in the emulsification process. Therefore the adsorption will occur on a faster time scale for the emulsification process.

Two different oil volume fractions were compared. For the emulsions with the lower oil fraction the difference in mean diameter of the emulsion subject agitation compared to that of the one that was not is smaller than the difference between the two emulsions with a higher oil fraction (Figure 6.2 & 6.3). This may be due to the initial droplet size being larger for the 1 ml emulsion. This experiment demonstrates that the limited coalescence of the emulsion can be controlled and by adding this agitation step better control of the size and stability of the emulsion is attained. In the following work the emulsions will undergo agitation on a carousel for 30 minutes.

Another possible explanation for the observations is the Ostwald ripening process, where small droplets dissolve and redeposit on larger droplets as a result of pressure differences existing between droplets of varying sizes. Due to the relatively low solubility of hexadecane in water[48] it is unlikely that this is occurring. According to Arditty et al. if the dispersed and continuous phases are immiscible Ostwald ripening occurs at a negligible rate.[9] One of the key features of Ostwald ripening is that average drop diameter keeps increasing.[178] Here a plateau is observed, though that is not to say that this is still occurring at a very slow rate. Additionally Pickering emulsifiers tend to adsorb at the interface with high detachment energies, unlike surfactant molecules which can adsorb and desorb.[23]

Further studies would be required to establish whether no Ostwald ripening is occurring. This can be achieved by taking into consideration the area of the droplet and the Laplace equation, $2d\gamma/dlnA > \gamma$. If this inequality is satisfied then the droplet should be in equilibrium and show no Ostwald ripening. The left had side of the equation can be determined experimentally from the dilational modulus. [231]

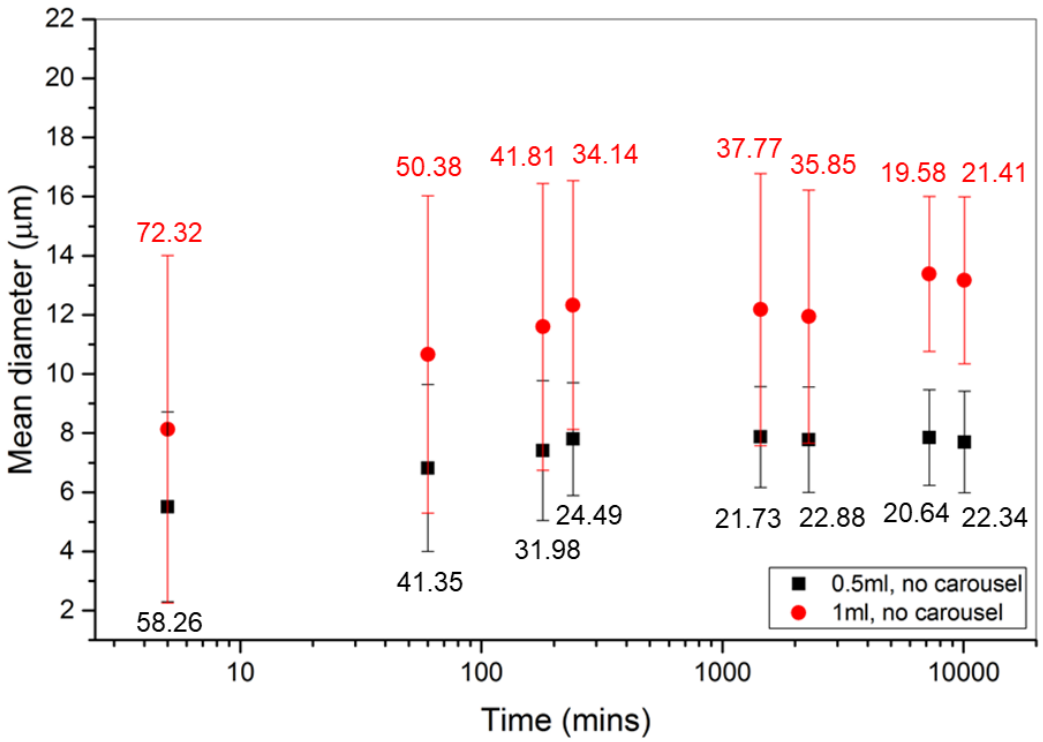

Figure 6.2: Diameter of the emulsion droplets as a function of time of hexadecane in Pt-PVP emulsions (oil $\phi = 0.05$ and 0.90) for samples not subject to agitation. Annotated numbers represent CV (%).

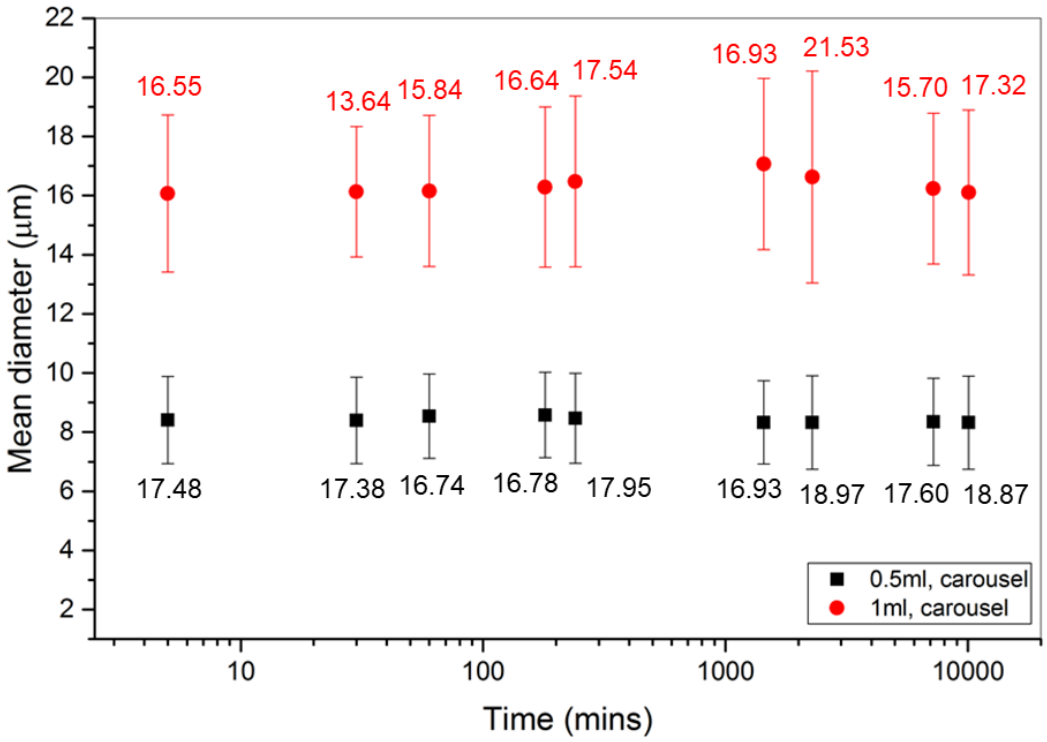

Figure 6.3: Diameter of the emulsion droplets as a function of time of hexadecane in Pt-PVP emulsions (oil $\phi = 0.05$ and 0.90) for samples subject to agitation for 30 mins on the carousel. Annotated numbers represent CV (%).

6.4 Effect of the addition of excess PVP before emulsification

Previously the importance in reducing the amount of PVP in the NP dispersion to attain a high density of catalytic sites at the oil-water interface to increase the efficiency of the subsequent electroless deposition mechanism has been stated. In order to demonstrate the importance of the presence of free PVP in the bulk on the emulsification process, emulsions were formed with a constant number of

nanoparticles, oil fraction and total volume, and differing amounts of excess PVP were added to the system. For this purpose, a fixed volume of PVP solutions(0.5 ml) at different concentrations was added to the suspension of Pt-PVP NPs (9.5 ml) after particle synthesis but prior to addition of the oil phase for the emulsification process. For the sample where no excess PVP was present, 0.5 ml of water was added to keep the volume and nanoparticle concentration constant across all tested samples. As mentioned in the previous chapters, the nanoparticle synthesis has been designed to minimise any excess PVP in the original dispersion and though it is possible that some free polymer chains may remain in these original suspensions, this amount is negligible as compared to the amount of PVP added in the other samples. Calculations of the ratio of polymer chains to Pt-NPs also suggest that there is no excess (Chapter 3.1.) Therefore for the emulsion with no excess PVP added the overall concentration of excess PVP is denoted as 0.00 wt%. PVP solutions were added from concentrations of 0.05 wt% to 2 wt%, giving overall PVP concentrations in the final suspensions used in the emulsification process of 0.0025 wt% to 0.1 wt%. The resulting dispersions were homogenised with hexadecane (0.75 ml) for 1 min at 40% amplitude with an ultrasonic processor while the sample was kept at a constant temperature (22 °C) in a water bath. Subsequently the emulsions were agitated on a carousel for 30 minutes then left to cream for 24 hours. The lower aqueous phase was removed for transmission analysis and replaced with milliQ water. The size distribution was measured for each of the emulsions.

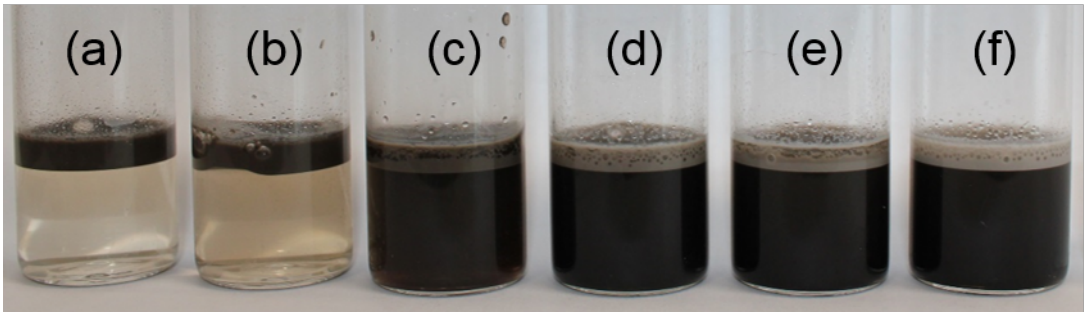

Figure 6.4: Digital photographs of emulsions prepared with different concentrations of PVP added to the NP dispersion before emulsification. Hexadecane (ϕ = 0.07) and Pt-PVP NP dispersions were homogenised at 40% amplitude for 1 min on an ultrasonic processor. Overall concentrations of PVP in aqueous nanoparticle phase are (a) 0.00 wt %, (b) 2.5 x 10^{-3} wt %, (c) 1.25 x 10^{-2} wt %, (d) 2.5 x 10^{-2} wt %, (e) 5.0 x 10^{-2} wt %, (f) 1 x 10^{-1} wt %

As can be observed in Figure 6.4, which shows digital photographs of the emulsion once creaming of the oil droplets appeared to be complete, the emulsions prepared with higher concentrations of excess PVP have a darker lower aqueous phase. This observation indicates that there is a higher concentration of nanoparticles in the bulk of the emulsions prepared in these conditions and hence a lower concentration of NPs at the droplet interface. Additionally, a lighter emulsion cream layer at higher concentrations of excess PVP can be observed, suggesting that the PVP has preferentially adsorbed at the droplet interface.

Furthermore, as the amount of excess PVP added increases, smaller droplets are created and there is an increase in the polydispersity of the emulsions as can be seen in Figure 6.5. There is more stabiliser available at higher excess PVP concentrations therefore more interface can be stabilised, hence resulting in smaller droplets overall. An increase in coalescence was observed with increasing excess PVP concentrations as some larger droplets are present in the optical micrographs (Figure 6.6) and digital images (Figure 6.4). The initial droplet sizes observed at high concentrations of excess PVP are lower, however as PVP is not as good a stabiliser as the nanoparticles so they destabilise quicker, therefore leading to coalescence of droplets. These larger droplets have a smaller contribution to

the overall interfacial area stabilised, hence why this is not reflected in the mean droplet diameter. The measurement of the size distribution is limited by the optical imaging measurement technique used. The ability of the imaging system to resolve the size of the droplets is limited to 1μm. So though there may be droplets smaller than this, they cannot reliably be measured. Due to the fast creaming rate of the very large droplets it is possible that these will also not be measured reliably. However, though this will skew the total interfacial area calculations, these are small errors compared to the changes seen in the trend.

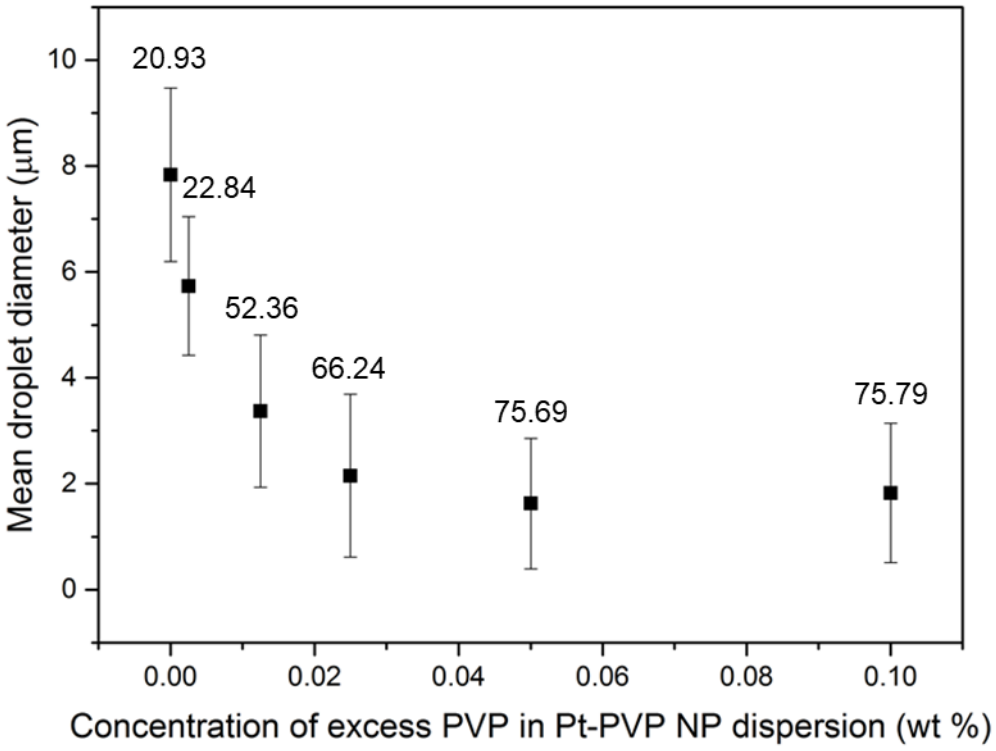

Figure 6.5: Mean droplet diameter of emulsions prepared with different concentrations of PVP added to the NP dispersion before emulsification. Overall PVP concentrations ranged from 0.00 wt % to 1 x 10^{-1} wt %. Hexadecane ($\phi = 0.07$) and Pt-PVP NP dispersions were homogenised at 40% amplitude for 1 min on an ultrasonic processor. The error bars represent the standard deviation of the mean. Annotated numbers represent CV (%).

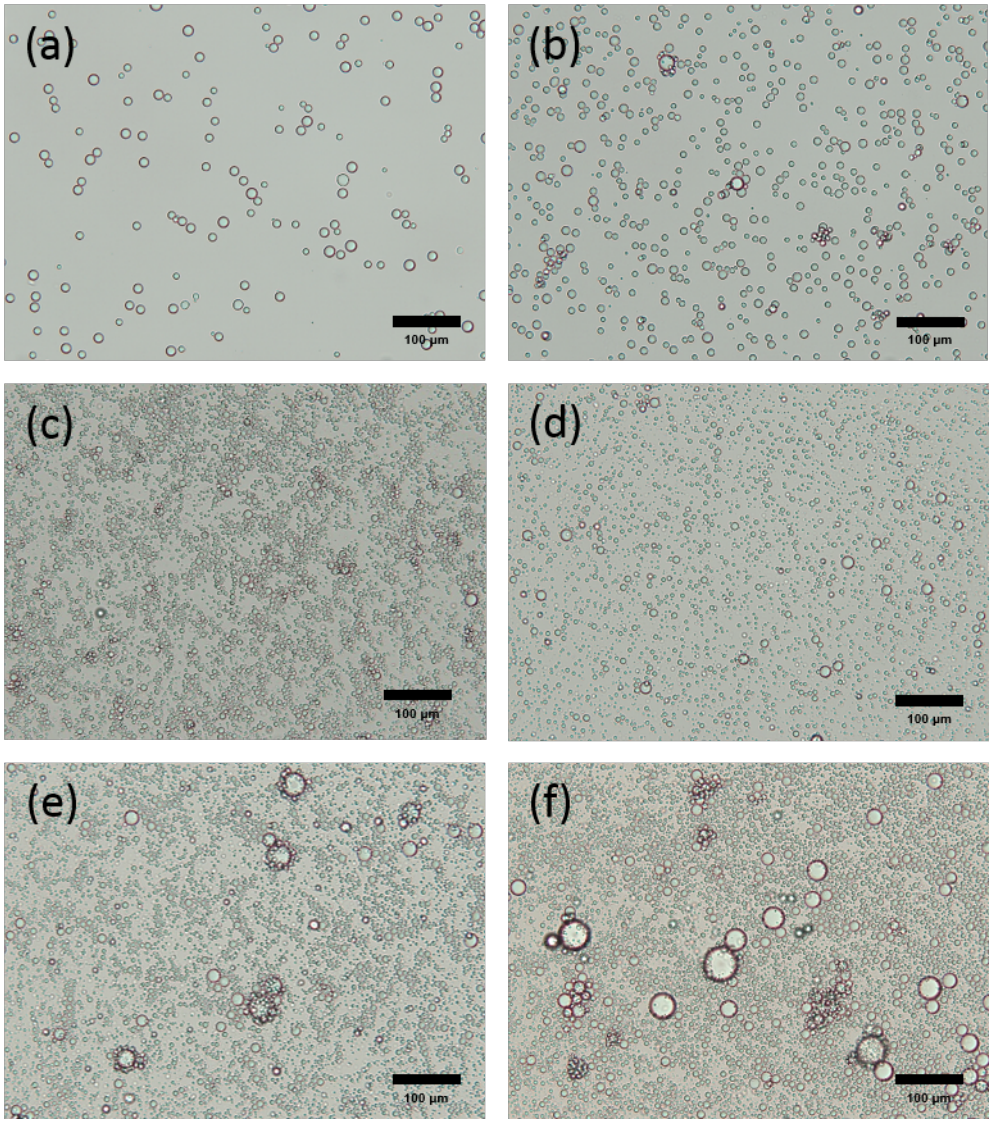

Figure 6.6: Optical micrographs of emulsions prepared with different concentrations of PVP added to the NP dispersion before emulsification. Hexadecane (ϕ = 0.07) and Pt-PVP NP dispersions were homogenised at 40% amplitude for 1 min on an ultrasonic processor. Overall concentrations of PVP in aqueous nanoparticle phase are (a) 0.00 wt %, (b) 2.5 x 10^{-3} wt %, (c) 1.25 x 10^{-2} wt %, (d) 2.5 x 10^{-2} wt %, (e) 5.0 x 10^{-2} wt %, (f) 1 x 10^{-1} wt %

In addition to measuring the transmission of the bulk nanoparticle aqueous

phase the LUMisizer can be used to study the displacement of the droplets as a result of density differences by measuring the transmission of emulsion samples over time. Homogenised samples of the emulsion were subject to centrifugation at 300 rpm while the transmittance was monitored across time as the emulsions creamed. Front tracking analysis measures the change in position across the cell of a particular transmission percentage over time (Figure 6.7) and the initial slope can be used to determine creaming velocities. Faster creaming velocities are observed for emulsions with lower excess PVP added, which would suggest larger droplets are present. This is in agreement with the larger mean diameters observed by the FlowCAM in Figure 6.5 and by the optical microscope in Figure 6.6.

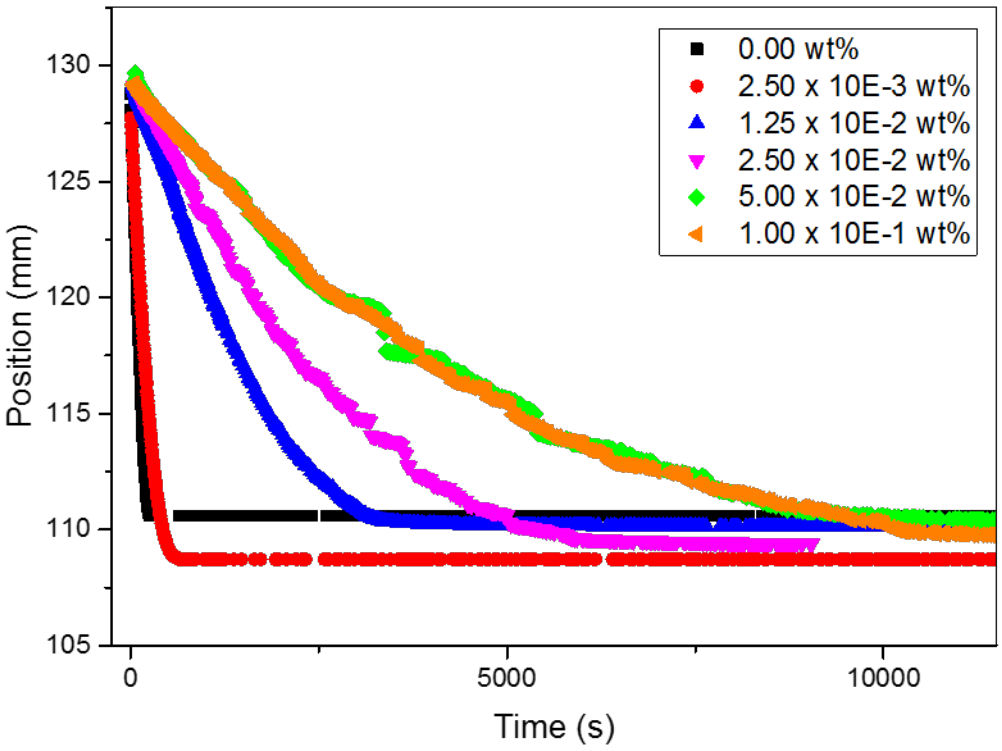

Figure 6.7: Front tracking profiles obtained from LUMIsizer emulsion creaming profiles at a transmission threshold of 10% for emulsions prepared with different concentrations of PVP in the NP dispersion. Experiments were carried out at 300 rpm and transmission measurements were taken over time.

The particle density at the interface was calculated by using the size distribution of the emulsions and the transmission of the aqueous phase (which related to the number of nanoparticles adsorbed at the interface) as detailed in Chapter 3. Again the LUMiSizer was used to obtain transmission values for the bulk aqueous nanoparticle phase and compared to a calibration to determine the concentration of nanoparticles remaining in the aqueous phase after emulsification. The interfacial area was calculated based on the measured size distributions of the emulsions from the FlowCAM. These resulting densities plotted against excess PVP concen-

tration clearly illustrate a decrease in particle density at the oil-water interface following emulsification with increasing PVP concentration in the nanoparticle suspension (Figure 6.8).

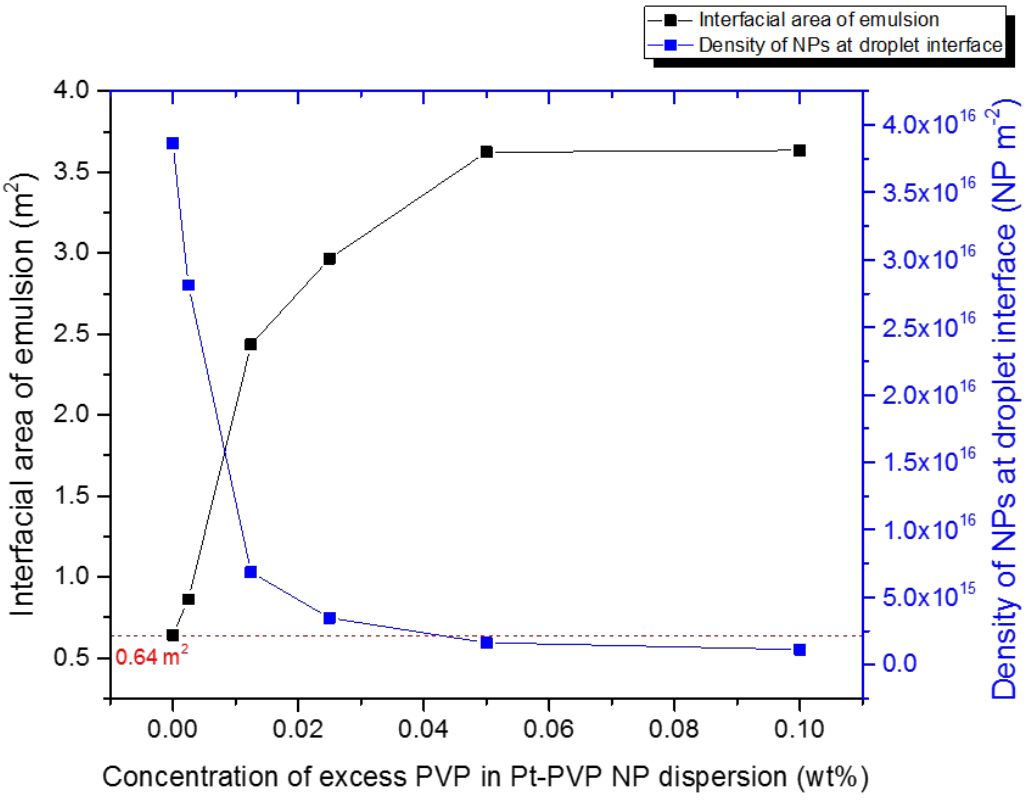

Figure 6.8: Nanoparticle density at the oil-water interface as a function of concentration of excess PVP in the NP dispersion. Emulsions were prepared with different concentrations of PVP added to the NP dispersion before emulsification. Overall PVP concentrations ranged from 0.00 wt % to 1 x 10^{-1} wt %. Hexadecane ($\phi = 0.07$) and Pt-PVP NP dispersions were homogenised at 40% amplitude for 1 min on an ultrasonic processor. The red line represents the interfacial area that the amount of Pt-PVP NPs used (9.5 ml) can stabilise (based on calculations detailed in Chapter 3 using an inter particle spacing of 2.9 nm and core diameter of 3.3 nm.)

The density of nanoparticles at the interface is reduced at higher excess con-

centrations of PVP due to the PVP competitively diffusing and adsorbing at the oil-water interface. As mentioned before there are errors associated with measuring the size distribution and hence the interfacial area from which it is derived. Moreover interfacial area calculations do not account for any coalesced oil layer on top, however these errors are small compared to the changes observed in the trend. The diffusion dynamics for spherical particles in solution can be predicted using the Stokes-Einstein relation. For a spherical particle of radius R, in a fluid of viscosity η, the diffusion coefficient D_{SE} is determined by Equation 6.1.

$$D_{SE} = \frac{k_B T}{6\pi\eta R} \tag{6.1}$$

Where k_B is the Boltzmann constant, T is the absolute temperature and R is the radius of the spherical particle. However, for nanoparticle systems this equation's validity is questionable as it does not account for microscopic interactions and diffusion properties are often hard to predict. Work by Almusallam and Scholl used Brownian dynamic simulations to incorporate a term for hydrodynamic interactions to describe diffusion properties of polymer grafted nanoparticles. In this particular article, simulations performed using the corrected diffusion equation were compared to experimental data with good agreement.[1] For small nanoparticles dispersed in polymer solutions and melts large deviations from D_{SE} have been observed both experimentally[240],[117] and by molecular dynamic simulations[143] when the particle size is comparable to the correlation length of the polymer. Dong et al.[65] argued that multiple length scales need to be taken into account and a microscopic viscosity (which would depend on particle size) may need to be considered when using Stokes-Einstein to establish diffusion coefficients for nanoparticles. They found that using experimental and mode-coupling theory (MCT) modelling methods that gold nanoparticle diffusion coefficients were decreased at higher polymer (PEG) volume fractions. The study investigated the effect of polymer concentration, polymer chain length and particle size of the diffusion coefficient and their theories were applicable for both unentangled and entangled polymer solutions. The size of the nanoparticles and polymers used in the study are comparable to the system used here. The diffusion coefficients will not be calculated here due to the aforementioned complexities but it is likely

that the Pt-PVP NPs and free PVP will have similar diffusion properties as they are both of a similar size and the stabilising layer of PVP on the NPs will result in them having similar chemical interactions. However interfacial tension measurements from Chapter 5 suggest that the PVP diffuses faster to the interface as the kinetics for adsorption were faster for PVP. Though the diffusion has not been quantified, observations would suggest that it diffuses faster. As the ratio of PVP to NPs present in the dispersion is drastically increased, the likeliness of a free PVP molecule reaching the interface before a nanoparticle becomes much higher.

This highlights the importance of reducing the amount of PVP in the NP synthesis and demonstrates control of the nanoparticle density at the interface, which has been highlighted already as being paramount to the success of the subsequent electroless deposition process. These observations agree with earlier cryo-TEM experiments in Chapter 5 where a lower density of Pt NPs was directly observed at the interface with the addition of a high excess of PVP.

6.5 Effect of oil fraction

In order to assess the volume of oil that could be emulsified by the nanoparticles the oil volume fraction was varied. Maximising the oil volume fraction and using all the nanoparticles for the bulk is more favourable from a manufacturing perspective as the materials are used more efficiently and washing cycles could be reduced. Pt-PVP NPs (synthesised as concluded from Chapter 4) (10 ml) were homogenised with hexadecane using an ultrasonic processor for 1 minute at 40% amplitude. Subsequently the emulsions were agitated to control the limited coalescence. The volume of hexadecane was changed from 0.1 ml to 4 ml, corresponding to an oil volume fraction (ϕ) from 0.01 to 0.29.

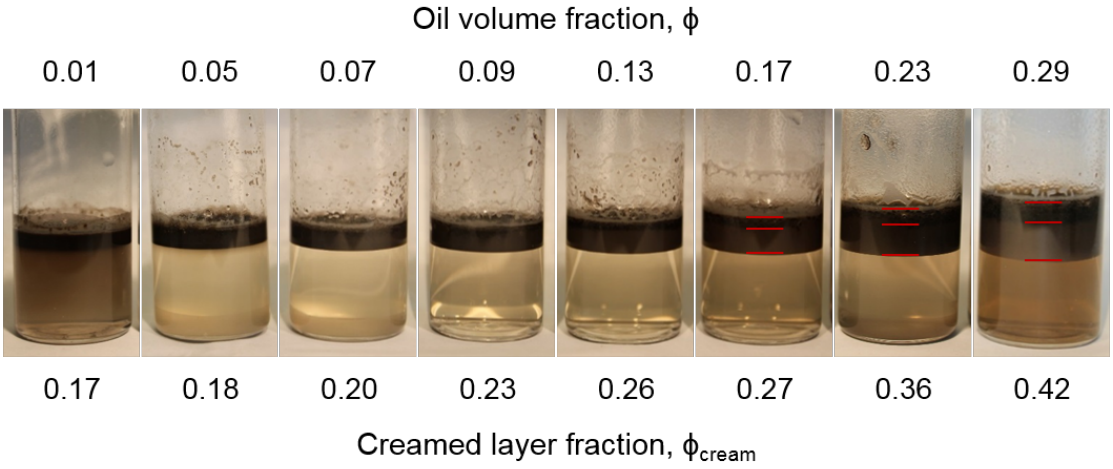

Figure 6.9: Digital photographs of emulsions prepared with different oil fractions (ϕ) (top number) and resulting cream layer volume fraction (ϕ_{cream}) (bottom number). Hexadecane and Pt-PVP NP dispersions (10 ml) were homogenised at 40% amplitude for 1 min on an ultrasonic processor.

As would be expected the volume fraction of the cream layer (ϕ_{cream}) increases with increasing oil volume fraction (ϕ) as observed in Figure 6.9. From these images two distinct cream layers can also be observed at higher ϕ, with a visible population of larger sized droplets (indicated by red lines on Figure 6.9). This relates to the broader size distributions with increasing ϕ (Figure 6.10). Some small oil droplets can be observed in these images (including for higher oil fractions), however these droplets are typically out of focus as compared to the larger ones and thus difficult to distinguish on the optical micrographs but could be identified under the microscope (Figure 6.11). The mean diameter increases with increasing ϕ, until $\phi = 0.23$ and appears to decrease/plateau as the oil volume fraction is increased further. At $\phi = 0.01$ droplet aggregation can be observed, possibly as a result of the presence of excess NPs in the system leading to depletion flocculation.[116],[126] Additionally an increasing amount of coalescence was observed immediately after creaming from $\phi = 0.17$ upwards which suggests that the emulsions are less stable.

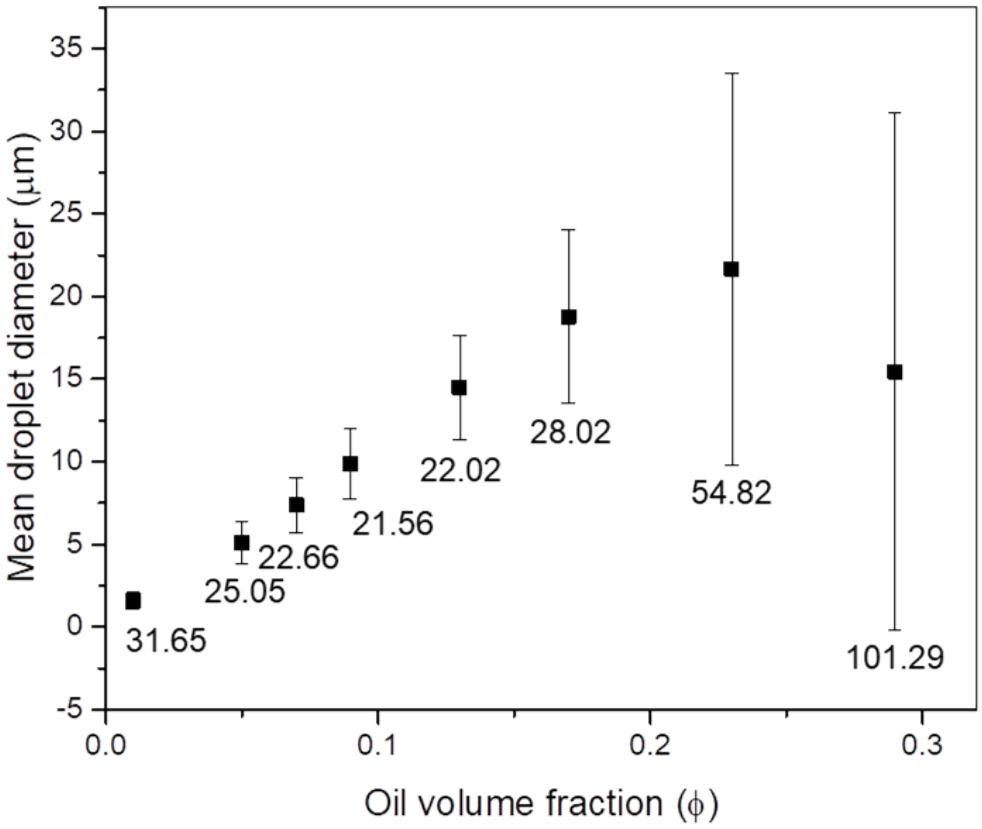

Figure 6.10: Mean droplet diameter of hexadecane in Pt-PVP NP emulsions at different oil fractions (ϕ). Oil fractions ranged from 0.01 to 0.29. Hexadecane and Pt-PVP NP dispersions (10 ml) were homogenised at 40% amplitude for 1 min on an ultrasonic processor. The error bars represent the standard deviation of the mean. Annotated numbers represent CV (%).

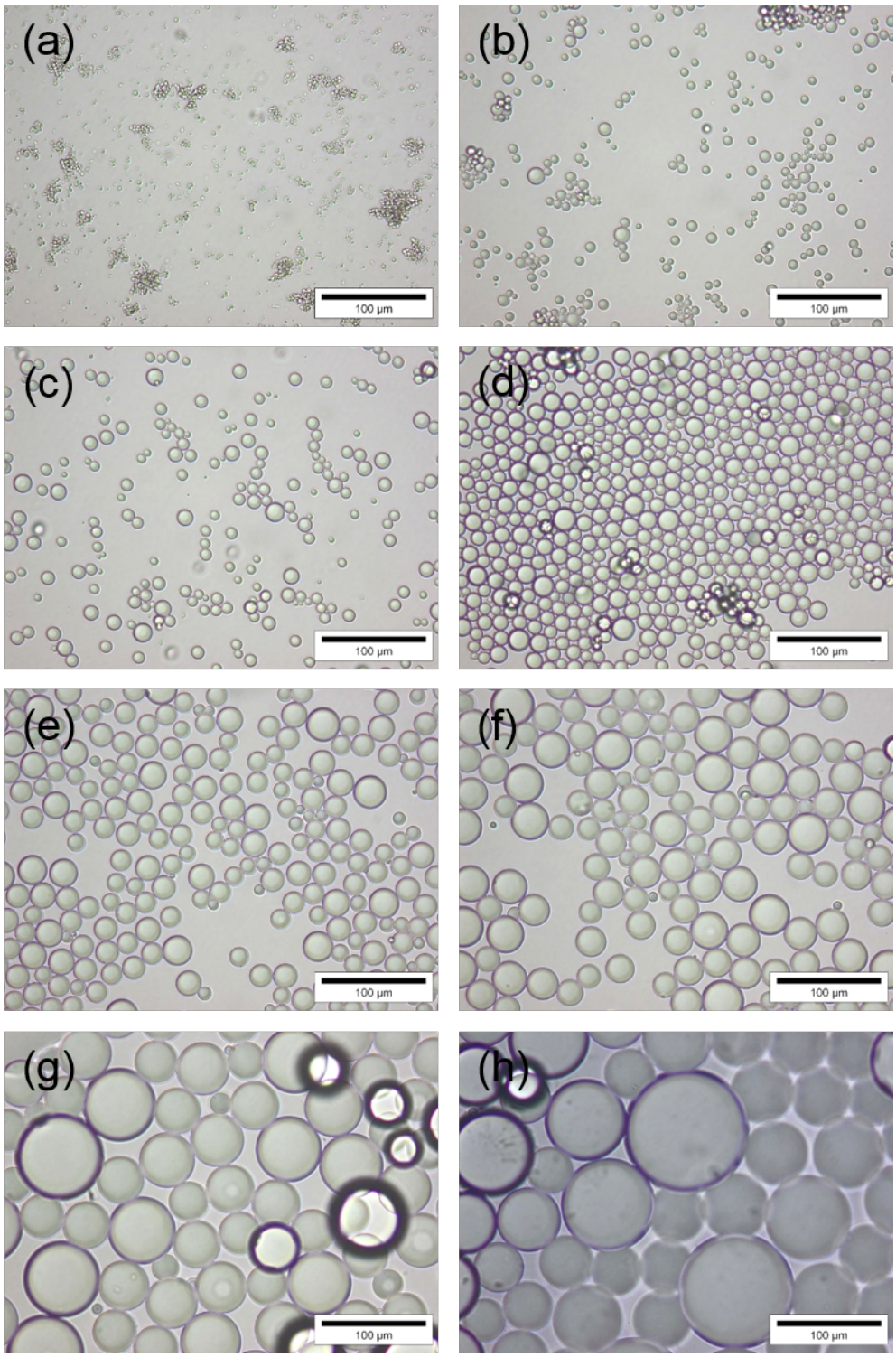

Figure 6.11: Optical micrographs of emulsions prepared with different oil volume fractions; (a) 0.01, (b) 0.05, (c) 0.07, (d) 0.09, (e) 0.13, (f) 0.17, (g) 0.23, (h) 0.29. Scale bar = 100 μm. Hexadecane and Pt-PVP NP dispersions (10 ml) were homogenised at 40% amplitude for 1 min on an ultrasonic processor.

Figure 6.12 illustrates that with increasing ϕ the interfacial area created increases slowly and then much more significantly beyond $\phi = 0.23$, hence the density of NPs adsorbed at the interface decreases accordingly. The surface coverage can be determined by considering ratio between the area that the nanoparticles in the system are able to stabilise (based on a core diameter of 3.3 nm and an interparticle spacing of 2.9 nm in a hexagonally packed array), represented by the red line on Figure 6.12, and the interfacial area created and hence stabilised by the nanoparticles for each emulsion. Near to maximum surface packing is obtained for ϕ values between 0.05 and 0.13 which supports the idea of limited coalescence whereby the particles reach an optimal stable packing density.[210],[238] At higher oil fractions (above $\phi = 0.17$) nanoparticle density at the interface decreases, which is reflected in the instability of the emulsion as the particle packing at the oil-water interface is less efficient. For $\phi = 0.01$ the area stabilised by the nanoparticles is less than the maximum packing (red line) suggesting that there is an excess of nanoparticles in the system. This could be caused by aggregation due to depletion flocculation leading to the apparent area seeming smaller.

At high volume fractions the barrier formed by the nanoparticles to prevent coalescence is less efficient. It is possible that during the emulsification process, which occurs at high energies due to the ultrasonic homogenisation, droplets are colliding with enough force to coalesce. Fan and Striolo[75] simulated the coalescence of Pickering emulsions and found that as the emulsion droplets come into contact bridging between stabilising particles may occur, which can lead to coalescence if the film between the two droplets is not sufficient. The coalescence threshold is determine by the stability of the thin film formed between two droplets as they collide. As suggested by Tambe and Sharma[229] for a less densly packed interface it is easier for particles move laterally at the oil-water interface rather than desorb from the interface. At higher NP packing densities this lateral movement becomes harder due to crowding. Additionally for our system it is possible that there is polymer entanglement at the interface which may inhibit particle movement at higher densities. Coalescence behavhiour as a function of surface coverage has been studied by Pawar et al.[192], who found that stability against coalescence was observed when the droplets are completely covered with

particles. However some studies have found that bridging of particles led to stabilisation of the droplets, whereby the particles on the emulsion droplets in the contact region form a dense, bridging monolayer as a result of strong capillary attraction.[103] The coalescence behaviour and dynamics of the emulsions could be further studied using the capillary aspiration technique, whereby droplets attached to the end of a capillary are bought into contact.[192], [256]

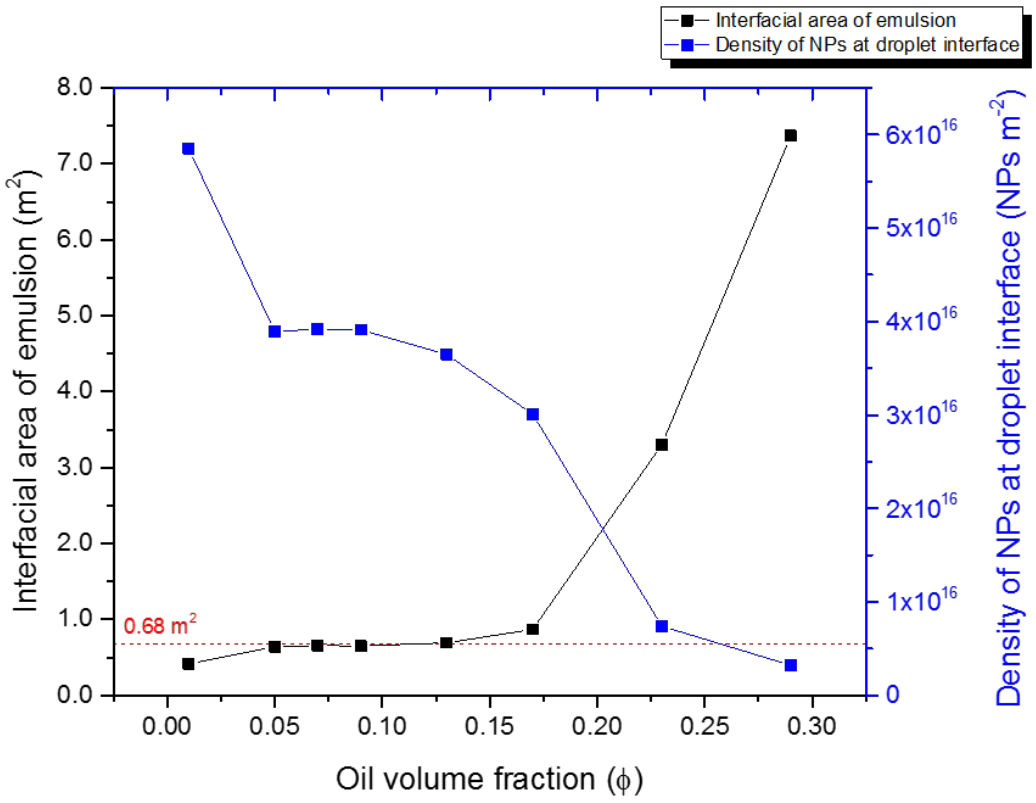

Figure 6.12: Nanoparticle density at the oil-water interface and interfacial area of emulsion as a function of oil volume fraction. Oil fractions ranged from 0.01 to 0.29. Hexadecane and Pt-PVP NP dispersions (10 ml) were homogenised at 40% amplitude for 1 min on an ultrasonic processor. The red line represents the interfacial area that the amount of Pt-PVP NPs (10 ml) used can stabilise (based on calculations detailed in Chapter 3 using an inter particle spacing of 2.9 nm and core diameter of 3.3 nm.)

6.6 Effect of the addition of excess salt to system before emulsification

As a result of the nanoparticle synthesis there are electrolytes present in the nanoparticle suspension (Equation 6.2). These ions in the suspension's continuous phase are likely to impact how the NPs behave at the interface and the resulting emulsions formed.[229], [238], [67], [81] Therefore, an experiment was designed to investigate the effect that the electrolyte concentration in the aqueous continuous phase of the nanoparticle suspensions has on their ability to act as efficient emulsifiers. The nanoparticle dispersion was dialysed to remove excess salt from the suspension using 8000 MW tubing to ensure that the particles and any polymer would not be removed from the suspension. Subsequently, sodium chloride salt was added into the Pt NP dispersions to create nanoparticles with known electrolyte concentrations (also resulting in a change of conductivity of each suspension sample). NaCl (0.5 ml) was added to Pt-PVP NP dispersions (9.5 ml) and subsequently emulsified with hexadecane (0.75 ml) for 1 min at 40% amplitude on an ultrasonic processor. NaCl solutions ranging from 5 - 2 x 10^{-4} M were added resulting in overall concentrations of 0.25 - 1 x 10^{15}M NaCl. This was followed by agitation for 30 minutes and then washing of the aqueous phase, which was used for analysis of the adsorption density at the droplet interface.

$$NaBH_4 + H_2PtCl_6 + 3H_2O \longrightarrow Pt + H_3BO_3 + 5HCl + NaCl + 2H_2 \quad (6.2)$$

Conductivity measurement were taken of each Pt-PVP NP dispersion prior to emulsification. The resulting conductivities are listed in Table 6.1. The conductivity of a solution of strong electrolyte is related to the concentration (at low concentrations, c < 10^{-2} M) according to Kohlrausch's Law. However Eslek found that there was sometimes large errors associated with these measurements (up to 16%).[73] It is possible that there are still some residual ions from the synthesis in the dialysed NP dispersion (Equation 6.2) so conductivity cannot be directly correlated to the concentration of NaCl as there could be multiple electrolytes present. Here caution should be taken when using the conductivities as a direct

correlation of concentration, but in this case it is a useful way to differentiate the samples.

Concentration of NaCl in Pt-PVP dispersion (mM)	Conductivity (μS cm^{-1})
0	8.35
0.05	100
0.5	896
Undialysed NPs	1808
5	8090
12.5	18840

Table 6.1: Concentration of NaCl in Pt-PVP NP dispersions before emulsification (NaCl added to dialysed NPs) and resulting conductivities of NP dispersion

With lower salt concentrations the emulsion size distribution is broader, and a much smaller size population can be observed for the two emulsions with the lowest aqueous phase conductivity (Figure 6.14). At higher aqueous phase conductivities the size distribution is visually less polydisperse, suggesting a more stable emulsion. There is possible aggregation at higher electrolyte concentrations (Figure 6.14) which may be a result of an increase in the polymer coiling (as described below) which reduces the steric barrier stabilising the droplets, hence they are able to approach closer and aggregate. Furthermore, stabilising polymer at the interface may be entangling with adjacent droplets.

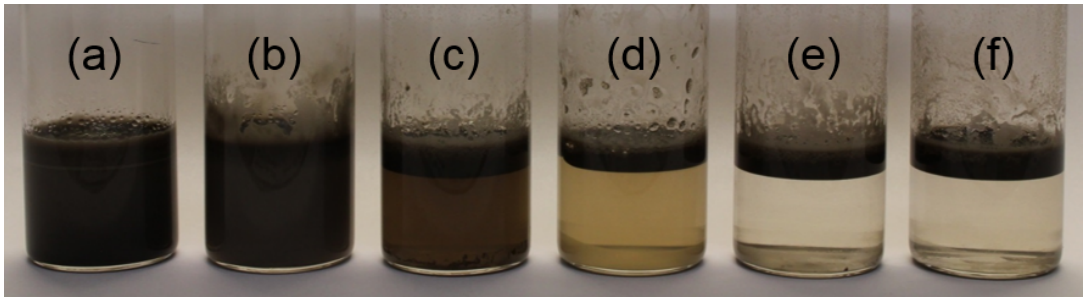

Figure 6.13: Digital photographs of emulsions prepared with different concentrations of NaCl added to the NP dispersion before emulsification. Hexadecane (ϕ = 0.07) and Pt-PVP NP dispersions were homogenised at 40% amplitude for 1 min on an ultrasonic processor. The resulting conductivities of the NP dispersions after the addition of NaCl are; (a) 8.35 μScm^{-1}, (b) 100.7 μScm^{-1}, (c) 896 μScm^{-1}, (d) 1808 μScm^{-1}, (e) 8090 μScm^{-1}, (f) 18840 μScm^{-1}. Emulsion (a) corresponds to the emulsion formed from the dialysed NPs without the addition of salt. Emulsion (d) corresponds to the emulsion formed from the undialysed NPs.

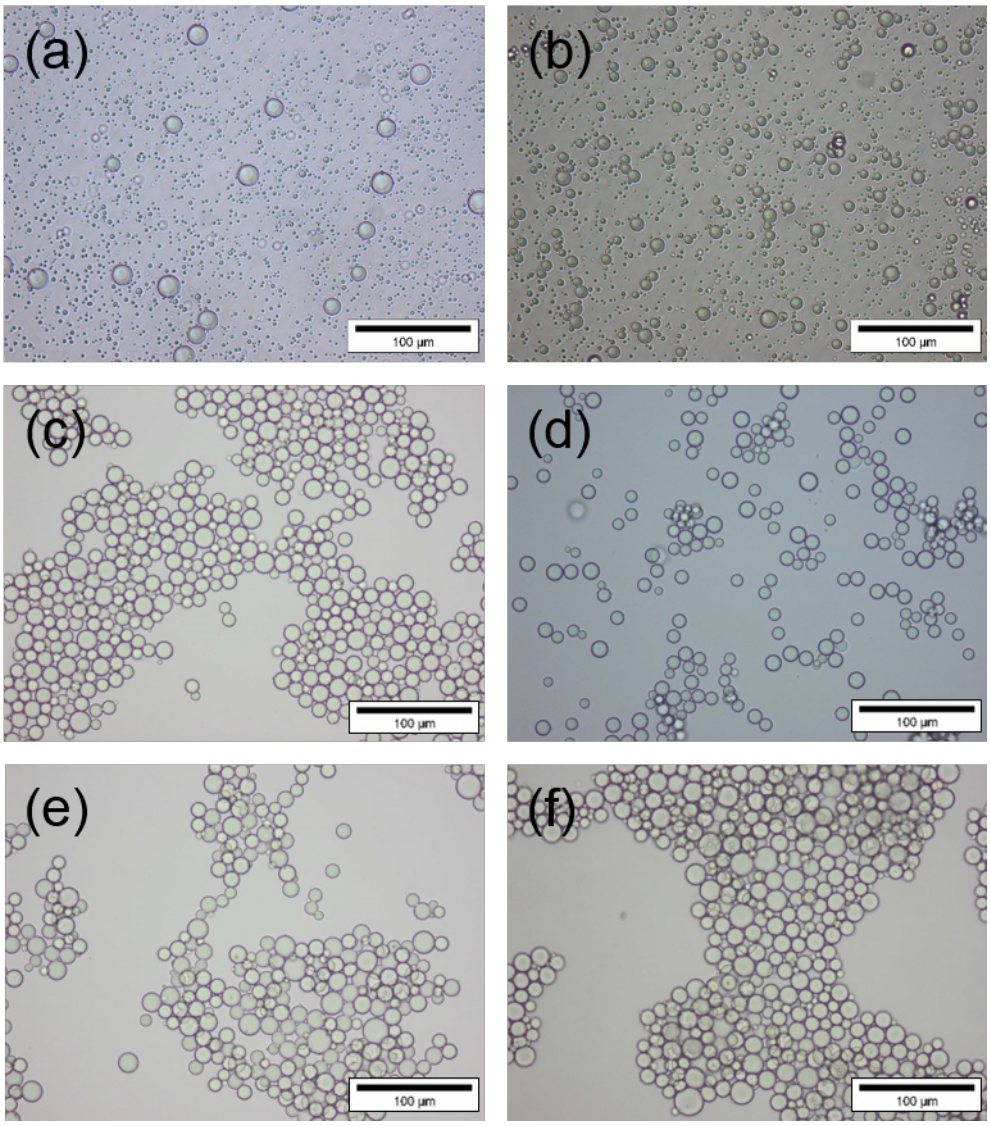

Figure 6.14: Optical micrographs of emulsions prepared with different concentrations of NaCl added to the NP dispersion before emulsification. Hexadecane (ϕ = 0.07) and Pt-PVP NP dispersions were homogenised at 40% amplitude for 1 min on an ultrasonic processor. The resulting conductivities of the NP dispersions after the addition of NaCl are; (a) 8.35 μScm^{-1}, (b) 100.7 μScm^{-1}, (c) 896 μScm^{-1}, (d) 1808 μScm^{-1}, (e) 8090 μScm^{-1}, (f) 18840 μScm^{-1}. Emulsion (a) corresponds to the emulsion formed from the dialysed NPs without the addition of salt. Emulsion (d) corresponds to the emulsion formed from the undialysed NPs.

6.6 Effect of the addition of excess salt to system before emulsification

It is apparent that the presence of some electrolyte is necessary to drive the adsorption of the nanoparticles to the interface. As can be observed from Figure 6.13 and Figure 6.16, with an increase in electrolyte concentration and hence conductivity the adsorption of NPs at the interface increases as a lower concentration of nanoparticles in the continuous aqueous phase is observed. These observations can be explained by the way in which PVP chains, which stabilise the NPs act in water. PVP undergoes specific interactions with water. Hydrogen bonding between protons of the solvent and cyclic tertiary amide groups of PVP, and hydrophobic intermolecular interactions between hydrocarbon groups, namely the polymer backbone and cyclic methylene groups result in these interactions. The polymer-solvent interaction via hydrogen bonding leads to swelling whereas the aforementioned hydrophobic intermolecular interactions cause compression of the chains into the coil and these two effects compensate for each other in solution. The canonical resonance forms highlight the potential for a partial negative charge to form on the oxygen in the pyrene ring as shown in Figure 6.15. The partial charge on the nitrogen is sterically hindered by the hydrocarbon backbone and nearby methyl groups.[169] In deionized water PVP exhibits a negative charge as suggested by the negative zeta potential.[12] Residual borohydride ions adsorbed at the interface will mainly contribute towards the negative charge on the nanoparticles.

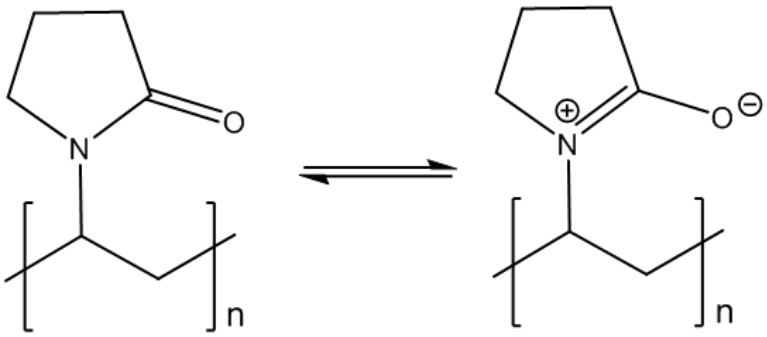

Figure 6.15: Resonance structures of PVP with a negative charge localised on the oxygen atom and positive charge localised on the nitrogen atom.

The addition of salt (electrolyte dependant) to solution affects the hydrogen

bonded structure of water and therefore the strength of hydrogen bonding between polymer and solvent. Güner found that in the presence of a salt, aqueous solutions of PVP exhibited an decrease in Huggins constant values. Huggins constants are a consequence of polymer solvent interactions. Therefore the addition of salt leads to an increasing degree of hydrophobic interactions of the polymer segment and subsequently the polymer coil contracts due to the increase in intermolecular association of the polymer coil.[94] The salts compete with the PVP for hydration which could lead to increased polymer entanglement at the interface, though it will mainly affect the affinity of the Pt-PVP NPs for the o/w interface as compared to its affinity for the solvent, which will be the predominant driving force for its adsorption at the interface. The oil-water interface may be expected to have a slight negative charge, due to impurities and dissolved CO_2, thus the approach of the negatively charged nanoparticles will be unfavourable. Therefore on addition of NaCl, the screening charge on the nanoparticles is increased, hence there is less repulsion and faster adsorption to the oil water interface will be facilitated.

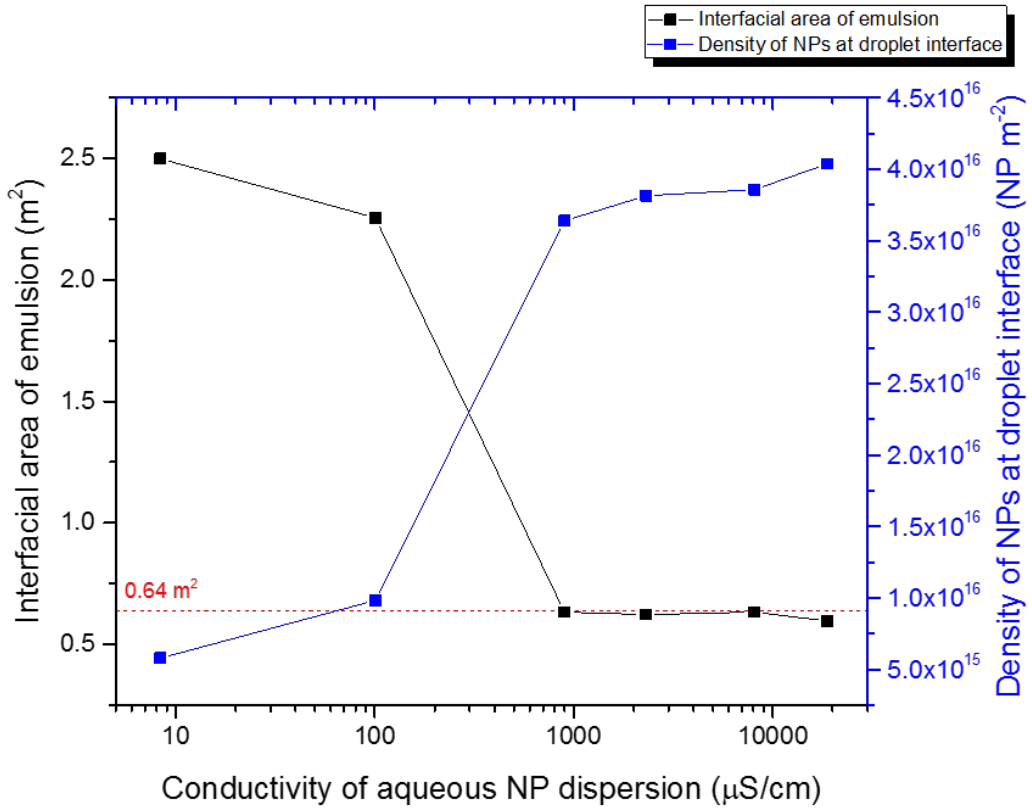

Figure 6.16: Nanoparticle density at the oil-water interface and interfacial area of emulsion as a function conductivity of aqueous NP dispersion. Hexadecane (ϕ = 0.07) and Pt-PVP NP dispersions were homogenised at 40% amplitude for 1 min on an ultrasonic processor. The red line represents the interfacial area that the amount of Pt-PVP NPs used (9.5 ml) can stabilise (based on calculations detailed in Chapter 3 using an inter particle spacing of 2.9 nm and core diameter of 3.3 nm.)

At lower electrolyte concentrations a higher than expected interfacial area is observed (Figure 6.16). This may be a result of the stabilising PVP on the NPs not contracting to as great an extent thus occupying a larger area at the interface. Therefore a smaller number of nanoparticles can occupy a larger area as the packing density is reduced. However these films are likely to be less robust as there is likely to be less polymer entanglement at the interface and thus the

emulsion less stable.

6.7 Conclusion

This chapter demonstrates that the particles synthesised in Chapter 4 were able to efficiently adsorb at the oil-water interface and stabilise o/w emulsions. It was found that controlling the limited coalescence immediately after emulsification allowed better control over the final emulsion size. As shown previously in Chapter 5, the importance of minimising the excess PVP in the emulsion system was again demonstrated in the case of the emulsions. As suggested before an increase of PVP in the Pt NP dispersion led to a decrease in the density of adsorbed NPs at the droplet interface, which can be detrimental for the subsequent electroless deposition process that these emulsions are used as a template for. For a given volume of nanoparticles the limit in stability with increasing oil fraction was obtained, suggesting that for the maximum particle concentration achieved in their synthesis a stable emulsion could be produced with an oil fraction from 0.05 to 0.13. These emulsions had near maximum surface coverages and support the idea of limited coalescence occurring for this system. Such volume fractions are likely to be sufficient, should these systems be eventually chosen to be manufactured. These results again agree with the particle density at the interface as calculated in Chapter 5. The particle concentration in the emulsion continuous phase has been accurately measured and correlated again to visual observations made of the emulsions and of the electron microscopy images in the previous chapter. Finally the influence of electrolyte concentration on the emulsion system was investigated and the importance of the presence of some salt in the system in order for the particles to act as efficient emulsifiers was demonstrated.

Chapter 7

Metallic coating of emulsion droplets

7.1 Synopsis

This chapter will examine the electroless deposition of a secondary metal onto the emulsion droplets, which will thereby encapsulate the oil core as illustrated in Figure 7.1. Firstly, this chapter will demonstrate successful deposition of thin secondary metallic films and the full retention of the encapsulated oil. Additionally, the components of the plating solution shall be investigated to explore control over the quality and thickness of the deposited secondary film. Finally, different release mechanisms will be explored including mechanical fracture, ultrasound and infrared radiation.

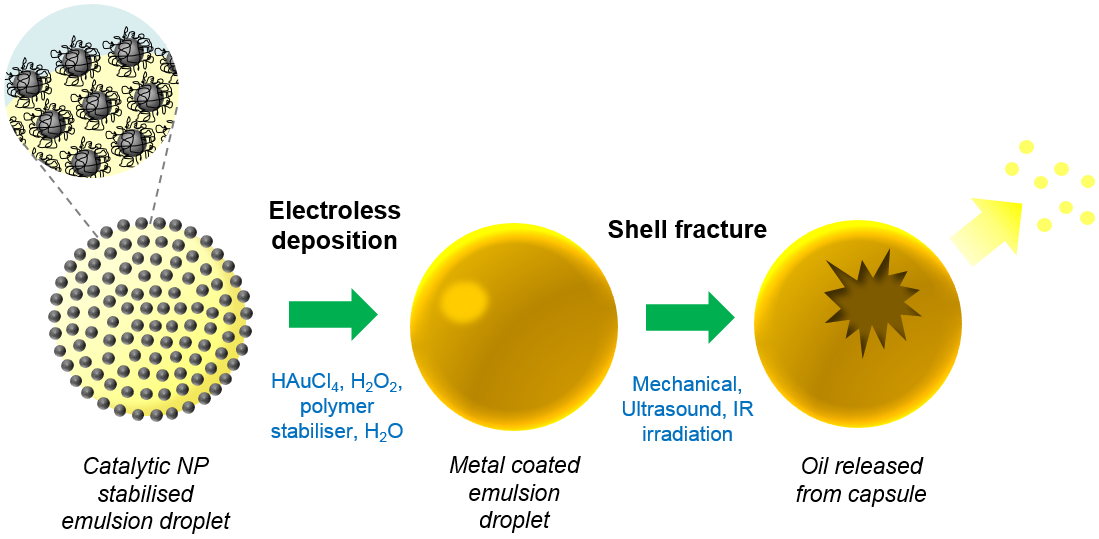

Figure 7.1: Schematic illustrating gold coating of emulsion droplet via electroless deposition onto the catalytic platinum nanoparticle emulsifiers to create microcapsules and subsequent shell fracture to release core.

7.2 Gold coating of Pt-PVP stabilised hexadecane droplets

As previously mentioned platinum nanoparticles can act as a catalyst for the growth of secondary gold films.[102] As in the previous chapter well-controlled Pickering emulsions are produced with a dense monolayer of Pt nanoparticles adsorbed at the droplet surface, the work in this chapter focuses on using these nanoparticles as catalysts to grow a gold film at the droplet interface and hence encapsulate the oil. As previously demonstrated in Chapter 6 a system where there are no excess nanoparticles in the bulk and the catalytic particles are mostly adsorbed at the interface is attained, therefore the subsequent electroless deposition process should grow the desired gold film solely at the oil-water interface.

Previous work on metal coating onto colloids has mainly been focused around applications on polymer particles and ceramic substrates, with less work on liquid

cores[181] and for encapsulation[226],[101] as described in Chapter 2.3.6. Conventional electroless plating methods often used formaldehyde or hydroxylamine as the reducing agent.[184] Here a simple method is implemented where $HAuCl_4$ and H_2O_2 are used to deposit the gold film, where H_2O_2 is used to reduce the Au^{3+} ions from the $HAuCl_4$ precursor to Au^0. The reaction can be explained by the following equations and with associated standard reduction electrode potentials (E^θ) (Equations 7.1, 7.2)[108]

$$2AuCl_4^- + 6e^- \longrightarrow 2Au + 8Cl^-(E^\theta = +1.002V) \tag{7.1}$$

$$3H_2O_2 \longrightarrow 3O_2 + 6H^+ + 6e^-(E^\theta = -0.695V) \tag{7.2}$$

These equations can be combined to give the overall equation, where the platinum nanoparticles act as a catalyst (Equation 7.3). Additionally, unlike many other electroless deposition methods, this method offers the advantage of not using cyanide in the plating solution, which is toxic and hazardous.[184]

$$2HAuCl_4 + 3H_2O_2 \xrightarrow{\text{Pt}} 2Au + 3O_2 + 8HCl \tag{7.3}$$

The standard redox potential for the overall reaction is +0.307 V which shows that H_2O_2 is thermodynamically capable of reducing $HAuCl_4$ to Au^0. It is thought that in the initial stage of the reaction, gold complexes are reduced by the hydrogen peroxide until metallic gold precipitates. Initially this process is catalysed by the platinum nanoparticles at the emulsion droplet interface. Subsequently a self-catalytic process occurs where the initial gold seeds catalyse the reduction of the precursor via hydrogen peroxide.[242] Without the presence of the platinum catalyst on the droplet interface the reduction reaction does not occur.

A plating solution comprising hydrogen peroxide, gold (III) chloride hydrate, polymer stabiliser and water, based upon methods by Hitchcock et al.[101] and Horiuchi et al.[102] was used. A polymer stabiliser is required in the plating solution to control the growth and provide steric stabilisation for the resulting gold capsules.

7.3 Demonstrating impermeability

Capsules were prepared from a hexadecane (0.75 ml) and Pt-PVP NP (10 ml) emulsion homogenised with an ultrasonic probe (see details in Chapter 3) at 40% amplitude for 1 minute (Figure 7.2). Following washing cycles the emulsion was placed in a plating solution consisting of PVP (5 ml, 0.2 wt%), water (10 ml), gold salt (2 ml, 180 mM) and hydrogen peroxide (1 ml, 1620 mM) as a reducing agent. The capsules were mixed for 30 minutes and subsequently washed after sedimentation.

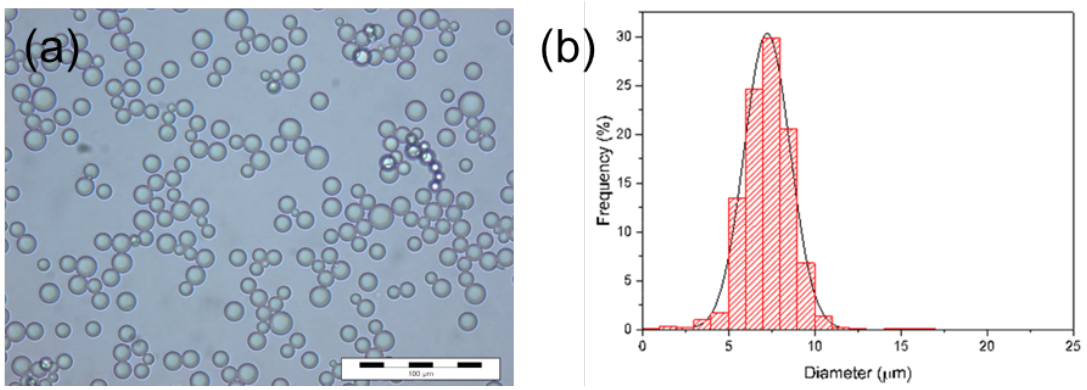

Figure 7.2: (a) Optical micrograph of emulsion prepared from a hexadecane (0.75 ml) and Pt-PVP NP (10 ml) emulsion homogenised at 40% amplitude for 1 minute, (b) and its corresponding size distribution measured by imaging flow cytometry.

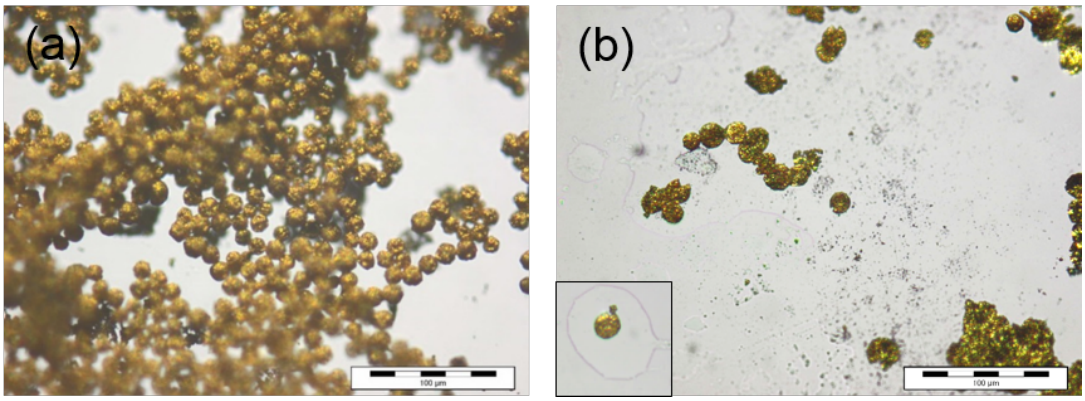

Figure 7.3: Optical micrographs of gold coated emulsion; (a) dried capsules before crushing (b) dried capsules after crushing, inset shows oil around capsule.

The capsule permeability was tested over time. The capsules were placed in an 4:1 (volume ratio) ethanol/ water continuous phase to mimic a full perfume formulation. The release was measured by gas chromatography (GC). Hexadecane solubility limit in ethanol is higher than the concentration used in this experiment so all oil can be dissolved by the continuous phase used here. Consequently, any oil leaking from the capsules would dissolve in the ethanol continuous phase and be detected by GC. Capsules were dispersed in ethanol in a 1:4 ratio and kept suspended at 40°C for periods of time up to 35 days. At different time intervals, the gold capsules were centrifuged and the resulting supernatant was analysed by GC.

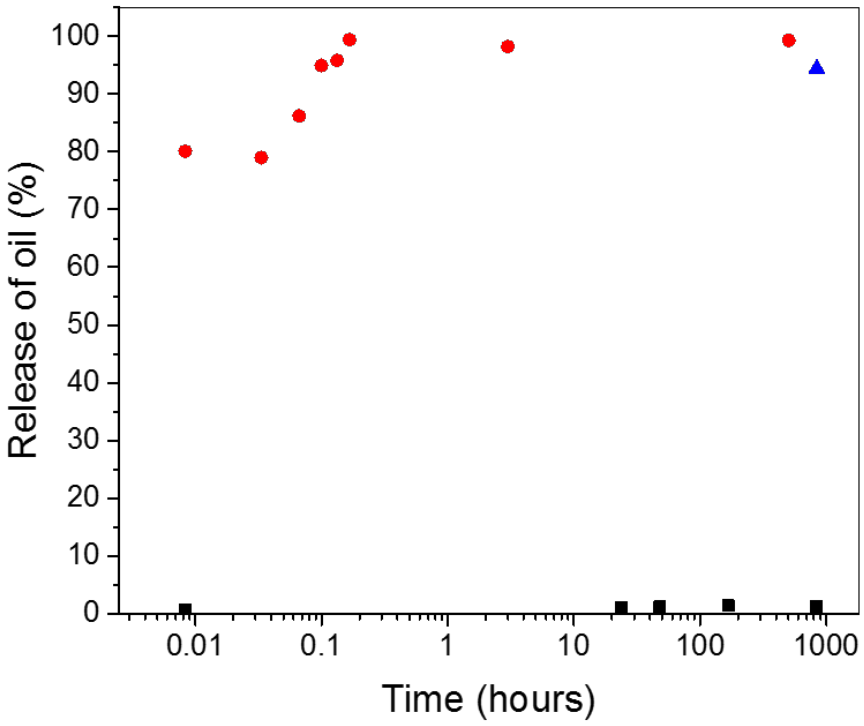

Figure 7.4: Release of oil core from capsule over time in a 4:1 ethanol:water continuous phase at 40°C. Black squares represent gold coated emulsion capsules, red circles represent uncoated PMMA shell capsules (data collected by Alison Tasker[101]), blue triangle represents release from crushed gold coated emulsion capsule.

Figure 7.4 demonstrates that the microcapsules (black squares) are able to fully retain the hexadecane core for over 30 days compared to polymer capsules (red circles) without any metal film which release most of their payload in less than 1 hour. This demonstrates the reduced diffusion and the benefit of a metal shell for encapsulating small species. The blue triangle illustrates the percentage of oil obtained from a mechanically fractured metal emulsion capsules. Micrographs of the dried capsules (Figure 7.3) illustrate that there is indeed oil within the capsule core.

7.4 Effect of polymer stabiliser

The role of the polymer in the plating solution is to provide steric stability to the capsules as they form. It was found that using PVP at a stabiliser in the plating solution sometimes led to rough, brittle shells that often aggregated. This is undesirable as a uniform coating is necessary to ensure the minimum amount of gold is used for cost-effectiveness purposes. Additionally, shell rupture can be controlled more efficiently with smooth, unaggregated capsules. In comparison, an uneven coating could lead to a differential in pressure across the capsule surface. Aggregation is undesirable as the microcapsules are unable to be dosed effectively. One possible reason for the observations is the influence of the stabilising polymer, as it is likely that PVP interacts with the gold salt ions prior to reduction.[72] This could then hinder the deposition of the gold at the interface and cause it to deposit in a non-uniform way. Additionally it has been found that PVP preferentially adsorbed on the Au(111) plane which promotes growth in a certain direction.[127] In an attempt to overcome this issue different polymer stabilisers were tested as an alternative to PVP including poly vinyl alcohol (PVA) and poly ethylene glycol (PEG)(Figure 7.5). PVA has been known to stabilise gold[241] and is highly stable and chemically inert. Additionally it is considered to be generally safe and biocompatible so is relatively safe when administered orally.[173] This makes PVA a suitable candidate for the stabilisation of the capsules in view of their potential medical applications. Different forms of functionalised PEG have also been shown to stabilise gold growth and are also already used in pharmaceutical products. Additionally PEG can be easily functionalised to help aid stability and improve bioavailability.[224]

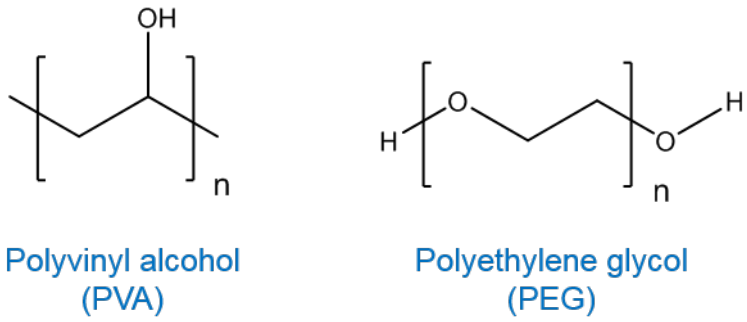

Figure 7.5: Chemical structures of PVA and PEG.

Microcapsules were prepared from a hexadecane (0.75 ml) and Pt-PVP NP (10 ml) emulsion homogenised with an ultrasonic probe at 40 % amplitude for 1 minute followed by agitation on the carousel for 30 minutes and washing of the aqueous phase to remove excess nanoparticles from the continuous phase. The emulsion (0.5 ml) was added to a plating solution of water (10 ml), polymer (10 ml, 0.05 wt%; 40 kDa PVP, 35 kDa PEG, 67 kDa PVA), gold (III) chloride trihydrate (2 ml, 180 mM). Subsequently hydrogen peroxide (1 ml, 1620 mM) was added to initiate the electroless deposition process. The ratio of gold salt and reducing agent remained constant for each sample (4.5 x molar excess to ensure full reduction of the metal salt in the process). Upon the addition of the H_2O_2 the samples were agitated for 30 minutes on a carousel and then left to sediment or cream.

Optical micrographs of the gold microcapsules in suspension in water and after drying were obtained. The PVP stabilised capsules in Figure 7.6 show a good gold covering however upon drying some appear to have collapsed which is unfavourable. These capsules all sedimented and exhibited some aggregation. The PEG stabilised gold microcapsules (Figure 7.7 did not appear to be evenly coated and were highly aggregated. This aggregation increased upon washing the capsules suggesting that the PEG did not stabilise the capsules well. This may be due to the highly hydrophilic nature of PEG, resulting in it having a low affinity for adsorption at the interface. A PEG functionalised with a more hydrophobic moiety may produce better results. The PVA coated microcapsules (Figure 7.8)

exhibited some aggregation however much less than the PEG. Additionally the capsules appeared intact upon drying. PVA and PVP are likely to have a higher affinity for the interface and therefore more likely to stabilise it better, however more work is needed to understand the interaction between the metal and the polymer and the exact mechanism of stabilisation.

Some of the capsules in Figures 7.6 - 7.8 do not appear spherical. These observations may be attributed to the surface roughness of the capsules as the gold films are relatively thick and is discussed further in the subsequent chapter. Additionally the interaction of the polymer with the capsules as the gold film is growing may contribute towards the surface roughness. For example PVP is known to interact with certain gold planes which may direct the growth in a particular direction.[127] Furthermore some variation in capsule shape can be observed across the samples. This can be accounted for by the variation of roughness across the samples and possible inconsistent mixing.

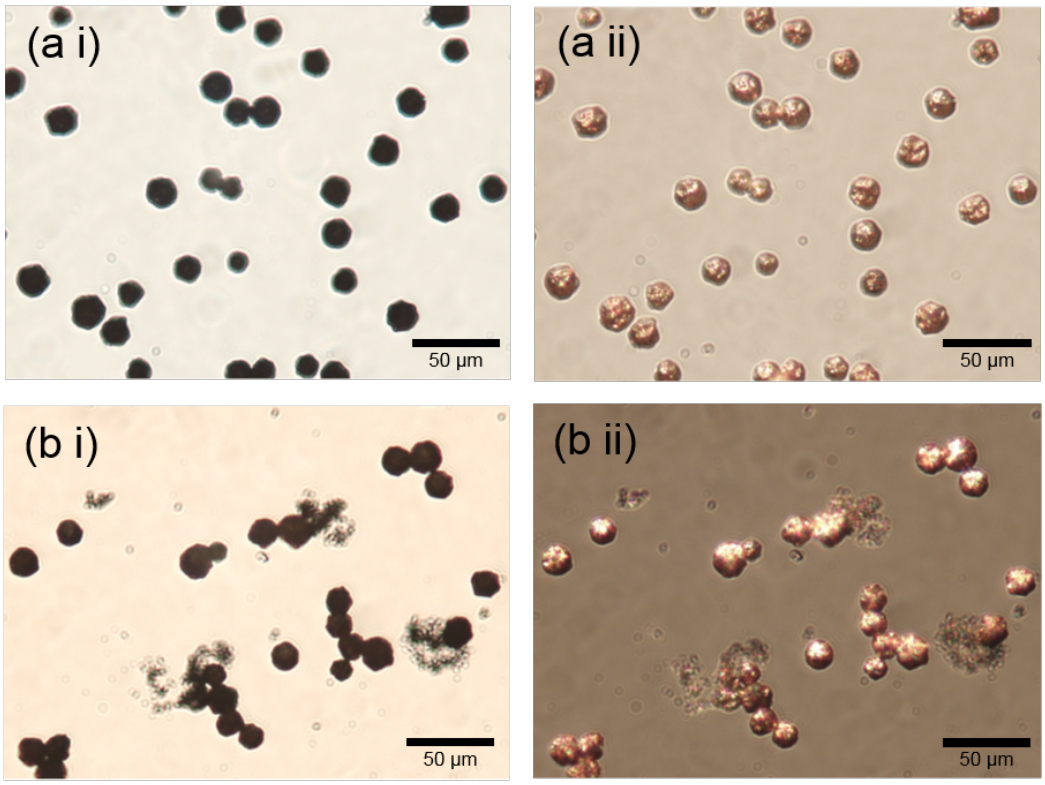

Figure 7.6: Optical micrographs of PVP stabilised gold microcapsules in suspension in water (a i) transmitted light, (a ii) reflected light and dried microcapsules (b i) transmitted light and (b ii) reflected light.

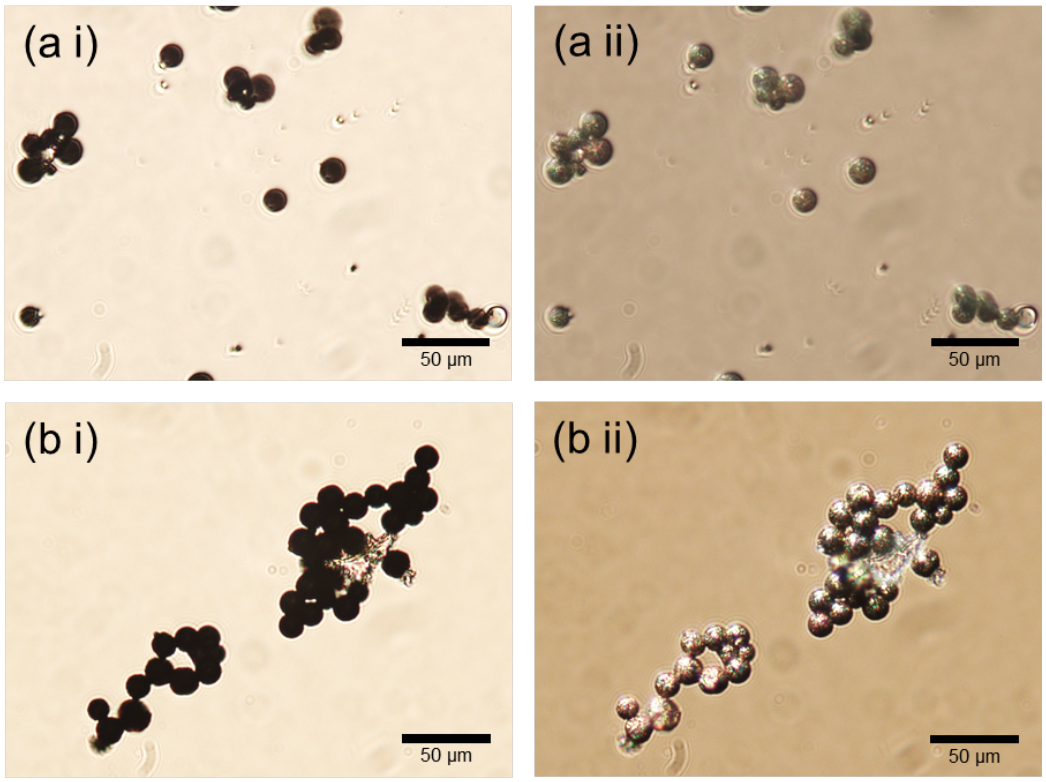

Figure 7.7: Optical micrographs of PEG stabilised gold microcapsules in suspension in water (a i) transmitted light, (a ii) reflected light and dried microcapsules (b i) transmitted light and (b ii) reflected light.

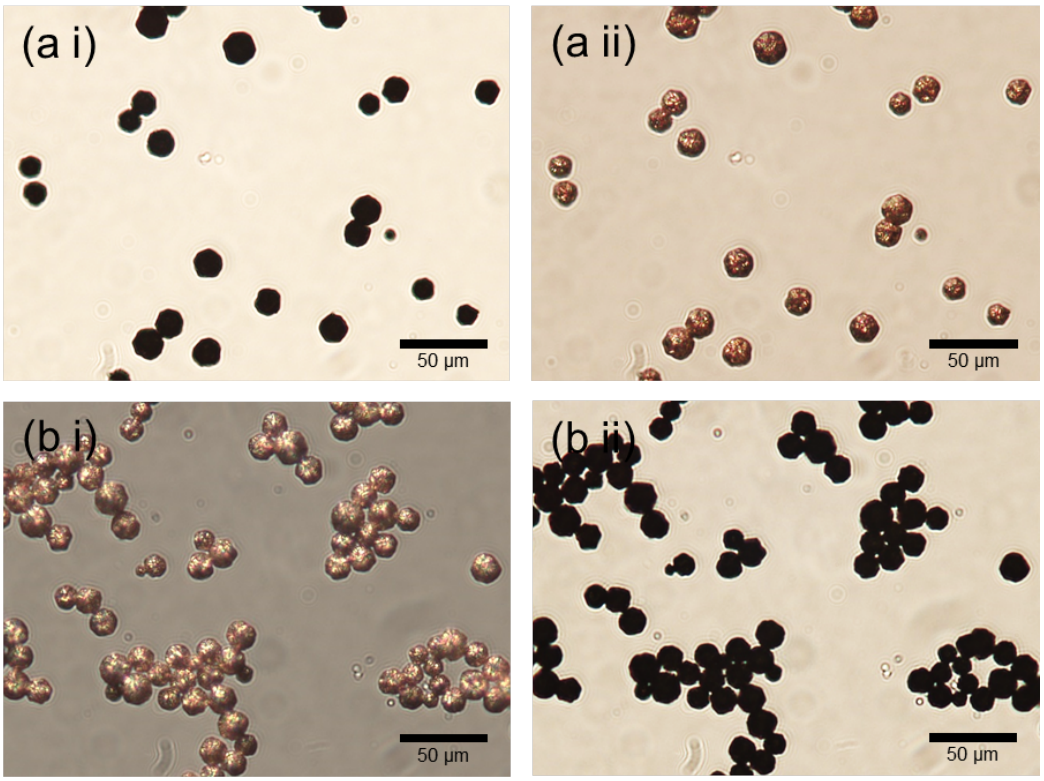

Figure 7.8: Optical micrographs of PVA stabilised gold microcapsules in suspension in water (a i) transmitted light, (a ii) reflected light and dried microcapsules (b i) transmitted light and (b ii) reflected light.

Bench top SEM micrographs were recorded for the samples to observe the morphology of the capsules in their dried state (Figure 7.9). Most of the PVP microcapsules (a) appear to be intact with some looking more brittle and wrinkled. The PEG (b) appear to have a more porous surface and there is evidence of cracks and broken shells. The PVA microcapsules (c) appear smoother and less collapsed. These observations corroborate the observations from the optical microscope images.

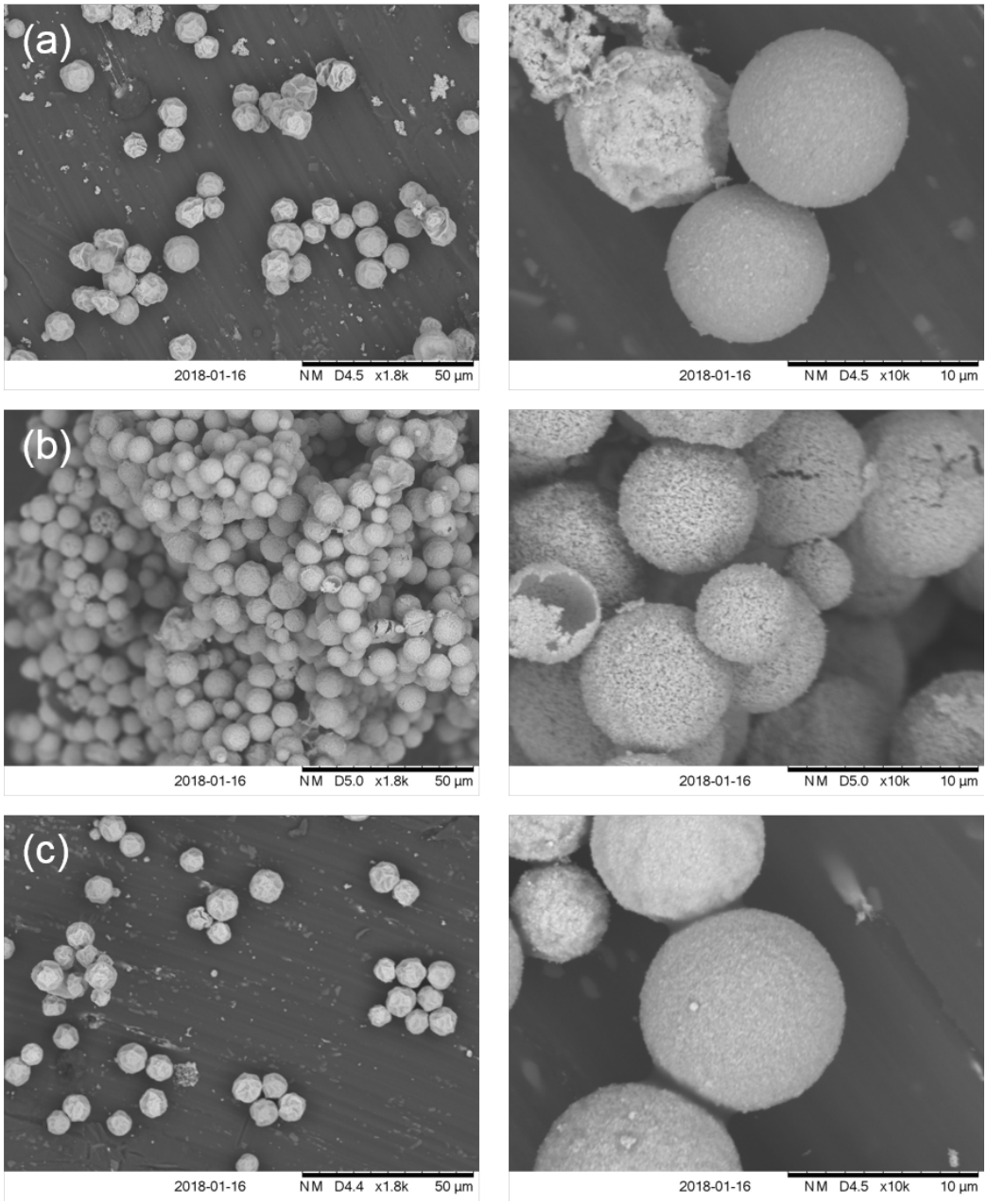

Figure 7.9: Bench top Scanning Electron micrographs of gold microcapsules prepared with 180 mM $HAuCl_4$ and stabilised with (a) 40 kDa PVP, (b) 35 kDa PEG and (c) 67 kDa PVA.

The PVA stabilised gold microcapsules appear most stable when dried and

aggregate the least compared to the PVP and PEG stabilised capsules, therefore 67 kDa PVA will be used in the plating solution for the next experiments.

7.5 Effect of gold salt concentration

Changing the concentration of gold salt used in the metal plating stage allows us to control the shell thickness of the secondary film on the surface of the oil droplets. This is useful as it allows us to tailor the capsule density, optical properties and mechanical stability. It also allows us to find the limits of the permeability of the shells. This is useful from a manufacturing perspective as it is more cost effective to reduce the amount of gold used for microencapsulation. Additionally by changing the shell thickness there is the potential to change the optical resonance which may be useful for optical sensors and imaging applications.[123], [249]

In this part of the work microcapsules were prepared from a hexadecane (0.75 ml) and Pt-PVP NP (10 ml) emulsion homogenised with an ultrasonic probe at 40 % amplitude for 1 minute followed by agitation on the carousel for 30 minutes and washing of the aqueous phase to remove excess nanoparticles from the continuous phase. The emulsion (0.5 ml) was added to a plating solution of water (10 ml), PVA (10 ml, 0.05 wt%, 67 kDa), gold (III) chloride trihydrate (2 ml). Subsequently hydrogen peroxide (1 ml) was added to initiate the electroless deposition process. The concentration of gold (III) chloride trihydrate added was varied from 180 mM to 12.5 mM. The ratio of gold salt and reducing agent remained constant for each sample (4.5 x molar excess to ensure full reduction of the metal salt in the process). Upon the addition of the H_2O_2 the samples were agitated for 30 min on a carousel and then left to sediment or cream.

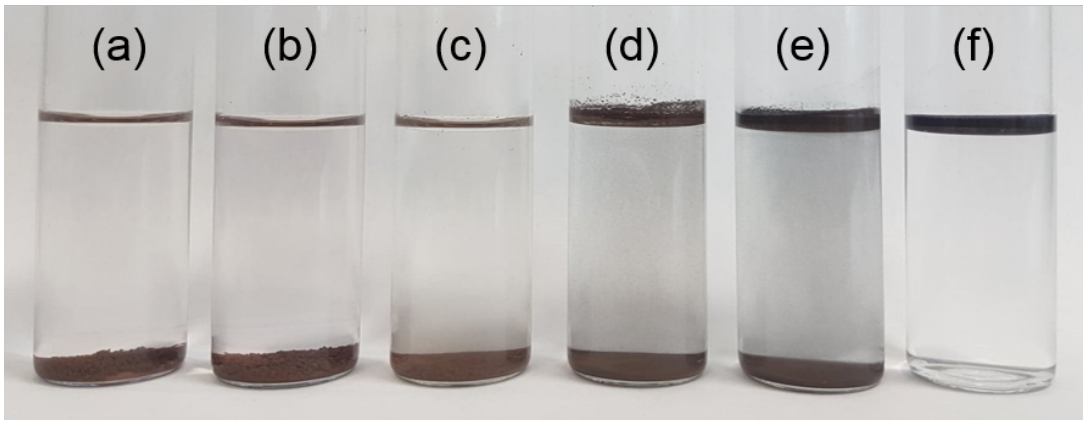

Figure 7.10: Digital photographs of the suspensions of gold microcapsules prepared at different concentrations of $HAuCl_4$; (a) 180 mM, (b) 100 mM, (c) 50 mM, (d) 25 mM, (e) 12.5 mM, and (f) 6.25 mM.

As can be observed from the digital photographs in Figure 7.10, capsules with gold concentrations of 50 mM and higher ((a) - (c)) fully sediment, whereas below this concentration creaming is observed for all samples with some sedimentation also observed in the case of (d) and (e). This relates well to the theoretical density calculations in Figure 7.11, where the microcapsule's specific density was calculated based on the measured size distribution of the emulsion ((via imaging flow cytometry) and the assumption that all gold is reduced at the oil-water interface. According to Stokes Law, the capsules with densities above the density of water (red line on Figure 7.11) should sediment and those below should cream. For (d) and (e) the microcapsules are close to the density of water therefore it is likely that some will cream and some will sediment as there is a distribution of droplet sizes and the resulting density within the same sample can depend strongly on the individual droplet sizes.

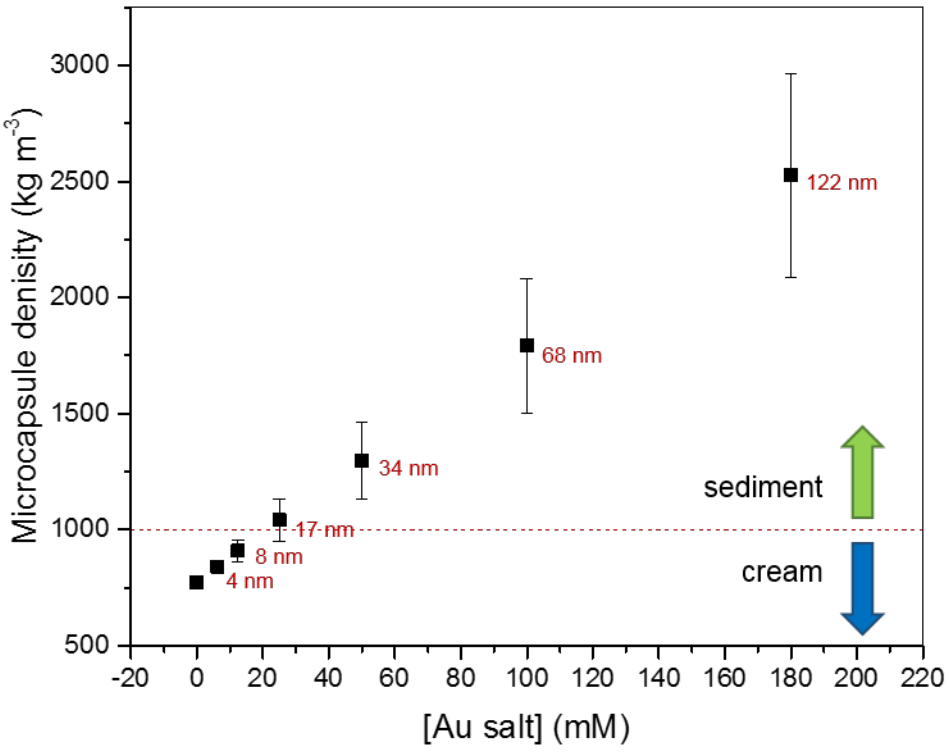

Figure 7.11: Theoretical microcapsule densities as a function of gold salt concentration added to the plating solution. The red line represents the density of water. The value at zero represents the uncoated emulsion. The annotated numbers indicate the theoretical shell thickness of the microcapsules calculated on the basis of the amount of gold salt added to the system and the total interfacial area derived from the measured particle size distribution.

Optical micrographs of the microcapsules (Figure 7.12 & 7.13) in suspension in water show that the emulsion droplets have been successfully plated with gold as the capsules do not transmit light through and appear to show a light-reflecting surface when observed in reflected light mode. With a reduction in the concentration of gold used the shells appear thinner as the capsules in the transmitted light micrographs (left hand side) appear less opaque. The shells

also appear to be smoother as the gold concentration is reduced. An increase in roughness with increase in film thickness has been observed by other members of the research group studying metal films and in literature.[106] This may be a result of the way in which the gold shell grows at the interface. It is thought that the gold initially grows on the catalytic platinum sites. These initial gold seed colloids grow until they coalesce with neighbouring gold seeds to form islands. Coalescence continues and a continuous shell is formed. This growth mechanism was observed by Oldenburg et al. who studied the growth of gold shells on silica particles from gold nanoparticle nucleation sites.[187] As there is a high excess of reducing agent the reaction will be occurring quickly, so these initial gold seeds may be larger and hence result in less uniform growth for higher concentrations of gold salt, leading to a less smooth shell. The more that the gold film is grown, the fewer growing crystals that are present, which therefore accentuates the roughness and thus non-spherical appearance. Additional experiments are required to support this theory. Further work into changing the concentration or rate of addition of the reducing agent may lead to smoother shells. The concentration of gold salt here for the thickest shell is similar to that used in Section 7.4 where the polymer stabiliser was varied therefore the non-spherical capsules observed there may be attributed to the shell roughness too.

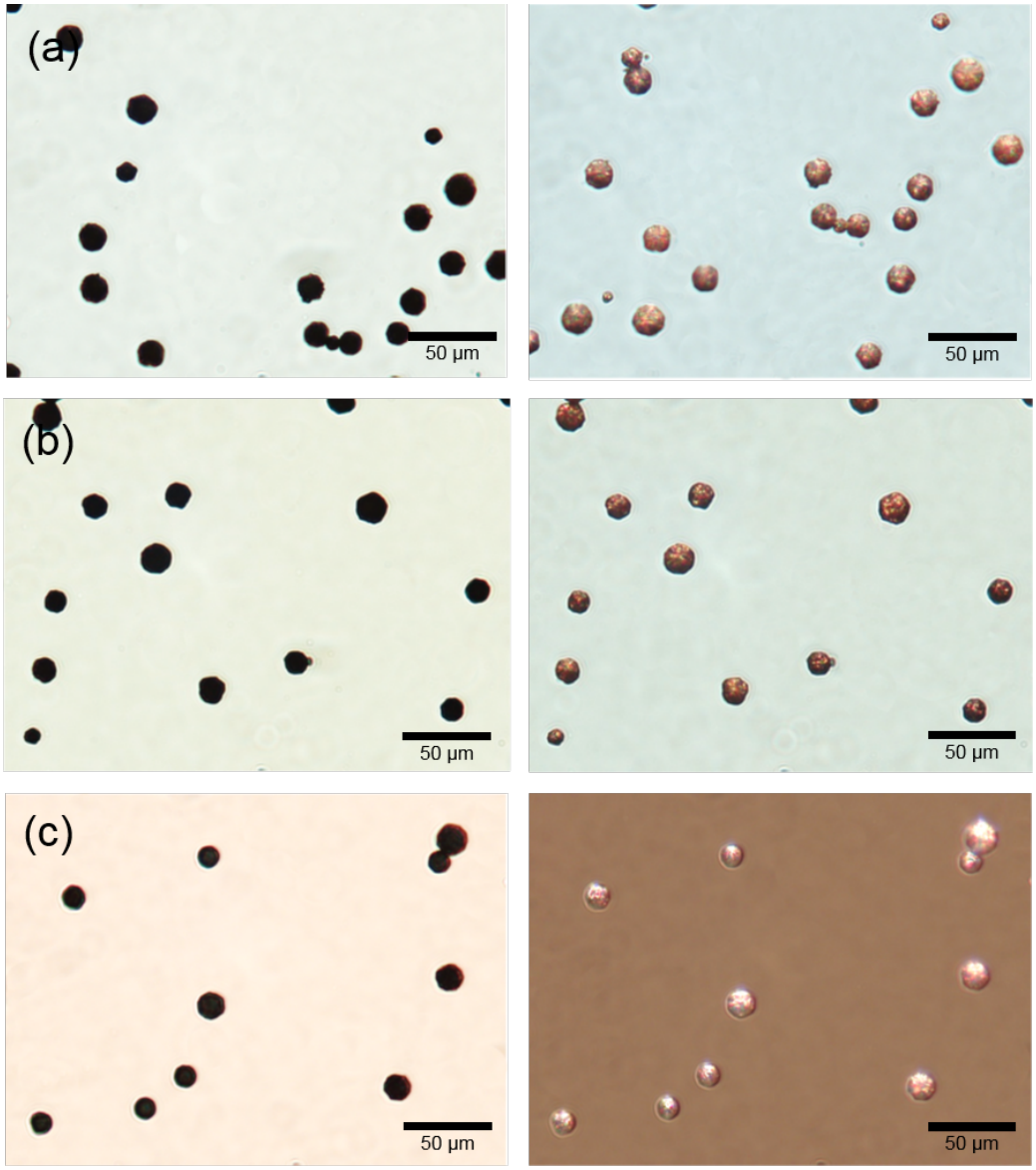

Figure 7.12: Optical micrographs of gold coated microcapsules in transmitted light (left) and reflected light (right) prepared with different concentrations of gold salt in the synthesis; (a) 180 mM, (b) 100 mM, (c) 50 mM.

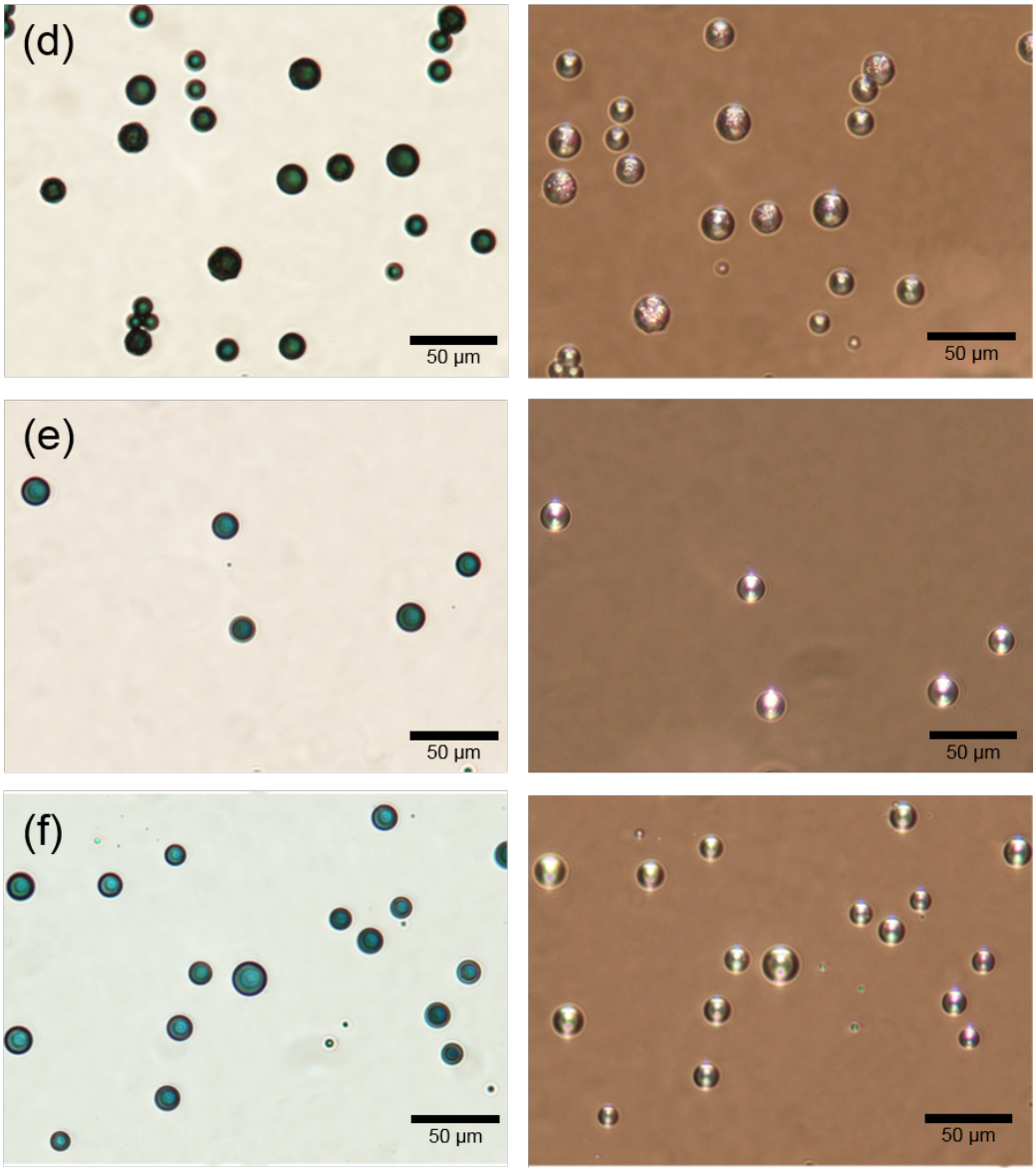

Figure 7.13: Optical micrographs of gold coated microcapsules stabilised with 67 kDa PVA in transmitted light (left) and reflected light (right) prepared with different concentrations of gold salt in the synthesis; (d) 25 mM, (e) 12.5 mM, (f) 6.25 mM.

The capsules were dried by allowing the water from the sample placed onto the microscope glass slide to evaporate at room temperature. Micrographs of

the dried capsules can be observed in Figure 7.14. Upon drying capsules (a) to (c) retained their 3D structure, whereas for (d) some have collapsed and some have retained their 3D structure and for (e) and (f) they have all collapsed. The theoretical thicknesses of the two thinnest shells are 4.4 nm (f) and 8.5 nm (e) respectively (Figure 7.11) therefore it might be expected that their resulting mechanical strength would be limited, which is seen to result in collapse of the microcapsules upon drying. However the thicker shells appear to have retained their spherical shape rather than bursting in most cases.

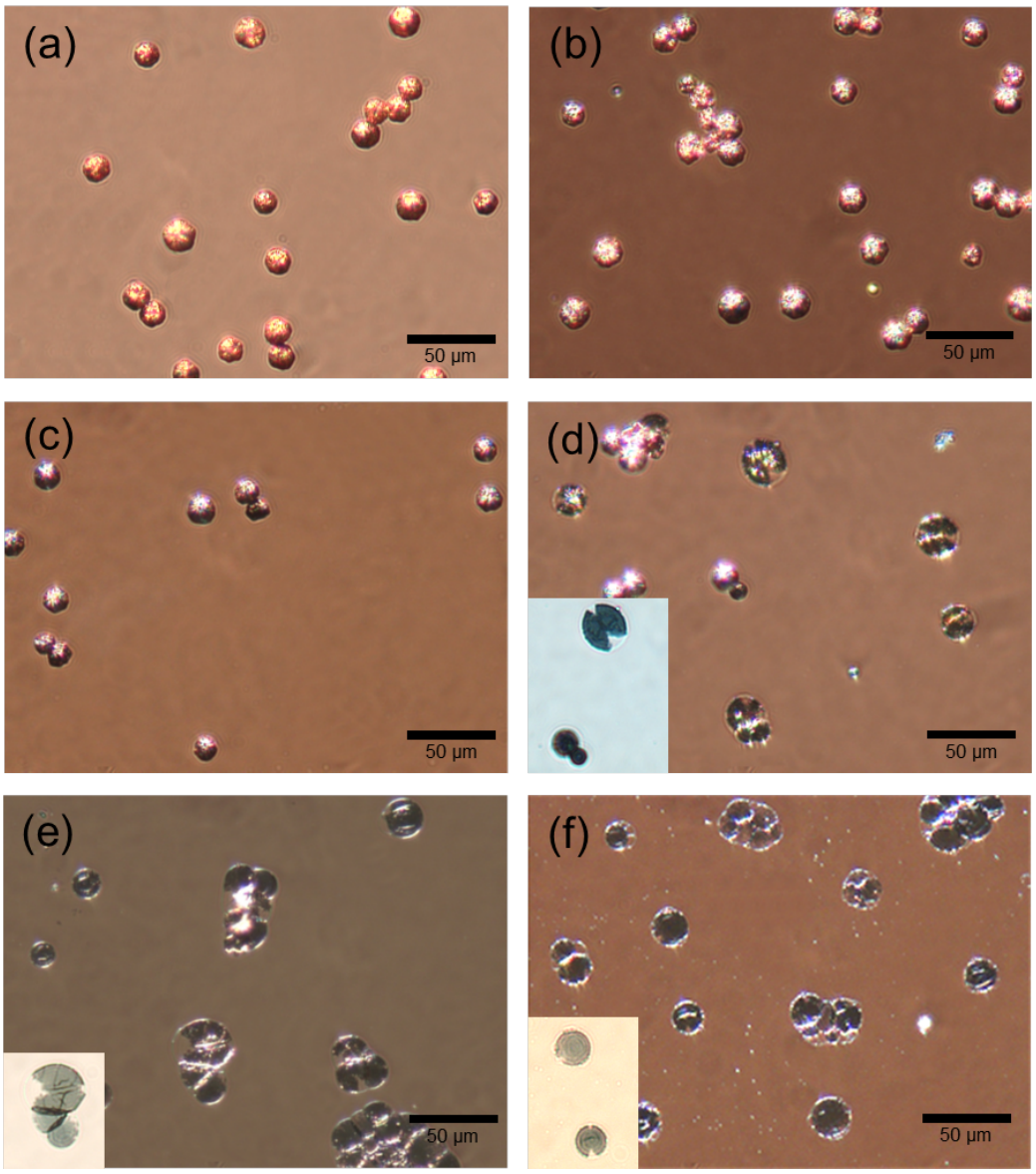

Figure 7.14: Optical micrographs of dried gold coated microcapsules stabilised with 67 kDa PVA in reflected light (inset is transmitted light) prepared with different concentrations of gold salt in the synthesis; (a) 180 mM, (b) 100 mM, (c) 50 mM, (d) 25 mM, (e) 12.5 mM, (f) 6.25 mM.

The microcapsules were visualised by SEM to better observe the surface morphology and roughness. Two types of SEM were used as they operate at differ-

ent vacuum pressures and can obtain different resolution images. The Hitachi TM3030 Bench Top SEM operates at lower vacuum pressure however is more suitable for low magnification images (Figures 7.15 & 7.16). The Hitachi SU8230 SEM operates at higher vacuum pressure and can obtain much higher resolution images (Figures 7.17 - 7.19). Here both instruments are useful as the microcapsules retain their spherical shape better in the Bench top unit, whereas they are far more likely to collapse in the Hitachi SU8230. However detailed surface morphology is only resolvable in the Hitachi SU8230 SEM.

The SEM micrographs confirm our earlier observations that there is an increase in surface roughness with an increase in gold concentration and hence shell thickness. This is particularly apparent when comparing the highest and lowest concentrations in Figure 7.17 and 7.18 as much larger features present on the interface of the thicker capsules (Figure 7.17) compared to that of the thinnest capsule (Figure 7.18). Wrinkling of some capsules is observed in most micrographs. This is most likely to be as result of the vacuum pressure of the SEM, however it is also possible that the wrinkles are formed during the electroless deposition process. It is possible that small temperature changes are occurring during the reaction which leads to the expansion of the hexadecane core, which retracts upon cooling, therefore resulting in a change in surface area and as a result the capsule may wrinkle. Alternatively the wrinkling could occur during drying or as a result of mixing during and/or after synthesis causing the microcapsules to come into contact with each other of the sample vial wall and hence denting the surface.

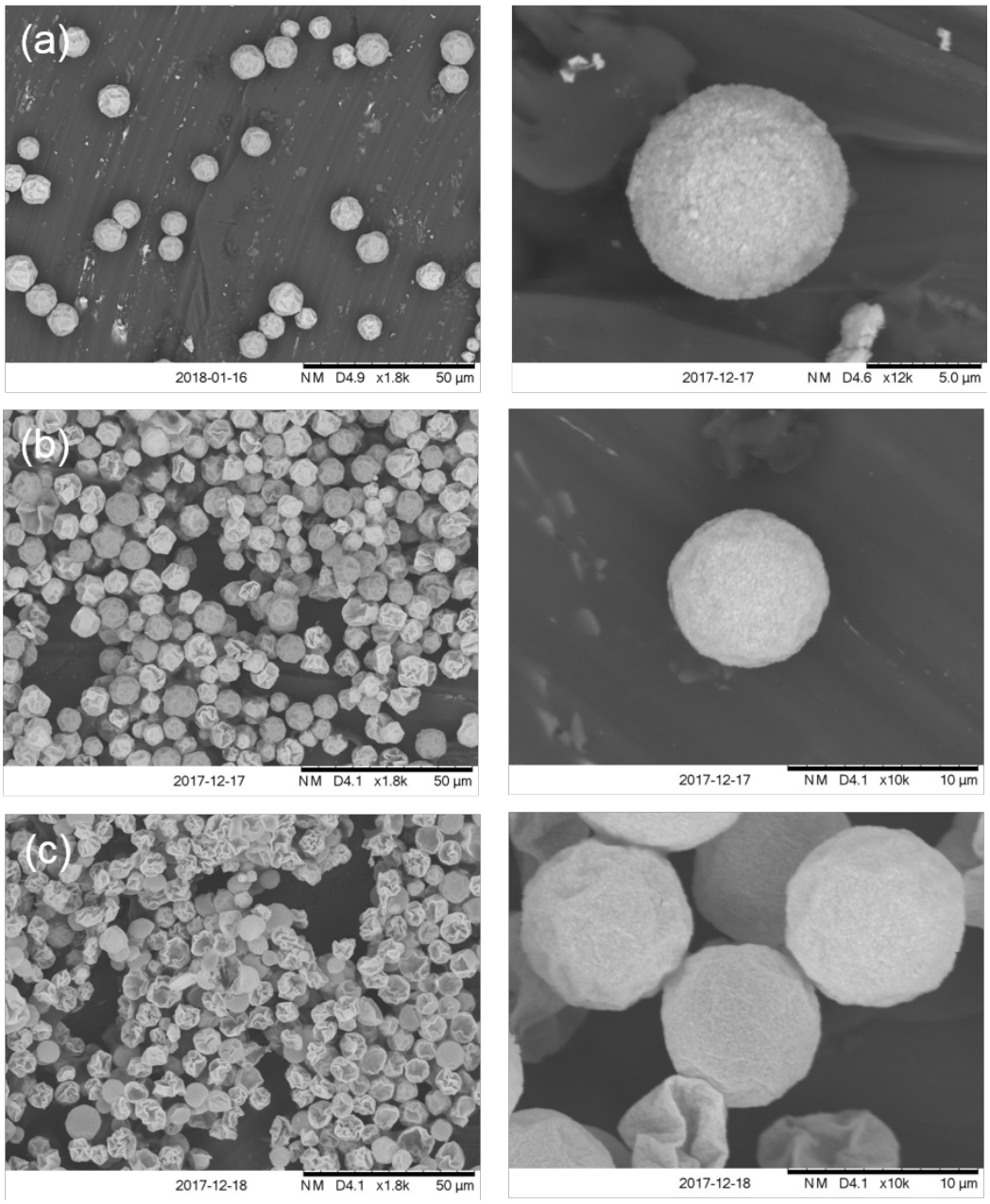

Figure 7.15: Bench top Scanning Electron micrographs of gold microcapsules stabilised with 67 kDa PVA prepared at different concentrations of gold salt in the synthesis; (a) 180 mM, (b) 100 mM, (c) 50 mM.

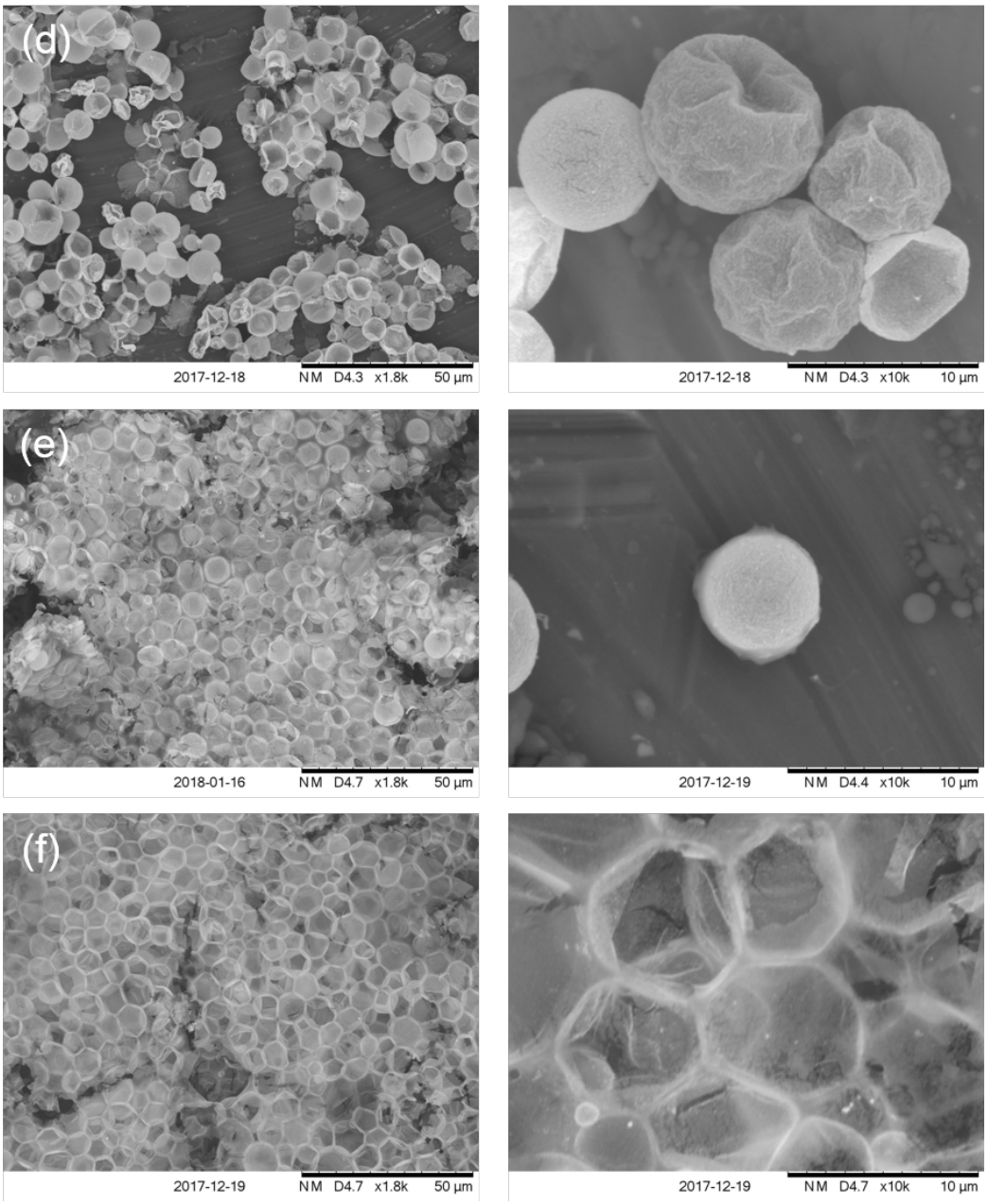

Figure 7.16: Bench top Scanning Electron micrographs of gold microcapsules stabilised with 67 kDa PVA prepared at different concentrations of gold salt in the synthesis; (d) 25 mM, (e) 12.5 mM, (f) 6.25 mM.

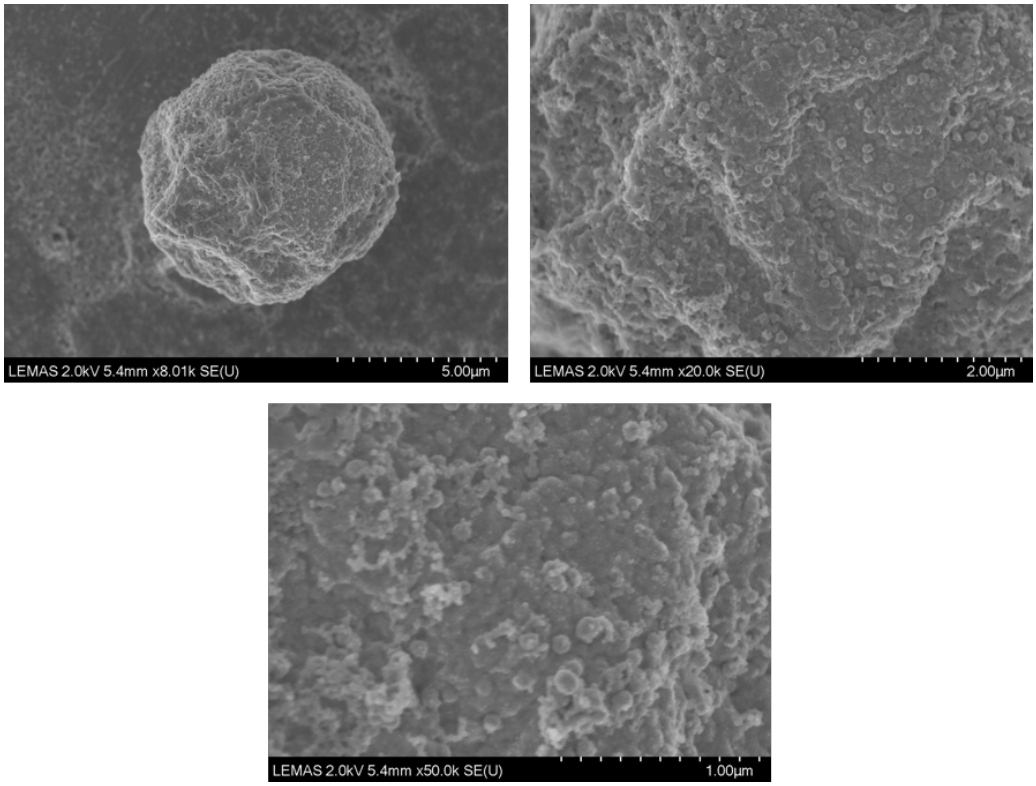

Figure 7.17: Scanning Electron micrographs of gold microcapsules stabilised with 67 kDa PVA prepared at 180 mM gold salt in the synthesis.

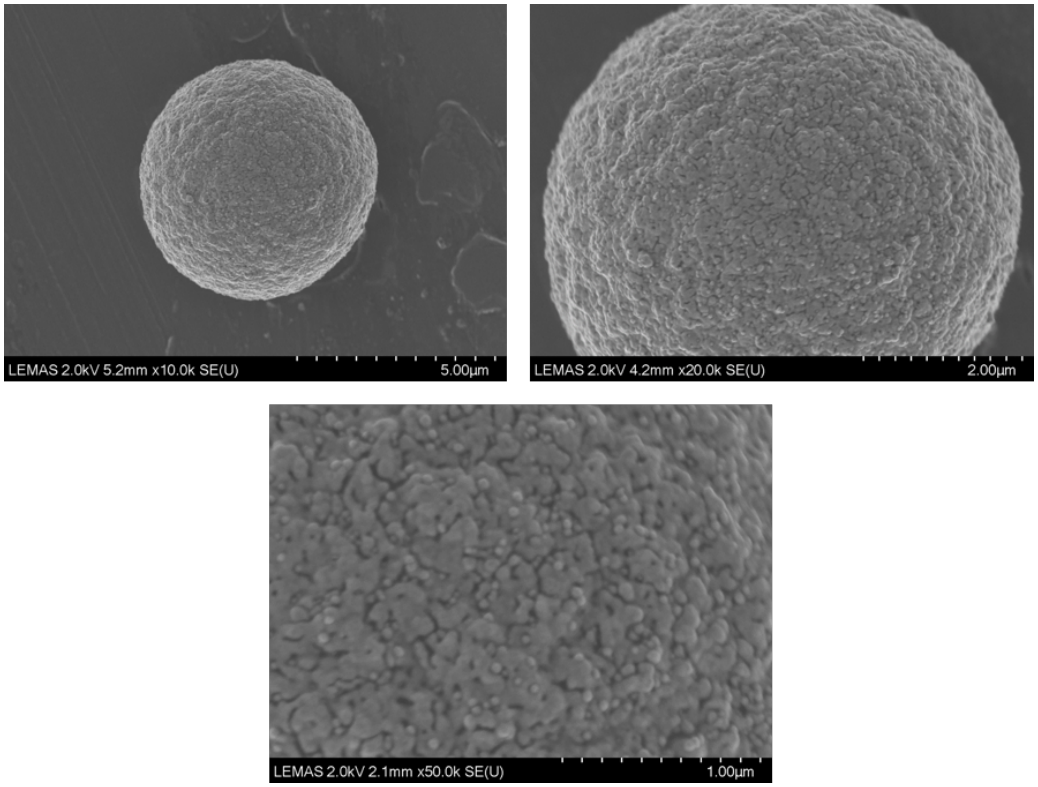

Figure 7.18: Scanning Electron micrographs of gold microcapsules stabilised with 67 kDa PVA prepared at 50 mM gold salt in the synthesis.

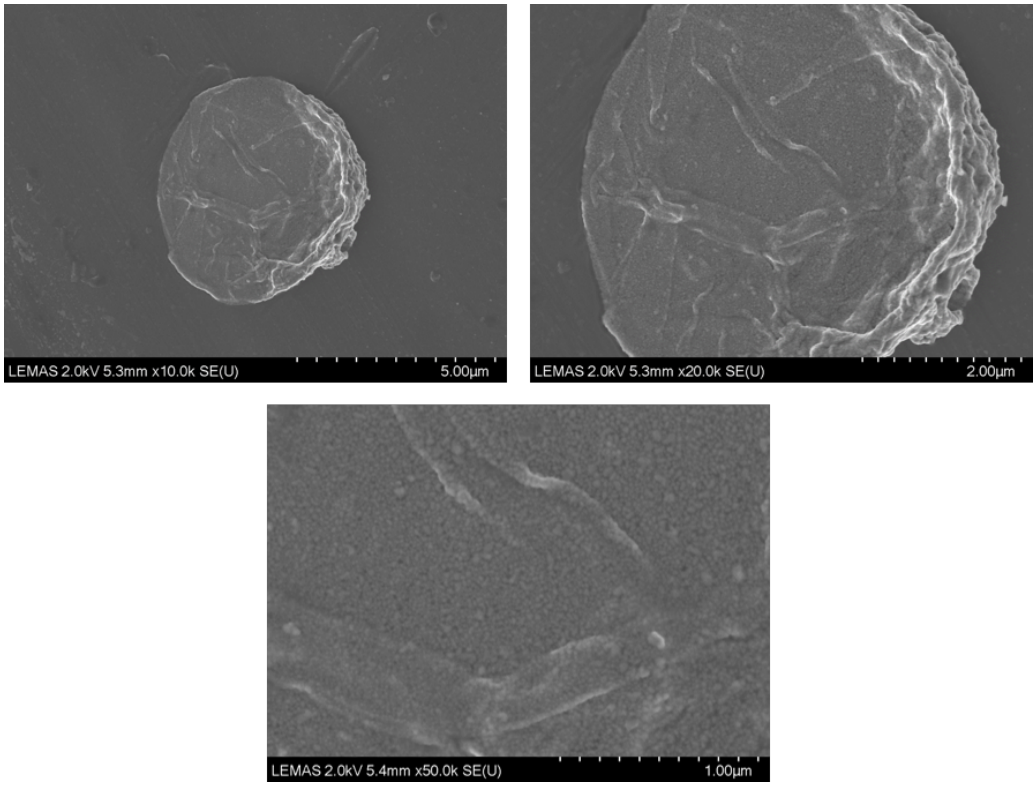

Figure 7.19: Scanning Electron micrographs of gold microcapsules stabilised with 67 kDa PVA prepared at 6.25 mM gold salt in the synthesis.

SEM images were recorded in cryo conditions in order to maintain the 3D structure of the microcapsules and allow us to study the morphology and shell thickness (via focussed ion beam (FIB). The FIB can directly mill the frozen sample surface, via the sputtering of ions and therefore cut through the frozen samples to create a cross section from which the shell thickness can be measured. After freezing, the sample is fractured, therefore exposing some of the capsules and subsequently coated with platinum to reduce charging while in the SEM.

The resulting micrographs for three different concentrations of gold can be observed in Figure 7.20. Wrinkling of the capsule shells is observed in these samples, however this represents only a few single capsules and not the bulk sample. Possible explanations for shell wrinkling have been discussed previously in the chapter. Additionally slight changes in the capsules may have occurred during

the freezing process. The right hand images in Figure 7.20 show the capsules where half of the capsule had been sheared off during sample preparation, resulting in a cross section being exposed. The right hand images of (a) and (b) show a FIB milled section where the sample can been milled while in the SEM to expose a cross section, hence the smoother appearance. A decrease in shell thickness can be observed with decreasing gold concentration, with the thinnest shell appearing to be close to the minimum required to form a continuous film. There also appears to be more variation in thickness/increase in roughness for the thicker gold shell which supports our previous observations. Though shell thickness cannot be quantitatively measured from these images due to the small sample size, these images clearly demonstrate the difference in shell thickness. Further work on cryo-SEM and other techniques such as thermogravimetric analysis (TGA) and atomic force microscopy (AFM) could be used to help quantify the shell thickness. For example, TGA could be used to compare the mass of hexadecane to gold in the sample and using a known interfacial area the thickness of the shell could be calculated (the mass of platinum would be considered negligible). Additionally methods such as x-ray photoelectron spectroscopy could be used to determine shell wall thickness for thin capsules wall which may be a challenge for other techniques.[203]

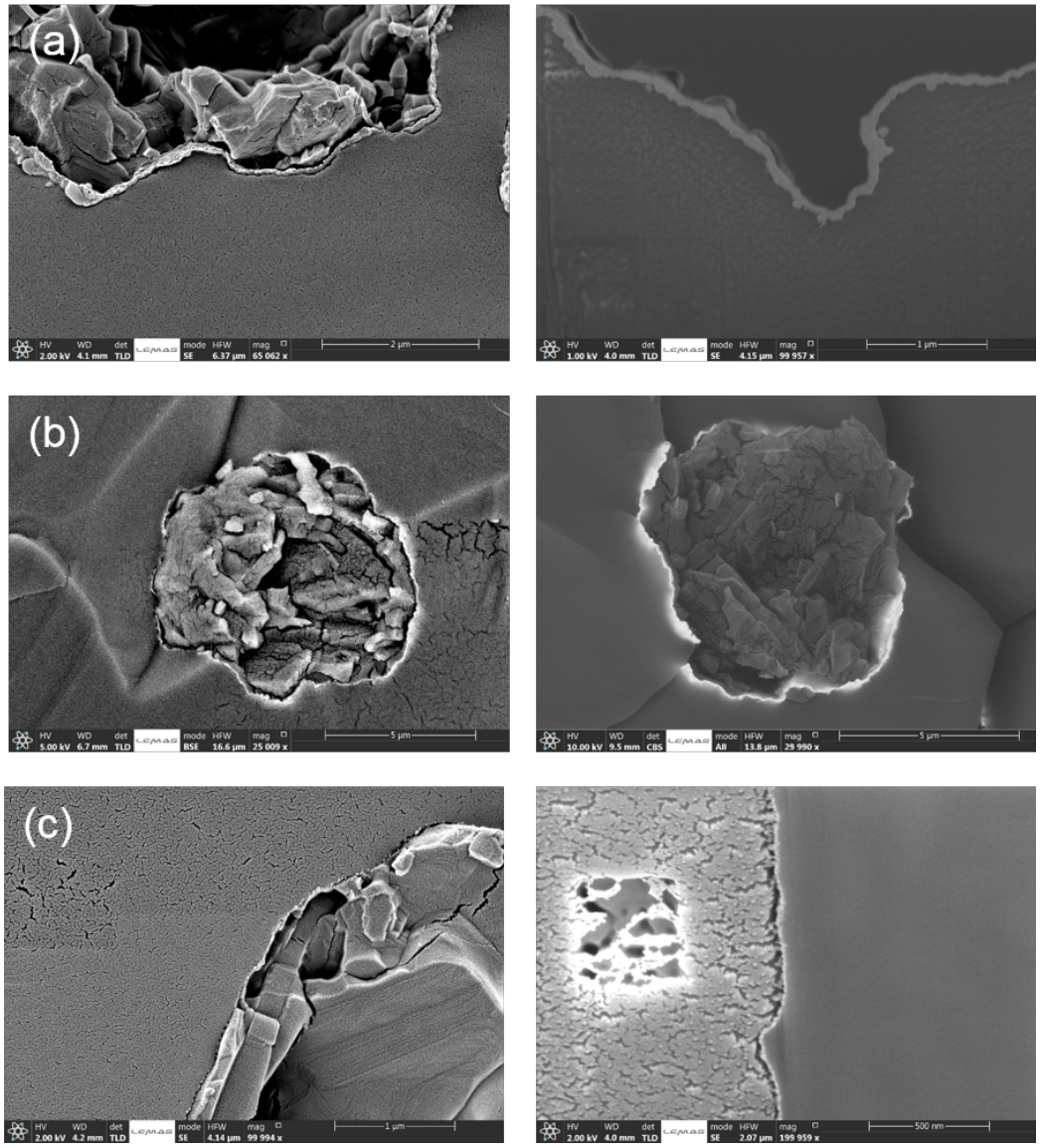

Figure 7.20: CryoSEM micrograph of gold microcapsules prepared with different concentrations of gold salt (a) 180 mM (left hand image shows a FIB section, (b) 50 mM and (c) 6.25 mM (left hand image is a FIB section)

An EDX spectrum was recorded for the capsules while under cryo-SEM conditions illustrating that there was gold at the interface. Figure 7.21 shows the false coloured EDX map where the yellow colour, representative of the presence of gold is situated on the surface of the droplet. The carbon corresponds to the

hexadecane core and the oxygen to the water, in which the sample is frozen.

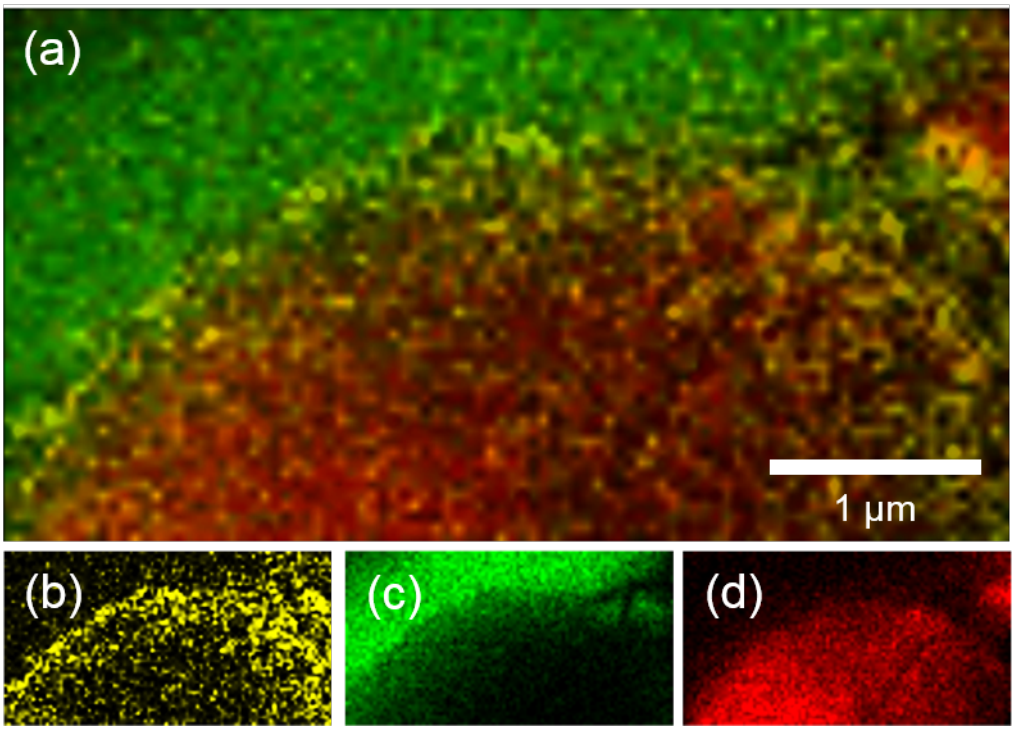

Figure 7.21: Cryo-SEM micrograph with EDX false colour mapping. EDX false colour of (a) overlay of Au, O and C, (b) Au - yellow (Au M map, (c) O - green (O K map) and (d) C - red (C K map)

Though some initial work has been carried out on the morphology of the gold film on the capsules, the segregation behaviour of the platinum and gold at the emulsion interface is yet to be determined. It is possible that the gold film is initially growing via a galvanic replacement reaction between Pt nanoparticles and the $AuCl_4^-$ ions. DaSilva et al. employed EDX techniques coupled with STEM to demonstrate significant metal segregation of AgAu particles obtained from the galvanic reaction of $AuCl_4^-$ ions and Ag particles. They also observed alloyed compositions depending on the Au concentration.[53] Platinum-gold alloys with a face-centred cubic structure have been reported in literature[236] ,[38] so in our case an alloyed structure is possible, as is a segregated structure. Further experiments employing characterisation techniques such as STEM, EDX[53]

and synchrotron high-energy X-ray diffraction (HE-XRD) coupled to atomic pair distribution function (PDF) analysis[38] could provide an insight into the composition of the gold-platinum film.

Further work is necessary in order to reduce the aggregation of the capsules. Alternative polymers or polymers of different molecular weights may offer a solution to this problem.

7.6 Improving stability

In order to improve the stability and reduce the aggregation of the capsules a higher molecular weight polymer was tested as a stabiliser in the plating solution. Higher molecular weight polymers have the potential to provide a larger steric layer at the interface and hence reduce aggregation. PVP (360 kDa) was tested as its lower molecular weight counterparts was able to go some way to stabilising the microcapsules. This is not an extensive study of longer chained polymers but some initial work to establish whether they may benefit the stability of the microcapsules.

Microcapsules were prepared from a hexadecane (0.75 ml) and Pt-PVP NP (10 ml) emulsion homogenised with an ultrasonic probe at 40 % amplitude for 1 minute followed by agitation on the carousel for 30 minutes and washing of the aqueous phase to remove excess nanoparticles from the continuous phase. The emulsion (0.5 ml) was added to a plating solution of water (10 ml), PVP (10 ml, 0.05 wt%, 360 kDa), gold (III) chloride trihydrate (2 ml, 180 mM). Subsequently hydrogen peroxide (1 ml, 1620 mM) was added to initiate the electroless deposition process. Upon the addition of the H_2O_2 the samples were agitated for 30 min on a carousel and then left to sediment.

As can be observed in Figure 7.22 the 360 kDa PVP produces smoother looking shells. Upon drying the microcapsules do not appear to collapse (Figure 7.22 (b)). Though there was still some aggregation observed, this is reduced compared to the lower molecular weight PVP, possibly due to the longer chain providing a larger steric barrier. The gold microcapsules appear smoother than other microcapsules synthesised with the same concentration of gold, as can be observed by the SEM micrographs in Figure 7.23. It is possible that the longer chain polymer

is able to better distribute itself on the microcapsule surface. Alternatively, the polymer may be diffusing slower than shorter chained polymers and therefore taking a longer time to reach the surface, which could allow the metal film to grow unhindered without the polymer.

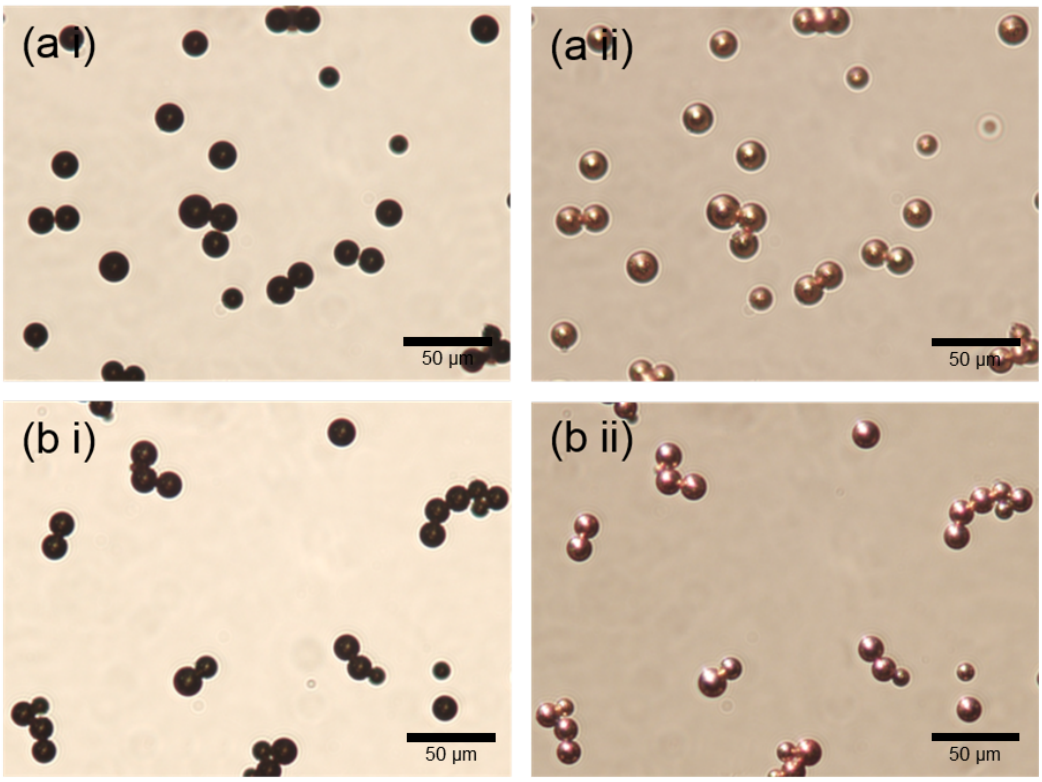

Figure 7.22: Optical micrographs of PVP (360 kDa) stabilised gold microcapsules in suspension in water (a i) transmitted light, (a ii) reflected light and dried microcapsules (b i) transmitted light and (b ii) reflected light.

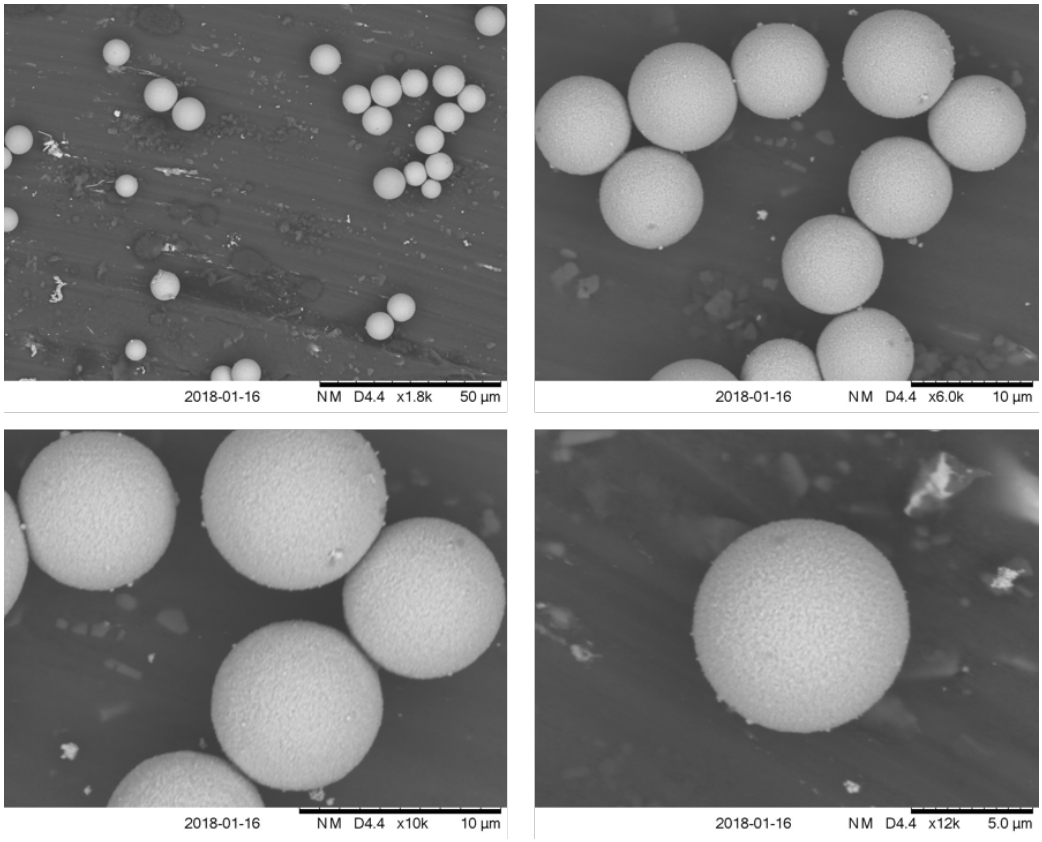

Figure 7.23: Bench top Scanning Electron micrographs of gold microcapsules stabilised with 360 kDa PVP.

It may be that an increase in the concentration of the polymer would lead to less aggregation and more stable microcapsules and this would make some interesting future work. Other longer chained polymers need to be investigated and their interaction with the metal capsules further probed.

7.7 Other release mechanisms

Aside from mechanical fracture, which has been shown to be suitable to release the core content of such metal-shell microcapsules, other release mechanisms have been investigated, particularly to suit potential medical applications. Indeed remote triggered release provides the option for expanding applications of these

microcapsules, for example in targeted drug delivery. In the pharmaceutical industry targeted delivery at a specific site is desirable so that only the affected part of the body is exposed to the drug, therefore minimising potential side effects. Here the potential for remotely breaking these impermeable metal shells via ultrasound and near infrared (NIR) irradiation is investigated. Capsules were tested at Queen Mary University in the laboratories of Prof. Gleb Sukhurokov. The preliminary experiments presented below examine the potential to further develop these routes (with no quantitative analysis has been carried out on the samples.)

7.7.1 Ultrasound

Ultrasound applies to sound waves with frequencies above human hearing (typically 20 kHz or higher). This type of acoustic energy has been utilised for many applications in biomedical areas, including for targeted drug delivery. For example, ultrasound has been employed for the delivery of therapeutic agents such as proteins, genetic material and chemotherapeutic agents by disrupting the membranes of the vesicles carrying the drugs[199].

Gold capsules were prepared from a hexadecane in Pt-PVP NP emulsion (0.5 ml) coated in a plating solution consisting of $AuCl_4$, (2 ml, 80 mM), PVP (5 ml 0.2 wt%), water (10 ml), H_2O_2 (1 ml, 360 mM). Capsules were imaged by SEM before and after ultrasound treatment (Figure 7.24.)

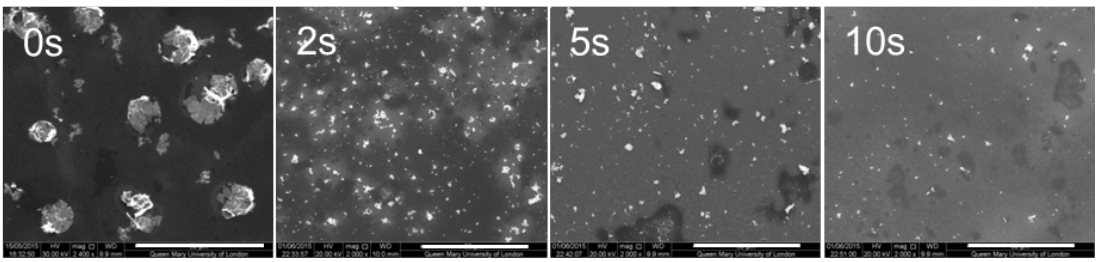

Figure 7.24: SEM micrographs of gold capsules subject to ultrasound treatment after 0, 2, 5 and 10 seconds at different magnifications. Scale bar = 50 μm

As can be seen in Figure 7.24, the capsules have been successfully broken

by ultrasound triggering within a few seconds. Though on drying the untreated capsules have collapsed, it is clear that the application of ultrasound mechanically shatters the capsule shells. Further work and imaging in a wet state would be useful to determine the effect of shell thickness, exposure time and energy input to optimise the system. However this initial result shows that it is a promising method for remote shell rupture.

7.7.2 NIR irradiation

Similarly to ultrasound treatment, the capsules were subject to infrared irradiation in an attempt to rupture the capsule wall. The capsules were prepared in the same way as detailed for the ultrasound experiments. Experiments were carried out with laser irradiation in a wet state and recorded by optical microscopy.

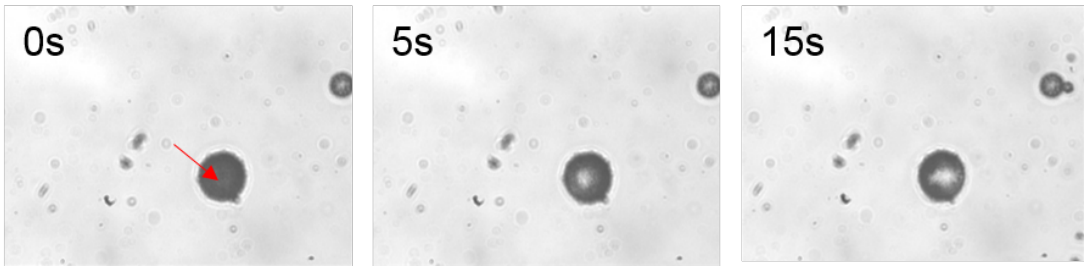

Figure 7.25: Optical micrographs of capsules after laser irradiation for 0, 5 and 15 seconds. The red arrow indicates the laser shooting position

Figure 7.25 illustrates that by shooting a single capsule a hole was obtained. With an increase in radiation time the size of the hole increases.

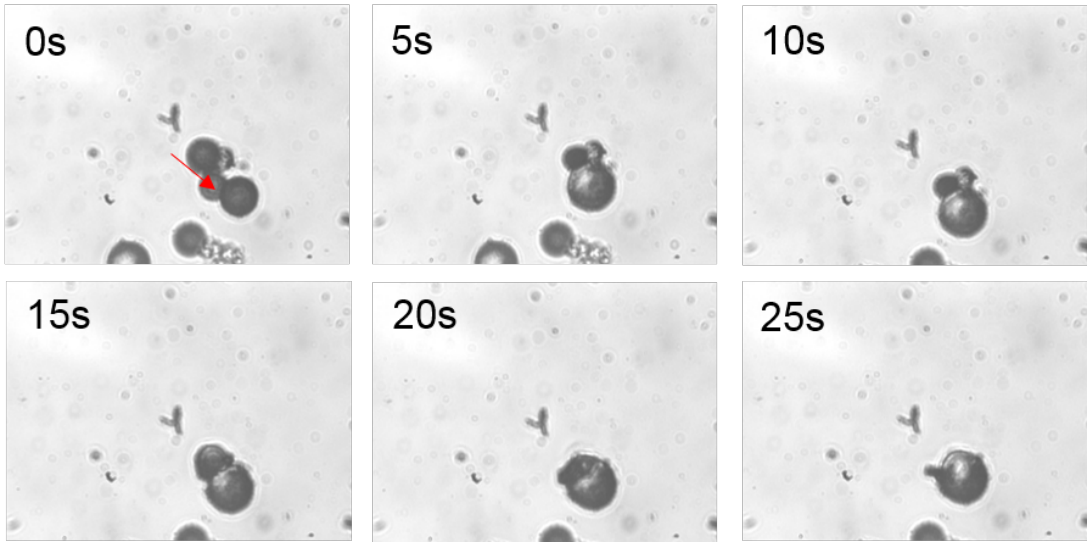

Figure 7.26: Optical micrographs of capsules after laser irradiation for 0, 5, 10, 15, 20 and 25 seconds. The red arrow indicates the laser shooting position

By shooting the connecting point of two capsules (Figure 7.26) with the NIR laser, it appears that the two targeted capsules merge with one another. This is likely a result of the leaking of oil from both capsules, which is likely to lead to a process of coalescence between the two capsules across the damaged areas of the capsule surfaces. This occurs from 5 s onwards and it is clear that the two capsules are almost fully merged by 20 s. A hole is also evident in the larger capsule. The application of NIR on the capsules may be less effective than ultrasound for potential applications as it is only able to target individual capsules.

7.8 Conclusion

This chapter has demonstrated the successful encapsulation of a hexadecane core by electroless deposition of a gold film on the previously optimised emulsion droplets. Under the conditions shown impermeability of the capsules has been demonstrated in an ethanol environment for 35 days and subsequent release of the oil upon mechanical fracture of the metal shell. The concentration of gold

salt in the gold plating solution was varied leading to the successful control of the capsule shell thickness and hence their overall density. Finally preliminary work was carried out on remote release mechanisms for the gold microcapsules including ultrasound and NIR irradiation. In particular the application of ultrasound shows promise for remote triggered release and potential application for drug delivery.

Chapter 8

Conclusions & future work

8.1 Conclusions

This work set out to develop a simple emulsion-based methodology that allows for the rapid and efficient production of thin metal-shell microcapsules capable of retaining small species and potentially remotely delivering the core contents when triggered. Though there are improvements still to be made, overall these aims have been achieved as summarised below.

In this work the synthesis of platinum nanoparticles via the reduction of hexachloroplatinic acid hydrate with sodium borohydride in the presence of PVP has been demonstrated. The amount of PVP stabiliser was minimised to ensure their efficient packing at the oil water interface where they are subsequently acting as catalysts for the electroless deposition of gold films.

Various techniques were utilised to evidence the presence of the Pt-PVP NPs at both 2D and 3D oil-water interfaces. A reduction in IFT was observed for the Pt-PVP NPs in hexadecane compared to that of water in hexadecane. The decrease was similar to that exhibited by PVP in hexadecane. The NPs took a much longer time to reach equilibrium compared to the PVP on its own. Additionally when excess PVP is added to the NP dispersion the kinetics are much more similar to that of PVP in hexadecane which suggests that the PVP diffuses faster and competitively adsorbs at the oil-water interface. Interfacial rheology experiments showed that the resulting nanoparticle film formed at the oil-water interface exhibited an increase in elastic properties over time.

The presence of these Pickering emulsifiers at the hexadecane-water interface was confirmed by electron microscopy techniques and EDX, where a densely packed array of nanoparticles was observed. This work is of particular interest as there are only very few examples of sub 10 nm particles being used as Pickering emulsifiers.[196],[131],[26] In particular cryo-TEM was used to resolve the Pickering nanoparticles at the droplet interface. This is a difficult measurement technique to observe sub-100 nm particles at a liquid-liquid interface and this work showed significant progress as compared to what is available in the literature.[54],[196],[153] It was found that free PVP molecules competitively adsorb at the interface, hence reducing the density of nanoparticles. This was visualised by cryo-TEM and is in agreement with the tensiometry measurements which suggested the PVP diffuses faster. These results demonstrates that it is paramount to limit the number of free polymer chains in the nanoparticle suspension to allow for a dense nanoparticle film at the oil-water interface to be obtained upon emulsification and justified the decision to minimise the PVP used in the nanoparticle synthesis.

The emulsification process and some key parameters were investigated in order to demonstrate control over the resulting emulsion characteristics (such as droplet diameter and size distribution and nanoparticle coverage). The limited coalescence process was investigated and optimised to facilitate as dense a nanoparticle film on the emulsion droplets as possible. As suggested before an increase of PVP in the Pt NP dispersion led to a decrease in the density of adsorbed NPs at the droplet interface. The particle density calculations agree well with particle densities observed and measured previously by cryo-TEM. For a given nanoparticle concentration stable emulsions could be produced with oil fraction from 5 % to 13 %. These emulsions exhibited maximum surface packing and support the idea of limited coalescence occurring for this system. The influence of electrolyte concentration of the nanoparticle dispersion was also investigated which confirmed the importance of screening the interactions between the charged oil-water interface and the charged nanoparticle surface for improving the nanoparticle adsorption efficiency.

Finally, the platinum nanoparticle stabilised oil droplets were used as scaffolds for the electroless deposition of gold films, thereby encapsulating the oil core. The

metal film at the interface can be produced at room temperature. Complete retention of the oil core within the metal-shell microcapsules was demonstrated over 35 days in an ethanol:water (4:1) environment at 40°C, and contrasted against the rapid release of oil from polymer (PMMA) capsules without a metal shell. The shell thickness and density of the capsules were varied by altering the concentration of gold salt in the metal plating solution. There is still improvement to be made on the electroless deposition process in order to obtain smoother shells and well dispersed capsules. This will hopefully lead to more robust thinner shells therefore allowing less of the secondary metal to be used which is beneficial from a manufacturing cost perspective. Preliminary ultrasound and IR radiation experiments were carried out in order to assess their viability to trigger the release of the capsule payload.

Overall this process meets the aims and objectives set out at the beginning of this thesis as a suitable catalytic nanoparticle emulsifier was synthesised and subsequently used as a scaffold for the electroless deposition of a secondary metal film. The process is a simple two-step process, which efficiently uses the materials and minimises waste. Emulsions are often produced industrially therefore this process would be easy to adapt for manufacture. Preliminary work on remote triggered release via ultrasound and IR irradiation show promise for potential application in drug delivery.

8.2 Future work

8.2.1 Metal nanoparticle synthesis

It would be interesting to further study the nanoparticle synthesis by examining the effect of particle size/polymer MW on the ability of the emulsifiers to adsorb at the oil-water interface. Additionally the influence of the polymer type chosen as the nanoparticle stabiliser could be investigated.

The method developed here produces a catalytic metal nanoparticle with a lower excess of stabilising polymer in the bulk dispersion. A low excess of polymer has the potential for increasing packing density of nanoparticles on a substrate for catalysis applications and therefore potentially improving efficiency. Platinum is

a commonly used catalyst for a broad range of applications such as hydrogenation reactions[13], antioxidant chemical reactions in nanomedicine[194], electrocatalysts used in fuel cells[156] and oxidation reactions.[171]

It is possible that other metal nanoparticles can be synthesised using the method developed here, which uses a low excess of polymer stabiliser, from suitable metal salt precursors such as gold, silver, palladium, ruthenium and rhenium as PVP has been shown as a viable stabiliser for these metal nanoparticles.[127] These metal nanoparticles provide the potential to catalyse the growth of other metals as well as other catalytic reactions. Additionally, metal nanoparticles have found applications in electronics, biomedicine, sensing, imaging and materials science.[168], [49]

8.2.2 Emulsifier

Here PVP was used as the stabiliser for the metal nanoparticles and subsequently the emulsifier. There is also the possibility to utilise surface crosslinkers to alter the structural and rheological properties of the emulsion therefore allowing more robust microcapsules to be synthesised as it was found that capsules with very thin shells often collapsed upon drying, which limits their applications. Both internal and external crosslinker could be utilised, for example an oil soluble crosslinker could be used to internally crosslink the emulsion.[79], [137], [86], [252] It is possible to crosslink PVP to create polymer gels by reactions with certain chemical reagents or irradiated with ultraviolet light or gamma rays. These gels have shown potential biomedical and industrial applications.[6], [151]

To increase the flexibility of the oils that could be encapsulated a diblock copolymer system could be utilised whereby the catalytic nanoparticles are subsequently adsorbed by electrostatic interactions to the hydrophilic polymer block after the formation of the emulsion droplets (Figure 8.1). This approach would allow for a wide range of oils to be encapsulated as the diblock copolymers adsorption properties could be designed to match specific interfaces.[209], [118]

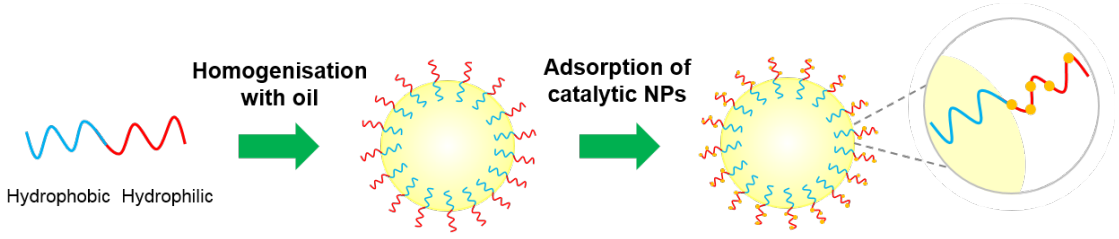

Figure 8.1: Schematic illustrating the formation of emulsion droplets with diblock copolymers and the subsequent adsorption of catalytic NPs (yellow dots on the inset of the right schematic) to the hydrophilic block.

8.2.2.1 Synthesis of diblock copolymers

Living polymerisation is a form of chain polymerisation from which chain transfer and termination are absent and the rate of chain initiation is fast compared to propagation, hence the number of kinetic chain carriers is essentially constant throughout. Such polymerisation methods allow the design and synthesis of block copolymers very precisely. Living polymerisation methods include anionic living polymerisation [206], cationic living polymerisation [8], living free radical polymerisation (including atom transfer radical polymerisation (ATRP) [135], stable free radical mediated polymerisation (SFRP) [121], nitroxide-mediated radical polymerisation (NMP) [58] and reversible addition fragmentation chain transfer polymerisation (RAFT). [119]

Some preliminary work has been carried out to synthesise suitable diblock copolymers via RAFT polymerisation. RAFT is a form of living radical polymerisation which offers many advantages;

- it has a high functional group tolerance
- it can be performed in a wide range of solvents (including water)
- it can be used on a wide range of monomers and reaction conditions
- it is simple to implement and relatively cheap compared to other technologies
- it produces polymers with a narrow polydispersity

- molecular weight can be predicted

The RAFT mechanism (Figure 8.2) involves a chain reaction whereby chains are initiated by radicals from an initiator adding to a monomer. Subsequently, propagation occurs via a degenerative chain transfer process where monomers are added to the radicals. The chain transfer process is aided by a chain transfer agent.[119], [167]

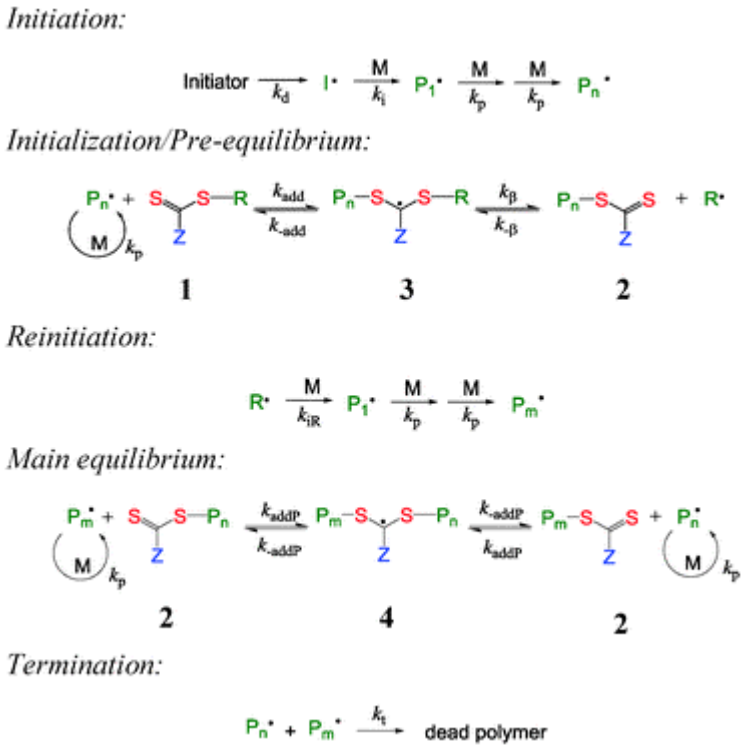

Figure 8.2: Schematic illustrating the RAFT polymerisation mechanism. Taken from Keddie[119].

Amphiphilic diblock copolymers were synthesised using the the RAFT technique. The first block, poly butyl acrylate (PBA) was synthesised from a designed reaction involving butyl acrylate monomer, 2-propionic acidyl butyl trithiocarbonate (PABTC) chain transfer agent and a V601 initiator in a dioxane solvent at 65°C for 4 hours (Figure 8.3).

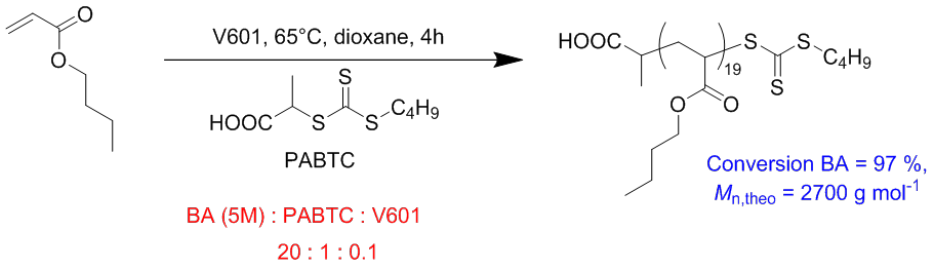

Figure 8.3: Reaction scheme for synthesis of Poly buytl acrylate

Subsequently a second block of bromoethyl acetate (PBrAc) was added to form poly butyl acyrylate-b-bromoethyl acetate (PBA-b-BrAc) using the same reaction conditions and a bromoacetate monomer. The second block was synthesised at different chains lengths. An example of the resulting NMR and GPC results can be found in the Appendix. Diblock copolymers were synthesised with high conversions and polydispersity indexes close to 1 in all cases illustrating that RAFT is a suitable technique for synthesising suitable diblock copolymers.

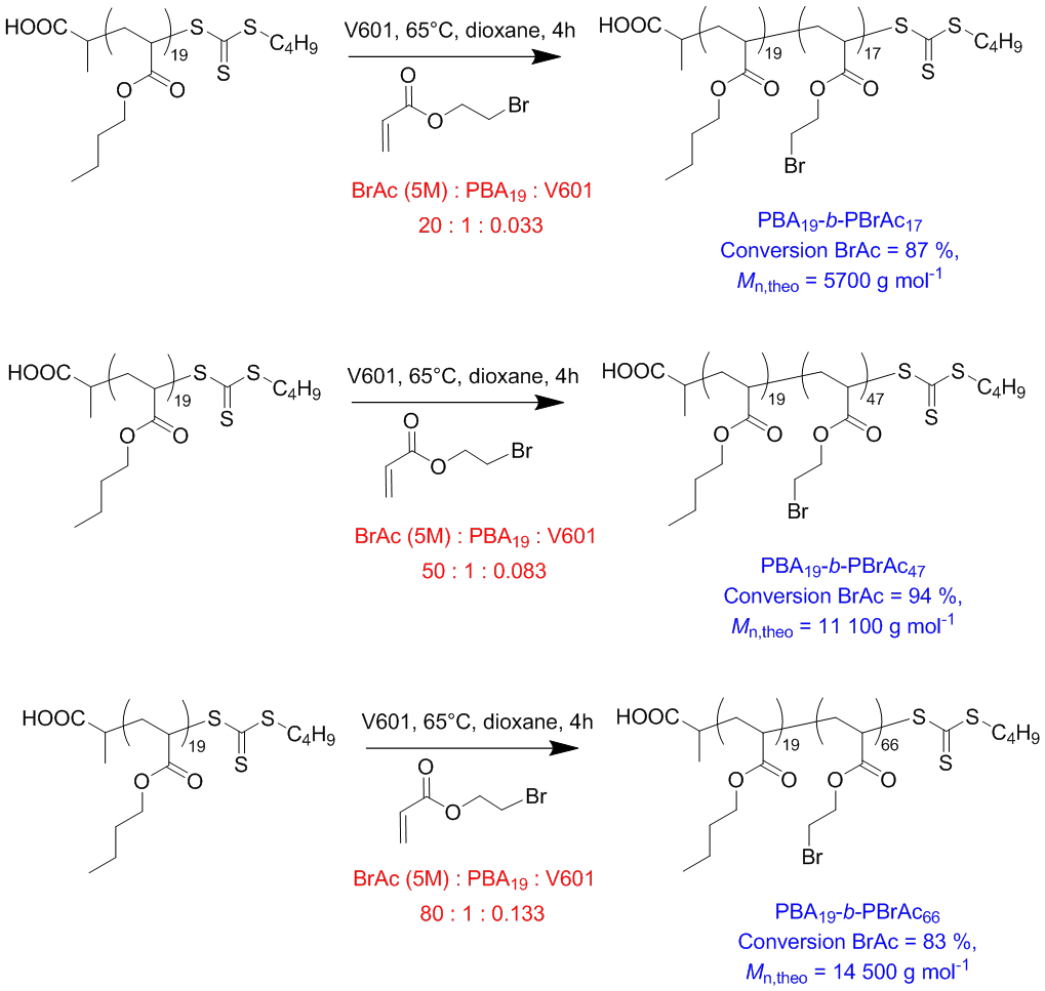

Figure 8.4: Reaction scheme for synthesis of PBA-BrAc with different BrAc block lengths

The bromoacetate group can be converted to a tertiary amine after synthesis by reacting with trimethylamine. Due to the limits in monomer combinations when creating diblocks via RAFT amine containing monomers cannot be directly used in the synthesis. The formation of the tertiary amine produces a positive charge, which can be utilised to adsorb negatively charged metal ions.

Figure 8.5: Reaction scheme for substitution of Br with TMA

8.2.3 Interfacial studies

Further experiments could be carried out to better understand the the particle film formed at the oil-water interface and the parameters that influence it. Interfacial tensiometry studies could be carried out to better understand the kinetics of adsorption of the nanoparticles at the oil-water interface (including with the addition of excess PVP.)

Dilational tensiometry experiments would allow us to investigate the interfacial rheology further by oscillation of the interface to determine the dilational modulus.[162]. In particular the effect of electrolyte concentration on the dilational elasticity modulus could be studied and compared to 2D interfacial rheology measurements. This would give us a better understanding of the particle film formation at the oil-water interface and optimise the electrolyte concentration in the emulsion system.

8.2.4 Secondary metal plating

More work is needed to improve the electroless deposition process to enable a smoother metal coating at the interface. Alternative stabilisers, concentration and rate of addition of reducing agent, reaction temperature and type of gold salt used could all be investigated as means for improving this step. In industry additives are sometimes added to improve the crystallinity of deposited layer in

electroless deposition baths so these could be incorporated in the plating solution. It would be interesting to test the mechanical strength of these capsules to determine their capability in relation to certain applications. For example, for a perfume application the capsules must be able to be broken by a reasonable shear force when applied to the body. Micromanipulation techniques could be utilised to determine the force required to rupture the microcapsule.[149], [96]

8.2.5 Microcapsule applications

There is still work required to optimise the final metal-shell microcapsule system in order to maximise the efficiency of the process, in particular for consistently producing thinner impermeable shells. This project's original aim was to encapsulate fine fragrance oils, however the technology implicated here could be utilised for other applications. For example this capsule system could be employed for drug delivery or flavour encapsulation. Further applications can be considered by the materials and conditions required of the final product as discussed below.

8.2.5.1 Alternative metal combinations

This work has focussed on the combination of a platinum catalyst catalysing the growth of gold because of the suitability of this metal combination as a model system to optimise the synthesis procedure - as described in the literature.[102], [4] These metals are expensive so may not be suitable for all applications, though often when encapsulating an expensive active ingredient the product profit margins are higher and the advantages of encapsulation outweigh the cost. A gold metal shell is useful for many applications due to its electrical, catalytic and optical properties, chemical stability, photonic energy adsorption and good biocompatibility.[122] For example, this provides potential for gold capsules to act as non-toxic carriers for drug and gene delivery applications.[91] In particular a combination such as gold and silver is favourable for applications such as fragrance encapsulation and drug delivery due to aforementioned advantages of gold and the antibacterial effects and lower cost of silver compared to platinum.

However there are many other metallic combinations possible which may be applied for different applications such as gold films deposited using palladium cat-

alysts[123], copper films deposited using cobalt catalysts[176], nickel films deposited using palladium catalysts[191], silver films deposited using gold catalysts[44], copper films deposited using silver catalysts[83], gold films deposited using gold catalysts[108], platinum films deposited using charged tin porphyrin catalysts[250] and gold, palladium and platinum films deposited using germanium catalyst.[202] One of the limiting factors in the choice of suitable metal combinations will be the application of the capsules as some metals may be unsuitable for particular uses. For example, metal for use within the body must be non-toxic and biocompatible, which would rule out the use of nickel or copper for instance.

In addition to protecting an active ingredient metal shells can impart other functionality such as optical, magnetic and electric properties. For example gold coated microcapsules have the potential to operate as optical sensors.[123] Silica core, gold shell nanoparticles, exhibited a change in optical resonance with changing gold shell thickness. This variation of light adsorption spanning across the visible and near infrared spectral regions is known as surface plasmon resonance (SPR) and has applications in biomedical imaging, optical materials and cancer treatments.[122] Magnetic capsules have the potential for application in bioseparation and biomedicine and offer the advantage of ease of separation and manipulation and potential to provide automation of devices[249]. Magnetic silica core particles coated in silver possess promising applications such as magnetic field targeted photothermal therapy agent and multimodal molecular probes by utilising the optical properties of Ag and magnetic properties of the core.[44] By using suitable magnetic nanoparticles a magnetic response can be imparted to the Pickering emulsion alone[69] and subsequently the metal-shell capsules.

8.2.5.2 Encapsulated core

Hexadecane is not an ideal encapsulant for a practical use however it was efficiently used in this thesis as a model system. Depending on the wettability of the oil phase with the emulsifier various oils can be encapsulated. For example dodecane and hexylsalysilate have been encapsulated in this way by other group members. A study of different oil cores would be useful, in particular oils that can carry bioactive substances.

It is also possible, if a suitable emulsifier was used to create water-in-oil emulsions so that an aqueous active ingredient could be encapsulated. This may prove challenging as there are less available metal salts that dissolve in the oil phase for the secondary metal shell deposition. Alternatively double emulsions could be created such as w-o-w emulsions again providing more possibilities for other encapsulated species. Double emulsions, in which droplets of the dispersed phase contain one or more types of smaller dispersed droplets have the potential to encapsulate both hydrophobic and hydrophilic molecules.[111]

Colloidal dispersions of gelled lipid nanoparticles (GLN) provide another potential scaffold for metal capsules. GLNs comprise organogels which are semi-solid systems in which a three-dimensional network of crosslinked fibres immobilises an organic liquid. Colloidal dispersions of GLNs can be prepared from organogels by combining an organic liquid and organic gelator and subsequent dispersion in a water phase with a suitable emulsifier or stabilising agent. In particular they offer a possible route to encapsulate compounds with poor water solubility used in pharmaceuticals, dermatology or cosmetics.[34] By incorporating a catalytic species into the stabiliser used to create the droplets a metal shell could be subsequently grown.

Phase change materials (PCMs) can be utilised for energy storage, thermal protection systems and passive cooling of electronic devices. Both inorganic and organic materials can be used as PCMs. Inorganic PCMs include metals, alloys, salts and salt hydrates, whereas organic PCMs are often paraffin or fatty acids/esters. Paraffin waxes offer favourable characteristics for comfort cooling and thermal storage applications such as high latent heat of fusion, negligible super-cooling, chemically inertness and stable low vapour pressure in the melt, however one of the main disadvantages is that they exhibit very low thermal conductvity.[129], [128], [267] The encapsulating shell is often polymer based and exhibits low thermal conductivity and stability. Additionally inorganic shells, such as silicon dioxide are often porous. These issues could be addressed by encapsulating the organic phase in a metallic shell that offers thermal conductive properties and thereby increasing the heat transfer rate.[114].

8.2.5.3 Release mechanisms

As shown in Chapter 7, some preliminary work has been carried out on remote release systems. Further systematic studies on ultrasound and IR irradiation as release mechanisms would allow us to optimise parameters such as energy input and exposure times as a function of shell thickness and microcapsule size. The ability to use these techniques to break the metal shells offers potential for use in biomedicine as drug delivery vehicles.[199] In addition to providing an inert surface that is easily modified chemically with bio-relevant species, a gold shell is useful for drug delivery due to the SPR response of the metal and the ability of certain wavelengths of light to penetrate human tissue, allowing the capsules to be triggered remotely.[122] Further studies on the SPR response as a function of shell thickness would be useful.

Other mechanisms can be employed to trigger the release of the payload such as electrical triggering, magnetically induced release, thermally induced release and chemical triggers. Magnetically responsive capsules can be manipulated and payload release triggered in the presence of a magnetic field. It may be possible by placing a chemically responsive trigger in the shell wall which results in change on porosity of the shell to release the payload upon appropriate stimulation. Changes in temperature could lead to the initiation of a reaction within the capsules core and initiate release at a potentially controlled rate.[74]

Appendix A

Supplementary data

A.1 RAFT synthesis of diblock copolymers

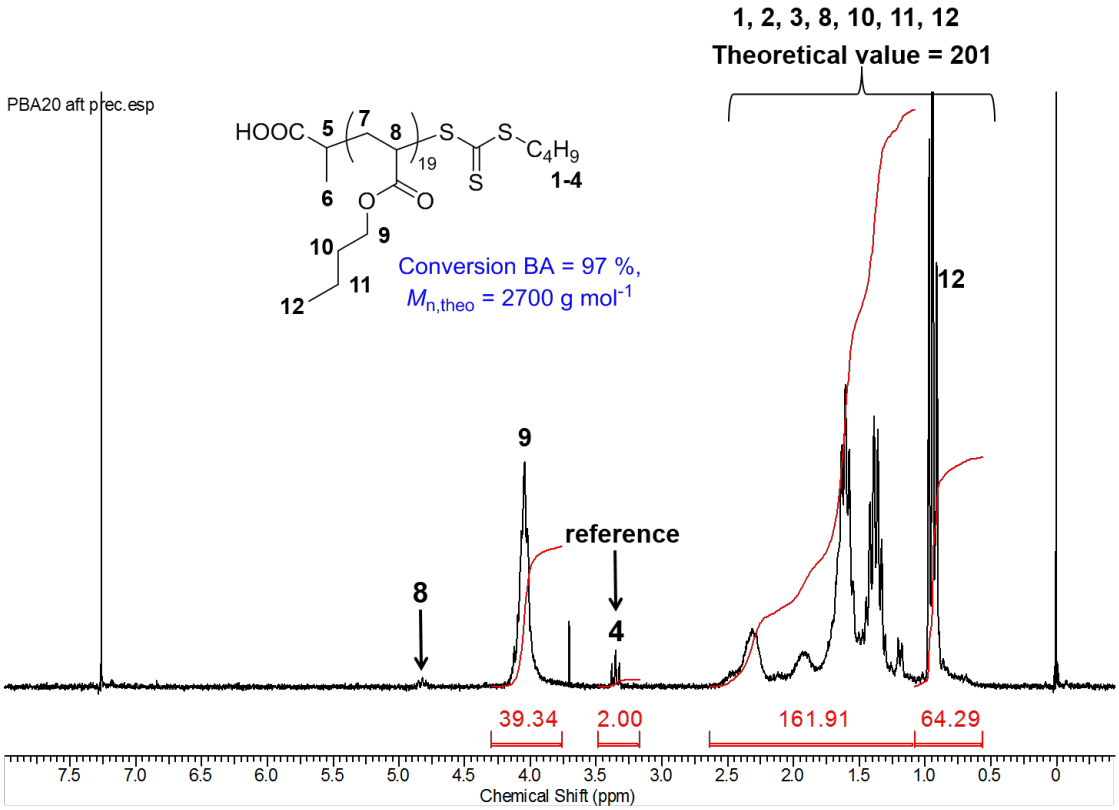

Figure A.1: NMR of PBA_{19} after precipitation

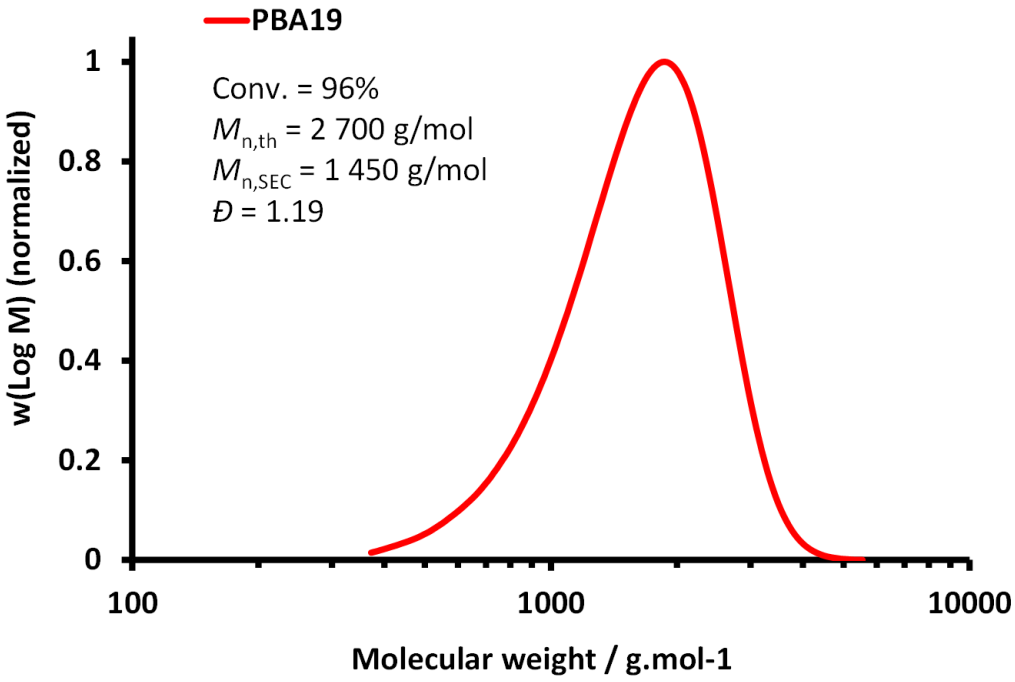

Figure A.2: GPC of PBA_{19} after precipitation

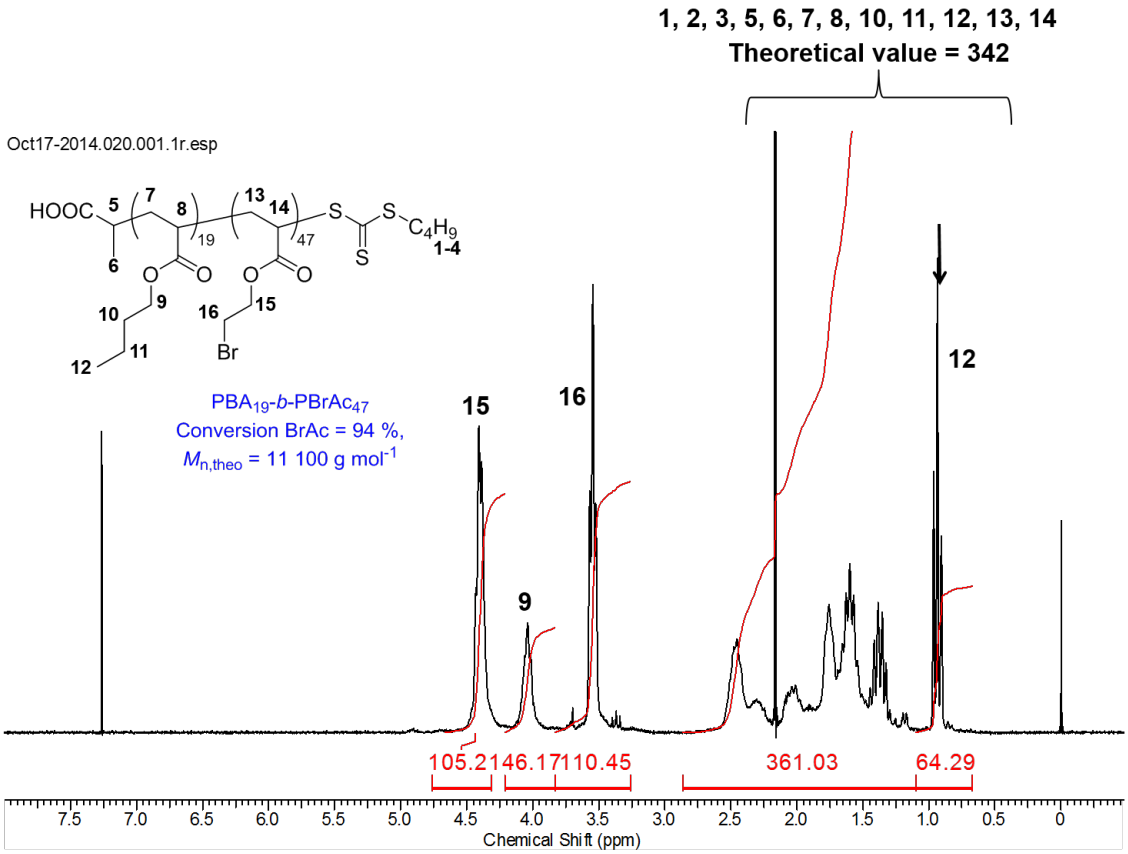

Figure A.3: NMR of PBA_{19}-b-$PBrAc_{47}$ after precipitation

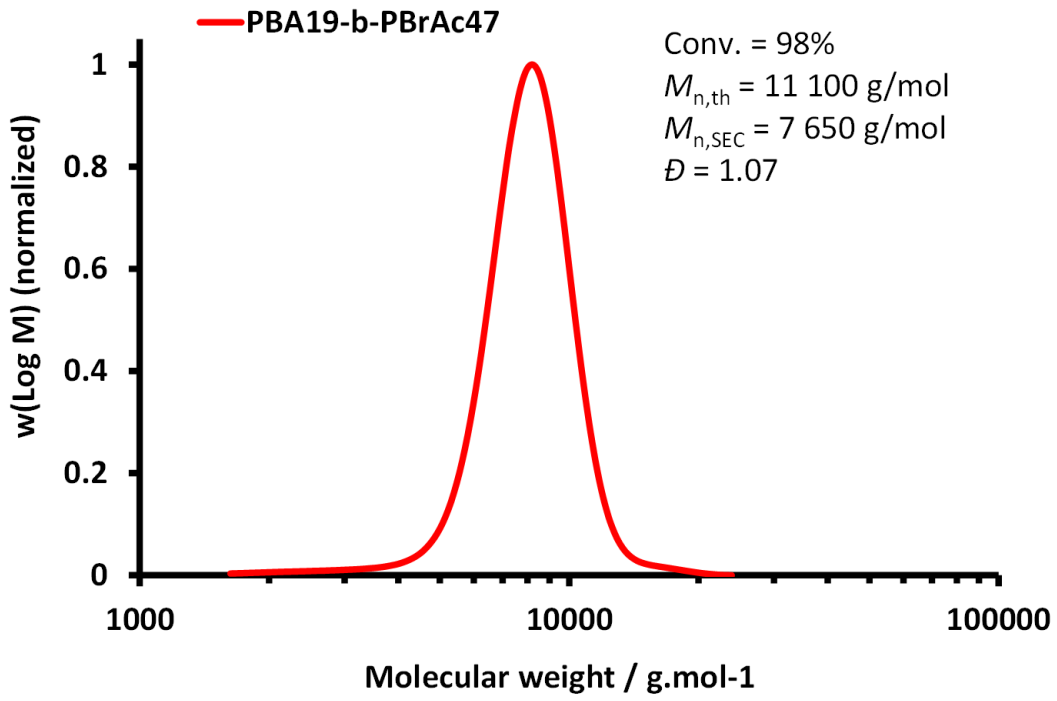

Figure A.4: NMR of PBA_{19}-b-$PBrAc_{47}$ after precipitation

References

[1] Abdulwahab, S.A. & David, S.S. (2005). Brownian dynamics study of polymer-stabilized nanoparticles. *Nanotechnology*, **16**, S409.

[2] Akbarzadeh, A., Rezaei-Sadabady, R., Davaran, S., Joo, S.W., Zarghami, N., Hanifehpour, Y., Samiei, M., Kouhi, M. & Nejati-Koshki, K. (2013). Liposome: classification, preparation, and applications. *Nanoscale Research Letters*, **8**, 102–102.

[3] Akoh, C. & Min, D. (2008). *Food Lipids: Chemistry, Nutrition, and Biotechnology, Third Edition*. Taylor Francis.

[4] Ali, H.O. & Christie, I.R. (1984). A review of electroless gold deposition processes. *Gold bulletin*, **17**, 118–127.

[5] Alvarez, N.J., Anna, S.L., Saigal, T., Tilton, R.D. & Walker, L.M. (2012). Interfacial dynamics and rheology of polymer-grafted nanoparticles at airwater and xylenewater interfaces. *Langmuir*, **28**, 8052–8063.

[6] Anderson, C.C., Rodriguez, F. & Thurston, D.A. (1979). Crosslinking aqueous poly(vinyl pyrrolidone) solutions by persulfate. *Journal of Applied Polymer Science*, **23**, 2453–2462.

[7] Andrade, C. (2015). Sustained-release, extended-release, and other time-release formulations in neuropsychiatry. *The Journal of clinical psychiatry*, **76**, e995–9.

[8] Aoshima, S. & Kanaoka, S. (2009). A renaissance in living cationic polymerization. *Chemical reviews*, **109**, 5245–5287.

[9] Arditty, S., Whitby, C.P., Binks, B.P., Schmitt, V. & Leal-Calderon, F. (2003). Some general features of limited coalescence in solid-stabilized emulsions. *The European Physical Journal E*, **11**, 273–281.

[10] Arias, J. (2014). *Nanotechnology and Drug Delivery, Volume One: Nanoplatforms in Drug Delivery*. CRC Press.

[11] Aronson, M.P. (1992). *Surfactant Induced Flocculation of Emulsions*, 75–96. Springer Netherlands, Dordrecht.

[12] Badoga, S., Pattanayek, S.K., Kumar, A. & Pandey, L.M. (2011). Effect of polymersurfactant structure on its solution viscosity. *Asia-Pacific Journal of Chemical Engineering*, **6**, 78–84.

[13] Bai, L., Wang, X., Chen, Q., Ye, Y., Zheng, H., Guo, J., Yin, Y. & Gao, C. (2016). Explaining the size dependence in platinum-nanoparticle-catalyzed hydrogenation reactions. *Angewandte Chemie International Edition*, **55**, 15656–15661.

[14] Bakry, A.M., Abbas, S., Ali, B., Majeed, H., Abouelwafa, M.Y., Mousa, A. & Liang, L. (2016). Microencapsulation of oils: A comprehensive review of benefits, techniques, and applications. *Comprehensive Reviews in Food Science and Food Safety*, **15**, 143–182.

[15] Bancroft, W.D. (1912). The theory of emulsification. i. *Journal of Physical Chemistry*, **16**, 177–233.

[16] Basketter, D.A., English, J.S.C., Wakelin, S.H. & White, I.R. (2008). Enzymes, detergents and skin: facts and fantasies. *British Journal of Dermatology*, **158**, 1177–1181.

[17] Becher, P. (1996). *Encyclopedia of Emulsion Technology*. CRC Press.

[18] Becker, R. & Doring, W. (1954). Kinetic treatment of the nucleation in supersaturated vapors. Report, National Advisory Committee for Aeronautics.

[19] Bergenholtz, J. (2001). Theory of rheology of colloidal dispersions. *Current Opinion in Colloid Interface Science*, **6**, 484–488.

[20] Beristain, C.I., Vazquez, A., Garcia, H.S. & Vernon-Carter, E.J. (1996). Encapsulation of orange peel oil by co-crystallization. *LWT - Food Science and Technology*, **29**, 645–647.

[21] Berry, J.D., Neeson, M.J., Dagastine, R.R., Chan, D.Y.C. & Tabor, R.F. (2015). Measurement of surface and interfacial tension using pendant drop tensiometry. *Journal of Colloid and Interface Science*, **454**, 226–237.

[22] Biggs, S. & Cayre, O. (2015). *Particle-Stabilized Emulsions as Templates for Hollow Spheres and Microcapsules*, 228–246. The Royal Society of Chemistry.

[23] Binks, B. & Horozov, T. (2006). *Colloidal Particles at Liquid Interfaces*. Cambridge University Press.

[24] Binks, B.P. (2002). Particles as surfactants - similarities and differences. *Current Opinion in Colloid Interface Science*, **7**, 21–41.

[25] Binks, B.P. & Olusanya, S.O. (2017). Pickering emulsions stabilized by coloured organic pigment particles. *Chemical Science*, **8**, 708–723.

[26] Bollhorst, T., Rezwan, K. & Maas, M. (2017). Colloidal capsules: nano- and microcapsules with colloidal particle shells. *Chemical Society Reviews*, **46**, 2091–2126.

[27] Bolten, D. & Turk, M. (2011). Experimental study on the surface tension, density, and viscosity of aqueous poly (vinylpyrrolidone) solutions. *Journal of Chemical Engineering Data*, **56**, 582–588.

[28] Borodko, Y., Habas, S.E., Koebel, M., Yang, P.D., Frei, H. & Somorjai, G.A. (2006). Probing the interaction of poly(vinylpyrrolidone) with platinum nanocrystals by uv-raman and ftir. *Journal of Physical Chemistry B*, **110**, 23052–23059.

[29] Borodko, Y., Humphrey, S.M., Tilley, T.D., Frei, H. & Somorjai, G.A. (2007). Charge-transfer interaction of poly (vinylpyrrolidone) with platinum and rhodium nanoparticles. *The Journal of Physical Chemistry C*, **111**, 6288–6295.

[30] Bouchemal, K., Brianon, S., Perrier, E., Fessi, H., Bonnet, I. & Zydowicz, N. (2004). Synthesis and characterization of polyurethane and poly(ether urethane) nanocapsules using a new technique of interfacial polycondensation combined to spontaneous emulsification. *International Journal of Pharmaceutics*, **269**, 89–100.

[31] Brooks, C.F., Fuller, G.G., Frank, C.W. & Robertson, C.R. (1999). An interfacial stress rheometer to study rheological transitions in monolayers at the airwater interface. *Langmuir*, **15**, 2450–2459.

[32] Callister, W.D. & Rethwisch, D.G. (2000). *Fundamentals of materials science and engineering*, vol. 471660817. Wiley London.

[33] Camargo, P.H.C., Rodrigues, T.S., da Silva, A.G.M. & Wang, J. (2015). *Controlled Synthesis: Nucleation and Growth in Solution*, 49–74. Springer International Publishing, Cham.

[34] Carranc Palomo, M., Martn Prieto, V. & Kirilov, P. (2017). Colloidal dispersions of gelled lipid nanoparticles (gln): Concept and potential applications. *Gels*, **3**.

[35] Castro, N., Durrieu, V., Raynaud, C., Rouilly, A., Rigal, L. & Quellet, C. (2016). Melt extrusion encapsulation of flavors: A review. *Polymer Reviews*, **56**, 137–186.

[36] Cates, M.E. (2017). Complex fluids: the physics of emulsions. *Soft Interfaces: Lecture Notes of the Les Houches Summer School: Volume 98, July 2012*, **98**, 317.

[37] Cayre, O.J., Noble, P.F. & Paunov, V.N. (2004). Fabrication of novel colloidosome microcapsules with gelled aqueous cores. *Journal of Materials Chemistry*, **14**, 3351–3355.

[38] Chang, F., Shan, S., Petkov, V., Skeete, Z., Lu, A., Ravid, J., Wu, J., Luo, J., Yu, G. & Ren, Y. (2016). Composition tunability and (111)-dominant facets of ultrathin platinumgold alloy nanowires toward enhanced electrocatalysis. *Journal of the American Chemical Society*, **138**, 12166–12175.

[39] Charcosset, C., Limayem, I. & Fessi, H. (2004). The membrane emulsification process - a review. *Journal of Chemical Technology and Biotechnology*, **79**, 209–218.

[40] Chen, C.W. & Akashi, M. (1997). Synthesis, characterization, and catalytic properties of colloidal platinum nanoparticles protected by poly (n-isopropylacrylamide). *Langmuir*, **13**, 6465–6472.

[41] Chen, D.T., Wen, Q., Janmey, P.A., Crocker, J.C. & Yodh, A.G. (2010). Rheology of soft materials. *Annual Review of Condensed Matter Physics*, **1**, 301–322.

[42] Chen, J., Mao, J., Zhao, J., Ren, M. & Wei, M. (2014). Surfactant-free platinum nanocubes with greatly enhanced activity towards methanol/ethanol electrooxidation. *RSC Advances*, **4**, 28832–28835.

[43] Chen, L., Okuda, T., Lu, X.Y. & Chan, H.K. (2016). Amorphous powders for inhalation drug delivery. *Advanced Drug Delivery Reviews*, **100**, 102–115.

[44] Chen, M., Kim, Y.N., Lee, H.M., Li, C. & Cho, S.O. (2008). Multifunctional magnetic silver nanoshells with sandwichlike nanostructures. *The Journal of Physical Chemistry C*, **112**, 8870–8874.

[45] Cheng, H., Xi, C., Meng, X., Hao, Y., Yu, Y. & Zhao, F. (2009). Polyethylene glycol-stabilized platinum nanoparticles: The efficient and recyclable catalysts for selective hydrogenation of o-chloronitrobenzene to o-chloroaniline. *Journal of colloid and interface science*, **336**, 675–678.

[46] Chevalier, Y. & Bolzinger, M.A. (2013). Emulsions stabilized with solid nanoparticles: Pickering emulsions. *Colloids and Surfaces A: Physicochemical and Engineering Aspects*, **439**, 23–34.

[47] Claesson, P.M., Blomberg, E., Frberg, J.C., Nylander, T. & Arnebrant, T. (1995). Protein interactions at solid surfaces. *Advances in Colloid and Interface Science*, **57**, 161–227.

[48] Coates, M., Connell, D.W. & Barron, D.M. (1985). Aqueous solubility and octan-1-ol-water partition coefficients of aliphatic hydrocarbons. *Environmental Science Technology*, **19**, 628–632.

[49] Conde, J., Doria, G. & Baptista, P. (2012). Noble metal nanoparticles applications in cancer. *Journal of Drug Delivery*, **2012**, 12.

[50] Cowsar, D. (1980). Novel fabric containing microcapsules of chemical decontaminants encapsulated within semipermeable polymers.

[51] Cullen, P., Romaach, R., Abatzoglou, N. & Rielly, C. (2015). *Pharmaceutical Blending and Mixing*. Wiley.

[52] Cussler, E. (1997). *Diffusion: Mass Transfer in Fluid Systems*. Cambridge University Press.

[53] da Silva, A.G.M., Rodrigues, T.S., Haigh, S.J. & Camargo, P.H.C. (2017). Galvanic replacement reaction: recent developments for engineering metal nanostructures towards catalytic applications. *Chemical Communications*, **53**, 7135–7148.

[54] Dai, L.L., Sharma, R. & Wu, C.y. (2005). Self-assembled structure of nanoparticles at a liquid liquid interface. *Langmuir*, **21**, 2641–2643.

[55] Dai, Z., Heilig, A., Zastrow, H., Donath, E. & Mhwald, H. (2004). Novel formulations of vitamins and insulin by nanoengineering of polyelectrolyte multilayers around microcrystals. *Chemistry A European Journal*, **10**, 6369–6374.

[56] Dandapat, A., Mitra, A., Gautam, P.K. & De, G. (2013). A facile synthesis of pt nanoflowers composed of an ordered array of nanoparticles. *Nanomaterials and Nanotechnology*, **3**, 11.

[57] Davey, W.P. (1925). Precision measurements of the lattice constants of twelve common metals. *Physical Review*, **25**, 753.

[58] Detrembleur, C., Sciannamea, V., Koulic, C., Claes, M., Hoebeke, M. & Jrme, R. (2002). Controlled nitroxide-mediated radical polymerization of styrene, styrene/acrylonitrile mixtures, and dienes using a nitrone. *Macromolecules*, **35**, 7214–7223.

[59] Dickinson, E., Golding, M. & Povey, M.J.W. (1997). Creaming and flocculation of oil-in-water emulsions containing sodium caseinate. *Journal of Colloid and Interface Science*, **185**, 515–529.

[60] Dinderman, M.A., Dressick, W.J., Kostelansky, C.N., Price, R.R., Qadri, S.B. & Schoen, P.E. (2006). Electroless plating of iron onto cellulose fibers. *Chemistry of Materials*, **18**, 4361–4368.

[61] Dinsmore, A.D., Hsu, M.F., Nikolaides, M.G., Marquez, M., Bausch, A.R. & Weitz, D.A. (2002). Colloidosomes: Selectively permeable capsules composed of colloidal particles. *Science*, **298**, 1006–1009.

[62] Discher, D.E. & Ahmed, F. (2006). Polymersomes. *Annual Review of Biomedical Engineering*, **8**, 323–341.

[63] Djoki, S. (2002). *Electroless Deposition of Metals and Alloys*, vol. 35 of *Modern Aspects of Electrochemistry*, book section 2, 51–133. Springer US.

[64] Donath, E., Sukhorukov, G.B., Caruso, F., Davis, S.A. & Mhwald, H. (1998). Novel hollow polymer shells by colloid-templated assembly of polyelectrolytes. *Angewandte Chemie International Edition*, **37**, 2201–2205.

[65] Dong, Y., Feng, X., Zhao, N. & Hou, Z. (2015). Diffusion of nanoparticles in semidilute polymer solutions: A mode-coupling theory study. *The Journal of chemical physics*, **143**, 024903.

[66] Dowding, P.J., Atkin, R., Vincent, B. & Bouillot, P. (2004). Oil corepolymer shell microcapsules prepared by internal phase separation from emulsion droplets. i. characterization and release rates for microcapsules with polystyrene shells. *Langmuir*, **20**, 11374–11379, doi: 10.1021/la048561h.

[67] Du, K., Glogowski, E., Emrick, T., Russell, T.P. & Dinsmore, A.D. (2010). Adsorption energy of nano-and microparticles at liquid liquid interfaces. *Langmuir*, **26**, 12518–12522.

[68] Du, N. & Pritzker, M. (2003). Investigation of electroless plating of niwp alloy films. *Journal of Applied Electrochemistry*, **33**, 1001–1009.

[69] Duan, H., Wang, D., Sobal, N.S., Giersig, M., Kurth, D.G. & Mhwald, H. (2005). Magnetic colloidosomes derived from nanoparticle interfacial self-assembly. *Nano Letters*, **5**, 949–952.

[70] Dubey, R. (2009). *Microencapsulation Technology and Applications*, vol. 59.

[71] E, S.H. (1957). Solid flavoring composition and method of preparing the same.

[72] Elizondo, N., Segovia, P., Coello, V., Arriaga, J., Belmares, S., Alcorta, A., Hernndez, F., Obregn, R., Torres, E. & Paraguay, F. (2012). *Green synthesis and characterizations of silver and gold nanoparticles*. InTech.

[73] Eslek, Z. & Tulpar, A. (2013). Solution preparation and conductivity measurements: An experiment for introductory chemistry. *Journal of Chemical Education*, **90**, 1665–1667.

[74] Esser-Kahn, A.P., Odom, S.A., Sottos, N.R., White, S.R. & Moore, J.S. (2011). Triggered release from polymer capsules. *Macromolecules*, **44**, 5539–5553.

[75] Fan, H. & Striolo, A. (2012). Mechanistic study of droplets coalescence in pickering emulsions. *Soft Matter*, **8**, 9533–9538.

[76] Fan, H. & Striolo, A. (2012). Nanoparticle effects on the water-oil interfacial tension. *Physical Review E*, **86**, 051610.

[77] Faraday, M. (1857). The bakerian lecture: Experimental relations of gold (and other metals) to light. *Philosophical Transactions of the Royal Society of London*, **147**, 145–181.

[78] Ferry, J. (1980). *Viscoelastic Properties of Polymers*. Wiley.

[79] Fielding, L.A. & Armes, S.P. (2012). Preparation of pickering emulsions and colloidosomes using either a glycerol-functionalised silica sol or core-shell polymer/silica nanocomposite particles. *Journal of Materials Chemistry*, **22**, 11235–11244.

[80] Franck, A. & Hodder, P. (2009). Measuring the rheological properties of ultrathin films at the water-air and water-oil interface by using a novel double wall ring (dwr) geometry. *Annual Transactions of the Nordic Rheology Society*, **17**.

[81] French, D.J., Taylor, P., Fowler, J. & Clegg, P.S. (2015). Making and breaking bridges in a pickering emulsion. *Journal of Colloid and Interface Science*, **441**, 30–38.

[82] Fujii, S., Hamasaki, H., Takeoka, H., Tsuruoka, T., Akamatsu, K. & Nakamura, Y. (2014). Electroless nickel plating on polymer particles. *Journal of Colloid and Interface Science*, **430**, 47–55.

[83] Fujiwara, Y., Kobayashi, Y., Sugaya, T., Koishikawa, A., Hoshiyama, Y. & Miyake, H. (2010). Adsorption promotion of ag nanoparticle using cationic surfactants and polyelectrolytes for electroless cu plating catalysts. *Journal of The Electrochemical Society*, **157**, D211–D216.

[84] Gabrielli, G., Cantale, F. & Guarini, G.G.T. (1996). Adsorption of amphiphilic mixtures and stabilization of suspensions of hydrophobic solids in water. *Colloids and Surfaces A: Physicochemical and Engineering Aspects*, **119**, 163–174.

[85] Gao, H.Y., Lin, J.Y.S., Li, Y.D. & Zhang, B.Q. (2005). Electroless plating synthesis, characterization and permeation properties of pd-cu membranes supported on zro2 modified porous stainless steel. *Journal of Membrane Science*, **265**, 142–152.

[86] Gao, N., Zhang, Z. & Dong, Q. (2013). Preparation and properties of two-component and double-crosslinking waterborne polyurethane-acrylic dispersions. *Open Journal of Organic Polymer Materials*, **Vol.03No.02**, 7.

[87] Gao, Y., Jiang, P., Liu, D., Yuan, H., Yan, X., Zhou, Z., Wang, J., Song, L., Liu, L. & Zhou, W. (2004). Evidence for the monolayer assembly of poly (vinylpyrrolidone) on the surfaces of silver nanowires. *Journal of Physical Chemistry B*, **108**, 12877–12881.

[88] Gaonkar, A., Vasisht, N., Khare, A., Sobel, R. & Oxley, J. (2014). *Microencapsulation in the Food Industry: A Practical Implementation Guide*. Elsevier Science.

[89] Garg, A.K. & De Jonghe, L.C. (1993). Metal-coated colloidal particles. *Journal of Materials Science*, **28**, 3427–3432.

[90] Garti, N. & McClements, D. (2012). *Encapsulation Technologies and Delivery Systems for Food Ingredients and Nutraceuticals*. Elsevier Science.

[91] Ghosh, P., Han, G., De, M., Kim, C.K. & Rotello, V.M. (2008). Gold nanoparticles in delivery applications. *Advanced Drug Delivery Reviews*, **60**, 1307–1315.

[92] Gimeno, M.C. (2009). *The Chemistry of Gold*, 1–63. Wiley-VCH Verlag GmbH Co. KGaA.

[93] Glaser, N., Adams, D.J., Bker, A. & Krausch, G. (2006). Janus particles at liquidliquid interfaces. *Langmuir*, **22**, 5227–5229.

[94] Gner, A. (1996). Properties of aqueous salt solutions of polyvinylpyrrolidone. i. viscosity characteristics. *Journal of Applied Polymer Science*, **62**, 785–788.

[95] Gouin, S. (2004). Microencapsulation: industrial appraisal of existing technologies and trends. *Trends in Food Science and Technology*, **15**, 330–347.

[96] Gray, A., Egan, S., Bakalis, S. & Zhang, Z. (2016). Determination of microcapsule physicochemical, structural, and mechanical properties. *Particuology*, **24**, 32–43.

[97] guila Hernndez, J., Trejo, A. & Garca-Flores, B.E. (2011). Volumetric and surface tension behavior of aqueous solutions of polyvinylpyrrolidone in the range (288 to 303) k. *Journal of Chemical Engineering Data*, **56**, 2371–2378.

[98] Hayward, R.C., Utada, A.S., Dan, N. & Weitz, D.A. (2006). Dewetting instability during the formation of polymersomes from block-copolymer-stabilized double emulsions. *Langmuir*, **22**, 4457–4461, doi: 10.1021/la060094b.

[99] Herman, S.J. (2009). *Applications II: Fragrance*, 305–329. Blackwell Publishing Ltd.

[100] Herrmann, A., Debonneville, C., Laubscher, V. & Aymard, L. (2000). Dynamic headspace analysis of the light-induced controlled release of perfumery aldehydes and ketones from -keto esters in bodycare and household applications. *Flavour and Fragrance Journal*, **15**, 415–420.

[101] Hitchcock, J.P., Tasker, A.L., Baxter, E.A., Biggs, S. & Cayre, O.J. (2015). Long-term retention of small, volatile molecular species within metallic microcapsules. *ACS Applied Materials Interfaces*, **7**, 14808–14815.

[102] Horiuchi, S. & Nakao, Y. (2010). Platinum colloid catalyzed etchingless gold electroless plating with strong adhesion to polymers. *Surface and Coatings Technology*, **204**, 3811–3817.

[103] Horozov, T.S. & Binks, B.P. (2006). Particle-stabilized emulsions: A bilayer or a bridging monolayer? *Angewandte Chemie International Edition*, **45**, 773–776.

[104] Hossain, M.J., Rahman, M.S., Rahman, M.S., Ali, M.A., Nandi, N.C., Noor, P., Ahmed, K.N. & Akhter, S. (2016). Optimized reduction conditions for the microfluidic synthesis of 1.3 0.3 nm pt clusters. *Journal of Nanostructure in Chemistry*, **6**, 49–56.

[105] Hosseinkhani, B., Callewaert, C., Vanbeveren, N. & Boon, N. (2015). Novel biocompatible nanocapsules for slow release of fragrances on the human skin. *New Biotechnology*, **32**, 40–46.

[106] Hrapovic, S., Liu, Y., Enright, G., Bensebaa, F. & Luong, J.H.T. (2003). New strategy for preparing thin gold films on modified glass surfaces by electroless deposition. *Langmuir*, **19**, 3958–3965.

[107] Hrvlgyi, Z. & Kiss, E. (2008). *Colloids for Nano- and Biotechnology*. Springer Berlin Heidelberg.

[108] Hu, J., Li, W., Chen, J., Zhang, X. & Zhao, X. (2008). Novel plating solution for electroless deposition of gold film onto glass surface. *Surface and Coatings Technology*, **202**, 2922–2926.

[109] Hvolbk, B., Janssens, T.V.W., Clausen, B.S., Falsig, H., Christensen, C.H. & Nrskov, J.K. (2007). Catalytic activity of au nanoparticles. *Nano Today*, **2**, 14–18.

[110] Illsov, A., Buko, M., Vikartovsk, A. & Gemeiner, P. (2013). Encapsulation as a useful tool for a biotechnological production of natural aromas. *Current Opinion in Biotechnology*, **24, Supplement 1**, S59–S60.

[111] Iqbal, M., Zafar, N., Fessi, H. & Elaissari, A. (2015). Double emulsion solvent evaporation techniques used for drug encapsulation. *International Journal of Pharmaceutics*, **496**, 173–190.

[112] Isa, L., Calzolari, D.C., Pontoni, D., Gillich, T., Nelson, A., Zirbs, R., Snchez-Ferrer, A., Mezzenga, R. & Reimhult, E. (2013). Coreshell nanoparticle monolayers at planar liquidliquid interfaces: effects of polymer architecture on the interface microstructure. *Soft Matter*, **9**, 3789–3797.

[113] Jackson, L. & Lee, K. (1991). *Microencapsulation in the food industry*, vol. 24.

[114] Jacob, R. & Bruno, F. (2015). Review on shell materials used in the encapsulation of phase change materials for high temperature thermal energy storage. *Renewable and Sustainable Energy Reviews*, **48**, 79–87.

[115] Jafari, S.M., He, Y. & Bhandari, B. (2007). Optimization of nanoemulsions production by microfluidization. *European Food Research and Technology*, **225**, 733–741.

[116] Jenkins, P. & Snowden, M. (1996). Depletion flocculation in colloidal dispersions. *Advances in Colloid and Interface Science*, **68**, 57–96.

[117] Karatrantos, A., Composto, R.J., Winey, K.I. & Clarke, N. (2017). Polymer and spherical nanoparticle diffusion in nanocomposites. *The Journal of Chemical Physics*, **146**, 203331.

[118] Karayianni, M. & Pispas, S. (2016). *Self-assembly of amphiphilic block copolymers in selective solvents*, 27–63. Springer.

[119] Keddie, D.J. (2014). A guide to the synthesis of block copolymers using reversible-addition fragmentation chain transfer (raft) polymerization. *Chemical Society Reviews*, **43**, 496–505.

[120] Keller, B. (2011). Nanotechnology for spilled oil encapsulation, remediation and recovery.

[121] Keoshkerian, B., MacLeod, P.J. & Georges, M.K. (2001). Block copolymer synthesis by a miniemulsion stable free radical polymerization process. *Macromolecules*, **34**, 3594–3599.

[122] Kim, B.S. & Lee, T.R. (2015). *The Development of Smart, Multi-Responsive Core@Shell Composite Nanoparticles*, Ch. 06. InTech, Rijeka.

[123] Kim, H., Daniels, E.S., Dimonie, V.L. & Klein, A. (2009). Palladiumcatalyzed electroless plating of gold on latex particle surfaces. *Journal of applied polymer science*, **112**, 843–849.

[124] Kim, J.W., Fernndez-Nieves, A., Dan, N., Utada, A.S., Marquez, M. & Weitz, D.A. (2007). Colloidal assembly route for responsive colloidosomes with tunable permeability. *Nano Letters*, **7**, 2876–2880, doi: 10.1021/nl0715948.

[125] Kim, K., Lee, H.B., Park, H.K. & Shin, K.S. (2008). Easy deposition of ag onto polystyrene beads for developing surface-enhanced-raman-scattering-based molecular sensors. *Journal of Colloid and Interface Science*, **318**, 195–201.

[126] Kim, K., Kim, S., Ryu, J., Jeon, J., Jang, S.G., Kim, H., Gweon, D.G., Im, W.B., Han, Y., Kim, H. & Choi, S.Q. (2017). Processable high internal phase pickering emulsions using depletion attraction. *Nature Communications*, **8**, 14305.

[127] Koczkur, K.M., Mourdikoudis, S., Polavarapu, L. & Skrabalak, S.E. (2015). Polyvinylpyrrolidone (pvp) in nanoparticle synthesis. *Dalton Transactions*, **44**, 17883–17905.

[128] Kousksou, T., Jamil, A., Rhafiki, T.E. & Zeraouli, Y. (2010). Paraffin wax mixtures as phase change materials. *Solar Energy Materials and Solar Cells*, **94**, 2158–2165.

[129] Krupa, I., Mikov, G. & Luyt, A.S. (2007). Phase change materials based on low-density polyethylene/paraffin wax blends. *European Polymer Journal*, **43**, 4695–4705.

[130] Kuroiwa, T., Horikoshi, K., Suzuki, A., Neves, M.A., Kobayashi, I., Uemura, K., Nakajima, M., Kanazawa, A. & Ichikawa, S. (2016). Efficient encapsulation of a water-soluble molecule into lipid vesicles using w/o/w multiple emulsions via solvent evaporation. *Journal of the American Oil Chemists' Society*, **93**, 421–430.

[131] Lacava, J., Ouali, A.A., Raillard, B. & Kraus, T. (2014). On the behaviour of nanoparticles in oil-in-water emulsions with different surfactants. *Soft Matter*, **10**, 1696–1704.

[132] Lakkis, J. (2016). *Encapsulation and Controlled Release Technologies in Food Systems*. Wiley.

[133] Lee, H., Choi, C.H., Abbaspourrad, A., Wesner, C., Caggioni, M., Zhu, T. & Weitz, D.A. (2016). Encapsulation and enhanced retention of fragrance in polymer microcapsules. *ACS Applied Materials Interfaces*, **8**, 4007–4013.

[134] Lee, I., Hammond, P.T. & Rubner, M.F. (2003). Selective electroless nickel plating of particle arrays on polyelectrolyte multilayers. *Chemistry of Materials*, **15**, 4583–4589.

[135] Lee, S.B., Russell, A.J. & Matyjaszewski, K. (2003). Atrp synthesis of amphiphilic random, gradient, and block copolymers of 2-(dimethylamino)ethyl methacrylate and n-butyl methacrylate in aqueous media. *Biomacromolecules*, **4**, 1386–1393.

[136] Lensen, D., Vriezema, D.M. & van Hest, J.C.M. (2008). Polymeric microcapsules for synthetic applications. *Macromolecular Bioscience*, **8**, 991–1005.

[137] Li, D., Hsu, R., Figura, B., Jacobs, R., Li, S., Horvath, S., Clifford, T. & Chari, K. (2016). Rheology and structure of surface crosslinked surfactant-activated microgels. *Soft Matter*, **12**, 7150–7158.

[138] Li, G., Prasad, S. & Dhinojwala, A. (2007). Dynamic interfacial tension at the oil/surfactant water interface. *Langmuir*, **23**, 9929–9932.

[139] Liaw, W.C., Cheng, Y.L., Chang, M.K., Lien, W.F. & Lai, H.R. (2016). The preparation of ni-plated polystyrene microspheres using 3-(trimethoxysilyl) propyl methacrylate as a bridging agent. *Polym J*, **48**, 91–99.

[140] Lin, K.J., Wu, H.M., Yu, Y.H., Ho, C.Y., Wei, M.H., Lu, F.H. & Tseng, W.J. (2013). Preparation of pmma-ni core-shell composite particles by electroless plating on polyelectrolyte-modified pmma beads. *Applied Surface Science*, **282**, 741–745.

[141] Lin, Y., Skaff, H., Bker, A., Dinsmore, A.D., Emrick, T. & Russell, T.P. (2003). Ultrathin cross-linked nanoparticle membranes. *Journal of the American Chemical Society*, **125**, 12690–12691, doi: 10.1021/ja036919a.

[142] Lin, Y., Skaff, H., Emrick, T., Dinsmore, A.D. & Russell, T.P. (2003). Nanoparticle assembly and transport at liquid-liquid interfaces. *Science*, **299**, 226–229.

[143] Liu, J., Cao, D. & Zhang, L. (2008). Molecular dynamics study on nanoparticle diffusion in polymer melts: a test of the stokes-einstein law. *The Journal of Physical Chemistry C*, **112**, 6653–6661.

[144] Liu, J.B., Dong, W., Zhan, P., Wang, S.Z., Zhang, J.H. & Wang, Z.L. (2005). Synthesis of bimetallic nanoshells by an improved electroless plating method. *Langmuir*, **21**, 1683–1686.

[145] Lobo, L. & Svereika, A. (2003). Coalescence during emulsification: 2. role of small molecule surfactants. *Journal of Colloid and Interface Science*, **261**, 498–507.

[146] Lokensgard, E. (2016). *Industrial Plastics: Theory and Applications*. Cengage Learning.

[147] Long, N.V., Ohtaki, M., Nogami, M. & Hien, T.D. (????). Effects of heat treatment and poly(vinylpyrrolidone) (pvp) polymer on electrocatalytic activity of polyhedral pt nanoparticles towards their methanol oxidation. *Colloid and Polymer Science*, **289**, 1373–1386.

[148] Long, N.V., Chien, N.D., Hayakawa, T., Hirata, H., Lakshminarayana, G. & Nogami, M. (2010). The synthesis and characterization of platinum nanoparticles: a method of controlling the size and morphology. *Nanotechnology*, **21**, 035605.

[149] Long, Y., Song, K., York, D., Zhang, Z. & Preece, J.A. (2016). Composite microcapsules with enhanced mechanical stability and reduced active ingredient leakage. *Particuology*, **26**, 40–46.

[150] LoPresti, C., Lomas, H., Massignani, M., Smart, T. & Battaglia, G. (2009). Polymersomes: nature inspired nanometer sized compartments. *Journal of Materials Chemistry*, **19**, 3576–3590.

[151] Loprgolo, L.C., Lugo, A.B. & Catalani, L.H. (2003). Direct uv photocrosslinking of poly (n-vinyl-2-pyrrolidone)(pvp) to produce hydrogels. *Polymer*, **44**, 6217–6222.

[152] Lorenceau, E., Utada, A.S., Link, D.R., Cristobal, G., Joanicot, M. & Weitz, D.A. (2005). Generation of polymerosomes from double-emulsions. *Langmuir*, **21**, 9183–9186.

[153] Lotierzo, A. & Bon, S.A.F. (2017). A mechanistic investigation of pickering emulsion polymerization. *Polymer Chemistry*, **8**, 5100–5111.

[154] Loxley, A. & Vincent, B. (1998). Preparation of poly(methylmethacrylate) microcapsules with liquid cores. *Journal of Colloid and Interface Science*, **208**, 49–62.

[155] Lu, Y.C. & Chou, K.S. (2008). A simple and effective route for the synthesis of nano-silver colloidal dispersions. *Journal of the Chinese Institute of Chemical Engineers*, **39**, 673–678.

[156] Luo, L., Engelhard, M.H., Shao, Y. & Wang, C. (2017). Revealing the dynamics of platinum nanoparticle catalysts on carbon in oxygen and water using environmental tem. *ACS Catalysis*, **7**, 7658–7664.

[157] Ma, Y. & Zhang, Q. (2012). Preparation and characterization of monodispersed ps/ag composite microspheres through modified electroless plating. *Applied Surface Science*, **258**, 7774–7780.

[158] Maa, Y.F. & Hsu, C.C. (1999). Performance of sonication and microfluidization for liquidliquid emulsification. *Pharmaceutical Development and Technology*, **4**, 233–240.

[159] Madene, A., Jacquot, M., Scher, J. & Desobry, S. (2006). Flavour encapsulation and controlled release a review. *International Journal of Food Science and Technology*, **41**, 1–21.

[160] Mahdi Jafari, S., He, Y. & Bhandari, B. (2006). Nano-emulsion production by sonication and microfluidizationa comparison. *International Journal of Food Properties*, **9**, 475–485.

[161] Mallory, G.O. & Hajdu, J.B. (1990). *Electroless Plating - Fundamentals and Applications*. William Andrew Publishing/Noyes, New York.

[162] Manga, M.S., Hunter, T.N., Cayre, O.J., York, D.W., Reichert, M.D., Anna, S.L., Walker, L.M., Williams, R.A. & Biggs, S.R. (2016). Measurements of submicron particle adsorption and particle film elasticity at oilwater interfaces. *Langmuir*, **32**, 4125–4133.

[163] McClements, D.J. (1999). *Food Emulsions: Principles, Practice and Techniques*. CRC Press LLC, United States of America.

[164] Mer, V.K.L. (1952). Nucleation in phase transitions. *Industrial Engineering Chemistry*, **44**, 1270–1277.

[165] Meyer, A. (1992). Perfume microencapsulation by complex coacervation. *CHIMIA International Journal for Chemistry*, **46**, 101–102.

[166] Mishra, M. (2015). *Handbook of encapsulation and controlled release*. CRC Press.

[167] Moad, G., Rizzardo, E. & Thang, S.H. (2009). Living radical polymerization by the raft processa second update. *Australian journal of chemistry*, **62**, 1402–1472.

[168] Mody, V.V., Siwale, R., Singh, A. & Mody, H.R. (2010). Introduction to metallic nanoparticles. *Journal of Pharmacy and Bioallied Sciences*, **2**, 282–289.

[169] Mohamed, A. & El-Gamal, M. (2014). Nano-sized composites containing polyvinyl pyrrolidone modified sodium silicates and method for making binders using same.

[170] Moshfegh, A.Z. (2009). Nanoparticle catalysts. *Journal of Physics D: Applied Physics*, **42**, 233001.

[171] Mostafa, S., Behafarid, F., Croy, J.R., Ono, L.K., Li, L., Yang, J.C., Frenkel, A.I. & Cuenya, B.R. (2010). Shape-dependent catalytic properties of pt nanoparticles. *Journal of the American Chemical Society*, **132**, 15714–15719.

[172] Muench, F., Schaefer, S., Hageluken, L., Molina-Luna, L., Duerrschnabel, M., Kleebe, H.J., Brotz, J., Vaskevich, A., Rubinstein, I. & Ensinger, W. (2017). Template-free electroless plating of gold nanowires: Direct surface functionalization with shape-selective nanostructures for electrochemical applications. *ACS applied materials interfaces*, **9**, 31142–31152.

[173] Muppalaneni, S. & Omidian, H. (2013). Polyvinyl alcohol in medicine and pharmacy: a perspective. *J. Dev. Drugs*, **2**.

[174] Murata, H. (2012). *Rheology - Theory and Application to Biomaterials*, Ch. 17. InTech, Rijeka.

[175] Nallamilli, T., Mani, E. & Basavaraj, M.G. (2014). A model for the prediction of droplet size in pickering emulsions stabilized by oppositely charged particles. *Langmuir*, **30**, 9336–9345.

[176] Narukeviius, L., Tamaauskait-Tamainait, L., ielien, A. & Jasulaitien, V. (2012). A co-based surface activator for electroless copper deposition. *Surface and Coatings Technology*, **206**, 2967–2971.

[177] Nelson, G. (2002). Application of microencapsulation in textiles. *International Journal of Pharmaceutics*, **242**, 55–62.

[178] Neogi, P. & Narsimhan, G. (2001). Ostwald ripening of oil drops in a micellar solution. *Chemical Engineering Science*, **56**, 4225–4231.

[179] Nitika Agnihotri, C.G.M.A., Ravinesh Mishra (2012). Microencapsulation a novel approach in drug delivery: A review. *Indo Global Journal of Pharmaceutical Sciences*, **2**, 1–20.

[180] Noble, P.F., Cayre, O.J., Alargova, R.G., Velev, O.D. & Paunov, V.N. (2004). Fabrication of hairy colloidosomes with shells of polymeric microrods. *Journal of the American Chemical Society*, **126**, 8092–8093.

[181] Nocera, G.M., Ben M'Barek, K., Bazzoli, D.G., Fraux, G., Bontems-Van Heijenoort, M., Chokki, J., Georgeault, S., Chen, Y. & Fattaccioli, J. (2014). Fluorescent microparticles fabricated through chemical coating of o/w emulsion droplets with a thin metallic film. *RSC Advances*, **4**, 11564–11568.

[182] Ohno, I. (2010). *Electroless Deposition of Alloys*, 499–506. John Wiley Sons, Inc.

[183] Ohno, I. (2010). *Electroless Deposition of Palladium and Platinum*, 477–482. John Wiley Sons, Inc.

[184] Okinaka, Y. & Kato, M. (2010). *Electroless Deposition of Gold*, 483–498. John Wiley Sons, Inc.

[185] Okubo, T. (1995). Surface tension of structured colloidal suspensions of polystyrene and silica spheres at the air-water interface. *Journal of Colloid and Interface Science*, **171**, 55–62.

[186] Okuro, P.K., de Matos, F.E. & Favaro-Trindade, C.S. (2013). Technological challenges for spray chilling encapsulation of functional food ingredients. *Food Technology and Biotechnology*, **51**, 171–182.

[187] Oldenburg, S.J., Averitt, R.D., Westcott, S.L. & Halas, N.J. (1998). Nanoengineering of optical resonances. *Chemical Physics Letters*, **288**, 243–247.

[188] Oxley, J. (2014). *Overview of Microencapsulation Process Technologies*, 35–46. Elsevier Science.

[189] Pandolfe, W.D. (1995). Effect of premix condition, surfactant concentration, and oil level on the formation of oil-in-water emulsions by homogenization. *Journal of Dispersion Science and Technology*, **16**, 633–650.

[190] Pastoriza-Santos, I. & Liz-Marzn, L.M. (2002). Formation of pvp-protected metal nanoparticles in dmf. *Langmuir*, **18**, 2888–2894, doi: 10.1021/la015578g.

[191] Patchan, M.W., Baird, L.M., Rhim, Y.R., LaBarre, E.D., Maisano, A.J., Deacon, R.M., Xia, Z. & Benkoski, J.J. (2012). Liquid-filled metal microcapsules. *ACS Applied Materials Interfaces*, **4**, 2406–2412, doi: 10.1021/am201861j.

[192] Pawar, A.B., Caggioni, M., Ergun, R., Hartel, R.W. & Spicer, P.T. (2011). Arrested coalescence in pickering emulsions. *Soft Matter*, **7**, 7710–7716.

[193] Pea, B., Panisello, C., Arest, G., Garcia-Valls, R. & Gum, T. (2012). Preparation and characterization of polysulfone microcapsules for perfume release. *Chemical Engineering Journal*, **179**, 394–403.

[194] Pedone, D., Moglianetti, M., De Luca, E., Bardi, G. & Pompa, P.P. (2017). Platinum nanoparticles in nanobiomedicine. *Chemical Society Reviews*, **46**, 4951–4975.

[195] Pelipenko, J., Kristl, J., Roic, R., Baumgartner, S. & Kocbek, P. (2012). Interfacial rheology: An overview of measuring techniques and its role in dispersions and electrospinning.

[196] Persson, K.H., Blute, I.A., Mira, I.C. & Gustafsson, J. (2014). Creation of well-defined particle stabilized oil-in-water nanoemulsions. *Colloids and Surfaces A: Physicochemical and Engineering Aspects*, **459**, 48–57.

[197] Piacentini, E. (2016). *Encapsulation Efficiency*, 706–707. Springer Berlin Heidelberg, Berlin, Heidelberg.

[198] Pickering, S.U. (1907). Cxcvi.-emulsions. *Journal of the Chemical Society, Transactions*, **91**, 2001–2021.

[199] Pitt, W.G., Husseini, G.A. & Staples, B.J. (2004). Ultrasonic drug delivery a general review. *Expert opinion on drug delivery*, **1**, 37–56.

[200] Polte, J. (2015). Fundamental growth principles of colloidal metal nanoparticles - a new perspective. *CrystEngComm*, **17**, 6809–6830.

[201] Pons, R. (2000). *Polymeric Surfactants as Emulsion Stabilizers*, 409–422. Elsevier Science B.V., Amsterdam.

[202] Porter, L.A., Choi, H.C., Ribbe, A.E. & Buriak, J.M. (2002). Controlled electroless deposition of noble metal nanoparticle films on germanium surfaces. *Nano Letters*, **2**, 1067–1071.

[203] Powell, C.J., Werner, W.S.M., Kalbe, H., Shard, A.G. & Castner, D.G. (2018). Comparisons of analytical approaches for determining shell thicknesses of coreshell nanoparticles by x-ray photoelectron spectroscopy. *The Journal of Physical Chemistry C*, **122**, 4073–4082.

[204] Prins, W. & Hermans, J.J. (1959). Theory of permeation through metal coated polymer films. *The Journal of Physical Chemistry*, **63**, 716–720, doi: 10.1021/j150575a017.

[205] Quellet, C., Schudel, M. & Ringgenberg, R. (2001). Flavors fragrance delivery systems. *CHIMIA International Journal for Chemistry*, **55**, 421–428.

[206] Quirk, R.P., Zhuo, Q., Jang, S.H., Lee, Y. & Lizarraga, G. (1998). *Principles of Anionic Polymerization: An Introduction*. ACS Publications.

[207] Richards, R. (2006). *Surface and Nanomolecular Catalysis*. CRC Press.

[208] Richards, R. & Bnnemann, H. (2005). Synthetic approaches to metallic nanomaterials. *Nanofabrication Towards Biomedical Applications: Techniques, Tools, Applications, and Impact*, 2.

[209] Riess, G., Nervo, J. & Rogez, D. (1977). Emulsifying properties, of block copolymers. oil-water emulsions and microemulsions. *Polymer Engineering Science*, **17**, 634–638.

[210] Rizzelli, S., Jones, E., Thompson, K. & Armes, S. (2016). Preparation of non-aqueous pickering emulsions using anisotropic block copolymer nanoparticles. *Colloid and Polymer Science*, **294**, 1–12.

[211] Rogers, J.A., Bao, Z., Baldwin, K., Dodabalapur, A., Crone, B., Raju, V.R., Kuck, V., Katz, H., Amundson, K., Ewing, J. & Drzaic, P. (2001). Paper-like electronic displays: Large-area rubber-stamped plastic sheets of electronics and microencapsulated electrophoretic inks. *Proceedings of the National Academy of Sciences of the United States of America*, **98**, 4835–4840.

[212] Roldan Cuenya, B. (2012). Metal nanoparticle catalysts beginning to shape-up. *Accounts of Chemical Research*, **46**, 1682–1691.

[213] Rosen, M.J. & Kunjappu, J.T. (2012). *Surfactants and interfacial phenomena*. John Wiley Sons.

[214] Roucoux, A., Schulz, J. & Patin, H. (2002). Reduced transition metal colloids: a novel family of reusable catalysts? *Chemical Reviews*, **102**, 3757–3778.

[215] Sadjadi, S. (2016). *Organic Nanoreactors: From Molecular to Supramolecular Organic Compounds*. Elsevier Science.

[216] Sagis, L. (2015). *Microencapsulation and Microspheres for Food Applications*. Elsevier Science.

[217] Saleh, N., Sarbu, T., Sirk, K., Lowry, G.V., Matyjaszewski, K. & Tilton, R.D. (2005). Oil-in-water emulsions stabilized by highly charged polyelectrolyte-grafted silica nanoparticles. *Langmuir*, **21**, 9873–9878.

[218] Sansukcharearnpon, A., Wanichwecharungruang, S., Leepipatpaiboon, N., Kerdcharoen, T. & Arayachukeat, S. (2010). High loading fragrance encapsulation based on a polymer-blend: Preparation and release behavior. *International Journal of Pharmaceutics*, **391**, 267–273.

[219] Saravacos, G. & Kostaropoulos, A. (2002). *Mechanical Processing Equipment*, book section 4, 134–207. Food Engineering Series, Springer US.

[220] Schlesinger, M. (2010). *Electroless Deposition of Nickel*, 447–458. John Wiley Sons, Inc.

[221] Schwarz, W. (1990). *PVP: a critical review of the kinetics and toxicology of polyvinylpyrrolidone (povidone)*. CRC Press.

[222] Sherman, P. (1968). *Emulsion science*. Academic Press.

[223] Shi, X. & Caruso, F. (2001). Release behavior of thin-walled microcapsules composed of polyelectrolyte multilayers. *Langmuir*, **17**, 2036–2042.

[224] Spadavecchia, J., Movia, D., Moore, C., Maguire, C.M., Moustaoui, H., Casale, S., Volkov, Y. & Prina-Mello, A. (2016). Targeted polyethylene glycol gold nanoparticles for the treatment of pancreatic cancer: from synthesis to proof-of-concept in vitro studies. *International journal of nanomedicine*, **11**, 791.

[225] Strawbridge, K.B., Ray, E., Hallett, F.R., Tosh, S.M. & Dalgleish, D.G. (1995). Measurement of particle-size distributions in milk homogenized by a microfluidizer - estimation of populations of particles with radii less-than 100 nm. *Journal of Colloid and Interface Science*, **171**, 392–398.

[226] Sun, Q. & Routh, A.F. (2016). Aqueous core colloidosomes with a metal shell. *European Polymer Journal*, **77**, 155–163.

[227] Swapan, K.G. (2006). Functional coatings by polymer microencapsulation. *WILEY-VCH Press, Weinheim*, 303.

[228] Tadros, T.F. (2013). *Emulsion Formation, Stability, and Rheology*, 1–75. Wiley-VCH Verlag GmbH Co. KGaA.

[229] Tambe, D.E. & Sharma, M.M. (1994). The effect of colloidal particles on fluid-fluid interfacial properties and emulsion stability. *Advances in Colloid and Interface Science*, **52**, 1–63.

[230] Tang, Z., Geng, D. & Lu, G. (2005). Size-controlled synthesis of colloidal platinum nanoparticles and their activity for the electrocatalytic oxidation of carbon monoxide. *Journal of Colloid and Interface Science*, **287**, 159–166.

[231] Taylor, P. (1998). Ostwald ripening in emulsions. *Advances in colloid and interface science*, **75**, 107–163.

[232] Tekin, R., Bac, N. & Erdogmus, H. (2013). Microencapsulation of fragrance and natural volatile oils for application in cosmetics, and household cleaning products. *Macromolecular Symposia*, **333**, 35–40.

[233] Tetsuya, O., Yutaka, O., Junji, S. & Masaru, K. (2006). Development of new electrolytic and electroless gold plating processes for electronics applications. *Science and Technology of Advanced Materials*, **7**, 425.

[234] Theron, F. & Sauze, N.L. (2011). Comparison between three static mixers for emulsification in turbulent flow. *International Journal of Multiphase Flow*, **37**, 488–500.

[235] Thompson, K.L., Armes, S.P., Howse, J.R., Ebbens, S., Ahmad, I., Zaidi, J.H., York, D.W. & Burdis, J.A. (2010). Covalently crosslinked colloidosomes. *Macromolecules*, **43**, 10466–10474.

[236] Tongsakul, D., Nishimura, S. & Ebitani, K. (2013). Platinum/gold alloy nanoparticles-supported hydrotalcite catalyst for selective aerobic oxidation of polyols in base-free aqueous solution at room temperature. *ACS Catalysis*, **3**, 2199–2207.

[237] Toshima, N. (2003). *Metal Nanoparticles for Catalysis*, book section 3, 79–96. Springer US.

[238] Tsabet, m. & Fradette, L. (2015). Effect of the properties of oil, particles, and water on the production of pickering emulsions. *Chemical Engineering Research and Design*, **97**, 9–17.

[239] Tu, W.x., Zuo, X.b. & Liu, H.f. (2008). Study on the interaction between polyvinylpyrrolidone and platinum metals during the formation of the colloidal metal nanoparticles. *Chinese Journal of Polymer Science (CJPS)*, **26**, 23–29.

[240] Tuteja, A., Mackay, M.E., Narayanan, S., Asokan, S. & Wong, M.S. (2007). Breakdown of the continuum stokeseinstein relation for nanoparticle diffusion. *Nano Letters*, **7**, 1276–1281.

[241] Tyagi, H., Kushwaha, A., Kumar, A. & Aslam, M. (????). Pva stabilized gold nanoparticles using ascorbic acid as a reducing agent. In *AIP Conference Proceedings*, vol. 1349, 419–420, AIP.

[242] Vaklev, N., Vasileva, P. & Dushkin, C. (2007). Synthesis of gold nanoparticles via hydrogen peroxide reduction enhanced by sonication. *Nanoscience and Nanotechnology*, **7**, 70–73.

[243] Van Rheenen, P.R., McKelvy, M.J. & Glaunsinger, W.S. (1987). Synthesis and characterization of small platinum particles formed by the chemical reduction of chloroplatinic acid. *Journal of Solid State Chemistry*, **67**, 151–169.

[244] Varona, S., Kareth, S., Martin, A. & Cocero, M.J. (2010). Formulation of lavandin essential oil with biopolymers by pgss for application as biocide in ecological agriculture. *Journal of Supercritical Fluids*, **54**, 369–377.

[245] Velev, O.D., Furusawa, K. & Nagayama, K. (1996). Assembly of latex particles by using emulsion droplets as templates. 2. ball-like and composite aggregates. *Langmuir*, **12**, 2385–2391.

[246] Viet-Long, N., Michitaka, O., Van Nong, N., Minh-Thi, C. & Masayuki, N. (2012). Structure and morphology of platinum nanoparticles with critical new issues of low- and high-index facets. *Advances in Natural Sciences: Nanoscience and Nanotechnology*, **3**, 025005.

[247] Vignati, E., Piazza, R. & Lockhart, T.P. (2003). Pickering emulsions: interfacial tension, colloidal layer morphology, and trapped-particle motion. *Langmuir*, **19**, 6650–6656.

[248] Walstra, P. (1993). Principles of emulsion formation. *Chemical Engineering Science*, **48**, 333–349.

[249] Wang, C., Zhang, C., Li, Y., Chen, Y. & Tong, Z. (2009). Facile fabrication of nanocomposite microspheres with polymer cores and magnetic shells by pickering suspension polymerization. *Reactive and Functional Polymers*, **69**, 750–754.

[250] Wang, H., Song, Y., Wang, Z., Medforth, C.J., Miller, J.E., Evans, L., Li, P. & Shelnutt, J.A. (2008). Silicametal coreshells and metal shells synthesized by porphyrin-assisted photocatalysis. *Chemistry of Materials*, **20**, 7434–7439.

[251] Wang, Y. & Pan, C. (2001). Dielectric behavior and magnetic properties of poly(styrene-co-acrylic acid)metal microspheres. *European Polymer Journal*, **37**, 699–704.

[252] Wang, Z., Gao, J., Ustach, V., Li, C., Sun, S., Hu, S. & Faller, R. (2017). Tunable permeability of cross-linked microcapsules from ph-responsive amphiphilic diblock copolymers: A dissipative particle dynamics study. *Langmuir*, **33**, 7288–7297.

[253] Wang, Z.F., Wang, B., Qi, N., Zhang, H.F. & Zhang, L.Q. (2005). Influence of fillers on free volume and gas barrier properties in styrene-butadiene rubber studied by positrons. *Polymer*, **46**, 719–724.

[254] Watanabe, Y., Fang, X., Minemoto, Y., Adachi, S. & Matsuno, R. (2002). Suppressive effect of saturated acyl l-ascorbate on the oxidation of linoleic acid encapsulated with maltodextrin or gum arabic by spray-drying. *Journal of Agricultural and Food Chemistry*, **50**, 3984–3987, doi: 10.1021/jf011656u.

[255] Wei, N., Hao, X., Sun, C., Lan, J. & Yang, S. (2010). Reversible thermochromism materials micro-encapsulation and application in offset printing ink. *Scientific Research*.

[256] Whitby, C.P. & Wanless, E.J. (2016). Controlling pickering emulsion destabilisation: A route to fabricating new materials by phase inversion. *Materials*, **9**, 626.

[257] Whithaus, S. & Blecker, L. (2016). *The Safe and Effective Use of Pesticides, 3rd Edition*. University of California Agriculture and Natural Resources.

[258] Wiley, R.M. (1954). Limited coalescence of oil droplets in coarse oil-in-water emulsions. *Journal of Colloid Science*, **9**, 427–437.

[259] Wuithschick, M., Witte, S., Kettemann, F., Rademann, K. & Polte, J. (2015). Illustrating the formation of metal nanoparticles with a growth concept based on colloidal stability. *Physical Chemistry Chemical Physics*, **17**, 19895–19900.

[260] Xia, Y., Xiong, Y., Lim, B. & Skrabalak, S. (2009). Shape-controlled synthesis of metal nanocrystals: Simple chemistry meets complex physics? *Angewandte Chemie International Edition*, **48**, 60–103.

[261] Yow, H.N. & Routh, A.F. (2006). Formation of liquid core-polymer shell microcapsules. *Soft Matter*, **2**, 940–949.

[262] ystein, S., Stanislav, S.D. & Johann, S.b. (2005). *An Experimental and Theoretical Approach to the Dynamic Behavior of Emulsions*, 1–106. Surfactant Science, CRC Press, doi:10.1201/9781420028089.ch1.

[263] Zhang, H., Liu, Y., Wang, C., Zhang, J., Sun, H., Li, M. & Yang, B. (2008). Directing the growth of semiconductor nanocrystals in aqueous solution: Role of electrostatics. *ChemPhysChem*, **9**, 1309–1316.

[264] Zhang, S., Shao, Y., Yin, G. & Lin, Y. (2009). Stabilization of platinum nanoparticle electrocatalysts for oxygen reduction using poly (diallyldimethylammonium chloride). *Journal of Materials Chemistry*, **19**, 7995–8001.

[265] Zhang, X.y. & Zhang, P.y. (2017). Polymersomes in nanomedicine - a review. *Current Medicinal Chemistry*, **13**, 124–129.

[266] Zhang, Z., Zhao, B. & Hu, L. (1996). Pvp protective mechanism of ultrafine silver powder synthesized by chemical reduction processes. *Journal of Solid State Chemistry*, **121**, 105–110.

[267] Zheng, Y., Zhao, W., Sabol, J.C., Tuzla, K., Neti, S., Oztekin, A. & Chen, J.C. (2013). Encapsulated phase change materials for energy storage characterization by calorimetry. *Solar Energy*, **87**, 117–126.

[268] Zhu, S.L., Tang, L., Cui, Z.D., Wei, Q. & Yang, X.J. (2011). Preparation of copper-coated -sic nanoparticles by electroless plating. *Surface and Coatings Technology*, **205**, 2985–2988.

[269] Zieringer, M.A., Carroll, N.J., Abbaspourrad, A., Koehler, S.A. & Weitz, D.A. (2015). Microcapsules for enhanced cargo retention and diversity. *Small*, **11**, 2903–2909.